8-2006

Design of an Active Stereo Vision 3D Scene Reconstruction System Based on the Linear Position Sensor Module

Julie Anne Morris
University of Tennessee - Knoxville

To the Graduate Council:

I am submitting herewith a thesis written by Julie Anne Morris entitled "Design of an Active Stereo Vision 3D Scene Reconstruction System Based on the Linear Position Sensor Module." I have examined the final electronic copy of this thesis for form and content and recommend that it be accepted in partial fulfillment of the requirements for the degree of Master of Science, with a major in Electrical Engineering.

M. A. Abidi, Major Professor

We have read this thesis and recommend its acceptance:

D. Page, B. Blalock, D. Bouldin

Accepted for the Council:
Carolyn R. Hodges

Vice Provost and Dean of the Graduate School

(Original signatures are on file with official student records.)

To the Graduate Council:

I am submitting herewith a thesis written by Julie Anne Morris entitled "Design of an Active Stereo Vision 3D Scene Reconstruction System Based on the Linear Position Sensor Module." I have examined the final electronic copy of this thesis for form and content and recommend that it be accepted in partial fulfillment of the requirements for the degree of Master of Science, with a major in Electrical Engineering.

M. A. Abidi
Major Professor

We have read this thesis
and recommend its acceptance:

D. Page

B. Blalock

D. Bouldin

Accepted for the Council:

Anne Mayhew
Vice Chancellor and
Dean of Graduate Studies

(Original signatures are on file with official student records.)

DESIGN OF AN ACTIVE STEREO VISION 3D SCENE RECONSTRUCTION SYSTEM BASED ON THE LINEAR POSITION SENSOR MODULE

A Thesis

Presented for the

Master of Science

Degree

University of Tennessee, Knoxville

Julie Anne Morris
August 2006

ACKNOWLEDGEMENTS

I would like to thank my parents for their constant support, advice, and patience. God has truly blessed me to have you as parents. Thank you for putting up with me.

Sincere thanks to Dr. Abidi for his support, both financially and through technological resources. Also thanks to the entire IRIS lab for the use of their facilities and especially Dr. Page for his help in the research process. Thank you also to Dr. Blalock and Dr. Bouldin for serving on my graduate committee.

Finally, I accept sole responsibility for any errors found in this document.

ABSTRACT

Active vision systems and passive vision systems currently exist for three-dimensional (3D) scene reconstruction. Active systems use a laser that interacts with the scene. Passive systems implement stereo vision, using two cameras and geometry to reconstruct the scene. Each type of system has advantages and disadvantages in resolution, speed, and scene depth. It may be possible to combine the advantages of both systems as well as new hardware technologies such as position sensitive devices (PSDs) and field programmable gate arrays (FPGAs) to create a real-time, mid-range 3D scene reconstruction system.

Active systems usually reconstruct long-range scenes so that a measurable amount of time can pass for the laser to travel to the scene and back. Passive systems usually reconstruct close-range scenes but must overcome the correspondence problem. If PSDs are placed in a stereo vision configuration and a laser is directed at the scene, the correspondence problem can be eliminated. The laser can scan the entire scene as the PSDs continually pick up points, and the scene can be reconstructed. By eliminating the correspondence problem, much of the computation time of stereo vision is removed, allowing larger scenes, possibly at mid-range, to be modeled.

To give good resolution at a real-time frame rate, points would have to be recorded very quickly. PSDs are analog devices that give the position of a light spot and have very fast response times. The cameras in the system can be replaced by PSDs to help achieve real-time refresh rates and better resolution. A contribution of this thesis is to design a 3D scene reconstruction system by placing two PSDs in a stereo vision configuration and to use FPGAs to perform calculations to achieve real-time frame rates of mid-range scenes.

The linear position sensor module (LPSM) made by Noah Corp is based on a PSD and outputs a position in terms of voltage. The LPSM is characterized for this application by testing it with different power lasers while also varying environment variables such as background light, scene type, and scene distance. It is determined that the LPSM is sensitive to red wavelength lasers. When the laser is reflected off of diffuse surfaces, the laser must output at least 500 mW to be picked up by the LPSM and the scene must be within 15 inches, or the power intensity will not meet the intensity requirements of the LPSM. The establishment of these performance boundaries is a contribution of the thesis along with characterizing and testing the LPSM as a vision sensor in the proposed scene reconstruction system.

Once performance boundaries are set, the LPSM is used to model calibrated objects. LPSM sensitivity to power intensity changes seems to cause considerable error. The change in power appears to be a function of depth due to the dispersion of the laser beam. The model is improved by using a correction factor to find the position of the light spot. Using a better-focused laser may improve the results. Another option is to place two PSDs in the same configuration and test to see whether the intensity problem is intrinsic to all PSDs or if the problem is unique to the LPSM.

TABLE OF CONTENTS

LIST OF TABLES

LIST OF FIGURES

1 INTRODUCTION

Machine vision allows a robot to see its surroundings. Robot vision describes the ability of a robot to reconstruct the scene surrounding the machine in three dimensions (3D) so that it can recognize objects in the scene and react accordingly. As research has been done to use robots in more applications, the importance for robots to "see" their surroundings has increased. For example, the Defense Advanced Research Projects Agency (DARPA) project challenges research teams to make a car autonomous and then navigate a roadway [DARPA, 2005]. In the competition, students faced problems when their visions systems had to deal with fog, shadows, or glare [Russell, 2005]. Many 3D robot vision systems also cannot currently provide real-time reconstruction rates of 30 frames per second (fps) or better. The Carnegie-Mellon University (CMU) camera has a refresh rate of 16.7 fps [Carnegie, 2005]. If a car used the CMU camera and was moving at 30 miles per hour, then it would see one frame every 2.63 feet, giving it very little time to process the information from the scene and react. If robot vision scene reconstruction could be made real-time and accurate for a wide range of distances, then the robot would have time to make good decisions and react accordingly.

This thesis focuses on the design and development of a 3D, real-time, mid-range scene reconstruction system. Contributions include the design of a 3D scene reconstruction system based on two position sensitive devices (PSDs) in a stereo vision configuration and using field programmable gate arrays (FPGAs) to perform computations, and characterization and testing of the linear position sensor module (LPSM) from Noah Corp as a vision sensor.

1.1 Motivation

One popular method of 3D scene reconstruction is to use an active vision system which interacts with the scene. A beam is emitted from the vision system. The beam hits an object in the scene and bounces back to the system. The amount of time that it takes for the beam to return is recorded and used to calculate the depth of the object. Since the beam travels at the speed of light, or 3.0×10^8 m/s, scenes that lie too close to the system are unable to accurately measure the time of flight of the beam. Therefore, active systems tend to be more accurate for long-range scenes.

Another active system, laser triangulation, places a laser and a camera near each other, both facing a scene. The laser highlights a point in the scene and the camera captures the picture. Geometry allows the depth of the point to be calculated. Laser triangulation is usually used for mid- to close-range systems.

Passive stereo systems are also popular for close-range scenes. These vision systems attempt to model human vision. Two cameras are placed in the same configuration as the

Table 1.1. Comparison of vision systems.

Company	Product	Range (meters)	Technology
3D Digital Corp. [2005]	Optix 400L	0.3 – 0.9	Triangulation
Minolta [2005]	Vivid 9i	0.6 – 2.5	Triangulation
Callidus Precisions Systems [2005]	Callidus CP 3200	40 – 80	Time of Flight
Leica Geosystems [2005]	HDS3000	Up to 50m	Time of Flight
PTGrey [2005]	Bumblebee	1.2	Stereo
Videre Design [2005]	STH-MDCS/-c Stereo Head	0.8 to 2.4	Stereo

camera and laser in laser triangulation. Both cameras take a picture of the scene. Equations determine which point in one picture corresponds to the same point in the other picture. Geometry then calculates the depth of the point. Since passive stereo systems face the problem of figuring out which points in each picture correspond to each other, stereo is more accurate for close-range scenes. If the scene becomes too large, then the correspondence problem increases and the time to determine a pair of points dramatically increases. Table 1.1 compares various vision systems currently available.

Each vision system has a recommended range of use. The majority of time of flight systems are usually recommended for use when a scene is greater than five meters away from the system. Laser triangulation systems tend to be recommended for use when scenes are within one meter of the system. Larger scenes become cumbersome for the laser triangulation system because the laser must travel to each point in the scene. Stereo vision systems also tend to be used for close-range scenes within one meter, but can be used for larger scenes. The correspondence problem limits stereo vision's ability to resolve larger scenes. Figure 1.1 shows how these visions systems fit together on a distance scale.

As can be seen from Figure, a gap exists for systems that can reconstruct mid-range scenes, or scenes ranging from one meter to five meters away. A good mid-range system could be used in such applications as indoor navigation. For example, a mid-range real-time vision system could be placed on a cart at a nursing station. The machine could then successfully navigate a hallway full of patients, carts, and other items, to carry supplies to a patient's room.

A mid-range system could also be used for reverse engineering applications for such groups as Automotive Research Center (ARC) or the Department of Energy (DoE). For example, automotive parts or other items could be placed in front of the system and modeled without probing or hurting the original item. With good resolution, complex parts such as propellers would have less error and the angles and curves of the item would be more exact.

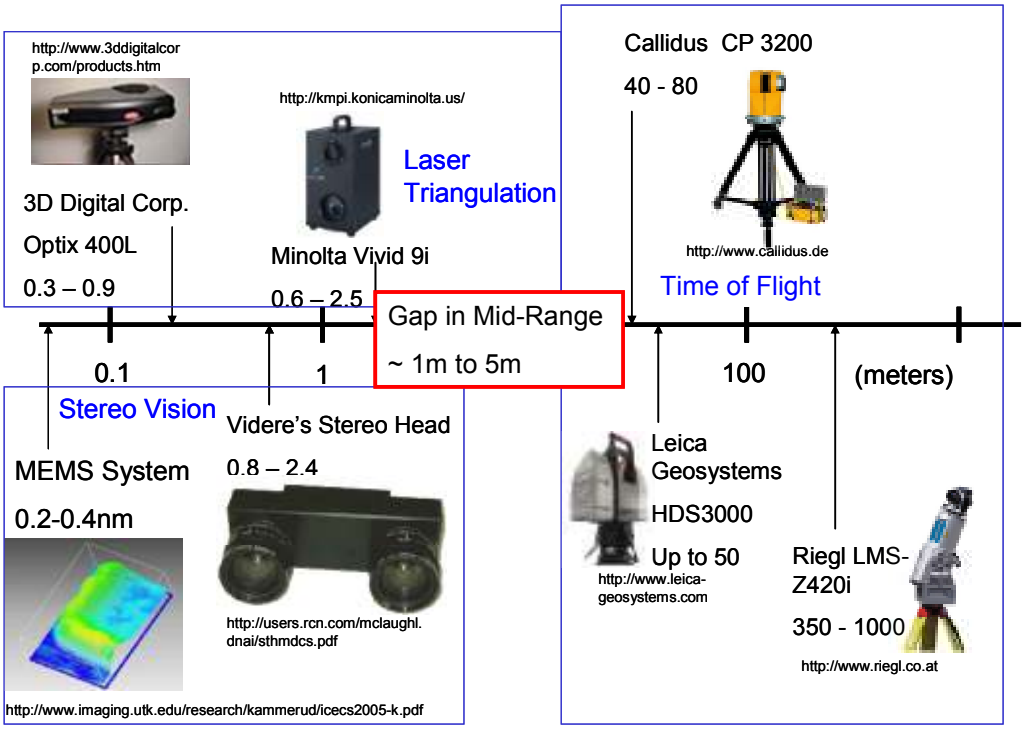

Figure 1.1: Different active and passive visions systems are used for different distance ranges.

Therefore, an accurate, real-time system needs to be developed for mid-range scenes. Advantages from laser triangulation and stereo vision can be used to create a hybrid vision system. Two cameras can be placed in a stereo vision configuration, facing a scene. A laser can be placed between the cameras, also facing the scene. When the laser is in the field of view of both cameras, then a single point is highlighted, eliminating the correspondence problem, thereby greatly reducing computation time. However, the laser also provides only one point of information instead of giving information for the entire picture. The laser must scan the entire scene while the cameras constantly pick up the x and y position of the beam until enough data is collected to reconstruct the scene. Therefore, special cameras with a low response time must be used.

Many active and passive systems tend to use charge coupled devices (CCDs) to collect data. CCDs are digital, dividing the picture into pixels. Digital devices result in a loss of accuracy in resolution due to pixel size, and loss of accuracy in each pixel due to bit storage size. The resolution of the acquired picture is directly related to the size of a pixel in the camera. Smaller pixels result in higher resolution, but require more memory to store the information. Each pixel holds digital data, usually stored in 8, 10, 12, or 16 bits. More bits translate to higher accuracy in the true color of each pixel, but again require more memory to store the value.

Two PSDs can replace the cameras of a passive stereo vision system. When enough incident light hits the active area of a PSD, current is generated. According to the characteristic equation of a PSD, the position of the light spot can be calculated from the current. PSDs have very low response times, usually between 0.8 μs and 10 μs. The output current is analog, giving more data at a faster rate than conventional CCDs.

After collecting data at a fast rate, the data sets must be plugged into stereo equations and the world coordinates of each point must be calculated. In traditional vision systems, software computes the equations. In the proposed system, FPGAs could perform the computations. Since FPGAs can do several operations in parallel, they should decrease computation time. However, since FPGAs are digital, the information will face the same accuracy problem that is faced by digital cameras. The number of bits used to store information will determine the accuracy of the output, with a higher number of bits meaning higher accuracy, but requiring more computation time and memory.

1.2 Problem Definition and Applications

It may be possible to combine the advantages of active triangulation systems and passive stereo vision along with new technologies to create a real-time, mid-range 3D scene reconstruction system. Two PSDs can replace the cameras in a stereo vision system configuration. A laser can be directed toward the scene to highlight a point, eliminating correspondence.

Since only one point can be highlighted at a time, data for the points in a scene must be collected at a high rate. Calculations on the data to give the depth must also be computed quickly. FPGAs can be used for computations by taking advantage of the parallelism that hardware can offer. The output can be sent to a computer via USB 2.0 or other high-rate technology to be displayed on a computer. Figure 1.2 gives a logical and physical block diagram of the proposed system.

Applications of the system would be determined by the performance boundaries. If the scene refresh rate is fast enough, then the system could be used for robot navigation. For example, the system could be placed on a robot that must go from a nursing station to a patient's room, navigating a hallway.

If the resolution is high enough, then the system can be used in reverse engineering applications. An object could be placed in the field of view and the system would give a 3D reconstruction of the object in CAD. Current reverse engineering systems, such as a coordinate measuring machine, require previous knowledge of the object, active interaction with the object, and a skilled operator. With this system, the object could be modeled without prior knowledge and without causing harm to the object.

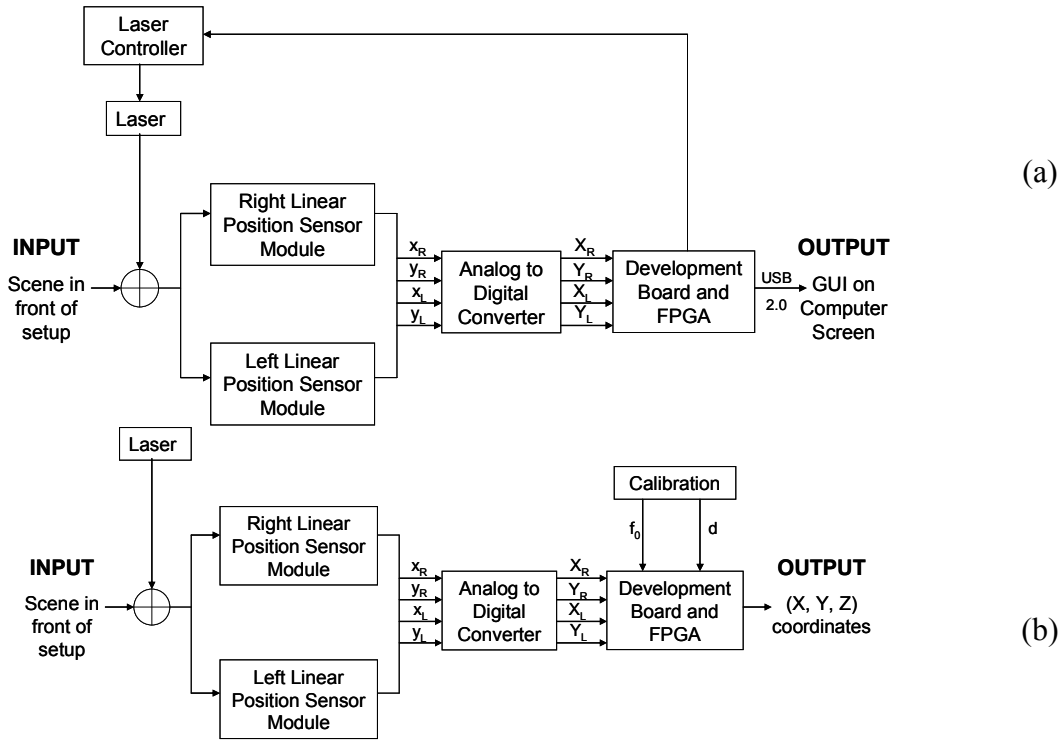

Figure 1.2: The proposed system can be viewed as (a) a physical block diagram and (b) as a logical block diagram.

1.3 Contributions

Contributions include:

- design and development of a 3D scene reconstruction system based on PSDs placed in a stereo vision configuration and FPGAs, and
- characterization and testing of the LPSM as a vision sensor in the proposed system.

A 3D scene reconstruction system is designed and developed to try to achieve real-time frame rates of scenes at mid-range distances. Two PSDs sit in a stereo vision configuration. As a laser scans the scene, the PSDs output the position of the laser point, giving two points to be applied to stereo vision equations. PSDs have already been used in active vision systems, but have not been applied to stereo vision systems since they require a light spot to be present in the field of view.

The LPSM is based on a PSD. Using the LPSM may reduce some of the problems faced by a stand-alone PSD because it already mounts the PSD in a case, amplifies the current

outputs, reduces noise in the output currents, and computes the position of the light spot. The LPSM is usually used in situations where a laser is shined directly into the LPSM, or is shined off of very reflective surfaces into the LPSM. In this thesis, the LPSM will be used in situations where a laser is shined off of diffuse surfaces at a variety of distances. Characterization and testing of the LPSM in these new conditions is analyzed.

1.4 Organization

In this paper, the proposed system is studied and the data acquisition system implemented. A literature review of current systems that use similar concepts and hardware is surveyed (Chapter 2). The theory behind active and passive systems is then studied, as well as background on the hardware and how it works (Chapter 3). The system choices are then implemented, tested, and analyzed (Chapter 4). The paper concludes with an analysis of the experiments and gives ideas for improvements (Chapter 5).

2 SURVEY OF 3D SCENE RECONSTRUCTION SYSTEMS

In this chapter, different approaches to 3D robot vision are surveyed. Some background information (Section 2.1) is provided before surveying current systems. Active robot vision systems using laser triangulation (Section 2.2) are explored. Specific types of laser triangulation, including systems that use point lasers and line lasers are studied. Passive stereo vision systems (Section 2.3) are also explored as an alternative solution to active vision systems. After the broad overview of active and passive systems, systems that use PSD devices are surveyed (Section 2.4). The interest in PSDs is due to their ability to potentially offer higher capture rates. Additional attempts at reducing computation time in vision systems with hardware is also explored (Section 2.5). Hardware can take the form of a CMOS solution or an FPGA solution. The survey concludes with a proposal for a new, real-time, accurate 3D scene reconstruction system (Section 2.6). Figure 2.1 shows a block diagram of the organization of the survey.

2.1 Background

Using laser triangulation, a laser and a PSD are pointed at a scene. The laser hits a point in the scene and a triangle can be drawn connecting the laser, the PSD, and the point in the scene. Given the distance between the laser and PSD and the angle that the laser is pointing, the depth of the point can be determined by:

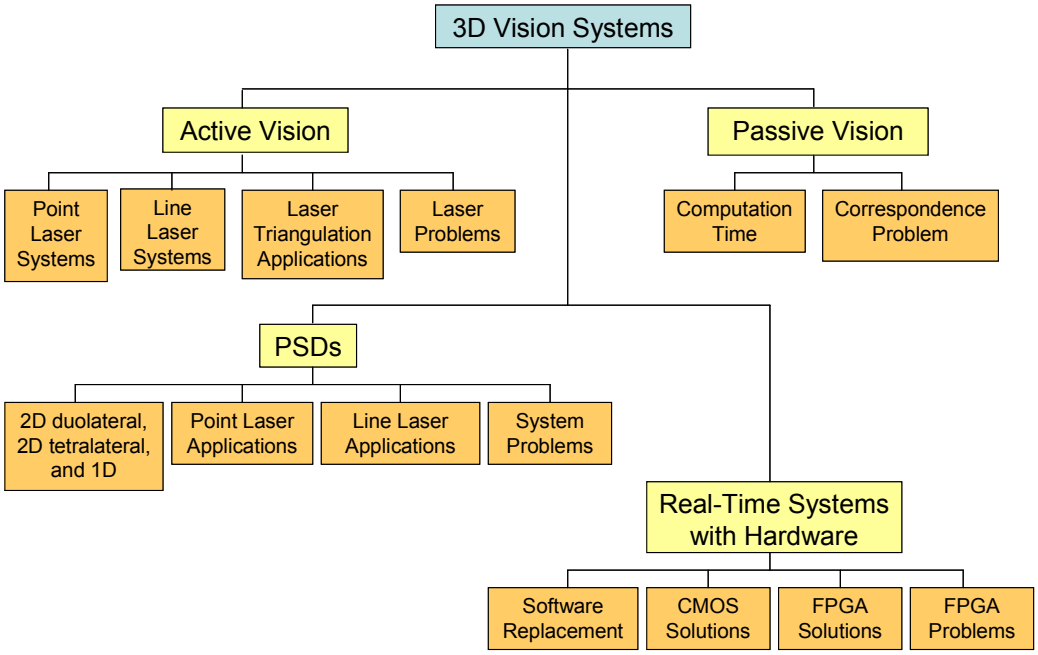

Figure 2.1: Chapter 2 surveys current 3D vision systems.

$$Z = \frac{f_0 * d}{x + f_0 * \tan(\theta)}, \tag{1}$$

where Z is the depth, f_0 is the focal length, d is the baseline, θ is the laser angle, and x is the position from the PSD.

In stereo vision, two PSDs face a scene. If the same point can be found in the picture by the left PSD and the picture by the right PSD, then two sets of coordinates, x_R, y_R, and x_L, y_L, can be found. A triangle can be drawn from the two PSDs to the point in the scene. Knowing the two coordinate points, the distance between the two PSDs, and the focal length of the PSDs, the point coordinates can be determined by:

$$Z = f_0 \frac{d}{x_L - x_R}, \tag{2}$$

$$X = \frac{Z}{f_0} x_L - \frac{d}{2}, \text{ and} \tag{3}$$

$$Y = \frac{Z}{f_0} y_L. \tag{4}$$

where X, Y, and Z are the coordinates, f_0 is the focal length, d is the baseline, and x_L, x_R, and y_L are the positions from the PSDs.

PSDs are devices made up of an n-layer and a resistive p-layer. When light hits the active area of a PSD, the photovoltaic effect causes a current to be created in the p-layer, which travels to electrodes. The current from the electrodes is input into a characteristic equation, giving an x and y position of the incident light.

Once a data set comprising the x and y positions of a point from the left and right PSDs, the baseline, and the focal lengths, is found, then the stereo equations can be used to calculate the coordinates of the point in 3D space. An FPGA can be used to implement the equations in hardware. An FPGA is a chip made up of an array of logic blocks. Different FPGAs have different configurations of logic in their unique logic blocks. Between the blocks run a grid of wires. The desired function can be coded in a hardware description language, and then programmed on an FPGA by connecting specific wires together and enabling certain parts of logic blocks.

2.2 Laser Triangulation

Active vision systems interact with a scene. In a point laser triangulation system, the laser sends a single beam to the scene. The point can be controlled either by tilting a mirror or by aiming the laser directly at the desired location. While the point sits at one

spot of the scene, the rest of the system calculates the coordinates of the spot. The point is then moved a very small distance, and the system calculates the coordinates of the new position. Once the laser has been moved over the entire scene and the point coordinates have been calculated, a 3D picture of the scene can be formed.

Beraldin [2000] uses laser triangulation for many applications. Artifacts and exhibits in museums, such as paintings or sculptures, can be scanned to create a 3D digital model, helping with documentation and research. He has also worked to develop portable systems for easier scanning and modeling of remote sites. These sites also add extra issues such as unknown terrain and sunlight. Laser triangulation has also been used to help scan scenes that are used in virtual reality simulators.

Point laser systems have the slowest data acquisition speeds of laser triangulation systems. The point laser must scan over each point in the scene before the entire scene can be reconstructed. The point must also stay at a specific spot for a period of time long enough for the camera to gather data before going on to the next point. Therefore, to reduce scene reconstruction time, a system can use a line laser instead of a point laser. [IVP Ranger, 2000]

Oike, *et al.* [2003] attempt to use a line laser along with a fabricated CMOS chip to achieve real-time 3D data acquisition rates. They also use a specialized image sensor comprised of one photodiode and three transistors to increase data acquisition speed. The data feeds into the CMOS image processing chip to recreate the image.

Konodo [2004b] uses the laser line method in his experiments with undersea vehicles. A navigation system which utilizes sheet laser beam light-sectioning allows the robot to find the general shape of an object. Only the shape of the object and the distance away need to be found to allow the robot to correctly navigate its surroundings. Konodo also uses [2004a] a sheet laser beam in his experiment with relative navigation. He determines which areas along the laser line are necessary for the robot to successfully navigate a scene. The areas usually have objects in the way of the robot's path. He then only calculates the depths in this region of interest instead of for the entire scene. This method helps the robot to save time in its calculations and in its decisions for navigation.

Besides point and line lasers, patterns can also be created on a given scene. Machines tend to use pattern lighting in conjunction with passive stereo vision. The major problem of stereo vision is correspondence, or matching a given point in one picture to the correct point in another picture. By using a pattern on a scene, the user can use the lines and edges created by the pattern lighting to solve the correspondence problem. Kim, *et al.* [2004] utilize structured lighting on an autonomous robot for easier extraction of specific features from a scene.

When using laser triangulation, certain problems arise due to the equipment. Lasers usually encounter three main problems: non-diffusing surfaces, shiny objects, and occlusion.

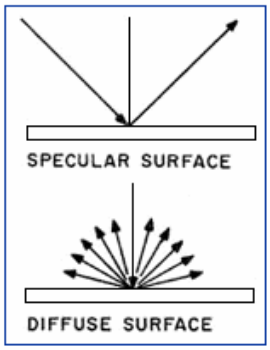

Figure 2.2: Laser beams reflect at one angle when striking specular surfaces and reflect uniformly in all directions when striking diffuse surfaces [Kennedy, 1998].

Two types of surfaces exist in a scene. Specular surfaces completely reflect a laser beam at the incident angle, according to Snell's Law. A specular surface could be a mirror, window, or lake. Diffuse surfaces usually cause a Gaussian distribution of a laser beam, as seen in Figure 2.2, with the peak occurring at the incident angle governed by Snell's Law. Different cameras look for different measures of reflectivity. Therefore, a diffuse sensor picks up a signal from a diffuse surface better than from a specular surface. Usually, surfaces display both specular and diffuse properties, although one is more dominant than the other.

Chen, *et al.* [1998] attempt to find a method to avoid spurious reflections. They explain that traditional algorithms assume that the light intensity around the center of a laser approaches zero. However, since surfaces are not ideal, the light intensity around the center is not zero, causing the calculated center to be shifted. Chen, *et al.* scan the scene once to find general shapes and then delete points that do not lie on the objects. They also use a look up table for comparison of shapes in the scene to known objects.

Another problem occurs when shiny objects lie in the scene. Lasers give off light at a specific frequency. Usually, lasers are at a much higher frequency than background light in a scene. Filters are used to pass through only the laser light to the camera and to better focus the laser beam on the device. Removing extra light reduces noise, improving accuracy. Some shiny objects reflect almost all light, causing them to appear white. This white light tends to have a much higher frequency than the rest of the background light in a scene, therefore appearing like another laser. PSDs have more trouble than CCDs when multiple lasers are present. If multiple light spots are present, then the PSD takes an average of the light spots. Therefore, if some white light is present along with the laser, the output of the PSD will be a point between the two objects.

Finally, the problem of occlusion is prevalent with lasers [IVP Ranger, 2000]. A laser beam originates from a point and cuts through air until it strikes an object. If an object

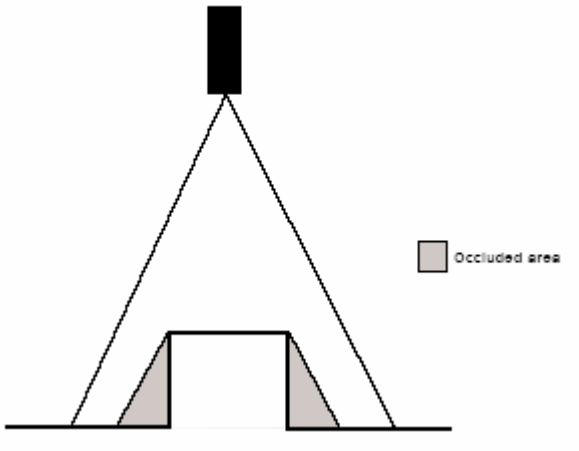

Figure 2.3: Occlusion causes part of the scene to be hidden from the laser [IVP Ranger, 2000].

protrudes too far from surrounding objects in the scene, then it can obstruct the laser. If this happens, then the laser cannot hit a point on the scene because it is hidden, as shown in the Figure 2.3. The occlusion problem can be solved by using multiple lasers or by using multiple sensors. An array of PSDs solves the problem from the sensor point of view, but increases cost and system complexity. A PSD array also causes the system to have a fixed resolution.

Chen, *et al.* [1999] attempted to reduce the occlusion problem. They decided that occlusion was based on the shape of the object and created an algorithm to find the best position of the camera compared to the position of the scene. The algorithm looks at an average of the contour of the object, checking convex and concave areas. Chen, *et al.* conclude that there will be some occlusion due to the nature of triangulation, but the low-occlusion method helps to reduce the problem as much as possible.

2.3 Stereo Vision

Laser triangulation is very good for close-range distances. Time of flight active systems are very good for determining 3D coordinates if the scene is long range. For mid-range scenes, stereo vision is the most common scene reconstruction system. Stereo vision is a mature subject that can be studied in textbooks [Faugeras, 1993; Hartley, 2000; Klette, 1998].

Progress has been made on bringing down the computation time of stereo vision systems by attempting to do preprocessing on the data [Silva, 2003]. Ferrari [1990] attempted an

algorithm where he runs through a scene twice – the first time building a coarse view of the scene, and then a second time to add detail to specific flagged areas of the scene.

Besides fighting with computation time, stereo vision also presents the problem of correspondence. Once the two pictures are found from the two cameras, it is difficult to determine which point from the first picture is the same point in the second picture. More computation must be done during calibration to determine extrinsic and intrinsic parameters, which must then be applied to the picture for every point to determine the corresponding point in the second picture. This algorithm elongates the computation time.

2.4 PSD Systems

Vision systems contain a camera, such as a CCD or a PSD, to determine the position of a light spot. CCDs are digital machines, divided into pixels, and therefore are only able to resolve an image to an accuracy level the same as the pixel size or pixel density. Unlike CCDs, PSDs are analog devices and are able to acquire data quicker. Since PSDs are analog, all of the data in a scene is in tact, allowing the accuracy of the equations to determine the accuracy of the system. PSDs have become popular, replacing the camera in many laser triangulation systems.

Three types of PSDs exist: one-dimensional, two-dimensional duolateral, and two-dimensional tetralateral. The type of system needed determines the type of PSD used. Each PSD calculates the position slightly differently due to their unique architectures [Hamamatsu, 2003].

Point lasers are the slowest system that uses PSDs, because the laser point must trace through the entire system. The laser points at one spot and the data for that spot is taken. The laser moves a very small amount to the next spot, and the system must take the data again. This process iterates through the entire scene.

Though the process for a point laser system is slow, people still use the system depending on the needs of the application. Beraldin, *et al.* [2003] create a system using a point laser to create a color image. An RGB laser reflects off of an object onto a diffracting optical element, splitting the laser into four separate beams: white, red, green, and blue. The white beam hits a discrete response position sensor, and the other three beams hit three separate continuous response position sensors. The data gathered from these four PSDs are fed into a chip which can calculate the color based on the proportions of the intensities of the colors.

Beraldin, *et al.* [2000] also found applications for point laser PSD systems by taking 3D images of artifacts and artwork, creating portable systems for rugged areas for 3D data acquisition, and helping to create virtual reality pictures. He takes pictures of artifacts for digital records and research, so the 3D model needs to be of archival quality, having very

high accuracy. Rugged systems need to be set up quickly, moved around easily, and must also deal with ambient light since they are usually used outdoors. Virtual reality systems need to have more flexibility in the objects they are able to depict, since they might have to represent objects with a wide range of sizes, colors, transparencies, and dimensions.

PSDs can only accurately measure the position of light when one spot is in the active area. If multiple spots of light hit the active area of the PSD, then the position will actually be an average of the intensity of the two spots.

Research has been done to attempt to make systems that offer higher accuracy. Marques *et al.* [1998] attempt to create a system using three lasers and a 2D tetralateral PSD. The lasers are parallel to one another in a triangular configuration. Since PSDs can only accurately measure one spot of light at a time, Marques *et al.* turn the lasers on sequentially, only taking data for one laser at a time. Once the system has gone through one iteration, data for three points around a given pixel is known. Vectors can be drawn between the points and the cross product is used to determine the incremental change in the position, giving a higher accuracy reading of the pixel.

Marques *et al.* [1994] also attempt to use three lasers in a similar configuration for another project. They attach a pre-processing unit to the system to do signal processing, reducing noise and computation time. The lasers switch on and off so that only one laser is on at any given time. The data acquired from the PSDs runs through a DC circuit, giving a discrete position. In this system, Marques *et al.* basically attempt to create a simple system for acquiring 3D images at a medium speed with average accuracy.

Funabiki and Tanaka [2002] use a single laser and two PSDs in their system. The laser-PSD system mounts onto a mobile robot which attempts to follow moving objects. A laser shines on an object, and both PSDs calculate the position of the object. Since both PSDs give a position, the angle from the PSD to the object can be calculated. If the object is not centered in the field of view, then the robot moves to center the object, and the process repeats. The measurable region of the PSD limits the field of view, so the object must stay within a narrow range for the configuration to work properly.

If only one 1D or 2D PSD is used in a system, then only a point laser can be used. However, this process can be slow since the point laser must be moved over the spots in the scene. To decrease data acquisition time, the point laser is often replaced by a line laser. PSDs can only pick up one light spot at a time. Therefore, if a line laser is used, then multiple PSDs must be used, creating an array. Only 1D PSDs can be used to create the array, with its respective equations used to calculate positions. The number of PSDs in the array dictates the number of "pixels" in the line laser. Therefore, more PSDs in the array correspond to higher resolution.

Araki, *et al.* [1992] attempt to use a line laser to speed up data acquisition, making a high speed, 3D scene reconstruction system. An array of PSDs is arranged in a vertical line.

The laser, also aligned vertically, sweeps from left to right across the scene. A rotating mirror controls the position of the laser beam. The analog current from the PSDs feed into analog-to-digital converters so that the information can be stored in memory.

De Bakker, *et al.* [1996] also use a line laser in their system. They attempt to improve speed by integrating the PSD onto the same piece of silicon that does signal processing, amplification, and demultiplexing. The system contains a digital part which outputs data for a 12-bit resolution picture. The PSD chip actually contains an array of 128 PSDs, but allows for concatenation of more devices, if needed.

Mizuno *et al.* [1994] utilize a line laser much like de Bakker's system. The laser and PSD array are arranged vertically, with the laser being directed by a rotating mirror. Mizuno *et al.* try to decrease image reconstruction time by using an analog chip to compute positions. The system has two CMOS chips per PSD, attempting to speed up the computation time. Four stages take place: "rough extraction for the background illumination," "first integration by charge amplifier without LED illumination," "second integration with LED illumination," and "selecting one array with the shift register." After the fourth stage, a signal from the PSD is selected and used as the final position.

Lasers introduce some error into a triangulation system in the form of occlusion and surface refracting problems, but PSDs can also introduce error into the system. One problem occurs when multiple light spots appear in the active area, causing the resulting position to be an average of the spots. PSDs also introduce noise and accuracy problems. Since people want to take pictures of different scenes, portability has also become an issue to overcome.

Beraldin, *et al*. [1999] attempt to create a portable, outdoor system for 3D image acquisition. Since the outdoors contain the sun, lakes, and other shiny, light-filled objects, PSDs can have trouble filtering out background light. Portable systems also have to be very rugged because their environment is unpredictable. Therefore, Beraldin, *et al.* decide to use a Biris camera comprised of a laser line, lens, and CCD camera. The camera is more rugged than a PSD and can filter out the background light using a developed algorithm. However, CCD cameras limit the accuracy of the final image and have slower computation times.

PSDs introduce speckle noise into the system. Gonzo [2003] tries to optimize PSDs to reduce speckle noise by creating a system that combines continuous and discrete reponse PSDs. Discrete response PSDs have better accuracy than continuous PSDs, but have a higher measurement uncertainty and have longer computation times. Continuous PSDs are faster and give a better value for the central location of the light spot. After the continuous PSDs pinpoint the center of the light spot, the point is sent to a discrete PSD chip, selecting a small, specific area of the discrete PSD dataset to calculate, reducing the amount of computation time necessary while providing the most accurate response possible.

Gonzo attempted a similar setup [2001] for further reduction of speckle noise. An RGB laser illuminates a point spot. The lens breaks up the laser beam into four beams: white, red, blue, and green. A discrete PSD picks up the white beam, while three separate, continuous PSDs are hit by the other three beams. He again uses the best of both worlds approach by combining the best features of both types of PSDs to calculate the smallest pixel size with the least speckle noise and fastest computation time.

Fujita and Idesawa [1999] attempt to fix the accuracy problem by changing the PSD architecture. They create a comb-structure PSD, which improves the uniformity of the resistive p-layer, by fabricating the photosensitive area separately from the rest of the photodiode. Since background light affects the apparent intensity of the light spot, they also create a circuit that subtracts the background light from the system before calculating the light spot.

Wang and Busch-Vishniac [1989] also attempt to improve the PSD itself to fix accuracy and sensitivity. They develop a "clover" shaped PSD, trying to get better linearity, resolution, and sensitivity than the tetraleteral and duolateral designs. The clover design contains eight point contacts and four short contacts at the corners of the active area, canceling noise and crosstalk between currents.

In an effort to continue to improve sensitivity and accuracy, people have experimented with using digital signal processing with analog position sensitive detectors or making the PSD itself digital. Makynen, *et al.* [2004] attempt to make a digital PSD. The system outputs a low-resolution binary image. Preprocessing hardware helps to reduce the computation time. The circuitry is also shielded from direct illumination in an effort to reduce computation time. Makynen, *et al.* separate the PSD itself into an array of 16 by 16 pixels to improve sensitivity. Makynen, *et al.* [1998] also attempt to make PSDs better by increasing the resisitivity of the p-layer. They demonstrate that the "best resolution is achieved by using the highest resistance that ensures the sensor bandwidth to be larger than signal bandwidth."

Simoni, *et al.* [2002] use both continuous and discrete PSDs to improve sensitivity and accuracy in his laser triangulation system. Two arrays of PSDs are in the system, one comprised of discrete response PSDs and one comprised of continuous PSDs. The continuous PSDs locate the light spot and tell the discrete response PSDs on which area to focus resolution. Therefore, the amount of computation needed by the discrete response array is decreased.

2.5 FPGA Systems

In a point laser triangulation system with PSDs, position data is acquired for each point. The system also contains constant characteristics such as the baseline and the focal length. Depending on the type of PSD used, two or four currents may be present. The laser controller supplies the angle that the laser points. As seen from the previous

sections, this data set must now be applied to equations to find the coordinates of the current point. If a stereo vision setup is used, then even more complex equations must be computed to find the coordinates of points in the scene. If a computer is placed in the system, the data can be fed into software programs to calculate the point. Another option is to use hardware to calculate the point, using either application specific integrated circuits (ASIC) chips or FPGAs.

Reves, *et al.* [2001] attempt to improve their software radio by integrating FPGAs. Reves, *et al.* use FPGAs separated into the functions of transmitter base station, receiver base station, mobile transmitter, and mobile receiver. The circuitry in each block is very complex. Therefore, to save space, the FPGAs are reconfigured while in use. Using FPGAs to do computations saves time; however, it requires a lot of space. The ability to reconfigure the FPGA in real-time allows the space to be reused. This process adds computation time back into the system, but not enough to greatly affect performance.

Software was also replaced by FPGAs in a machine by Donninger, *et al.* [2004] that plays chess. Donninger, *et al.* implement the search algorithm from previous software-based chess-playing computers on an FPGA to take advantage of the parallelism available in hardware. This greatly reduces the search time for the next move. Information gathered by the machine during games can be added into the system, but requires more space on the FPGA.

Since its invention in the 1980s, many chips are based on complimentary metal oxide semiconductor (CMOS) technology. In CMOS, a chip is fabricated based on NMOS transistor logic. The compliment of the NMOS transistor configuration is created and implemented using PMOS transistors. By attaching the output of these two configurations, a system is created which gives strong zero and strong one signals according to the logic equation it implements.

Viarani, *et al.* [2004] attempt to change the PSD pixel itself using CMOS technology. CMOS allows readout and processing electronics to be fabricated on the same die. Viarani, *et al.* found that this integration reduces system cost. However, the laser in the system needs to have higher power due to the change in the gain of the CMOS photodetector. Viarani, *et al.* also found that the CMOS pixel has less noise.

Nisi, *et al.* [2003] also integrate CMOS technology into his triangulation system. Two arrays of photodetectors are used, one of continuous PSDs, and the second of discrete PSDs. Each array collects information at the same time. A CMOS chip processes all of the signal information in parallel to find both spot intensity estimation and spot position detection. The CMOS chip also allows color detection in the scene.

Oike, *et al.* [2002] utilize CMOS 3-Metal 1-Poly-Si technology to fabricate a PSD comprised of a 64 by 64 matrix of photodetectors to solve the problem of background illumination. Each pixel contains 24 transistors and is controlled by signals that run the

length of the pixel array. During test, the pixels were able to suppress extra noise from even harmonics, but were unable to fully suppress noise from odd harmonics.

Oike, *et al.* used a similar design when attempting to make real-time VGA quality 3D images [2004b]. The photodiodes made up a 640 by 480 pixel array fabricated using 0.6 μm CMOS technology. A laser line was used for triangulation instead of a point line to acquire data faster. The system achieved 65.1 range maps per second and 0.87 mm resolution at 1200 mm.

In trying to again increase frame rate, Oike, *et al.* [2004a] used a chip that contained "a pixel array, bit-streamed column address generators, row-parallel processors with 18b registers and output buffers, and an on-chip controller with a PLL." The chip was fabricated with 0.18 μm 1-poly 5-metal CMOS technology, where each pixel had 24 FETs. The controller was built on-chip to increase speed. Oike, *et al.* also implemented a search algorithm for the row and column pixels to reduce time.

CMOS circuits tend to be realized in either ASIC chips or FPGAs. In an ASIC chip, the designer must manually place every transistor on the silicon. Therefore, timing, routing, and space are minimized. Many of the above mentioned vision systems used ASIC chips to increase system speed. FPGAs began to gain popularity because they were able to be reprogrammed on the fly in the field and were able to be used for a wide variety of projects. Therefore, one type of chip could be fabricated and be put in a much larger number of systems, reducing cost and time to market. Although FPGAs are not as space-efficient, the density of gates on a chip continued to increase, reducing the difference in space for FPGAs and ASICs. Now, FPGAs tend to be preferred over ASICs due to their lower cost and comparable performance. Routing, timing, and other factors continue to try to be improved on FPGA chips.

Many people have conducted studies to attempt to optimize routing on chips and on systems with multiple FPGAs. Ejnioui and Ranganathan [2000] attempt to find a better algorithm for routing. Many routing systems have evolved into a switch matrix, comprised of horizontal and vertical wires that can be programmed using SRAM. The proposed algorithm creates several vectors with many possible vertexes. The vertexes are mapped to a constraint satisfaction problem and the optimal solution is chosen. The algorithm helps to minimize CPU processing time to find routing.

FPGAs have already been integrated into some 3D vision applications. The chips are especially popular with stereo vision systems due to the large computations necessary in passive systems. Rajda [2001] uses a Xilinx FPGA in his stereo vision system. The algorithm contains four main steps: "compute census values for each pixel in left and right image, compute Hamming distance for each pair of pixels, sum over a larger window to improve statistics," and "find the maximum of the array of similarity measures." Rajda worried about time delay, but only ran into this problem when pipelining was necessary. He also reconfigured the FPGA at real-time to conserve space.

Rose, *et al.* [1999] combine FPGAs and PSDs in his system. The system contains several FPGAs, labeled even and odd. All of the even FPGAs contain a program, and all of the odd FPGAs contain a second program. The system goal is to set flags to know when data is ready and then to read the data. Two modes are available, time of flight and PSD. The PSD mode calculates which events should be digitized and recorded. Although the PSD is not being used for 3D reconstruction, the FPGAs are still used to reduce PSD equation computation time.

Filho, *et al.* [2005] also created a system combining PSDs and FPGAs. The PSD is used in conjunction with a Gas Electron Multiplier. The PSD acquires data at specified times. The FPGA controls the system and tells the PSD at what times to take data. X-ray images can then be acquired with 512 by 512 pixel resolution.

Although FPGAs tend to be faster than software and can process in parallel, they still have some problems. FPGAs are able to implement addition and subtraction. Many FPGAs have built in carry-chains to aid in the speed of addition and subtraction. However, many chips still have trouble implementing multiplication and division. Companies have tried adding multiplier chains to their logic blocks, but the arithmetic still has limited capability. If the multiplication or division necessary is small, then look-up tables are sometimes more efficient than carrying out the arithmetic.

Programming FPGAs also presents a problem because FPGAs are not under strict regulations. Each company provides their own software for their products, putting a slight twist on their own designs. In other words, a Xilinx chip cannot be programmed unless the user also has the software made by Xilinx. Software determines the efficiency of place and route, how close logic blocks are to each other on the chip, and many other important features. The user interface to the software can also be confusing and must be relearned if chips from different companies are used, or if the company decides to switch to newer software.

Benkrid, *et al.* [2000] attempt to improve the software tools used with FPGAs in image processing applications. By looking at the type of arithmetic needed for image processing, Benkrid, *et al.* found ways of improving the mapping of operations to the FPGA. For example, they found that parallel addition is better than serial addition. Therefore, if addition is implemented, it is mapped in a parallel fashion to the FPGA. For division, Benkrid, *et al.* decide between look-up tables or a multiplication combined with a shift operation, depending on the size of the inputs.

2.6 Summary

The focus of this chapter has been current 3D modeling systems. Active systems implementing laser triangulation and passive stereo vision systems were examined. Next, the use of PSDs in 3D modeling systems was studied. Finally, the use of FPGAs to reduce computation time for vision systems was examined.

Laser triangulation and stereo vision systems tend to be used for close-range scenes. The need to scan an entire scene with a laser limits the distance that laser triangulation systems can operate while the correspondence problem limits the distance that stereo vision systems can operate. By placing two PSDs in a stereo vision configuration and using a laser to scan the scene, a mid-range scene reconstruction system may be realized.

The new configuration eliminates the correspondence problem, improving computation time as compared to normal stereo vision. However, a laser still needs to scan the entire seen, like in laser triangulation. Since the PSD is an analog device, it has a faster response time than CCDs, allowing it to gather more points in a shorter amount of time.

Using the LPSM is proposed over the use of a stand-alone PSD. The LPSM is based on a PSD, but comes pre-mounted and also takes care of signal processing and light spot position computation. Therefore, the LPSM may eliminate some problems seen by using a stand-alone PSD.

With the proposed data acquisition system, x and y position data sets from the two PSDs would be gathered at high rates. The data sets would have to be applied to stereo equations to find the coordinates of each point. FPGAs can be used to achieve faster computation rates, possibly allowing for real-time refresh rates. Due to the parallelism in hardware, the equations can be computed faster. Also, multiple points' coordinates can be computed simultaneously. The combination of all of these technologies could help to realize an accurate, real-time 3D reconstruction system.

3 BACKGROUND AND SYSTEM THEORY

The proposed system attempts to achieve two main goals: 1) a hybrid system mixing the advantages from laser triangulation and stereo vision, and 2) real-time operation using FPGAs. Therefore, both laser triangulation systems and stereo vision systems need to be studied to determine the advantages and disadvantages of each system and how their individual properties can be combined to form a new system. Next, the new system will have its own challenges in achieving real-time operation. New hardware technologies need to be studied to overcome these issues.

3.1 Laser Triangulation

Laser triangulation systems are an active vision system that tends to be used for close-range scenes. The main disadvantage of laser triangulation is the time it takes to collect enough points to create one image of the scene. The number of points collected also affects resolution.

3.1.1 System Setup

Certain fundamental elements are needed in a system that acquires data to reconstruct a 3D scene. In a passive stereo system, or a system that does not directly interact with the scene it is capturing, two cameras are used. The two cameras point at a scene and capture two unique images. It is possible to pick a point in the scene and draw a line from that point to one camera, another line from the first camera to the second camera, and a final line from the second camera to the original point, creating a triangle. Since the user is able to control the cameras, the angles between the camera and the point are known and the distance between the two cameras, or the baseline, is known. Therefore, geometry and algebra can be used to determine the distance from the cameras to the point.

In laser triangulation, a laser replaces one of the cameras of stereo vision. The laser interacts with the scene, so the system is now said to be active. However, similar principles to stereo vision are used to calculate the depth of the object.

Many types of cameras are able to be used for laser triangulation. CCDs or PSDs are usually used. PSDs collect information analogously while CCDs are digital. With either device, a lens must be used to focus the scene onto the active area of the device.

Unlike stereo vision, the laser is usually placed above the lens of the camera instead of next to the lens. The camera sits behind the lens, and the middle of the lens lines up with the middle of the camera. The distance from the camera to the lens is referred to as the focal length, or f_0.

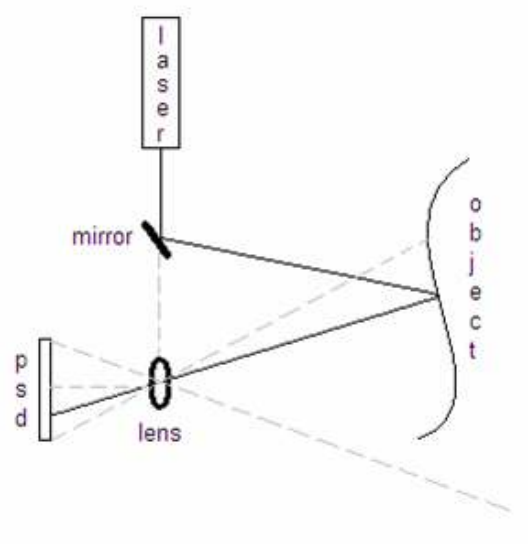

Figure 3.1: A typical laser triangulation setup contains a laser, camera, and lens.

The user controls the laser and moves it around the scene. The laser can be either a point laser, meaning that the beam hits one point of the scene at a time and reflects, or it can be a line, meaning that it illuminates an entire horizontal or vertical line of the scene. Coded patterns can also be used, but are less common. The user controls the laser by either directly moving the laser or by deflecting the laser using a mirror, and moving the mirror to direct the beam. If a mirror is used, then it is placed above the lens of the PSD, and the laser is placed above the mirror, pointing down towards the lens. The angle at which the laser points is called θ. The distance from the lens to the mirror is called the baseline, represented by the variable d. The entire system can be seen in Figure 3.1 [Kennedy, 1998; Dumberger, 2002; Beraldin, 2000].

3.1.2 Laser Triangulation Geometry

Laser triangulation is based on the point laser setup. Equations for a line laser system can be extracted by applying the point laser equations to the system. The equations are based on some previous knowledge of the system and also on the acquired data.

First, the user must set a coordinate system. The X-axis lies along the line running from the laser through the mirror to the lens, as seen in Figure 3.2. The middle of the lens corresponds to X=0. The Z-axis is the depth of the object, so it lies ninety degrees from the X-axis, going from the lens-mirror-laser line to the scene. The lens, mirror, and laser beam lie at Z=0. The Y-axis comes out of the paper, towards the reader. The current point in the scene that the point laser hits is located at *(X, Y, Z)*.

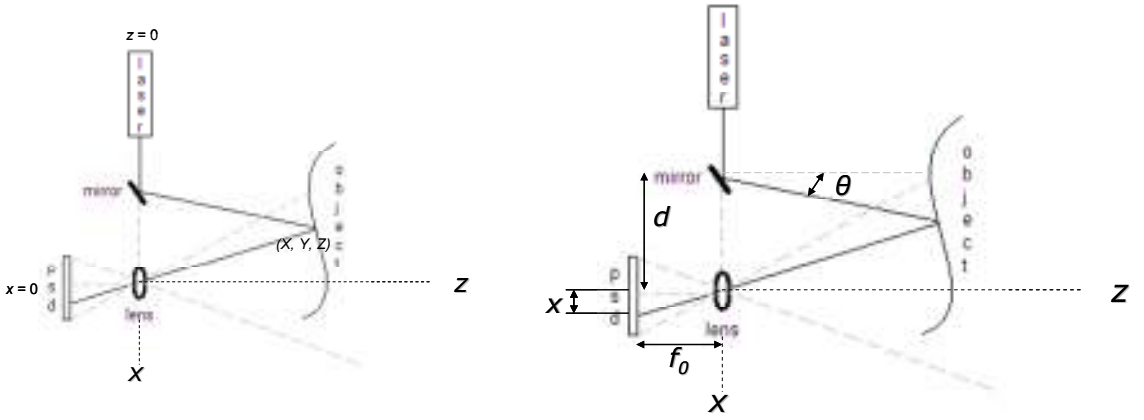

(a) (b)

Figure 3.2: (a) A coordinate system can be placed on the laser triangulation setup and (b) the variables can be superimposed on the system.

To derive the point laser equations, certain variables must be set by some type of calibration or prior knowledge of the system. The focal length, f_0, is the distance from the lens to the PSD. The baseline, d, is the distance from the lens to the mirror. If no mirror is used, then the baseline is the distance from the lens to the laser origin. The user finds these variables by either calibrating the system or by estimation.

All other variables are either controlled by the user or acquired by the system. θ is the angle, in radians, from the Z-axis to the laser beam and is controlled by the user. The distance from the middle of the PSD to the point where the light hits the device is called x. Specific equations calculate x according to the type of PSD.

Once the necessary variables are known, two equations can be found from the setup. The first equation is based on the principle of similar triangles. The first triangle connects the object to the point on the PSD where the beam hits. The other two lines of the triangle run parallel to the X- and Z- axis, forming a right angle. The second triangle lies inside the first triangle. The extra line of the smaller triangle runs from the middle of the lens to the middle of the PSD, parallel to the Z-axis, as shown in the Figure 3.3.

The length from the lens to the PSD, f_0, is known from calibration. The distance from the middle of the PSD to the light spot is x. Due to the orientation of the coordinate system, the corresponding edges of the large triangle are known as Z and X, or the coordinates of the point in the scene. The principle of similar triangles can then be used to create the ratio:

$$\frac{x}{f_0} = \frac{X}{Z}. \qquad (5)$$

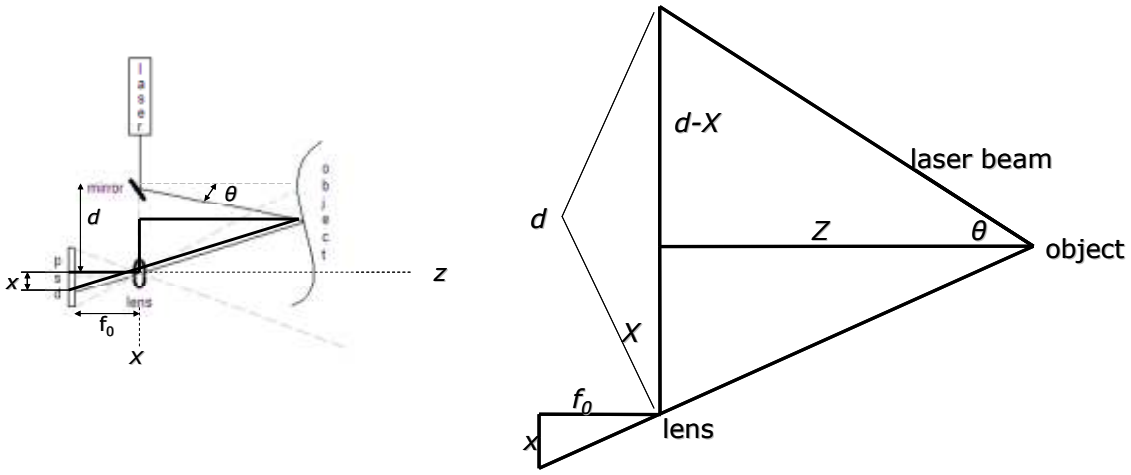

(a) (b)

Figure 3.3: (a) Similar triangles can be superimposed on the system setup and (b) used to create a ratio.

The other initial equation comes from the triangle formed by the laser beam. By connecting the current point on the object to the laser, and drawing lines parallel to the *X*-axis and *Z*-axis, another right triangle is found. The angle from the *Z*-axis to the laser beam is already known as θ. From calibration, the distance from the laser to the PSD is known as *d* and the distance where the object sits along the *X*-axis is known as *X*. Therefore, the distance along the *X*-axis in this triangle can be called (*d*-*X*). Now, the tangent of the triangle gives:

$$\tan(\theta) = \frac{(d - X)}{Z}. \tag{6}$$

3.1.3 Laser Triangulation Equation Derivation

Beraldin [2000] shows the derivation of the depth equation from initial equations () and (). Algebraic manipulation results in the depth equation in the final form of:

$$Z = \frac{f_0 d}{x + f_0 \tan(\theta)}. \tag{7}$$

With a point laser system, the *Y* coordinate equals the point where the lens and laser are placed along the *Y*-axis. The PSD is assumed to have a very narrow field of view in the y direction, only picking up a light point along the *X*-*Z* plane where the system sits. To collect data for the entire scene, the system is moved along the y axis, taking data for points along the current plane before being moved again.

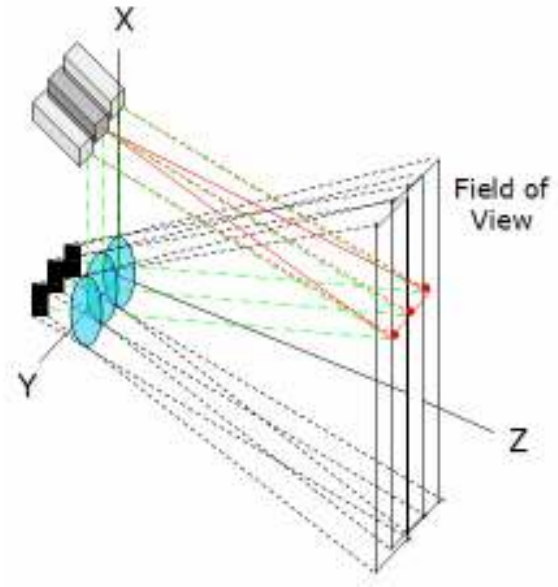

Figure 3.4: An array of PSDs can be used with a line laser.

3.1.4 Line Laser Triangulation

The depth equation for line laser triangulation is the same as the depth equation for point laser triangulation. A line can be viewed as a set of points lying next to each other. The user can decide how many points should make up the line. Smaller point size results in higher resolution, but requires more computation. Each point needs its own PSD instead of using a single device, as shown in Figure 3.4. The system can then be viewed as a series of triangles. Therefore, the same geometry rules apply, yielding the same depth equation. Each point gives its own unique depth due to each device's unique baseline and the distance where the light spot hits each device.

3.2 Stereo Vision

Stereo vision provides a passive solution to modeling a 3D scene. The main disadvantage of stereo vision is known as the correspondence problem, discussed later. The correspondence problem adds a lot of computation time, affecting resolution and frame rate.

3.2.1 System Setup

A stereo vision system requires at least two pictures of the same scene, usually from two different cameras. Unlike laser triangulation, no interaction with the scene takes place. The coordinates of each point in the scene are calculated from geometry, much like laser triangulation. [Klette, 1998; Faugeras, 1993; Hartley, 2000; Chapter 9, 2005; Geiger, 2005; Stereo Vision, 2005; Stereopsis, 2005]

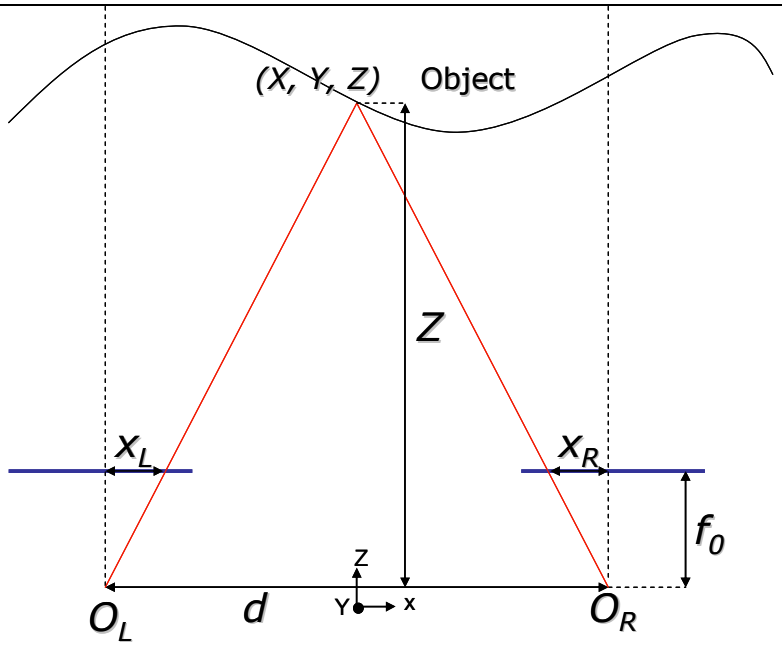

Figure 3.5: A typical stereo vision setup has two PSDs facing the scene.

3.2.2 Base Case Coordinate Derivation

For the stereo vision base case, two PSDs lie along the same plane, facing a scene, as shown in Figure 3.5. The distance between the lens and the PSD is the focal length, f_0. The distance between the middle of the two lenses is the baseline, d. The focal lengths and baseline variables are found from calibration of the system. The Z direction runs from the lens to the object, with Z=0 at the baseline. The X direction runs along the baseline, with X=0 at the middle of the baseline. The two PSDs are usually placed equidistant from the point X=0. The Y direction is perpendicular to the X-Z plane, with the positive Y direction coming out of the page toward the reader.

To find the depth of the scene, each point in the two pictures must be analyzed separately. Assume a point is chosen in the scene. Lines can be drawn from the middle of each lens to the point in the scene. The lines intersect the PSDs, giving x_R and x_L. Connecting these lines along with the baseline gives two similar triangles, as shown in Figure 3.6.

The principle of similar triangles gives:

$$\frac{d + x_L - x_R}{Z - f_0} = \frac{d}{Z}. \tag{8}$$

With algebraic manipulation, the depth can be solved, yielding:

$$Z = f_0 \frac{d}{x_L - x_R}. \tag{9}$$

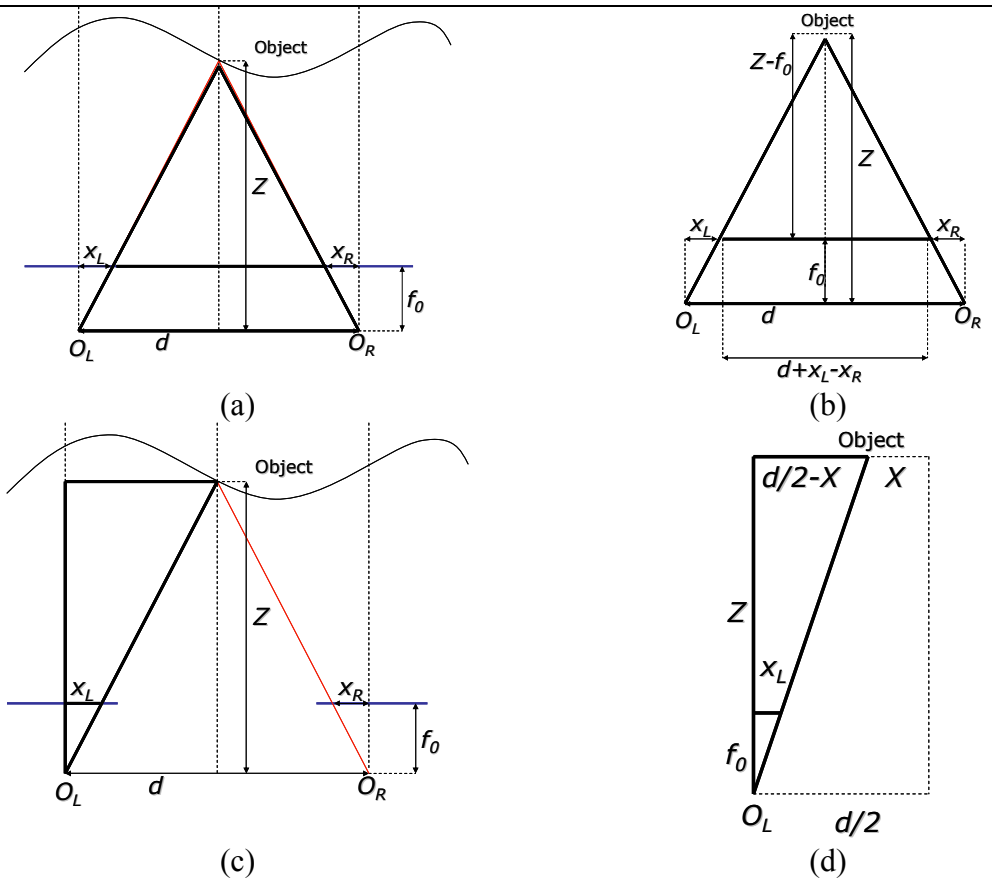

Figure 3.6: Stereo vision uses similar triangles, (a) in the system and (b) showing relationships, to find the depth. The X coordinate is found using triangles, shown (c) in system and (d) the relationships.

Geometry can also be used to find equations for the *X* and *Y* coordinates. A triangle can be drawn following the current point in the scene to one of the lenses in the system. The other two sides of the triangle follow the *X*-axis and *Z*-axis to form a right triangle. Again, similar triangles can be used to give:

$$\frac{f_0}{x_L} = \frac{Z}{\frac{d}{2} - X}, \tag{10}$$

and manipulation can solve for the X coordinate, giving:

$$X = \frac{Z}{f_0} x_L - \frac{d}{2}. \tag{11}$$

The *Y* coordinate is found much like the *X* coordinate. However, the *Y* axis begins along the line where the lenses lie. Therefore, the baseline does not affect the *Y* value, yielding:

$$Y = \frac{Z}{f_0} y_L . \tag{12}$$

3.2.3 Correspondence Problem

The biggest problem in stereo vision is called the correspondence problem. Two pictures are acquired by two cameras in the system. From these two pictures, the coordinates must be found for each point. The correspondence problem refers to the difficulty in determining exactly which points in each picture correspond to the same point in the scene.

To solve this problem, many systems use calibration. A known scene is placed in front of the cameras, and the cameras provide two pictures. Since the scene is already known, the points are already known, and matrices can be found that contain calibrated values. These matrices are then added into the depth equation for all other scenes.

Calibration is computationally expensive. Active 3D vision systems solve the correspondence problem by replacing one of the cameras with a laser, creating laser triangulation. Another way to get rid of the correspondence problem is to place a laser along the baseline of a stereo vision system. The laser can highlight a single point in the system. The laser beam highlights a single point in the two images from the cameras. The highlighted point in each picture represents the same point in the scene. Stereo equations can then be used to calculate the coordinates of the point.

3.2.4 Degrees of Freedom

The above equations only hold true for the specific system setup when both cameras lie along the same plane and both cameras are aligned perpendicularly to the scene. If either of the PSDs are offset, either by translation or rotation, then the equations quickly become more complex. For example, one of the cameras may be rotated around its center by an angle, α, in the X direction, as shown in Figure 3.7.

The value for x_L is now skew. If it is possible to find the value that x_L would be for a PSD that is perpendicular to the scene, then the original stereo equations can be used. Using geometry, x_L can be brought back to the basic setup position by:

$$x_L = \frac{\sin(90 + \tan^{-1}(\frac{f_0 \cos(\alpha) - x_{LR} \sin(\alpha)}{f_0 \sin(\alpha) + x_{LR} \cos(\alpha)}) - \alpha)}{\sin(90 - \tan^{-1}(\frac{f_0 \cos(\alpha) - x_{LR} \sin(\alpha)}{f_0 \sin(\alpha) + x_{LR} \cos(\alpha)}))} x_{LR} . \tag{13}$$

Then, the original stereo equations can be applied to find the coordinate of a point.

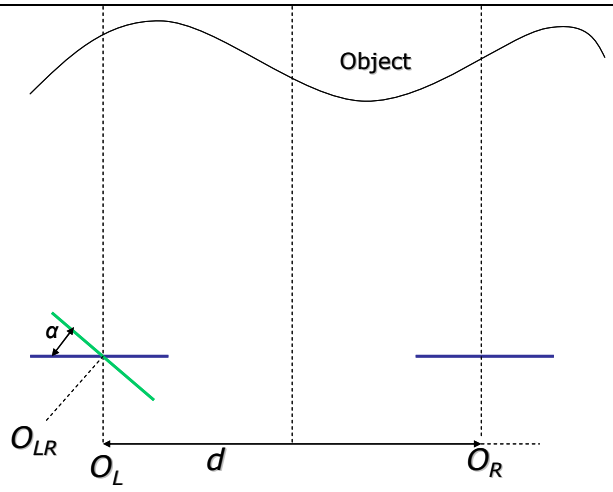

Figure 3.7: One or both of the PSDs in stereo vision can be rotated.

The PSDs have six degrees of freedom comprising three degrees of rotation and three degrees of translation. Klette, Schluns, and Koschan [1998] give four simultaneous equations,

$$[-x_L \sin(\theta) - f_0 \cos(\theta)]X + [x_L \cos(\theta) - f_0 \sin(\theta)]Z = -[\frac{b}{2} x_L \sin(\theta) + \frac{b}{2} f_0], \quad (14)$$

$$[-x_R \sin(\theta) - f_0 \cos(\theta)]X + [x_R \cos(\theta) + f_0 \sin(\theta)]Z = -[\frac{b}{2} * x_R \sin(\theta) - \frac{b}{2} * f_0], \quad (15)$$

$$[-y_L \sin(\theta)]X + [-f_0]Y + [y_L \cos(\theta)]Z = [\frac{b}{2} y_L \sin(\theta)], \text{ and} \quad (16)$$

$$[y_R \sin(\theta)]X + [-f_0]Y + [y_R \cos(\theta)]Z = -[\frac{b}{2} y_R \sin(\theta)], \quad (17)$$

that take all degrees into consideration. When solved, the coordinate of a specific point in the scene is determined. The equations are very complex and computationally expensive.

3.3 PSD Operation

Laser triangulation systems sometimes use PSDs in place of a camera. PSDs are used to find the coordinates of a spot of light. In contrast to CCDs, PSDs provide information analogously because they are not comprised of discrete elements. Instead, PSDs rely on the surface resistance of a photodiode.

PSDs are divided into different categories: one-dimensional and two-dimensional. The two-dimensional PSDs are divided into duo-lateral and tetra-lateral types. All PSDs are known for their excellent position resolution, high-speed response, and wide spectral

response range. Two-dimensional PSDs will usually have more distortion on the edges of its active area than one-dimensional PSDs [Hamamatsu, 2003; Sitek, 2005].

3.3.1 PSD Basics

A PSD is a p-n junction separated by silicon or some other insulator. The p-layer is resistive and has two electrodes, as seen in Figure 3.8. A common node connects to the n-layer, grounding the device. The distance between the two electrodes is called the resistive length, *L*, and has a uniform resistance.

When incident light hits the active area of the p-layer, the phenomenon called the photovoltaic effect occurs. The light energizes an electron on the p-layer. When the electron gets excited, a hole is created and the electron moves, creating electric current. The electric current flows to either electrode, where the current can be measured. Since the layer is uniformly resistive, equations can be used to determine where the light spot hits the device.

A scene contains a lot of light at different frequencies. Lasers operate at a higher frequency than background light in a scene. A lens placed in front of the PSD filters out the majority of the background light, only allowing light at laser frequency levels to pass through, and focuses the beam onto the PSD. As more background light is filtered out, the noise decreases.

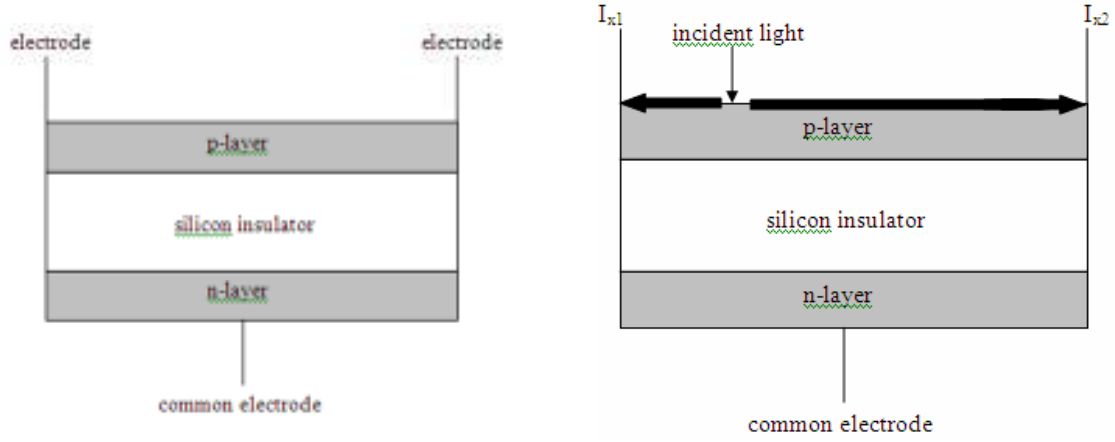

(a) (b)

Figure 3.8: (a) A PSD is a p-n junction separated by an insulator. (b) When incident light hits the PSD, current is generated.

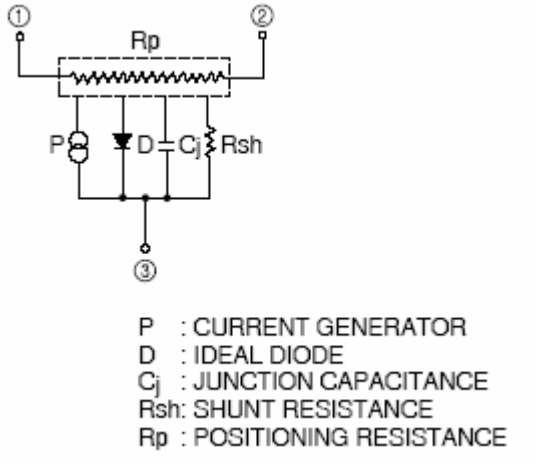

Figure 3.9: The 1D PSDs act like potentiometers [Hamamatsu, 2003].

3.3.2 Position Calculation

The 1D PSDs are able to calculate the position of a light spot in one direction only. The equivalent circuit looks like Figure 3.9.

When the laser light hits the active area, then the PSD acts like a potentiometer. Since the resistance in the p-layer is uniform, a ratio of the two currents can give the position of the light spot. This position corresponds to the distance, x, in laser triangulation, and $x_L$or x_R in stereo vision. The equation for finding the position of the light spot is:

$$\frac{I_{x2} - I_{X1}}{I_{x1} + I_{X2}} = \frac{2x}{L_x}, \tag{18}$$

where I_{x1} and I_{x2} are the currents from the electrodes, x is the position to be found, and L_x is the resistive length, or the distance between the electrodes.

The 2D PSDs calculate both the x and y positions of a light spot. Therefore, two extra electrodes are needed. The two electrodes are placed ninety degrees from the first two electrodes. On a duolateral PSD, they are placed on the n-layer, and the n-layer is resistive. The light penetrates through the silicon layer of the PSD and the photovoltaic effect creates current in both the p-layer and n-layer, creating a circuit like the one in Figure 3.10.

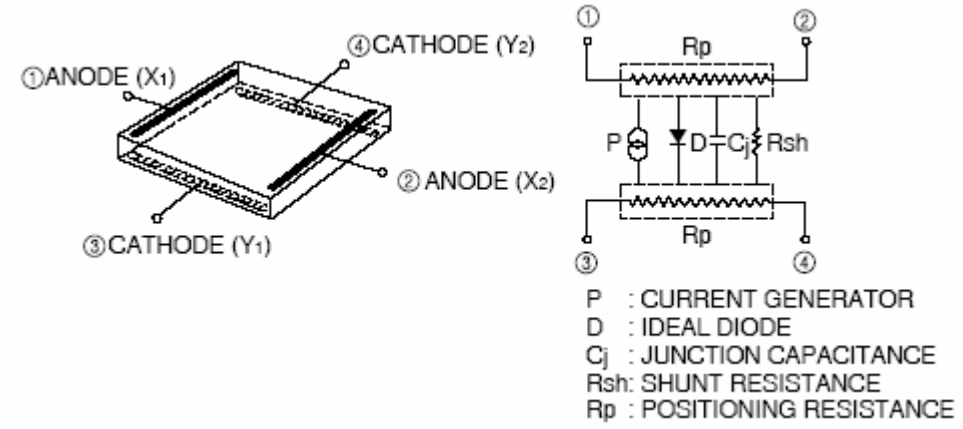

Figure 3.10: The 2D duolateral PSDs create four currents [Hamamatsu, 2003].

The current ratios allow the x position to be found by:

$$\frac{I_{x2} - I_{X1}}{I_{x1} + I_{X2}} = \frac{2x}{L_x}, \tag{19}$$

and the y position to be found by:

$$\frac{I_{Y2} - I_{Y1}}{I_{Y1} + I_{Y2}} = \frac{2y}{L_y}, \tag{20}$$

where I_{x2} and I_{x1} are the currents from the p-layer, I_{y1} and I_{y2} are the currents from the n-layer, x and y are the positions to be found, and L_x and L_y are the resistive lengths on the p-layer and n-layer, respectively.

The tetralateral PSD also calculates an x and y coordinate for a beam of light. The four electrodes are placed on the p-layer in a ninety degree configuration from one another. When the light spot hits the PSD, current is generated in four directions, creating the circuit in Figure 3.11.

Using the currents acquired, the x position can be found by:

$$\frac{(I_{x2} + I_{Y1}) - (I_{x1} + I_{Y2})}{I_{x1} + I_{X2} + I_{Y1} + I_{Y2}} = \frac{2x}{L_x}, \tag{21}$$

and the y position can be found by:

$$\frac{(I_{x2} + I_{Y2}) - (I_{x1} + I_{Y1})}{I_{x1} + I_{X2} + I_{Y1} + I_{Y2}} = \frac{2y}{L_y}, \tag{22}$$

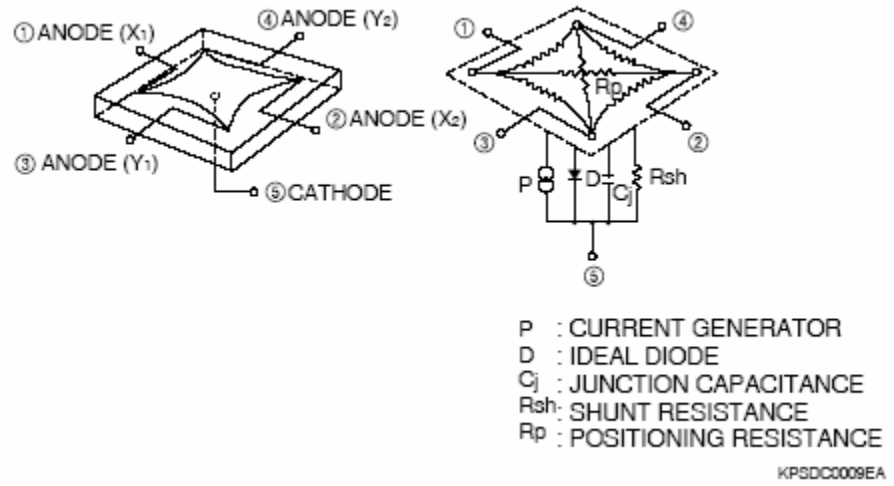

Figure 3.11: The 2D tetralateral PSDs create four currents in the p-layer [PSDs, Hamamatsu].

where I_{x1}, I_{x2}, I_{y1}, and I_{y2} are the currents from the electrodes, x and y are the positions to be calculated, and L_x and L_y are the resistive lengths between their respective electrode pairs.

The tetralateral configuration must take into account the four currents to calculate either the x position or the y position because the currents are generated in the same layer. If all currents are not considered, then more noise is introduced into the circuit. As the light beam nears the edge of the active area of the PSD, more distortion occurs.

3.3.3 1D, 2D, and Array PSDs

The requirements of a system determine which type of PSD should be used. Each type of PSD has different levels of accuracy, distortion, and equation complexity. Also, some types of PSDs cannot be used for different types of lasers.

The 1D PSDs have the simplest equations to calculate and are therefore the least computationally expensive. However, they also provide the least amount of information, only telling the location of a light spot in one direction. The position has the least amount of noise since only two currents are generated. The active area on a 1D PSD can be as large as 30 mm, allowing it to pick up light from a larger scene or giving higher resolution.

The 2D PSDs offer more information since they give both the x and y position of a light spot. However, the equations are more complex, causing longer computation time. The extra currents in the photodiode also cause more noise in the circuit. Since the duolateral configuration spreads the electrodes farther apart than the tetralateral configuration, there is smaller position detection error and higher position resolution. However, the

tetralateral configuration has a higher-speed response time and can accurately find the position with a low dark current. A special type of tetralateral PSD is being developed called a pin-cushion type, which improves the active area and electrodes. These improvements bring the position detection error of the tetralateral PSD to the same level as the duolateral PSD.

If only one 1D or 2D PSD is used in a system, then only a point laser can be used. However, this process can be slow since the point laser must be moved over every spot in the scene. To decrease data acquisition time, the point laser is often replaced by a line laser. PSDs can only pick up one light spot at a time. Therefore, if a line laser is used, then multiple PSDs must be used, creating an array. Only 1D PSDs can be used to create the array. If 2D PSDs are used to create the array, then multiple light spots are present in either the x or y direction and average out to the middle of the PSD. The number of PSDs in the array dictates the number of pixels in the line laser. Therefore, more PSDs in the array correspond to higher resolution.

3.4 Field Programmable Gate Arrays

Computation time remains a problem for many 3D modeling systems due to software's limitation of only doing one operation per clock edge. FPGAs offer parallelization of operations, performing multiple operations per clock edge.

3.4.1 FPGA Origination

In a point laser triangulation system with PSDs, data is acquired for every point. The system contains constant characteristics such as the baseline and the focal length. Depending on the type of PSD used, two or four currents may be present. As seen from the previous sections, this data set must now be applied to equations to find the coordinates of the current point.

Since some of the variables in the equations depend on other values that must be calculated, the equations must be solved in a specific order. First, the x and y values must be calculated using the respective equation for the PSD in the system. Once the x and y values are known, the Z coordinate can be calculated using the stereo depth equation. The X and Y coordinate can be calculated once Z is known.

The data can be fed into a software program that calculates these equations. Software is serially based. In other words, software programs can only do one task at a time. Therefore, it must process one equation before going on to the next equation. Each equation has a certain amount of computation time associated with it. Software must load the equation, perform the calculation, and store the answer elsewhere before it can go on to the next task, causing long computation times.

Engineers began looking for solutions other than software to make systems faster and more efficient. Hardware started to become a popular way to attempt to solve these problems. At first, ASIC chips were designed and fabricated, but recently, people have begun looking to FPGAs for their hardware solution needs.

Both ASIC and FPGA chips provide the same hardware solution to a problem by running electrical pulses through a series of gates. In hardware, multiple processes can occur in parallel. Therefore, multiple equations can be calculated at the same time, reducing computation time. Also, variables and equations do not have to be loaded or stored. Inputs can be hooked directly to pins on a chip and can be used immediately upon arrival. In the case of a line laser, the data sets for several points can be available at the same time. Software has to calculate each equation for a single point before going on to the equations for the next point. In hardware, data from multiple points can be input to the chip at the same time, and the equations for each of the points can be calculated simultaneously.

The two most popular hardware solutions are ASIC chips and FPGAs. Equations can be found that implement the necessary computations using gates. The gates must then be laid out onto either the ASIC chip or FPGA. Engineers design ASIC chips by laying out every transistor individually. The process tends to be more time-intensive, since the engineer plans where to put each gate and transistor. However, this also allows more control over the design space and the delay times between gates.

ASIC chips were very popular due to the control over signal propagation time and space. However, die size has been steadily decreasing, and signal speed has been increasing. Therefore, size and time delay for FPGAs has begun to rival that of ASIC chips while supplying other advantages. FPGAs allow for instantaneous implementation because they can be reprogrammed on the fly. A person can program a design onto an FPGA, test the implementation, and fix any problems on the same chip. An ASIC chip only allows one design and must be thrown out if the design does not work. FPGAs can also be reprogrammed during run-time. Some systems in the field contain embedded FPGAs which can be easily upgraded instead of taking the entire machine apart to replace a single chip [Oldfield, 1995; Trimberger, 1994; Brown, 1996].

3.4.2 FPGA Structure

Field programmable gate arrays are comprised of units called logic blocks. The logic blocks are laid out in a 2D array, surrounded by wires. Each company uses a slightly different logic block for each FPGA family to provide better density, computations, or another desired effect. To program the FPGA, wires inside the chip are connected to create the equations. Input and output pads surround the array, as seen in Figure 3.12.

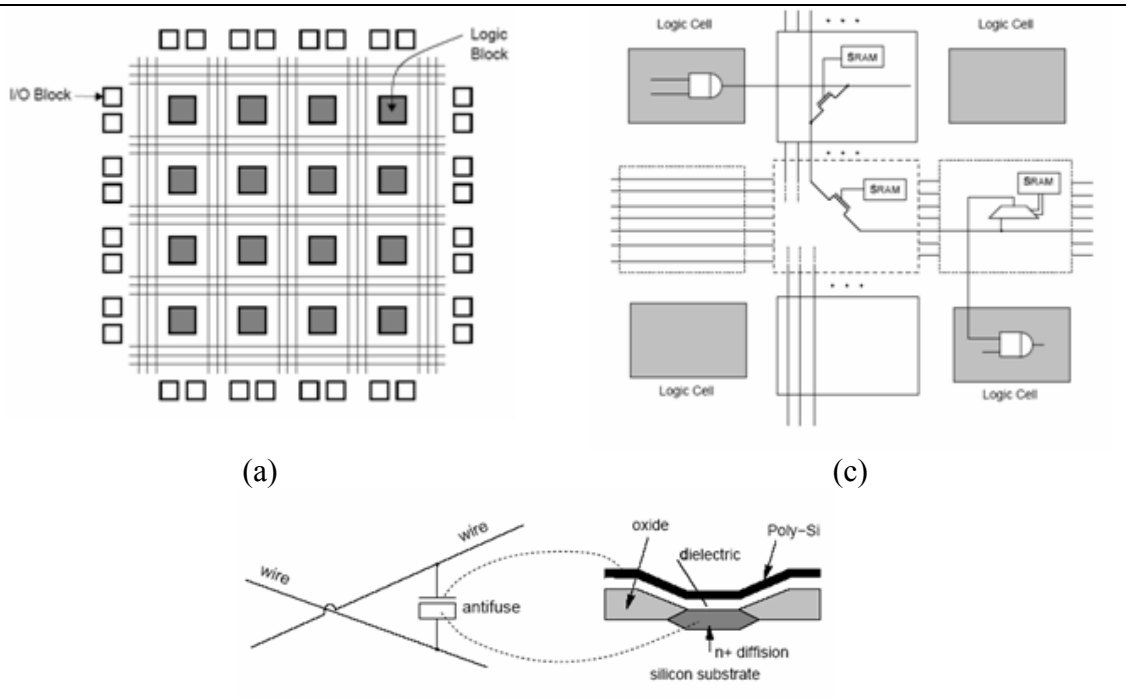

Figure 3.12: (a) FPGAs are comprised of logic blocks laid out in a 2D array. (b) Connections in FPGAs can be programmed by antifuses (c) or by SRAM [Brown, 1996].

The wire connections can be created either by antifuse technology or controlled by SRAM. Antifuses contain three layers, top and bottom conductive layers separated by a middle insulating layer. Before programming, the anitfuse is considered an open circuit due to the insulating layer. To program, a high electric current runs through the fuse and the middle layer because a low-resistance link between the top and bottom layers. Antifuse-based FPGAs are non-volatile, retaining the program even after power is lost, but cannot be reprogrammed.

In contrast, SRAM controlled FPGAs are volatile, so connections can be programmed by reprogrammed, but are lost when power is removed. Transistors connect two wires and the SRAM attaches to the gate of the transistor. To turn the transistor on, the SRAM gives a high signal to the gate of the transistor, creating a short circuit and connecting the wires.

3.4.3 Logic Blocks

The main manufacturers of FPGAs include Xilinx, Atmel, and Altera. Due to the quickly changing market, other companies enter and exit the FPGA market frequently. Each company carries different families of FPGAs, trying to minimize some aspect of hardware computation, whether it is density, speed, or a combination of factors. To

achieve these different qualities, the building blocks, or logic blocks, of the FPGAs are unique for each family.

Two main Xilinx families include the Virtex 4 and Spartan chips. The logic blocks are referred to as configurable logic blocks, or CLBs. The CLBs are separated into four slices, which are then grouped into two pairs. The two slices on the left are grouped together to form SLICEM, while the two slices on the right are grouped together to form SLICEL, as shown in Figure 3.13[Xilinx, 2005a; Xilinx, 2005b].

Each slice contains a number of digital logic elements including flip-flops, Nands, distributed RAM, shift registers, and look-up tables (LUTs). Look up tables, or function generators, hold the output values for a given function and can therefore generate the answer for an equation very quickly. The delay for a LUT is independent of the function. Multiplexers are present so that LUTs can be combined to implement larger functions. Muxes also allow CLBs to be connected to each other. The Virtex 4 contains specialized areas to help with arithmetic logic including fast look ahead carry logic.

SLICEM of the CLB contains both memory and logic functionality, while SLICEL only contains logic elements. By separating the functions, the CLB retains a lot of functionality while reducing size, allowing either a decrease in size of the chip, or allowing more CLBs to be placed on the chip. The Virtex CLB also offers two fast-carry logic chains to speed up arithmetic operations.

The Spartan CLBs are broken into the same slice configuration as the Virtex 4. However, the mechanics of the individual slices differ to achieve different qualities, as can be seen in Figure 3.14. The Spartan is made for digital signal processing and other data processing applications. Each Spartan CLB also contains three separate LUTs, so bigger functions can be processed faster. The Virtex has a much higher density, and is therefore more expensive, offering more computing power and the ability to user PowerPC or Microblaze [Xilinx, 2005a].

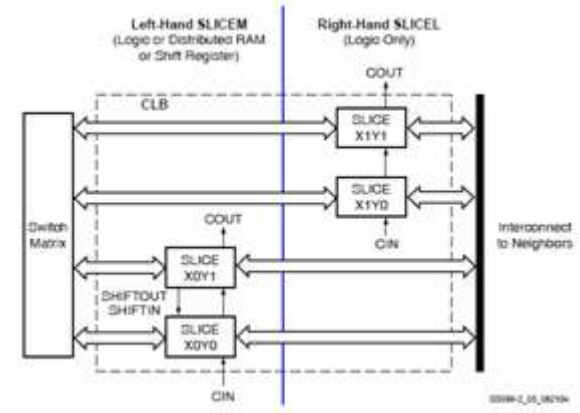

Figure 3.13: The Xilinx CLB is made up of 4 slices. [Xilinx, 2005b].

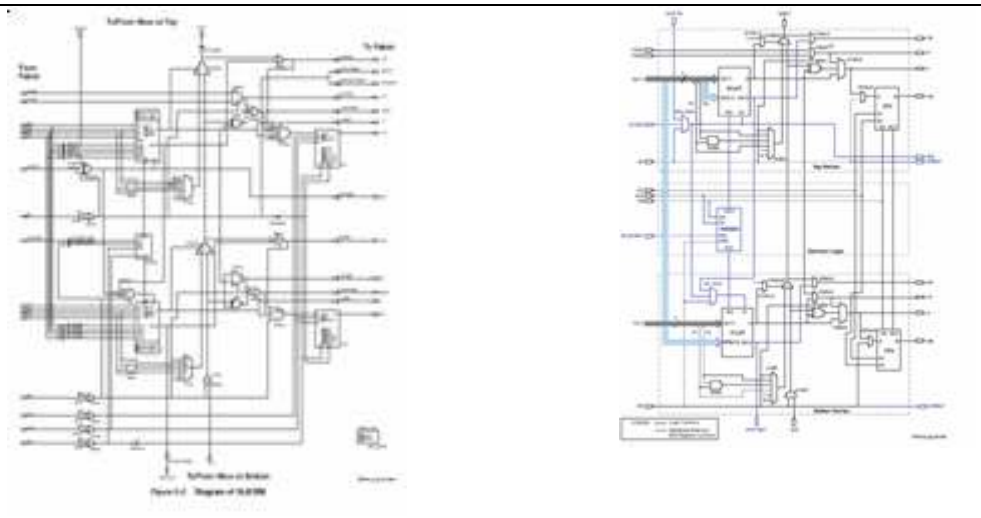

(a) (b)

Figure 3.14: (a) SliceM of a Virtex4 [Xilinx, 2005b] has different logic than (b) SliceM of a Spartan[Xilinx, 2005a].

Atmel refers to their logic block as "the cell", as seen in Figure 3.15. The main Atmel FPGA, the AT40KAL, is based on a cell containing two three-input LUTs so that either two functions of three inputs or one function of four inputs can be created. Each cell also has an extra And gate for more efficient multiplication array implementation. A D-flip-flop allows an output to be held and fed back into the system. All of these elements allow the cell of the Atmel FPGA to be configurable for random logic, arithmetic, multiplication, and counter implementations [Atmel, 2004].

Altera offers several FPGA solutions, including the Stratix, which offers high density, and the Cyclone, which offers low cost. The main building block of these FPGAs is called the logic element or Adaptive Logic Module (ALM). Each ALM in the Stratix offers multiple LUTs, programmable registers, full adders, a carry chain, a register chain, and more. These resources allow random logic, extended LUT, arithmetic, and shared arithmetic implementation. The registers also allow for data storage and easy execution of state machines [Altera, 2005a; Altera, 2005b].

The Cyclone offers fewer elements than the Stratix in its ALM. It includes one four-input LUT, one programmable register, a carry chain, and a register chain. Since each ALM contains less functionality, it offers a lower-cost solution. The Cyclone can still implement random logic functions and arithmetic. It can also be configured to make D, JK, T, and SR operation using its register and take up to six inputs.

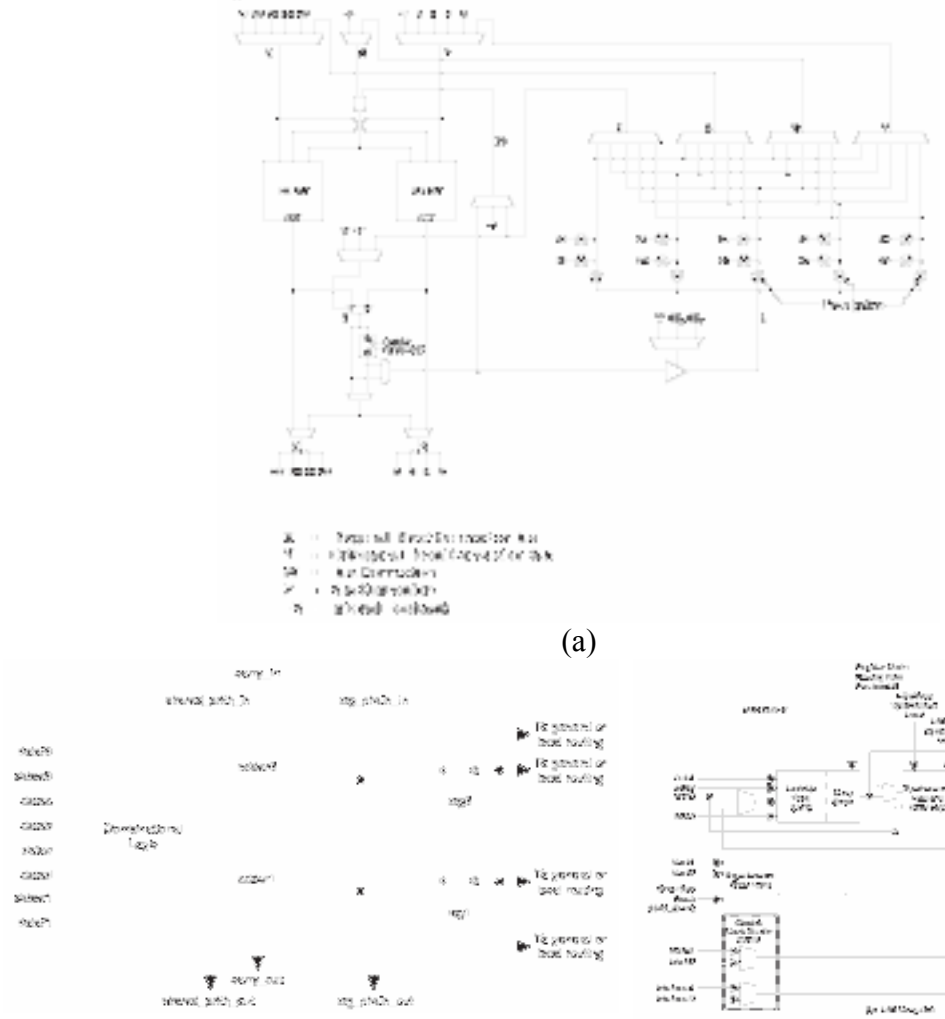

(a) (b) (c)

Figure 3.15: (a) The Atmel "Cell" contains 2 LUTs [Atmel, 2004]. (b) The main building block of the Altetratix is the ALM [Altera, 2005b].. (c) The Altera Cyclone ALM is based on a four-input LUT[Altera, 2005a].

3.4.4 Routing

The individual logic block of each type of FPGA determines the density of the FPGA and how many functions it can implement. These logic blocks must interact with other logic blocks on the chip. Therefore, it is very important for the FPGA to manage routing efficiently to maintain signal integrity and retain high speed. In general, logic blocks are organized in a 2D array, with blocks lined up horizontally and vertically and wires running between all of the blocks. The number of wires placed between the logic blocks can help to make the chip faster by offering more routing options, but also decreases density. Therefore, each company has a slightly different routing option to make their chip as efficient as possible.

Xilinx uses wires of different length to maximize speed in their chips, as shown in Figure 3.16. All of the wire connections are SRAM based. Twenty four lines are available for connections from horizontal lines to vertical lines and are referred to as general routing matrix wires. Ninety-six wires of smaller length are available to carry signals from one CLB to another CLB, as long as the CLBs are within six blocks from each other. Twelve longlines are available to carry signals across the chip in either direction, in case logic blocks that need each other's signals are placed far apart. All of these interconnections allow many options for routing, ensuring fast signal propagation [Xilinx, 2005a; Xilinx, 2005b].

Atmel's busing network contains five identical planes. Each bus plane contains two express buses separated by a middle, local-bus resource, as seen in Figure 3.17. The local-bus lines can carry a signal between logic blocks that are four elements apart or closer.

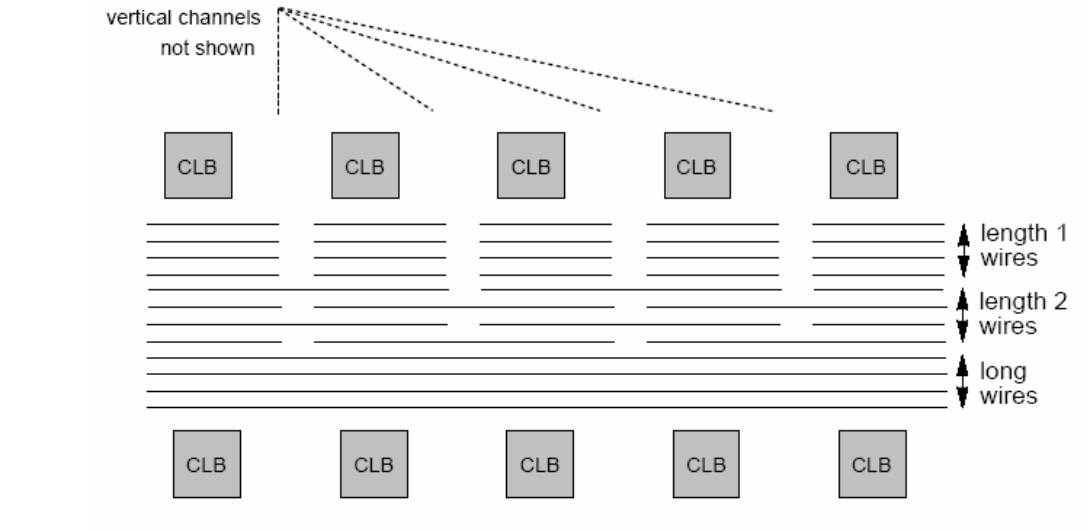

Figure 3.16: Routing in Xilinx FPGAs has many multiple-length wires[Brown, 1996].

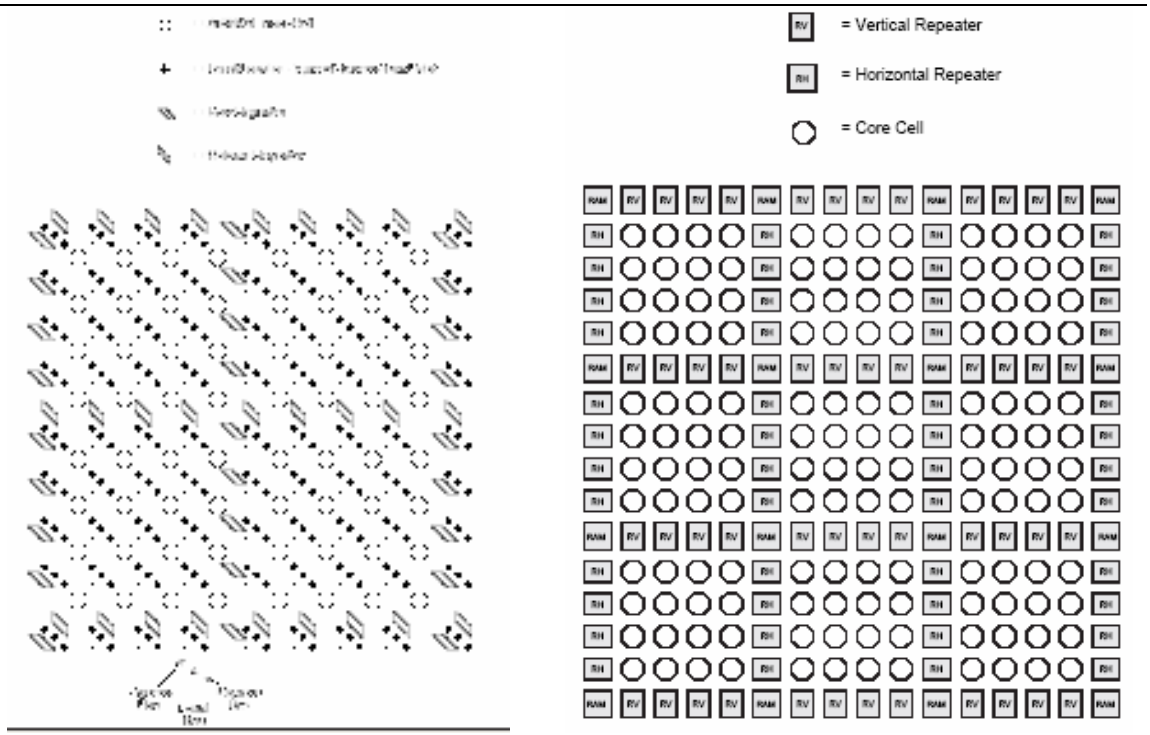

(a) (b)

Figure 3.17: Atmel's routing scheme contains 5 (a) bus planes and is laid out as seen in the (b) floor plan [Atmel, 2004].

Express bus lines span eight cells. Connections are made with repeaters, dubbed horizontal or vertical based on the wires that they connect. Express bus lines skip a repeater using a programmable pass gate to create longer wires with faster propagation times. Connections between two local wires are made using pass gates, while express to express connections use separate pass gates [Atmel, 2004].

Altera uses two separate types of interconnections. First, Altera groups their logic elements into groups of eight ALMs called logic array blocks (LABs). LAB signals tend to carry control signals, such as clock or synchronous reset. Eight wires run to each ALM in the LAB, as seen in Figure 3.18. The wires can carry either global control signals, or up to four non-global control signals.

Altera refers to its general routing matrix as MultiTrack Interconnections. It contains separate types of wires for row interconnections and column connections, as shown in Figure 3.19. Within the row and column connections lie different types of wires for faster signal propagation time. Many wires are available for specific connections between certain logic blocks. Row connections include direct link, connecting LABS to adjacent blocks, R4s, connecting blocks within four blocks of each other, and R24s, providing a high speed solution for signals traveling the length of the chip. Column

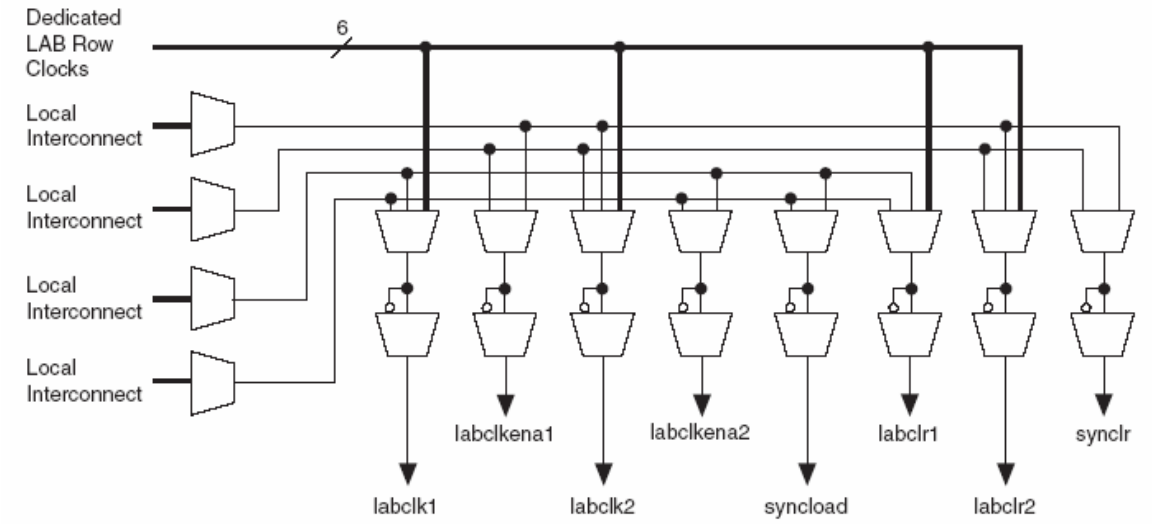

Figure 3.18: Altera LAB interconnections usually carry control siganls[Altera, 2005a].

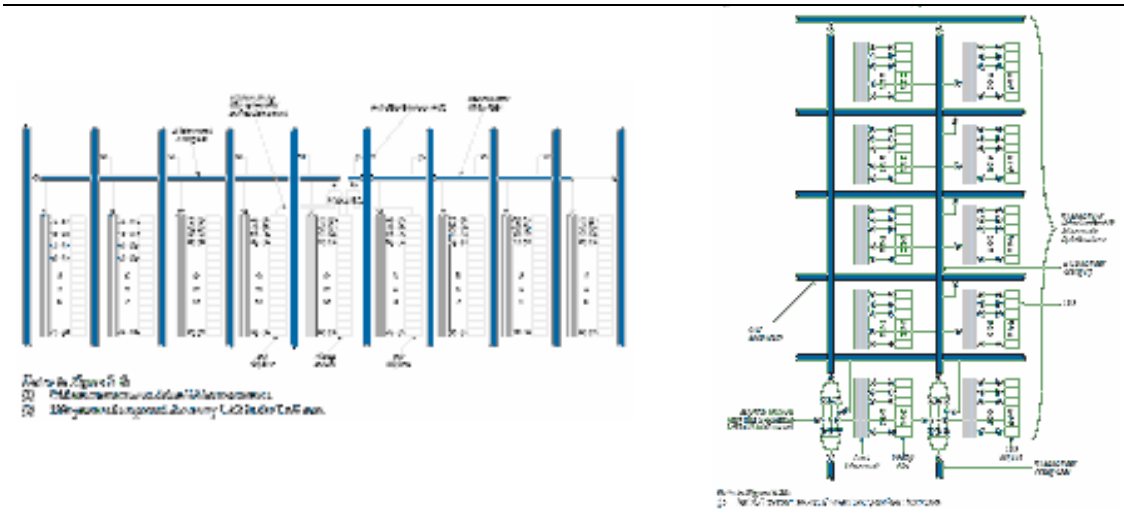

(a) (b)

Figure 3.19: Altera Routing Structure is divided into (a) Rows and (b) Columns [Altera, 2005a].

interconnections include register chains within a LAB, C4s, connecting blocks within four blocks of each other, and C16s, allowing signals to quickly travel the length of the chip.

3.4.5 Other Considerations

Through the use of specialized logic building blocks and routing, companies have attempted to give a variety of FPGA solutions which minimize cost, maximize speed, or provide high density. These companies have also attempted to provide superior software for placement of logic on their chips. They give solutions to routing of global clocks to keep signal integrity and minimize delay. If the clock signal corrupts, then state machines implemented on the chip do not work. Memory is also placed on chips, giving storage area options. More onboard memory allows higher speeds so that external memory does not have to be attached. The package that the chip is placed in also plays an important role, determining the number of input and output pins and planning the routing between the pads and the logic on the chip.

3.5 Hardware Selection

For the system to operate in real time, it must produce pictures at 30 frames per second or better. Therefore, it can take no longer than 0.033 seconds to acquire the data for a pixel and output it to the screen. The time to move the laser, have stable outputs on the electrodes of the PSD, allow the FPGA to receive the readings, and calculate the point using the FPGA all contribute to the total time needed to calculate a single pixel.

Next, the resolution of the picture must be satisfactory. The system should be able to acquire good images for scenes ranging from 0.5 feet to greater than 15 feet. The first point for error in resolution occurs at the PSD. The active area of the PSD and the layout of the active area contribute to the resolution. Once the currents are fed into the FPGA, more error can occur depending on the number of bits used to describe the current as a digital signal. High resolution in the PSD and a larger number of bits used in the FPGA translate to more expensive parts.

All of the parts chosen also need to be a reasonable cost. If the parts are all expensive, then the entire system becomes even more expensive and thus unmarketable. However, as cheaper parts are used, then the computation time increases, slowing down the system, and the resolution decreases, causing the picture to appear more blurry.

Table 3.1. Hamamatsu 2D PSDs

Part No.	Active Area (mm)	Structure	Rise Time	Resolution	Error	Package	Price
S1200	13 x 13	Tetra-lateral	1.5 us	1.4um	150um	Ceramic	$526.40
S1300	13 x 13	Duo-lateral	0.8 us	1.4um	80um	Ceramic	$1776.60
S1880	12 x 12	Pin-cushion (improved tetra)	1.5 us	1.5um	80um	Ceramic	$789.60
S1881	22 x 22	Pin-cushion	3 us	2.8um	150um	Ceramic	$3948.00
S2044	4.7 x 4.7	Pin-cushion	0.3 us	0.6um	40um	Metal	$180.48
S5990-01	4 x 4	Pin-cushion	1 us	0.7 um	70um	Ceramic chip carrier	Discontinued 22.56
S5991-01	9 x 9	Pin-cushion	2 us	1.5 um	150um	Ceramic chip carrier	Min 2 pieces $57.15
S7848	2 x 2	Tetra-lateral	20 us	?	20um	Plastic	Min 5 pieces $16.92
S7848-01	2 x 2	Tetra-lateral	20 us	?	20um	Plastic	Min 5 pieces $16.92

3.5.1 PSDs

First, a choice must be made between 1D PSDs and 2D PSDs. If a line laser is used, then two arrays of one-dimensional PSDs are needed. If a point laser is used, then either four one-dimensional PSDs or two two-dimensional PSDs are needed.

On a regular television monitor, a point laser scans through every pixel at a rate of thirty frames per second. Therefore, it is possible for a point laser in this system to scan a scene at the same rate, meaning that a line laser is not necessary to achieve real time scanning speeds. Since an inexpensive PSD is about twenty dollars, and two arrays of these PSDs would cost much more than two PSDs of any type, it is better to use a point laser and two PSDs.

Next, either four 1D PSDs or two 2D PSDs must be placed on either side of the point laser. The 2D PSDs are known for good dark current, high resolution, and fast current output. Since many 2D PSDs are also affordable, it is decided to use two 2D PSDs for the system.

The main manufacturer of PSDs is Hamamatsu. They carry a range of duo-lateral, tetra-lateral, and pin-cushion tetra-lateral PSDs. Table 3.1 compares the different types of 2D PSDs offered. [Hamamatsu, 2001; Hamamatsu, 2004; Hamamatsu, 2005]

All of the errors for the PSDs are less than 150 µm. Since the smallest scene is about six inches away, 150 µm is undetectable to the human eye. The resolution for the worst PSD is 1.5 µm, which is also undetectable to the human eye from a distance of six inches or greater. Therefore, the resolution and error are a big concern for any of these parts.

The amount of time to have a good current on the outputs of the PSD takes away from the amount of time the FPGA can take to calculate the coordinate. Therefore, a smaller rise time is preferable.

Considering the rise time, cost, and error, a low end solution of the S7848 is recommended. A mid-range solution of the S5991-01 is recommended, and a high-range solution of either the S5991-01 or the S2044 is recommended.

Once the PSD is purchased, it has to be mounted. The outputs also have to be connected to an FPGA and the FPGA needs to be programmed to calculate the x and y positions of a light spot. Another option is to purchase a product that includes a PSD and already calculates positions. The Noah Corporation offers a linear position sensor module (LPSM) based on a 2D duolateral PSD. The PSD is mounted in a 1.25" x 2.5" case with a bezel plate on the front for a lens. The product outputs the x and y positions as a DC signal between -10 Volts and +10 Volts. The LPSM is recommended for the system because it meets all technical requirements and combines tasks for easier implementation and reduction of the chance for mechanical failure.

3.5.2 Lasers

A point laser needs to be chosen as the source of light for LPSM. The PSD in the module is sensitive to a specific wavelength and intensity. The specification shows that the PSD will pick up laser light at a nominal beam power range of 0.001 mW to 1 mW and with a spectral range of 350nm to 1100nm. The values given in the specification refer to the reflection of the laser beam off of any object in the scene. Therefore, the actual power for the laser beam needs to be larger. A laser beam with 5 mW to 10 mW power is preferred, with a wavelength of about 600 nm. Table 3.2 shows a variety of lasers available.

Another consideration for the laser is the beam size and fan angle. A laser beam emits from a point. However, as the beam moves further away from its source, it slowly gets larger, spreading out over a given distance. The beam can be viewed as a cone instead of a true beam. The fan angle refers to the angle at which the beam spreads out. The beam size is the diameter of the laser beam at the exit face of the laser, but grows larger due to the fan angle. A smaller beam size and fan angle helps to give better focus and less power intensity loss. [Edmund Optics, 2005]

3.5.3 Laser Scanning System

Many laser scanning systems direct either a point laser, line laser, or pattern laser. Each system runs into its unique difficulties in implementation. For this system, a point laser is being used to scan the entire field of view at very high speeds, bringing such problems

Table 3.2. Summary of lasers

Company	Product	Power (mW)	Wavelength (nm)	Beam Size (mm)	Fan Angle (mRad)	Price
Thorlabs	CPS184: Visible Laser Module	4.5	650	4.4 x 1.2	?	$79.50
Thorlabs	CPS196: Focusable Laser Module	4.5	635	2.45 x 0.54	0.6 x 1	$143.00
Edmund Optics	NT54-006: Rocket Laser Pointer	<5	640 +- 10	adjustable	?	$49.95
Edmund Optics	NT52-840: Laser Pointer - Best Buy	<5	650	3.6 x 3	?	$49.95
Edmund Optics	NT53-546: Laser Pointer - Spectra	5	650	1/8 inch	?	$26.75
Edmund Optics	NT47-112: Laser Diode Premiere	5	655	6 x 2 (ellipse)	<0.5	$335.00
Edmund Optics	NT57-108: Laser Diode Premier	5	655	5 x 5	<0.5	$505.00
Edmund Optics	NT54-183: Laser Diode w/ Key	10	670	3.8 x 0.9	0.40 x 0.93	$390.00
Edmund Optics	NT54-180: Laser Diode w/ Key	10	635	3.8 x 0.9	0.40 x 0.93	$460.00

as physical limitations in speed, physical stress on the moving laser, and accurate control of the laser movement.

In some systems, the laser can be deflected using a mirror which is controlled by a motor. Stepper motors provide an accurate and repeateable method of moving the mirror. However, stepper motors usually only rotate up to about 10,000 rpm. According to the resolution and size of the field of view, the laser may have to move faster, meaning extra gear ratios would have to be added to the system. Another option is to use servo motors. Although they are not always as repeatable as stepper motors, they are easy to control and have variable accuracy.

Since a point laser is being used, the laser will have to move at very high speeds that may not be able to be reached. Several solutions exist to slow down the necessary speed of the laser. First, a polygonal mirror can be used to deflect the beam. The mirror reduces the necessary speed by a factor of the number of sides on the mirror. Another option is to use a line laser instead of a point laser. A line laser allows the entire scene to be scanned with one sweep of the laser instead of needing multiple scans. Laser scanning systems are developed, tested, and hardware decisions made in Chapter 4.

3.5.4 A/D Converter

Analog to digital converters (A/D converters) take an analog signal as its input and converts it to a binary number. A/D converters have several parameters to define their specific configuration including resolution, speed, and architecture.

3.5.4.1 A/D Basics

The resolution defines the number of bits in the binary number representation of the signal. Common resolutions include 8-bit, 16-bit, and 24-bit.

Speed refers to the sampling rate of the chip. The analog input signal contains continuous information. At a certain time interval, the value of the input signal is sampled. The sampled value is then converted to a digital signal. A higher sampling rate gives more samples per second for better time resolution. The speed can range from as slow as 128 samples per second (SPS) to high speed chips of 10 MSPS and higher.

Two of the most popular architectures of A/D converters are the ramp or staircase A/D converter and the successive-approximation (SAR) A/D converter. For the ramp style converter, the input voltage is assumed to be positive and a reference voltage internal to the chip is set to zero volts. At every clock cycle, the internal voltage is increased by one level and is compared to the input voltage. Once the internal voltage exceeds the input voltage, then the value is sent to the output.

Since this process must go through every voltage until the correct level is found, the process can take up to 2^n clock cycles. It is also very limiting since it only takes positive voltages. The SAR architecture helps to eliminate the necessity of positive input voltages and increases speed.

The SAR architecture acts much like a number-guessing circuit. As an example, say that the resolution is 8 bits and the internal reference voltage is 2.55 V. Therefore, the most significant bit would refer to either 0V if set to “0” or 1.28V if set to “1”. The input voltage is compared to 1.28V. If the input voltage is greater than 1.28V, then the most significant bit is set to 1. Otherwise, the bit is set to 0. To find the next bit, the input voltage is compared to 1.28V times the most significant bit plus 0.64V, or one-fourth of the internal reference voltage. The bit is again set to “0” or “1” based on whether the input voltage is higher or lower. This process continues until all bits are set.

3.5.4.2 Resolution Validation

The signal from the LPSM is analog. However, the inputs to the FPGA need to be digital. Therefore, an A/D converter must be used to convert the signals to an appropriate format.

Many parameters must be considered for the A/D converter. The input voltage levels, sampling rate, bit resolution, and output voltage levels must all be considered. The LPSM outputs are the inputs to the A/D converter, so the input voltage levels must go from approximately -10 V to 10 V. The FPGA inputs need to be between 0 V and 5 V, so this range is set to the output voltage levels.

The LPSM gives valid outputs every 100 μs, according to the specification. The A/D converter should sample at a rate greater than 100 μs in the event that the LPSM is able to give a better data rate. A sampling rate of 10 μs is chosen. If sampled every 10 μs, then the A/D converter will give a valid data output every 10 samples.

Finally, a resolution must be chosen. Eight bits gives 255 levels, while twelve bits gives 4095 levels, and sixteen bits gives 65535 levels. The smallest necessary distance is the focal length, corresponding to 13 mm. From the table of possible resolutions versus frame rates, the best resolution makes each pixel 69 mm by 98 mm. The baseline for stereo vision systems is typically $1/10^{th}$ of the distance of the distance. Therefore, the largest baseline is approximately 500 mm, but will probably not reach that level.

Looking at all of the possible inputs, 8 bits should be able to allow for good resolution of all inputs. Chips from TI, National Instruments, and Analog Devices were surveyed, but an 8 bit resolution chip with a voltage range of -10 V to 10 V could not be found. Therefore, the 16 bit chip ADS7805 from TI was chosen. A sample was ordered from TI and was hooked up on a breadboard to test its functionality before purchasing the ADS7805 mounted on an EVM board. Only the 8 most significant bits need to be connected. The lower 8 bits can be disregarded.

3.5.5 FPGAs

Xilinx, Altera, and Atmel provide FPGA solutions. Xilinx and Altera have more options than Atmel and offer more support, so families from these two companies are considered. The Virtex 4 and the Spartan 3 are offered by Xilinx while the Stratix II and the Cyclone II are offered by Altera.

For the basic system, only addition, subtraction, and division need to be implemented. Using the worst-case PSD choice, the FPGA needs to output a coordinate within 0.33313 seconds, corresponding to a frequency of about 30.02 MHz or faster. Both companies have low-end chips that run at 40MHz or better, so speed is not a big factor.

Higher-end systems will have to handle sines, cosines, and tangents to allow more flexibility in the position of the PSDs. The best way to implement these functions in an FPGA is by using a look-up table. The amount of bits used to store a value in the table and the number of entries in the table will determine the desired amount of on-board memory.

Finally, the number of input and output pins is also an important consideration. More I/O pins means that more information can be sent into and out of the FPGA. If the data for more points can be given to the FPGA at the same time, then more parallel processing of the coordinates can occur. This allows the points to be output faster, causing the real-time data rate to increase.

Since Xilinx offers a university support program, free software, and reasonably-priced development boards, the Xilinx families were chosen. Table 3.3 summarizes the Xilinx FPGAs. [Williams, 2005]

The Virtex series is much more expensive than the Spartan. Although the Virtex offers a much higher speed and more logic, the system does not require these resources. Therefore, the choice is narrowed to a Spartan 3 device.

3.5.6 Development Boards

Several companies offer development boards for FPGAs. Development boards offer a place to mount an FPGA so that it can be programmed. These boards also offer a variety of peripherals including extra memory, USB connections, PS2 connections, LCDs, JTAG, and a variety of other hardware. Components on the boards are already hooked

Table 3.3. FPGA comparison

Part No	FPGA	Speed	I/O Pins	Price
XC3S50-4VQ100C	Spartan 3	40 MHz	100	$5.65
XC3S50-4PQ208C	Spartan 3	40 MHz	208	$10.55
XC3S200-4FT256C	Spartan 3	40 MHz	256	$19.35
XC3S200-4TQ144C	Spartan 3	40 MHz	144	$11.40
XC3S400-4FG456C	Spartan 3	40 MHz	456	$35.60
XC3S400-4TQ144C	Spartan 3	40 MHz	144	$16.60
XC3S1000-4FT256C	Spartan 3	40 MHz	256	$35.25
XC3S1000-5FT256C	Spartan 3	50 MHz	256	$40.55
XC3S1500-4FG320C	Spartan 3	40 MHz	320	$55.95
XC3S1000-5FG320C	Spartan 3	50 MHz	320	$43.60
XC3S1000-5FG676C	Spartan 3	50 MHz	676	$74.45
XC4VLX15- 10FF668C	Virtex 4	100 MHz	668	$141.56
XC4VLX25 – 10FF668C	Virtex 4	100 MHz	668	$274.03
XC4VLX40- 10FF668C	Virtex 4	100 MHz	668	$432.47
XC4VLX60- 10FF668C	Virtex 4	100 MHz	668	$535.00
XC4VLX80 – 10FF1148C	Virtex 4	100 MHz	1148	$1128.58
XC4VLX100-10FF1148C	Virtex 4	100 MHz	1148	$1913.25
XC4VLX160-10FF1148C	Virtex 4	100 MHz	1148	$3098.80
XC4VLX200- 10FF1513C	Virtex 4	100 MHz	1513	$5832.53

up and ready to interface with the FPGA. A board can only support one family of FPGA since the connections and pin layout vary between different types of FPGAs.

Since information needs to be input and output quickly from the FPGA, we would like to find a development board that supports the Spartan 3 chip and offers USB2.0 connections for communication with a computer. Trenz Electronics offers a micromodule for the Spartan 3 with USB2.0 capabilities. The module is powered by the USB connection. If more power is needed, an adapter must also be purchased. Two high-speed connectors, one for input and one for output, lie on either side of the FPGA. The micromodule can be used as a standalone board, or can be attached to a carrier board. The carrier board provides another source of power to the board and attaches extra peripherals. The board costs approximately $200 and is recommended for use due to its capabilities and high speed [Trenz Electronics, 2005].

3.5.7 Computer Software and PC Criteria

A computer is needed to display the collected points. The computer needs to have a USB 2.0 port to take input from the FPGA. To properly display the picture, the video card should have at least 32 bit true color or better. The CPU speed should be at least a Pentium 4, 1GHz processor or better.

The points can be stored in a text editor, such as notepad, Wordpad, or MS Word. The data can then be displayed in a program such as RapidForm 2004. Once the data points are stored on the computer, they can be manipulated to be displayed in a program of the user's choice. For more advanced applications, the computer may also need a compiler for the user's choice of programming languages.

3.6 Summary

The components of the proposed system have been chosen. The LPSM serves as the light-collecting device. A lens is used to focus light onto the active area of the PSD in the LPSM. The lab already has a laser that can be used to scan the scene to be modeled. The LPSM, lens, and laser comprise the data acquisition system.

The data acquisition system will send x and y datasets to the A/D converter board. The data should be able to be connected to the EVM board, along with control signals, and then output the data as digital signals, ready for computation. Once digitized, the data can be sent to the FPGA on the Tektronics platform.

Now that the system has been designed on paper, the different parts of the system need to be tested to find performance boundaries. The system is broken into parts for testing since different sections of the system depend on the performance of other sections. The

data acquisition system, and more specifically the LPSM, is primarily tested because it will determine scene distance, resolution, and frame rate.

The data acquisition system is based primarily on the LPSM, so the LPSM needs to be characterized and tested first. Once the LPSM has been characterized, the rest of the data acquisition system can be built and objects can be modeled. Using calibrated objects, the accuracy of the system can be studied as well as how to fix error. Then, laser scanning systems can be evaluated to find the best approach for controlling the laser for the final system.

4 LENS CHARACTERIZATION

A lens is attached to the LPSM using an SM1A10 C-Mount adapter from Thorlabs. The lens focuses light from a large scene onto the small active area of the LPSM and determines the field of view. Tests must be conducted to find the distance between the lens and the LPSM for best focus.

4.1 Lens Field of View

The lens has an associated field of view. As the scene moves farther away from the lens, a larger area can be seen. The field of view is based on the focal length of the lens, 13 mm, and the size of the active area that the image is trying to be focused on, which is 4 mm by 4 mm for the LPSM.

As seen in Figure 4.1, geometry rules can be used to find the field of view size.

Using similar triangles, a proportion can be found:

$$\frac{\frac{s}{2}}{f} = \frac{\frac{p}{2}}{d}, \tag{23}$$

where s is the active area of the LPSM, f_0 is the focal length, d is the distance from the lens to the scene, and p is the field of view length. Filling in the known values for variables and simplifying with algebra, the field of view is approximately equal to one-third of the distance from the lens to the scene.

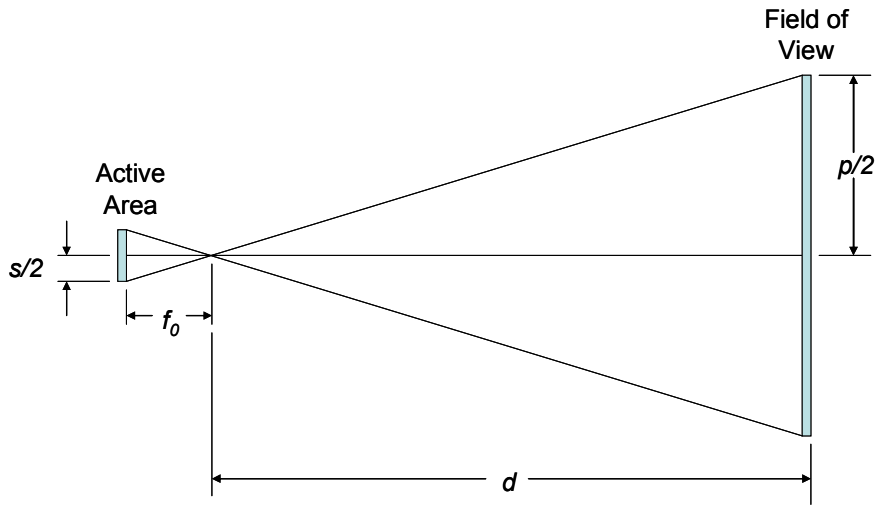

Figure 4.1: Geometry can be used to find the lens field of view.

4.2 Focusing Glass Experiment

A lens is used to collect light and focus the light on a plane behind the lens. The place where the light is focused behind the laser depends on the focal length of the lens and the distance from the lens to the object that needs to be in focus. These three variables are related by:

$$\frac{1}{p}+\frac{1}{q}=\frac{1}{f}, \tag{24}$$

where p is the distance from the object to the lens, q is the distance from the back of the lens to the plane where the image is focused, and f is the focal length.

Laser light shines at a much higher intensity than the rest of the background light. The laser light is also focused at a point. As the point becomes smaller, the light becomes more intense, and it appears like it is coming from infinity. Therefore, p is approximately infinity. As p approaches infinity, then q approaches f.

A laser can be reflected off of a surface in front of the lens. If a slightly opaque surface is placed behind the lens, then the laser light, as focused by the lens, can be seen. As the surface is held at different distances away from the lens, the laser light goes in and out of focus. Starting close to the lens, the laser light is unfocused. As the surface is moved farther away from the lens, the laser light becomes more focused until the surface is approximately the distance of the focal length away from the lens. At this point, the laser light appears as a pinpoint of light. As the surface continues to move further away from the lens, the laser light goes out of focus.

Two types of transparencies were used as a focusing glass to try to see the focused and unfocused laser light. The white film transparency was too opaque and reduced the power of the laser too much to see the laser spot unless it was almost perfectly focused, as seen in Figure 4.2. A slightly less opaque transparency was also used. The more transparent film allowed more laser power through so that unfocused laser could be seen better.

4.3 Lens Filter Characterization

A filter can be placed on the lens to try to help reduce the amount of background light hitting the LPSM. The filter only allows light of specified wavelengths through. All other light hitting the filter does not pass through.

A spectral meter can be used to find the wavelengths that are allowed to pass through the filter. With the help of Phil Evans in the University of Tennessee Physics Department, the Shimadzu Scanning Spectrophotometer UV-250 was used with a wavelength range of 190 nm to 900 nm. The result was printed on thermal paper and shows a peak wavelength of 690 nm with a tolerance of about ±10 nm.

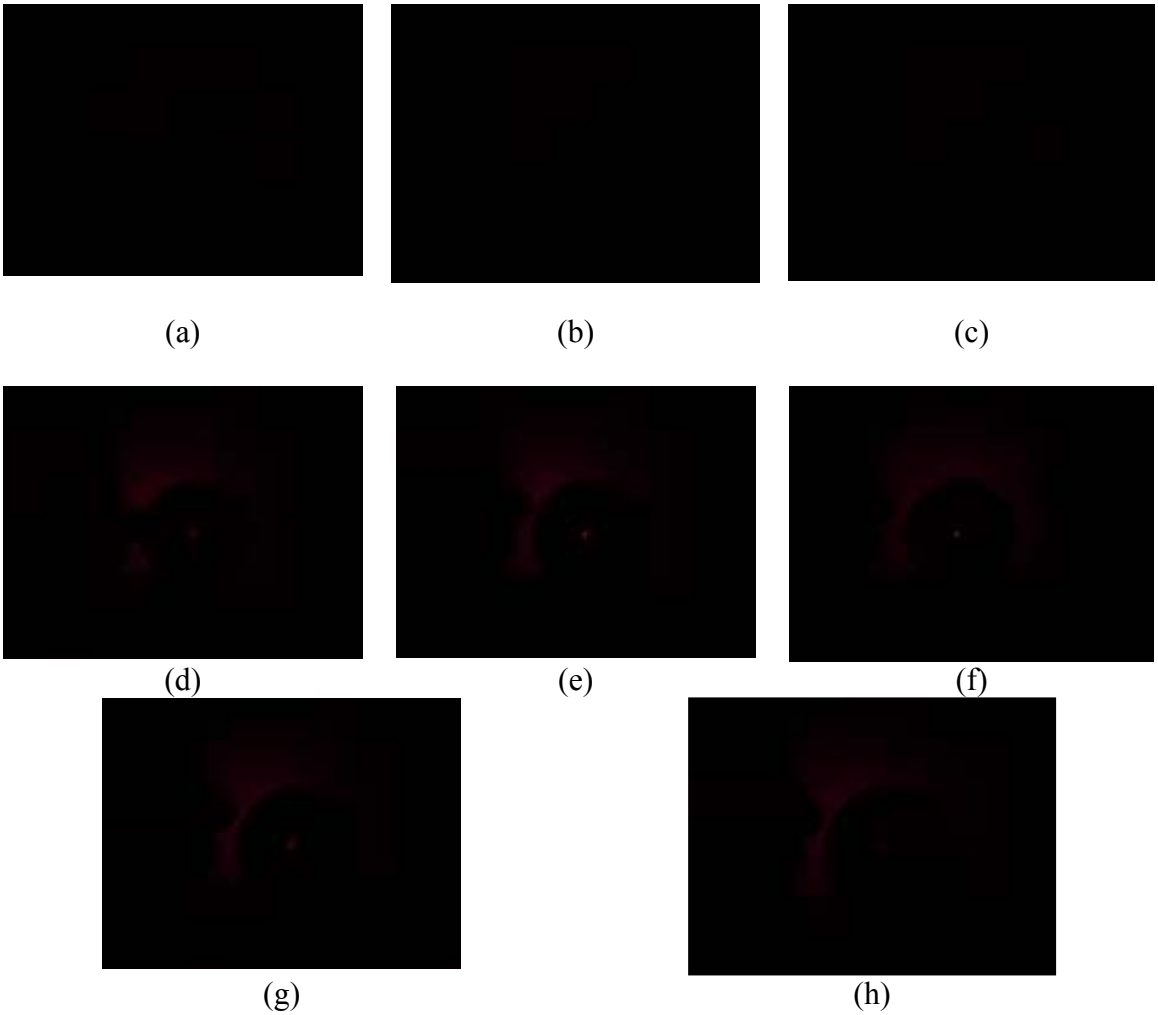

Figure 4.2: As the white film is pulled further away from the lens, the laser point goes from (a) out of focus, (b) to in focus at distance f, (c) and then out of focus, but cannot be seen well. As the more clear transparency is pulled away from the lens, the laser point goes from (d) out of focus, (e) to more in focus, (f) to focused at distance f, (g) to out of focus, (h) and then completely out of focus.

To help view the graph, points were taken from the printout graph and were input into Excel. Figure 4.3 shows a peak wavelength of 690 nm with a tolerance of approximately ±10 nm.

(a) (b)

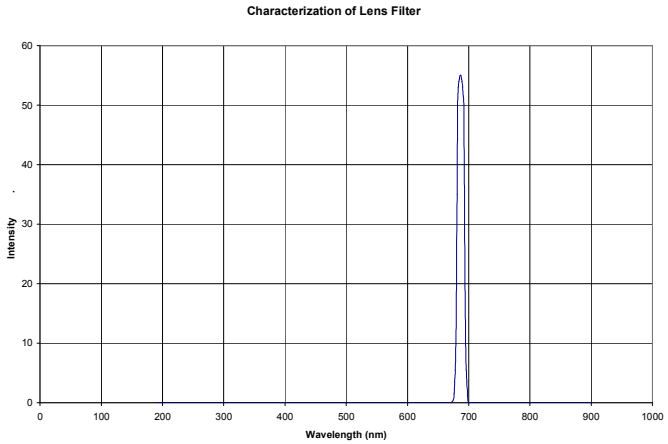

(c)

Figure 4.3: (a) A filter is placed on the lens to help with background light (b)The spectrophotometer shows what wavelengths pass through the filter. (c) The spectral analysis was input into Excel for a clearer graph.

5 LPSM CHARACTERIZATION AND LASER TESTS

The specification of the LPSM gives a range of light intensity levels for the operating region as well as the response time. These factors need to be tested for validation and to determine the requirements for other parts of the data acquisition system, such as laser power and wavelength for the point laser. Characterizing the LPSM will give system performance boundaries such as scene distance and resolution.

5.1 General Experiments and Preparation

Before other characterization experiments can occur, the basic operation of the LPSM and the laser must be known, such as the response time and the wavelength. Validating the response time of the LPSM gives a better idea of the possible resolutions. The laser must be characterized to validate its wavelength. Since the laser is high power, filters can be made to vary the laser power level for future experiments.

5.1.1 LPSM Response Time from Specification

When light hits the active area of the LPSM, the photovoltaic effect occurs, creating a current. The currents travel to the electrodes and are then converted into normalized voltage levels corresponding to the x and y positions. The length of time required for good values to appear on the outputs once there is a valid input is known as the response time and can be found from the frequency response diagram shown in Figure 5.1, given in the specification.

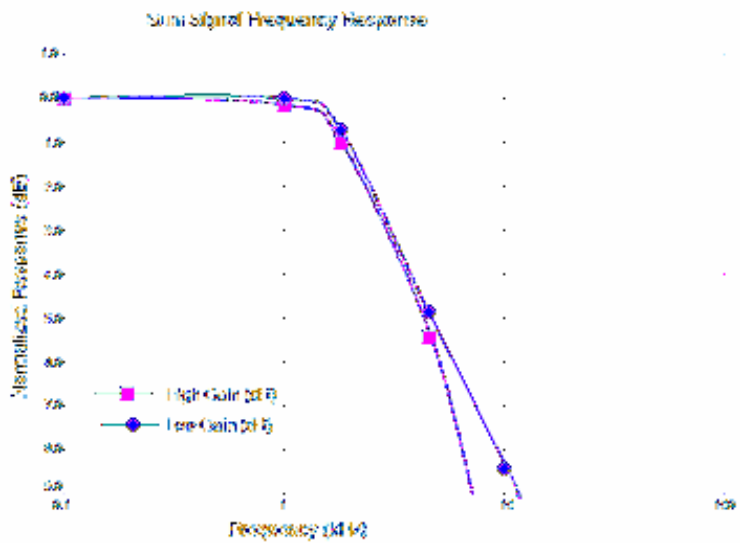

Figure 5.1: The response time can be found from the frequency response diagram.

To solve for the rise time or the response time, the time it takes for the signal to change from its 10% voltage value to its 90% voltage value needs to be found. Since the signal is DC, a step function can approximate the signal. Therefore, the voltage equation is:

$$V = V_{in}(1 - e^{-\frac{t}{\tau}}). \tag{25}$$

To find the time it takes to rise from 10% of the voltage to 90% of the voltage, compute:

$$t_{10\%-90\%} = t_{90\%} - t_{10\%}. \tag{26}$$

At $t_{10\%}$, V=0.1V_{in}, and at $t_{90\%}$, V=0.9V_{in}. By plugging these values into the voltage equation and then plugging those values into the time equation, it can be found that:

$$t_{10\%-90\%} = 2.195\tau. \tag{27}$$

The frequency at the -3dB point is inversely proportional to the time constant according to:

$$F_{3dB} = \frac{1}{2\pi\tau}. \tag{28}$$

Therefore, by substitution:

$$t_{10\%-90\%} = \frac{0.35}{F_{3dB}}. \tag{29}$$

From the above graph, the -3dB point is at approximately 4 kHz. By subbing 4 kHz into the above equation, the rise time is approximately 88μs. The Noah Corporation claims that the LPSM has a response time of 100μs. Since the frequency had to be approximated from the graph, it stands that 100μs seems to be close to the true response time of the LPSM.

5.1.2 LPSM Response Time from Experiment

If the LPSM responded ideally, then the x and y signals would look perfectly triangular when the laser sweeps through the field of vision. However, the signal has a curve in it. The curve could be due to the response time of the LPSM or due to edge distortion. Therefore, the response time of the LPSM needs to be tested. The procedure followed was:

1. Place the laser next to the LPSM and aim the laser so that it registers at 5V on the oscilloscope.
2. Place the poster 3 inches from the LPSM.
3. Set the oscilloscope to trigger on the rising edge.
4. Turn the laser on and hold a thick object between the LPSM and poster to block the beam, as shown in Figure 5.2.
5. Quickly remove the object. Capture the image on the oscilloscope and measure the rise time.
6. Move the poster 1 inch further away and repeat.

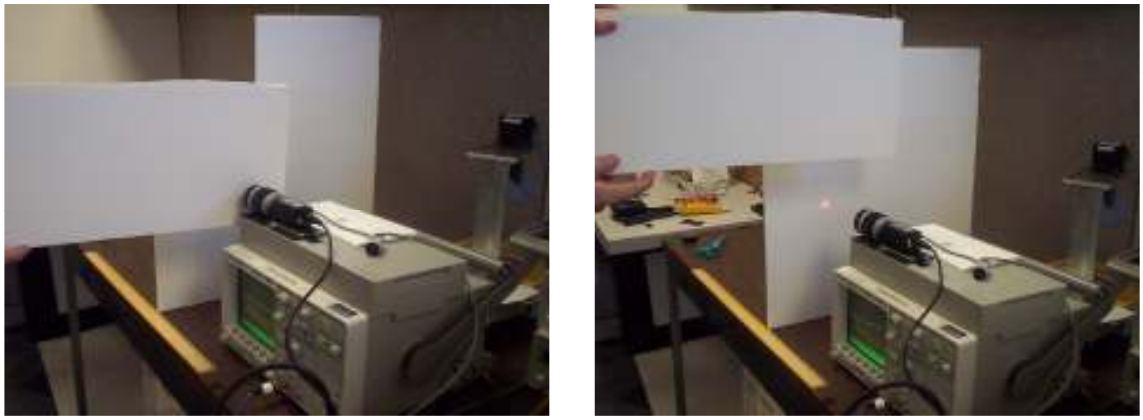

(a) (b)

Figure 5.2: (a) A piece of foam blocks the laser so that the LPSM does not see anything. (b) As soon as the piece of foam is removed, the laser is present, acting like a step function. The rise time can then be measured using the oscilloscope.

From the experiment in Section 5.4.5, the LPSM can only pick up the laser at distances within 11 inches, so the rise time was only recorded for distances between 3 inches and 11 inches. The oscilloscope has a function to measure the rise time of the signal, as seen in the waveforms in Figure 5.3.

The response time changes with distance. The shape of the curve does not appear to be linear. Although the spec says that the response time should be approximately 100 µs, the response time ranges from 480 µs to 900 µs. The response time also increases as distance increases.

Even though the laser power is within the operation threshold of the LPSM, the power at different distances may cause the discrepancy in the rise times. Table 5.1 summarizes the results for all distances.

5.1.3 Laser Characterization

To perform tests on the PSD or LPSM, a single point laser is used. Filters are placed in front of the laser to create a variety of power levels for testing. The laser used is the LASIRIS <500mW red laser, as seen in Figure 5.4. The laser is a point laser, but has a large fan angle. Therefore, if the laser strikes an object more than about two feet from the source, the beam appears to be a small line, growing larger with distance. Lenses are available to be placed in front of the laser to create a variety of shapes.

(a) (b) (c)

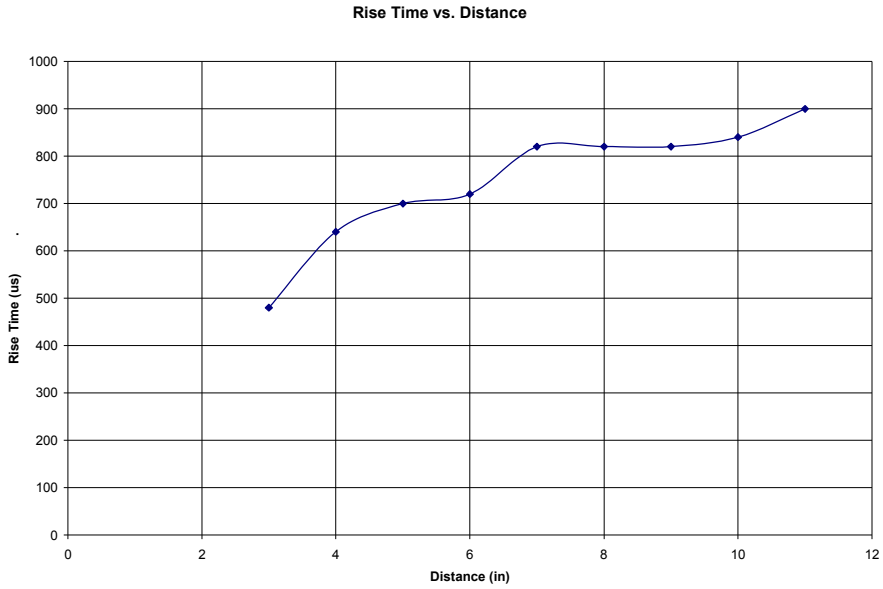

(d)

Figure 5.3: The oscilloscope measures the rise time of the signals, as shown for the waveforms at (a) 3 inches, (b) 7 inches, and (c) 11 inches. (d) The rise time is plotted again the distance.

Table 5.1. LPSM rise time at different distances

Distance (in)	Rise Time (μs)
3	480
4	640
5	700
6	720
7	820
8	820
9	820
10	840
11	900

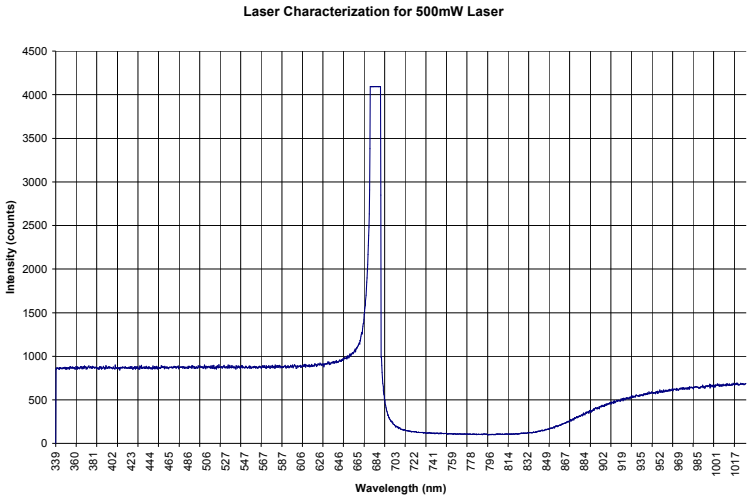

(a) (b)

Figure 5.4: (a) The <500mW laser from LASIRIS is used to perform experiments. (b) The spectral meter shows the characterization of the laser.

The Ocean Optics USB 2000 Spectral Meter was used to find the wavelengths that are emitted from the laser. The beam of the laser is pointed into a collecting area on the spectral meter. The spectral meter then creates a chart showing how many photons in a span of wavelengths are hitting the collecting area. A bell curve forms around the peak intensity wavelength. The laser emits mostly wavelengths at approximately 690nm, but has a tolerance of about ±10nm.

5.1.4 Filter Creation

The laser used to perform the experiments is rated at <500mW. To lower the power, filters are created using PowerPoint. A black box is first created and copied to create four rows of four black boxes each. The opaqueness of the boxes is changed so that the boxes range from 0% to 100% at 6.25% increments. The filters are placed directly in front of the laser. Depending on the opaqueness of the box, a different amount of laser light will be allowed to pass.

The amount of light that is able to go through the transparency also depends on the type of transparency. Three types of transparencies were tried. The first transparency, seen in Figure 5.5, was white film. The white film had too much color in it and therefore did not allow much of the laser light through. The filters were also printed on a clear transparency especially created for printing on HP printers.

(a) (b)

(c)

Figure 5.5: (a) The filters were printed on a white film transparency and (b) on a clear transparency. (c) The filter attached to the laser using foam board.

The filters were also printed on another clear transparency paper. However, the color on the third transparency was not very uniform. Therefore, it was decided to use the HP transparency instead of the third type of transparency.

Next, a way to hold the filter close to the laser was needed. A circle was cut into the middle of a piece of foam board. The laser could be placed into the circle, and then the appropriate filter could be pinned to the foam board. Therefore, the correct filter could lay flat at the origin of the laser beam and could be easily changed.

The filters diffused the beam in multiple directions, as seen in Figure 5.6. There was a spot that appeared where the majority of the laser beam intensity passed through the filter, but there was a lot of light scattered around the spot. As the filter allowed less light through, the light was diffused more and the intense spot was less apparent. By 75% opacity, the light could barely be seen on the poster, so filters greater than or equal to 75% opacity were not used. The diffusion, if not symmetrical, could cause inconsistencies in the data since a PSD takes an average of all light in the scene.

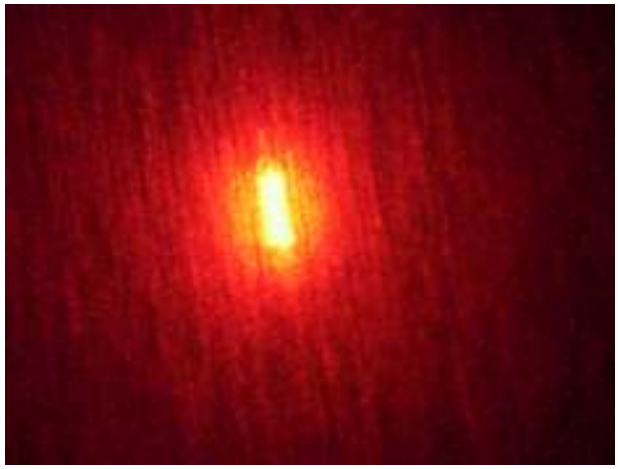

Figure 5.6: The filter caused the laser beam light to scatter, although there was a more intense spot in the middle.

5.2 Tests with White Poster

According to the specifications for the LPSM, it is expected that a laser can be shown in front of the LPSM, and as the laser moves across the scene, the voltage output should vary from -10 V to +10 V, linearly. The laser is first reflected off of a white poster board so that the LPSM can be tested with a uniform surface that does not absorb much of the laser power. Environment variables such as background light, laser power levels, and scene distance are tested to see how the LPSM reacts.

5.2.1 Voltage and Distance Range at Different Light Levels

In order to try to get consistent, reproducible data, some extra steps were taken. First, all items on the table between the poster board and LPSM/laser setup were removed. Next, the table was completely wiped down and dried off to remove any extra dirt or dust. During the testing, other measures were taken, such as the background lux level, before each filter measurement to ensure comparable light levels.

The poster board was pinned to the cubicle wall to cover as much area as possible. Six green pins were used on the edges of the poster board and on the overlap of the 2 pieces, as far away from the field of view as possible. The oscilloscope and power supply were placed six feet away from the poster board. The LPSM was set on top of the power supply, allowing it to be about 12 inches off of the table. According to calculations from the lens, the field of view from six feet should be approximately two feet by two feet, so holding the LPSM one foot off of the table should not cut off the field of view. Two multi-meters were attached to the outputs of the LPSM to read the x and y voltage levels. The laser was set on a tripod next to the LPSM and was controlled with a pan-tilt.

(a)

(b)

(c)

Figure 5.7: (a) The system is setup so that the LPSM and laser are 6 feet from the poster. Two lux readings were taken with the meter (b) sitting on the tabletop and (c) facing the scene.

A set procedure was used:

1. Set the lux meter on the table, as shown in Figure 5.7. Stand somewhere and in a position that you can remember. Every time this reading is taken, stand in the same position so that reflections and absorptions of light from your body and clothing remain fairly constant.
2. Record the reading
3. Hold the lux meter up to the lens, facing away from the lens. Stand somewhere and in a position that you can remember. Every time this reading is taken, stand in the same position so that reflections and absorptions of light from your body and clothing remain fairly constant. These lux meter measurements are to establish that approximately the same background light level is present for all experiments that are not conducted in the dark.
4. Record the reading.
5. Ensure correct filter is pinned in front of laser.

6. Turn on laser.
7. Move laser to the left. Voltage readings should decrease. When they become stable and begin increasing, mark the point and record the voltage.
8. Move laser to the right. Voltage readings should increase. When they become stable and begin decreasing, mark the point and record the voltage.
9. Move the laser up. Voltage readings should decrease. When they become stable and begin increasing, mark the point and record the voltage.
10. Move the laser down. Voltage readings should increase. When they become stable and begin decreasing, mark the point and record the voltage.
11. Take the ruler and measure the distance between the horizontal points and vertical points. Record.
12. Move the laser back to the center of the poster board, so that it is in front of the LPSM.
13. Get the laser power meter and hold the sensor 1 inch from laser. Record.
14. Hold the laser power meter sensor at the poster board, with laser hitting it, as seen in Figure 5.8. Record value.
15. With the laser hitting the middle of the poster board, hold the laser power meter sensor at the lens, facing the poster board. Record value.

(a) (b) (c) (d)

Figure 5.8: Laser power meter was used to read laser power at (a) the laser, (b) the poster board, and at the lens, as can be seen from (c) the front and (d) the back.

16. Repeat with new filter.
17. Once all measurements have been taken with all filters, then repeat the experiment with a different light level or with lens filter.

The white film transparency was used in the dark with the results shown in Table 5.2. The voltage range was so low even with a 0% and 6% filter that it was determined that the white film took away too much of the laser's power to give good readings. Therefore, the white film transparency was disregarded for further tests.

Tables 5.3-5.5 summarize the data for different background light levels and with or without the lens filter.

Table 5.2. Experiment with no lens filter, no background light, white transparency

Filter	Power 1 inch from laser (mW)	Power at Poster (mW)	Power at Lens (mW)	Room Lux Table (Lux)	Room Lux Lens (Lux)	Min Voltage (V)	Max Voltage (V)	Voltage Change (V)
0%	3.73	0.104	0.013	0	0	9.55	10	0.45
6%	1.92	0.059	0.1	0	0	9.63	9.78	0.15

Table 5.3. Experiment with no lens filter, daylight, clear transparency

Filter	Power 1 in. from laser (mW)	Power at Poster (mW)	Room Lux Table (lux)	Room Lux Lens (lux)	Min Voltage (V)	Max Voltage (V)	Change in V (V)	Distance (in)	Volt/In (V/in)
0%	40	29.9	892	395	-0.5	1.3	1.8	22	0.0818
6%	40	4.04	898	361	0.1	1.06	0.96	23.5	0.0409
13%	40	6.55	892	388	-0.16	0.99	1.15	20	0.0575
19%	40	3.27	890	375	-0.01	0.8	0.81	18.5	0.0438
25%	28.5	0.722	922	349	0.12	0.65	0.53	18.25	0.0290
31%	24.01	0.228	860	270	0.22	0.6	0.38	17.75	0.0214
38%	14.3	0.186	860	291	0.26	0.5	0.24	15.75	0.0152
44%	8.59	0.188	877	301	0.28	0.48	0.2	15	0.0133
50%	10.25	0.205	863	294	0.3	0.5	0.2	17.25	0.0116
56%	8.65	0.168	903	289	0.33	0.49	0.16	15.25	0.0105
63%	6.8	0.142	858	326	0.31	0.5	0.19	15	0.0127
69%	7.17	0.19	873	261	0.28	0.44	0.16	19.5	0.0082
75%	6.04	0.143	872	313	0.36	0.46	0.1	16.5	0.0061

Table 5.4. Experiment with lens filter, daytime, clear transparency

Filter	Power 1 in from laser (mW)	Power at Poster (mW)	Room Lux Table (lux)	Room Lux Lens (lux)	Min Voltage (V)	Max Voltage (V)	V Change (V)	Distance (in)	Volts per inch (V/in)
0%	40	30.93	1023	445	5.13	10	4.87	35.25	0.1382
6%	40	5.09	978	398	7.07	10	2.93	36	0.0814
13%	40	7.39	1027	415	6.33	9.86	3.53	35	0.1009
19%	40	3.97	1016	452	6.74	9.9	3.16	34	0.0929
25%	24.94	0.678	981	423	7.91	9.9	1.99	34	0.0585
31%	20.78	0.222	1012	409	8.66	10	1.34	29	0.0462
38%	12.73	0.148	1007	459	9.08	10	0.92	34.5	0.0267
44%	10.03	0.162	1012	463	9.24	10	0.76	26	0.0292
50%	9.19	0.161	1035	445	9.18	9.83	0.65	32.5	0.0200
56%	8.3	0.195	1030	467	9.32	10	0.68	29.5	0.0231
63%	6.71	0.152	967	501	9.34	9.92	0.58	31.25	0.0186
79%	6.52	0.147	1013	512	9.3	10	0.7	33.5	0.0209
75%	6.38	0.099	1027	458	9.41	10	0.59	30.25	0.0195

Table 5.5. Experiment with no lens filter, no background light, clear transparency

Filter	Power 1 in from laser (mW)	Power at Poster (mW)	Room Lux Table (lux)	Room Lux Lens (lux)	Min Voltage (V)	Max Voltage (V)	Change in V (V)	Distance (in)	Volt/In (V/in)
0%	40	30.14	0	0	-0.86	10	10.86	28.5	0.3811
6%	40	4.38	0	0	1.73	9.78	8.05	32	0.2516
13%	40	5.34	0	0	1.11	9.7	8.59	35	0.2454
19%	40	3.45	0	0	2.14	9.68	7.54	31.75	0.2375
25%	33.19	0.42	0	0	4.22	9.85	5.63	33.5	0.1681
31%	21.3	0.12	0	0	5.5	9.82	4.32	31.5	0.1371
38%	12.28	0.103	0	0	7	10	3	29.5	0.1017
44%	10.54	0.105	0	0	7.25	10	2.75	26.25	0.1048
50%	9.65	0.125	0	0	7.36	10	2.64	25	0.1056
56%	8.66	0.106	0	0	7.7	10	2.3	24	0.0958
63%	6.12	0.08	0	0	7.94	10	2.06	34	0.0606
79%	6.4	0.052	0	0	8.1	10	1.9	23.5	0.0809
75%	5.45	0.063	0	0	8.28	10	1.72	25	0.0688

First, it can be seen that as the power from the output source decreases, the minimum voltage increases, as seen in Figure 5.9. Next, as the laser power decreases, the maximum voltage power tended to stay fairly constant, decreasing only slightly. Power output from the source was compared with amount of voltage change. Figure 5.10 shows that as power decreases, the amount of voltage change decreases.

Next, the distance where the minimum voltage and the where the maximum voltage were found was compared to the laser power from the source. The distance tended to remain constant, regardless of the laser power change.

Finally, the amount of voltage change was compared with the distance that voltage change occurred. This parameter showed how quickly the voltage changed per inch. With faster voltage change, the resolution would be better. With slower voltage change, the resolution would be worse.

Overall, the module does not seem consistent in telling the voltage at a specific point. The voltage at a point seems to depend on the background light and on the power of the laser. The lens filter seemed to help give better results than operation in the light; however, operation in the dark seemed to give the best and most consistent results.

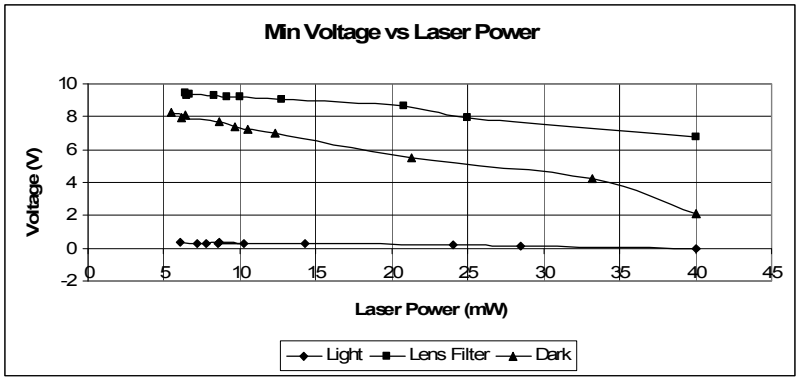

(a)

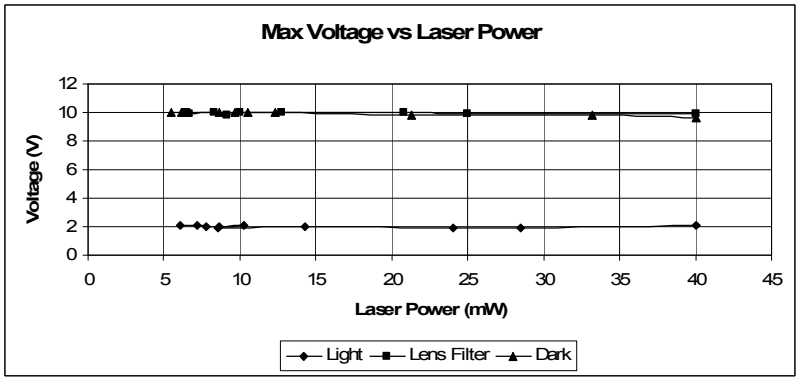

(b)

Figure 5.9: (a) As the laser power decreases, the minimum voltage increases. (b) The maximum voltage stayed fairly constant.

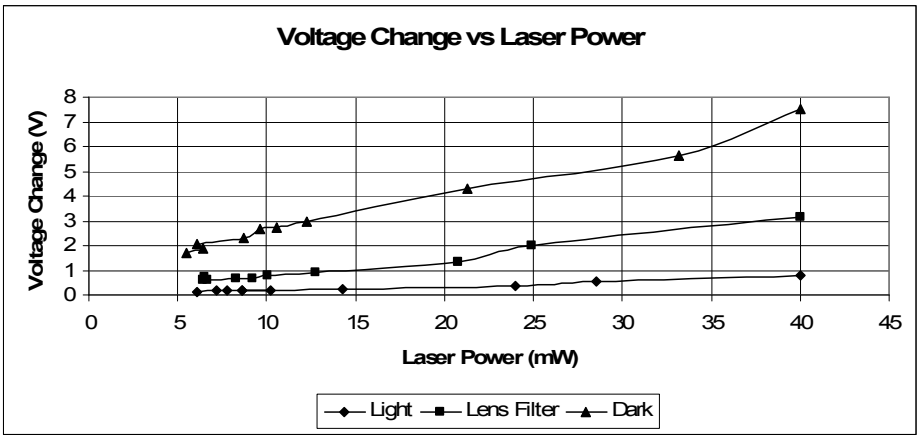

(a)

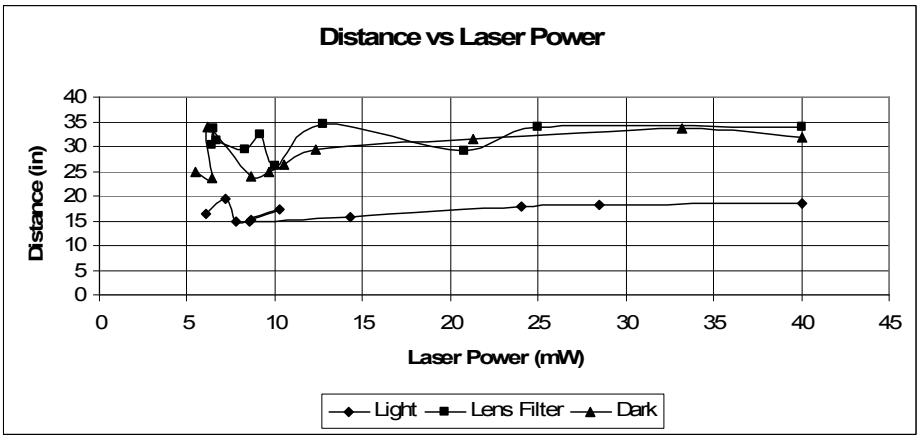

(b)

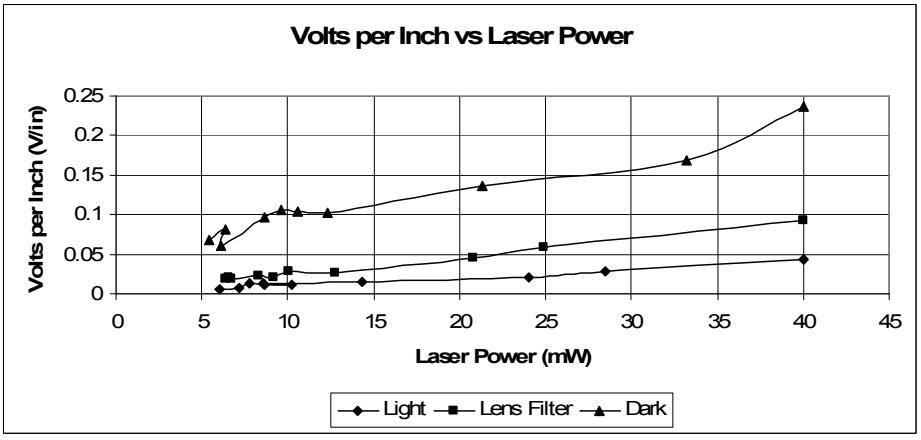

(c)

Figure 5.10: (a) The chart compares laser power at the source with voltage change. (b) Distance between minimum and maximum voltages remain fairly constant regardless of laser power. (c) As the laser power decreases, the rate of change in voltage decreases, giving worse resolution.

5.2.2 Voltage at Set Distance

Moving the laser as far to the left and right as possible and then checking the voltage results in a variety of distances. The voltage tends to change linearly in the middle of the field of view, but as the laser reaches the edges of the active area of the LPSM, the voltage change reduces, becomes stable, and then begins to change in the opposite direction. Therefore, a better judge of change in voltage for different environments and distances would be to pick two points in the field of view of the LPSM and check the voltages at these two points.

Very similar procedural steps as the voltage and distance range experiment were used:

1. Set the lux meter on the table. Stand somewhere and in a position that you can remember. Every time this reading is taken, stand in the same position so that reflections and absorptions of light from your body and clothing remain fairly constant.
2. Record the reading
3. Hold the lux meter up to the lens, facing away from the lens. Stand somewhere and in a position that you can remember. Every time this reading is taken, stand in the same position so that reflections and absorptions of light from your body and clothing remain fairly constant. These lux meter measurements are to establish that approximately the same background light level is present for all experiments that are not conducted in the dark.
4. Record the reading.
5. Ensure correct filter is pinned in front of laser.
6. Turn on laser.
7. Move the laser to point on the left mark. Record the voltage.
8. Move the laser to the center point. Record the voltage.
9. Move the laser to the right mark. Record the voltage.
10. Change the filter, light conditions, distance, or other parameter and repeat.

The poster was six feet away from the laser and LPSM for all tests. The first test had all of the lights on, giving a reading of 1058 lux, and had no lens filter, giving the data in Table 5.6.

Tables 5.7-5.9 summarize the data for different background light levels and with or without the lens filter.

Table 5.6. Data with background light, no lens filter

Filter	Power 1 in from laser (mW)	Min Voltage (V)	Max Voltage (V)	Change in Voltage (V)	Distance (in)	Volt/In (V/in)	X Center (V)
No filter	40	-0.78	0.74	1.5200	10	0.1520	0.04
0%	40	-0.68	0.58	1.2600	10	0.1260	0.0200
6%	40	-0.4	0.34	0.7400	10	0.0740	0.0000
13%	40	-0.46	0.39	0.8500	10	0.0850	0.0000
19%	40	-0.36	0.31	0.6700	10	0.0670	0.0100
25%	36.02	-0.21	0.2	0.4100	10	0.0410	0.0000
31%	24.14	-0.15	0.13	0.2800	10	0.0280	0.0000
38%	16	-0.12	0.06	0.1800	10	0.0180	-0.0100
44%	14.48	-0.09	0.04	0.1300	10	0.0130	0.0000
50%	11.8	-0.12	0.03	0.1500	10	0.0150	-0.0200
56%	9.39	-0.11	0.01	0.1200	10	0.0120	-0.0400
63%	7.06	-0.09	0	0.0900	10	0.0090	-0.0400
69%	6.5	-0.11	0	0.1100	10	0.0110	-0.0500

Table 5.7. Data with background light and lens filter

Filter	Power 1 in from laser (mW)	Min Voltage (V)	Max Voltage (V)	Change in V (V)	Distance (in)	Volt/In (V/in)	X Center (V)
No filter	40	7.73	8.56	0.8300	10	0.0830	8.15
0%	40	7.94	8.78	0.8400	10	0.0840	8.32
6%	40	8.37	8.91	0.5400	10	0.0540	8.64
13%	40	8.22	8.89	0.6700	10	0.0670	8.5
19%	40	8.35	8.98	0.6300	10	0.0630	8.77
25%	36.02	8.84	9.14	0.3000	10	0.0300	8.97
31%	24.14	9.12	9.41	0.2900	10	0.0290	9.3
38%	16	9.5	9.66	0.1600	10	0.0160	9.57
44%	14.48	9.74	9.88	0.1400	10	0.0140	9.75
50%	11.8	9.68	9.88	0.2000	10	0.0200	9.7
56%	9.39	9.68	9.8	0.1200	10	0.0120	9.75
63%	7.06	9.81	9.9	0.0900	10	0.0090	9.86
69%	6.5	9.8	9.83	0.0300	10	0.0030	9.82

Table 5.8. Data with dimmed lights and no lens filter

Filter	Power 1 in from laser (mW)	Min Voltage (V)	Max Voltage (V)	Change in V (V)	Distance (in)	Volt/In (V/in)	X Center (V)
No filter	40	1.26	6.89	5.6300	10	0.5630	4.5
0%	40	1.7	7	5.3000	10	0.5300	4.6
6%	40	3.15	6.91	3.7600	10	0.3760	5.07
13%	40	2.74	6.78	4.0400	10	0.4040	4.99
19%	40	3.65	6.96	3.3100	10	0.3310	5.36
25%	36.02	4.74	7.22	2.4800	10	0.2480	6.03
31%	24.14	5.46	7.51	2.0500	10	0.2050	6.52
38%	16	6.51	8.07	1.5600	10	0.1560	7.2
44%	14.48	6.96	8.19	1.2300	10	0.1230	7.63
50%	11.8	6.96	8.32	1.3600	10	0.1360	7.67
56%	9.39	7.12	8.36	1.2400	10	0.1240	7.72
63%	7.06	7.66	8.56	0.9000	10	0.0900	8.1
69%	6.5	7.56	8.5	0.9400	10	0.0940	8.04

Table 5.9. Data with no lights and no lens filter

Filter	Power 1 in from laser (mW)	Min Voltage (V)	Max Voltage (V)	Change in V (V)	Distance (in)	Volt/In (V/in)	X Center (V)
No filter	40	1.87	7.78	5.9100	10	0.5910	5.09
0%	40	2.28	7.83	5.5500	10	0.5550	5.13
6%	40	3.93	7.89	3.9600	10	0.3960	5.97
13%	40	3.45	7.76	4.3100	10	0.4310	5.71
19%	40	4.23	7.85	3.6200	10	0.3620	6.24
25%	36.02	5.42	8.21	2.7900	10	0.2790	6.9
31%	24.14	6.41	8.56	2.1500	10	0.2150	7.6
38%	16	7.43	9.13	1.7000	10	0.1700	8.3
44%	14.48	7.92	9.41	1.4900	10	0.1490	8.59
50%	11.8	7.87	9.45	1.5800	10	0.1580	8.62
56%	9.39	8.07	9.55	1.4800	10	0.1480	8.83
63%	7.06	8.62	9.82	1.2000	10	0.1200	9.18
69%	6.5	8.5	9.6	1.1000	10	0.1100	9.17

From the data, it can be seen that the minimum voltage tends to decrease as the laser power increases, as seen in Figure 5.11. The maximum voltage tends to decrease as laser power increases, as can be seen in Figure 5.12. It follows that the voltage change would increase as laser power increases.

The distance between the maximum and minimum voltages was 10 inches. By dividing the voltage change by 10 inches, the volts per inch is found. High volts per inch means that the voltage level changes faster as the laser point moves, giving better resolution. The volts per inch increases as laser power increases.

5.2.3 Voltage at Set Point with Different Surfaces

Different surfaces have different reflectivity. White surfaces reflect light very well. Red surfaces reflect red light, but absorb most other light. Black surfaces absorb almost all light. Shiny surfaces reflect light differently than diffuse surfaces. The material also causes light to reflect in different ways. Therefore, a tan surface on a cardboard box was tested in comparison to white poster. The same point was marked on both surfaces, so it is expected that for correct operation, the voltage should be the same regardless of what surface is present. The same distance grid that was used in the experiment for voltage at a set point at different distances was used for this experiment.

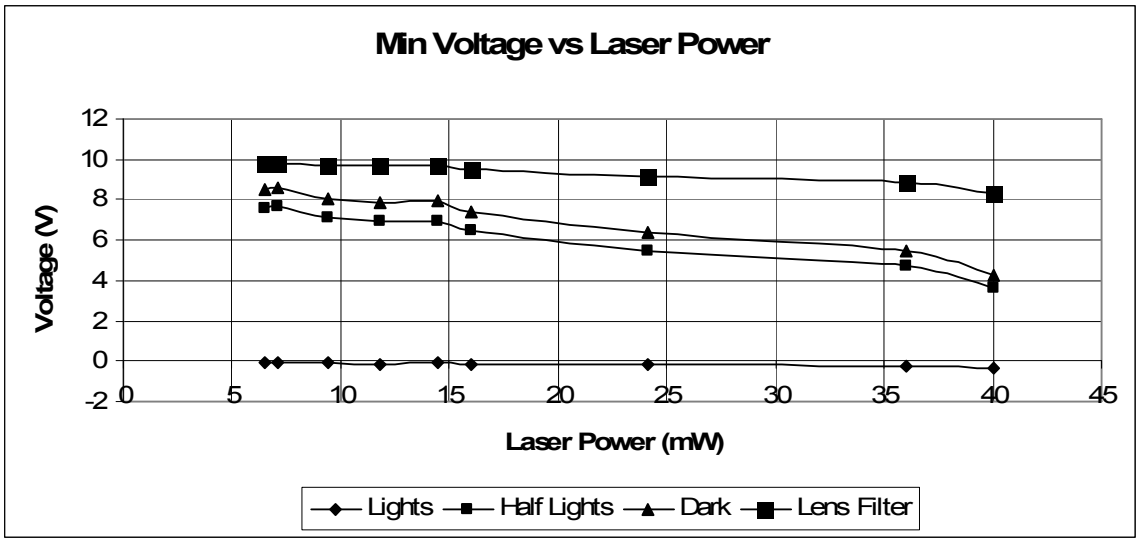

Figure 5.11: The minimum voltages tends to decrease as laser power increases.

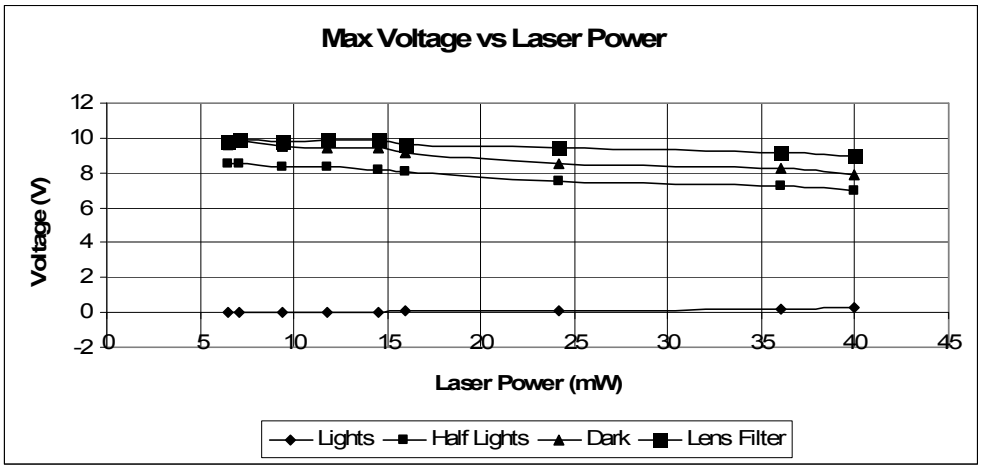

(a)

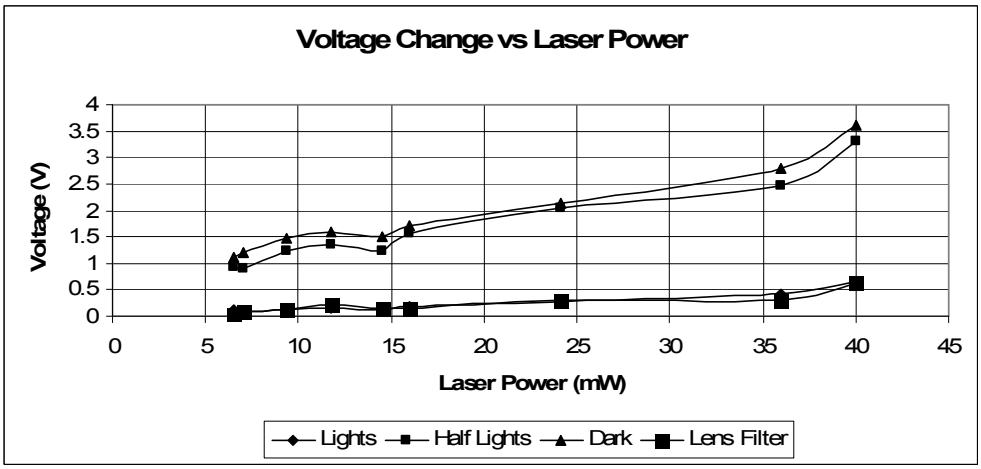

(b)

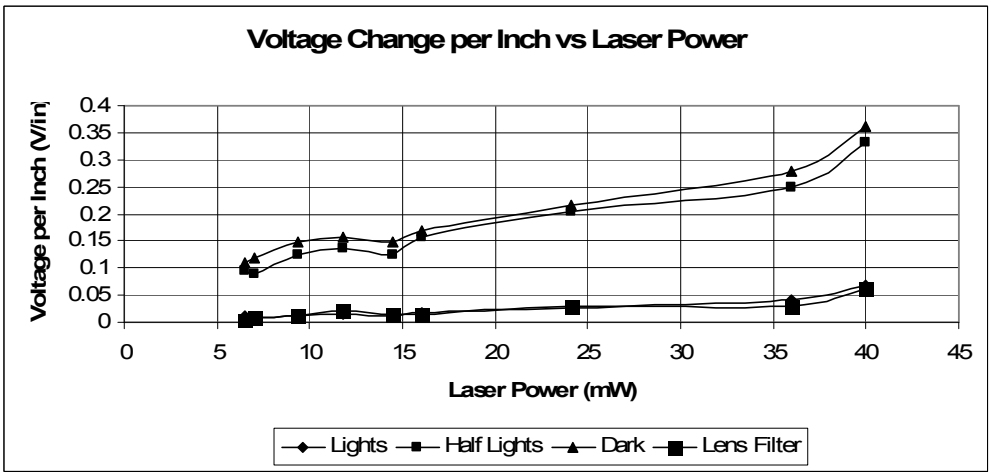

(c)

Figure 5.12: (a) The maximum voltage tends to decrease as laser power increases. (b) The voltage change increases as laser power increases. (c) As the laser power increases, the volts per inch increase, giving better resolution.

The poster was attached to the box so that it could be moved. The point was marked by pushing a push-pin through the spot. When the poster was removed, a tiny hole showed what point to use for the box test.

The procedure was:

1. Align the lens/LPSM to point along the table.
2. Set the box so that the edge is on the table and the front sits directly behind one of the marked distances, as seen in Figure 5.13.
3. Point the laser at the marked point.
4. Record the voltage.
5. Move the box to another distance and repeat.

The data in Table 5.10 was collected and graphed. As seen in Figure 5.14, the voltage levels differ with surface and with distance, even though it is the same point. Therefore, if the system was in use and a voltage level was collected, then it would depend on the surface and distance of the point. This means that the depth cannot accurately be determined because the voltage cannot be translated to a set distance.

5.2.4 Voltage at Set Point at Different Distances

The poster was again mounted on a box so that it could easily be moved to different distances. Six-inch distance increments were measured from the lens and laser setup up to 5.5 feet. A point was marked on the poster near the center. According to projective geometry, since the point is close to the center of the field of view, the voltage should change slightly as the poster is moved further away, but should not change very dramatically. If the point were closer to the edge of the field of view, the voltage would change more.

(a) (b)

Figure 5.13: The box was moved to different distances, like the set point, different distances experiment with poster board.

Table 5.10. Voltage of same point on different surfaces and distances

Distance (ft)	Voltage, Poster (V)	Voltage, Box (V)
1	-1.67	-1.28
1.5	0.05	0.01
2	0.63	1.21
2.5	0.67	1.66
3	1.47	2.19
3.5	1.98	3.19
4	2.43	3.7
4.5	3.21	4.97
5	3.24	4.75

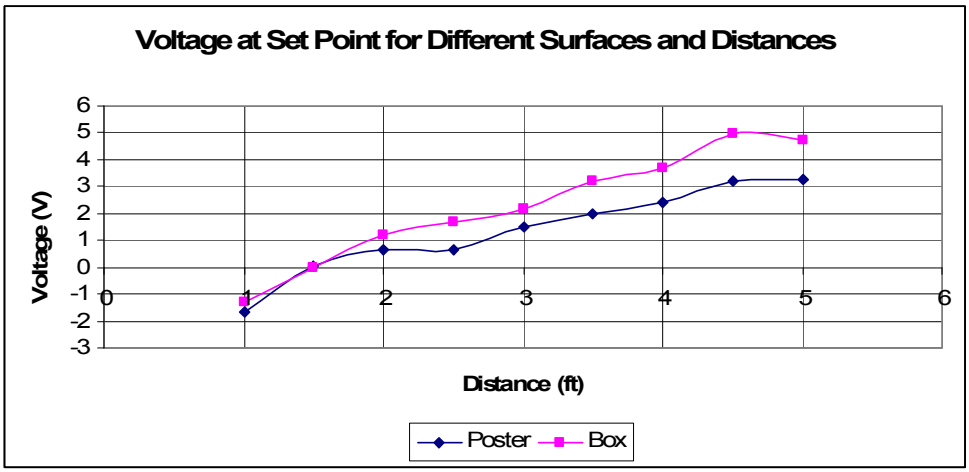

Figure 5.14: The voltages are not the same for different distances and different points.

The procedure was:

1. Align the lens/LPSM to point along the same line as the table.
2. Align the box so that one edge is on the table and the front sits directly behind one of the marked distances.
3. Move the laser beam to hit the marked point.
4. Record the voltage.
5. Move the poster to another distance, as seen in Figure 5.15. Repeat the above steps.

The data in Table 5.11 was collected during the experiment.

As the distance increases, the voltage level increases. The voltage is supposed to remain fairly constant because the point is near the center of the field of view, but the graph shows that the voltage increases about 4.5 Volts. The voltage should change slightly due to projective geometry.

(a)

(b)

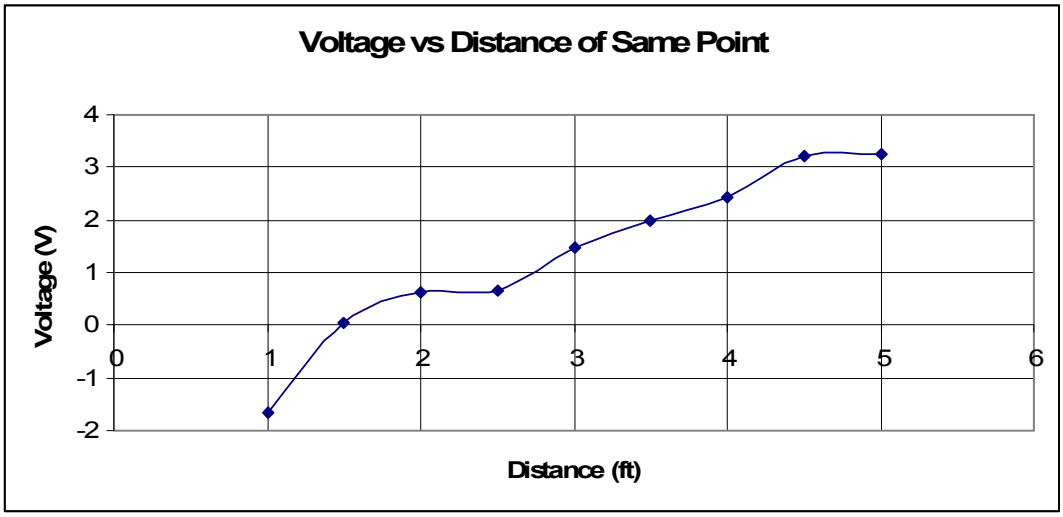

(c)

Figure 5.15: Voltages were taken starting at (a) close distances and then moved (b) further away. (c) The voltage changed dramatically as distance changed.

Table 5.11. Data comparing poster distance to voltage

Distance (ft)	Voltage (V)
1	-1.67
1.5	0.05
2	0.63
2.5	0.67
3	1.47
3.5	1.98
4	2.43
4.5	3.21
5	3.24

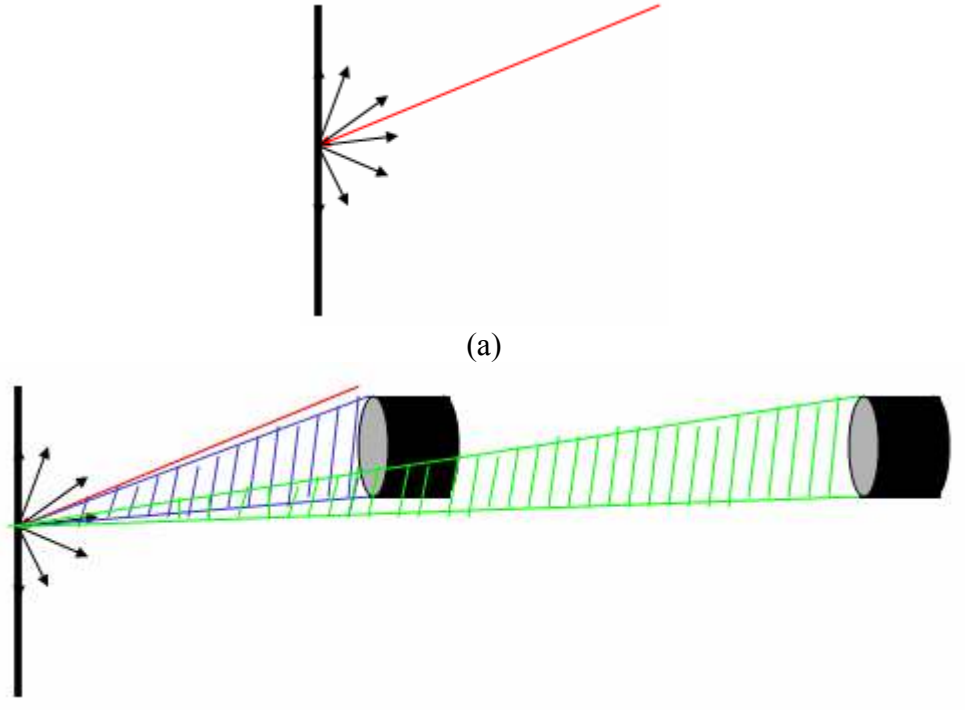

(a)

(b)

Figure 5.16: (a) When a laser hits a diffuse surface, the reflected light is spread out uniformly. (b) The blue triangle shows how the closer lens picks up more light, while the green triangle of the farther away lens picks up less light.

For a diffuse surface, the laser hits the surface and some of the light is reflected and some of the light is absorbed. The light that is reflected spreads out uniformly in all directions, as seen in Figure 5.16.

When a lens is placed facing the surface, it sees some of the reflected light. Two lines can be drawn from the lens to the reflection point, forming a triangular shape. When the light is closer, this triangle covers more incident reflection lines, meaning that it picks up more reflected light. If the lens is moved further away from the scene, then the triangle becomes narrower, and fewer incident rays are picked up, causing less light to hit the lens. Therefore, the reason that the voltages from the LPSM are different with different distances seems to be that it is picking up different amounts of light and thus different amounts of power. At closer distances, more light is picked up, causing a certain voltage reading. As the distance becomes larger, then less light and less power is picked up, changing the voltage.

5.2.5 Testing with Various Lasers

The system was tested with a variety of lasers power levels and colors. Testing with various wavelengths showed to which wavelengths the LPSM was sensitive. Testing with different power levels helped determine system performance boundaries.

Table 5.12. Various lasers tested

Laser Type	Laser Color	Wavelength (nm)	Rated Power (mW)	Actual Power (mW)	Voltage Range (V)	Distance Range (in)
HeCd	Blue	441.6	70	--	8.3-10	16.5
HeCd	Blue	325	20	--	Did not register	
HeNe	Red	652	5	0.13	Did not register	
HeNe	Red	652	30	13	7.8-10	16.5
Ar+	Green	514	7	--	10.9-11.2	--

The poster was set up six feet away from the laser and lens/LPSM. The lens and LPSM faced the poster. The laser was pointed to the same height as the lens/LPSM and moved to the left and right. The voltage change and distance range in the X direction were then recorded, along with the laser specifications. Lasers of under 40mW were checked for their true power output at the source. The data is shown in Table 5.12.

The LPSM did not seem to respond well to the blue laser, even though the blue laser was rated at 70mW. It did respond to the red and green lasers, as long as the power level was sufficient.

The LPSM responded to the green laser at 7mW, though the voltage readings were above the -10V to 10V threshold. The Ar+ laser power could be adjusted from 7mW to 2 W. As the power increased, the laser got brighter. However, if the power was turned up very high, the laser could not sustain the power level for too long and the brightness would diminish. When the laser got above 1 W, the voltage readings went from 9V to -9 volts, although the red indicator light remained red for the entire experiment.

The Ar+ green laser was used last. The green laser could not give readings in the good threshold range even when the power was greater than 500mW. Therefore, it was determined that the LPSM must be more sensitive to wavelengths near the red range.

5.2.6 Conclusions

In these tests, the laser power, the background light level, the distance, and the surface types were varied. Voltage readings were taken at the boundaries of the field of view, as well as in the middle of the field of view.

It was found that results could only be reliably reproduced in the dark. Background light had a big effect on the voltage readings. However, none of the readings from three feet to fifteen feet were within the threshold given on the specification of the LPSM. Therefore, the same experiments may be able to be performed and give consistent, expected results if the laser power level is within the LPSM threshold.

Most of the power of the laser is diffused when it strikes the surface of the poster. Different methods can be used to increase the laser power. The laser itself can be changed by either getting a better focused laser, or by increasing the laser power. Since lasers that are well-focused and high-powered cost thousands of dollars, this option is probably the most expensive. Another option is to change the poster to a specular surface, such as a mirror. The mirror will reflect the majority of the laser, but will only reflect it in one direction.

5.3 Tests with Mirror

The poster board is replaced with a mirror to try to reflect more laser power. By reflecting more laser power, the light level may be within the specified good operation region. Conducting similar tests within the good operation region may result in more consistent results.

5.3.1 Mirror Experiments Setup

More experiments were conducted using a mirror. A mirror is a shiny surface, causing more than 90% of the incident laser light to be reflected. Almost all of the light is reflected at one angle instead of spreading out uniformly like a diffuse surface.

A mirror was acquired that was 4 feet tall by 8 feet wide. The mirror was mounted onto a hand truck, as seen in Figure 5.17, so that it would sit perpendicularly to the floor and be able to be moved easily. Books were placed on the bottom of the hand truck to ensure that the back of the hand truck was standing straight.

Next, a file cabinet was moved to the middle of the floor. The cabinet was lined up so that it sat parallel with the table. The power supply, lens, laser, and other materials were placed on the cabinet. Tape was used to mark where the cabinet was sitting so that the setup could be easily replicated.

Some of the experiments required that the mirror be placed at specified distances away from the lens and laser setup. The mirror also needed to remain perpendicular to the table so that the angle that the laser hit the mirror at did not change. Therefore, the table edge was marked on the floor from 1 foot to 8 feet away from the cabinet. Six inch increments were measured going away from the file cabinet so that the mirror could be set on the tape marks. Two points at each distance were marked to ensure that the mirror's relative angle to the cabinet would be the same.

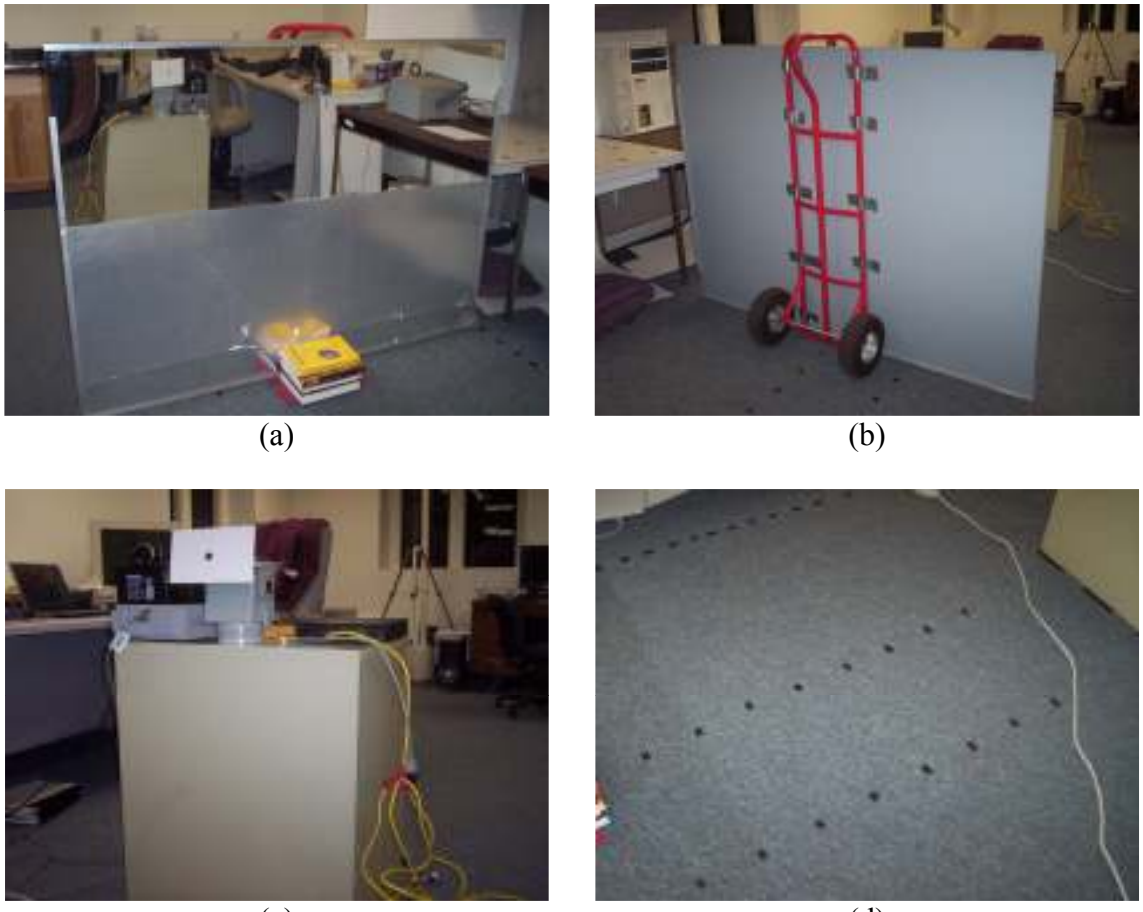

(a) (b)

(c) (d)

Figure 5.17: A large mirror was mounted on a hand truck so that it would sit perpendicularly to the ground and could be moved easily. (a) Front. (b) Back. (c) The lens/LPSM, power supply, laser, and other materials were placed on a filing cabinet. (d) Tape marks on the floor showed six inch increments in distance from the file cabinet.

5.3.2 Laser Power Compared to Poster

The mirror was placed three feet away from the setup. With no lights on, the laser was reflected off of the mirror, into the lens. The laser power behind the lens was then taken, giving the data in Table 5.13. Different filters were used in this experiment. A similar experiment was done with poster board instead of with a mirror and those results are included in the table.

Figure 5.18 gives a chart of the data. The mirror reflects over 90% of the light, and when directed at the lens, gives a much higher power level than the poster. The reflection of the laser light from the mirror depends on the distance between the laser and the lens. The angle at which the laser light reflects depends on the incident angle. No matter where the laser and lens are placed, the distance that the reflection successfully hits the lens is a lot smaller than the field of view used for the poster board. Therefore, as soon as the reflection does not hit the lens, the power goes to zero, so the poster would have a high power reading.

5.3.3 Laser Power at Different Light Levels

The LPSM was removed from the lens and the lens was placed in the setup, aligned with the table. The laser reflected almost perfectly off of the mirror at a single angle. Therefore, the laser can be aligned so that the reflection hit the lens, as seen in Figure 5.19.

Table 5.13. Data on laser power behind lens

Filter	Laser Power (mW)	Power Behind Lens Poster (uW)	Power Behind Lens Mirror (mW)
0%	>40	1.24	19.74
6%	>40	1.07	5.72
13%	>40	1.03	3.79
19%	>40	0.76	1.83
25%	40.00	0.46	0.35
31%	30.37	0.34	0.051
38%	21.28	0.23	0.046
44%	16.36	0.17	0.016
50%	15.21	0.15	0.03
56%	14.96	0.12	0.019
63%	12.39	0.12	0.013
69%	11.47	0.11	0.017

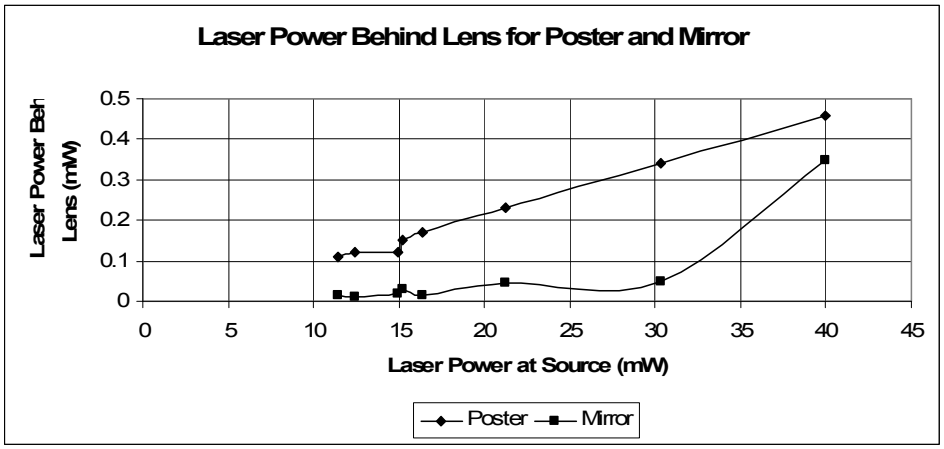

Figure 5.18: When the laser reflection from the mirror hits the lens, then it records a higher laser power than with the poster.

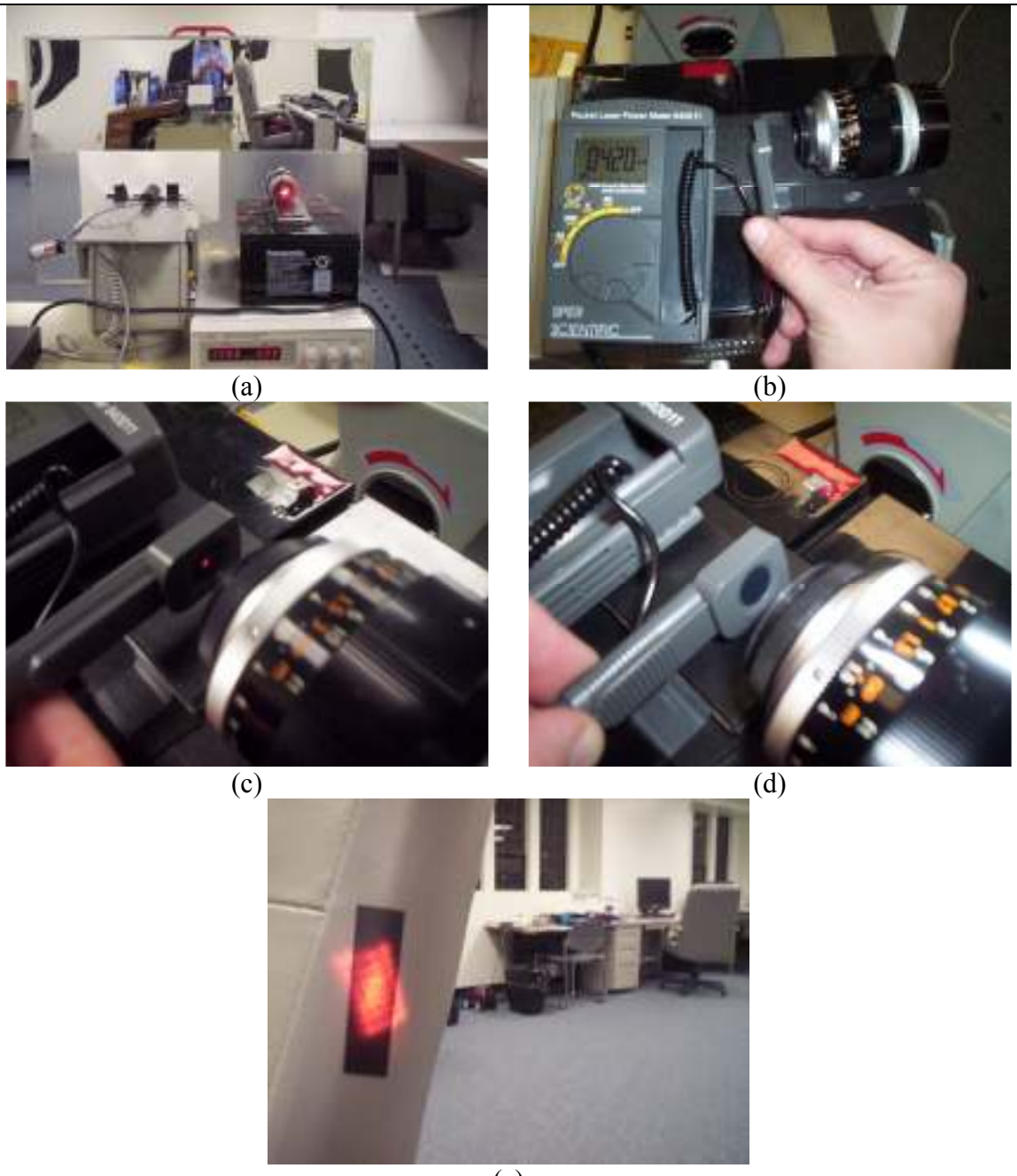

Figure 5.19: (a) The laser can be directed so that the reflection hits the lens. (b) The power of the light getting through the lens can be measured. (c)When laser light is reflected into the lens, then the light can be seen. (d) If the laser light is reflected elsewhere, then no laser light can be seen. (e) The laser is targeted so that the reflection hits the tape instead of the lens.

The lens focuses the light at a certain point behind the lens. The laser power meter can be used to find the power of the light at its focused point. The sensor is held behind the lens where the light becomes the smallest possible point. This point should give the highest power reading because it is the most focused and most intense.

When the laser light reflection is aimed at the lens, then a small light spot can be seen and focused on the sensor of the laser power meter. However, if the reflection is not hitting the lens, then no laser light can be seen coming through the lens.

The power behind the lens needs to be measured with different filters and at different light levels. The following procedure was followed:

1. Line up the lens with the edge of the table.
2. Set up the mirror 6 feet away from the file cabinet.
3. Turn on the laser with desired filter. Using the laser power meter, measure the power at the source.
4. Point the laser so that the reflection hits the lens.
5. Place the laser power meter sensor behind the lens so that the light is focused on the sensor.
6. Record the power reading.
7. Move the laser so that the reflection is targeted onto the black piece of tape.
8. Place the laser power meter sensor behind the lens so that the light is focused on the sensor.
9. Record the power reading.
10. Change the filter on the laser and repeat the above steps.
11. Change the background lighting and repeat the above steps.

The data in Table 5.14 was collected.

When the laser was reflected at the target instead of onto the lens, then no laser light could be seen. The laser power meter was held at different distances behind the lens, but a reading of 0.0mW was always read. This supports the fact that almost all laser light gets reflected at a specific angle.

At the 31% laser light filter, the laser could no longer be seen behind the lens, so no power measurements were able to be taken. Figure 5.20 shows the laser power readings.

From the graph, it can be seen that the laser power behind the lens tends to increase as the laser power at the source increases when no lights are present. The power at half light tends to be more inconsistent. The inconsistencies could be due to the mirror reflections. If different objects are in the mirror, then the light hitting the lens may be slightly different. In the dark, there should be no other reflections, giving better data. In conclusion, the light level does affect the laser power level behind the lens.

Table 5.14. Data comparing power at different light levels

Filter	Laser Power at Source (mW)	Lights On (mW)	Half Lights (mW)	No Lights (mW)
0%	>40	6.27	6.73	6.36
6%	>40	0.88	1.51	0.98
13%	>40	0.71	0.83	1.183
19%	>40	0.43	0.39	0.525
25%	40.00	0.084	0.096	0.092
31%	30.37	*could not see laser	0.0088	0.011
38%	21.28	--	0.016	0.0067
44%	16.36	--	0.0138	0.0065
50%	15.21	--	0.00491	0.0082
56%	14.96	--	0.0179	0.0082
63%	12.39	--	0.00673	0.0062
69%	11.47	--	0.022	0.0041

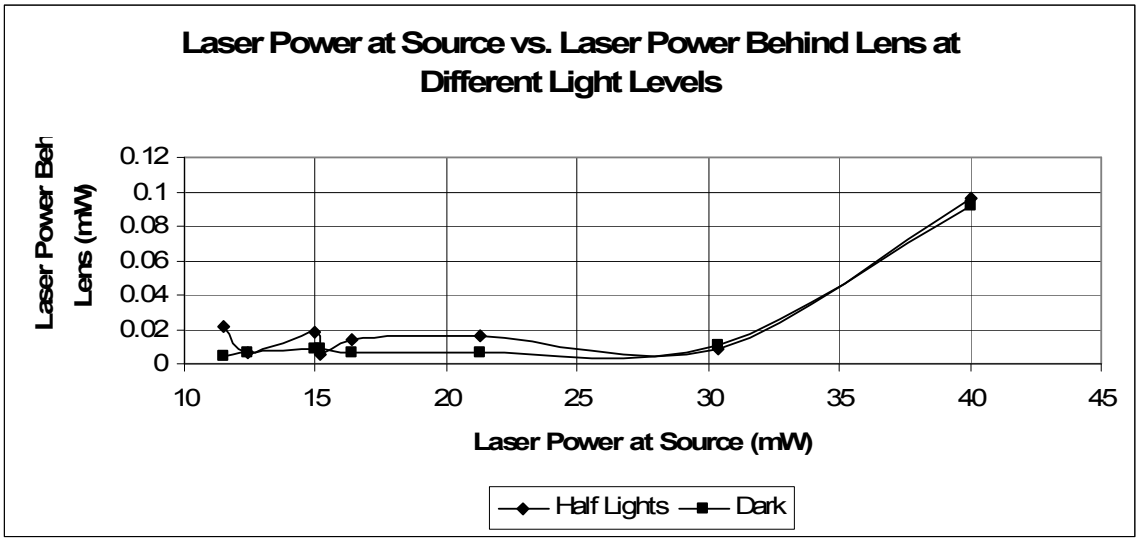

Figure 5.20: The laser power behind the lens depends on the laser power source and background lights.

5.3.4 Laser Power Levels at Different Distances

Next, the laser power levels at different distances were measured. No filters were used on the laser. The following procedure was used:

1. Move the mirror to 6 feet and align it with the table and marks on the floor.
2. Point the laser so that the reflection hits the lens.
3. Using the laser power meter, find the power of the laser behind the lens and record.
4. Change the background light level and repeat.
5. Move the mirror closer by 1 foot and repeat.

The data in Table 5.15 was collected.

The data was used to create the graph in Figure 5.21. The laser power level tends to follow the same trend, regardless of light level. However, the laser power does change according to how much background light is present. This may be due to extraneous reflections in the mirror when any extra light is present. In general, as distance increases, the laser power decreases, as expected. This could again pose inconsistencies in the voltage levels of the LPSM because different power levels seem to cause different voltage readings.

5.3.5 Voltage at 2 Set Points at Various Light Levels

The mirror was set six feet away from the lens and laser setup. Two points were marked and the voltage levels at these points were taken with different filters and at different light levels. This experiment tests to see how much the background light conditions affect the LPSM.

Table 5.15. Data of laser power levels varying background light and distance

Distance (ft)	Lights On (mW)	Half Lights (mW)	No Lights (mW)
3	16.24	15.37	17.4
4	10.27	13.03	11.48
5	5.48	4.65	4.17
6	4.63	9.12	8.47

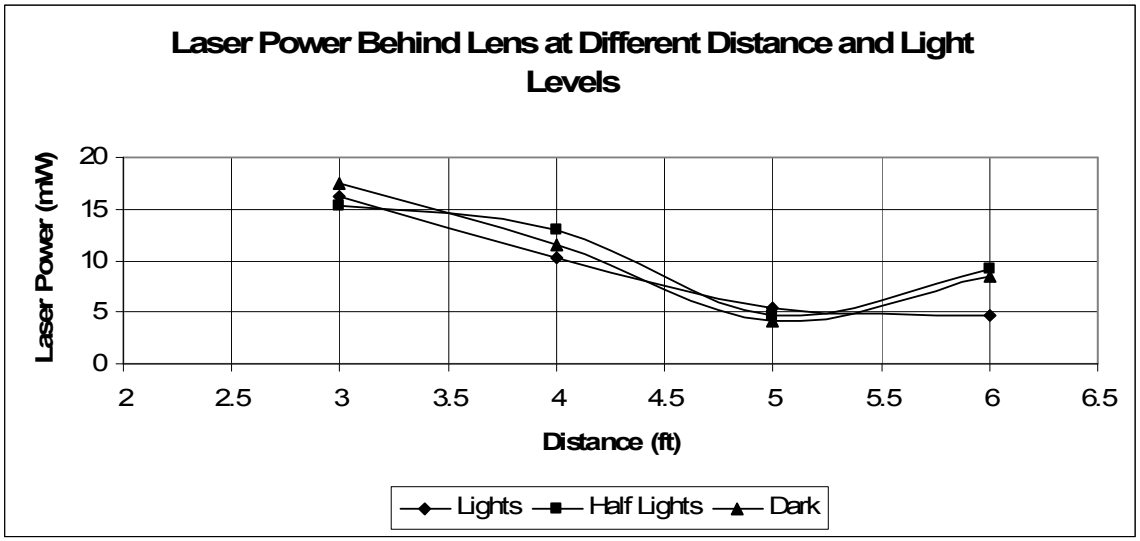

Figure 5.21: As distance increases, the laser power tends to decrease.

Two points were chosen that were 5 inches apart. When the laser was pointed at either point, the LPSM low light indicator was red. As the laser was moved from one point to the other, there was a small area where the low light indicator was green. The two points were always outside of this green light area to ensure consistency in the data.

The procedure followed was:

1. Set up the mirror 6 feet from the lens and laser setup.
2. Turn on the laser on.
3. The laser will only be moving horizontally. Get two pieces of white paper and tape them to the mirror, above the laser so that no laser light hits the paper. The paper will be used to mark the two points where the laser will shine, as shown in Figure 5.22.
4. With the correct light level and the correct filter, move the laser to point at the indicated left point. Record the voltage.
5. Move the laser to point to the right point. Record the voltage.
6. Change the filter and repeat.
7. Change the light level and repeat.

Figure 5.22: White paper was taped to the mirror to indicate the two points where the laser should be directed.

The data in Table 5.16 was collected when all lights were on. After the 19% filter, the light could not be seen, so the laser could not be correctly pointed to the two indicated points. A filter was then placed on the lens and the experiment was repeated with all of the lights on. Table 5.17 summarizes the data. The data in Table 5.18 was collected with half of the lights on. The laser could be seen with all filters. The data in Table 5.19 was collected with no lights on.

As seen in Figure 5.23, as laser power increases, the minimum voltage decreases. The minimum voltage tends to be higher with no background lights than with some background lights. As seen in Figure 5.24, the maximum voltage tends to be lower when no lights are on. The maximum voltage decreases as laser power increases, regardless of light level.

Subtracting the maximum and minimum voltage gives the voltage change. As the laser power increases, the voltage change tends to decrease. This is opposite of the behavior in diffuse surfaces, which had a larger voltage change at high laser powers.

The filters cause the laser light to spread out more. Therefore, the light is hitting the mirror at different angles and all of the light is not getting reflected at the same angle. This means that the LPSM may be picking up spurious reflections that would not be present with a true point laser. The voltage change may decrease, unlike the diffuse surfaces, due to the difference in reflections. The inconsistencies in the patterns may be due to the diffusion from the laser filters.

Table 5.16. Data for experiment with lights

Filter	Power at laser source (mW)	Min Voltage (V)	Max Voltage (V)	Change in Voltage (V)	Distance (in)	Volt/In (V/in)
No filter	>40	0.6	1.98	1.3800	5	0.2760
0%	>40	-0.16	1.36	1.5200	5	0.3040
6%	>40	-0.1	0.3	0.4000	5	0.0800
13%	>40	-0.43	0.23	0.6600	5	0.1320
19%	>40	-0.55	1.36	1.9100	5	0.3820

Table 5.17. Experiment with lens filter and lights on

Filter	Power at laser source (mW)	Min Voltage (V)	Max Voltage (V)	Change in Voltage (V)	Distance (in)	Volt/In (V/in)
No filter	>40	-1.05	9.15	10.2000	5	2.0400
0%	>40	-3.6	2.83	6.4300	5	1.2860
6%	>40	-4.18	-1.98	2.2000	5	0.4400
13%	>40	-3.65	-2.12	1.5300	5	0.3060
19%	>40	-3.83	-2.14	1.6900	5	0.3380

Table 5.18. Experiment with dim lights and no lens filter

Filter	Power at laser source (mW)	Min Voltage (V)	Max Voltage (V)	Change in Voltage (V)	Distance (in)	Volt/In (V/in)
No filter	>40	-2.35	7.67	10.0200	5	2.0040
0%	>40	-3.93	-0.35	3.5800	5	0.7160
6%	>40	-4.06	-3.34	0.7200	5	0.1440
13%	>40	-4.35	-3.1	1.2500	5	0.2500
19%	>40	-4.24	-3.28	0.9600	5	0.1920
25%	40.00	-3.73	-2.77	0.9600	5	0.1920
31%	30.37	-3.42	-1.6	1.8200	5	0.3640
38%	21.28	-3.15	-0.67	2.4800	5	0.4960
44%	16.36	-3.47	-0.32	3.1500	5	0.6300
50%	15.21	-3.32	0	3.3200	5	0.6640
56%	14.96	-3.6	-0.53	3.0700	5	0.6140
63%	12.39	-2.9	1.29	4.1900	5	0.8380
69%	11.47	-3.15	0.38	3.5300	5	0.7060

Table 5.19. Data with no background lights

Filter	Power at laser source (mW)	Min Voltage (V)	Max Voltage (V)	Change in Voltage (V)	Distance (in)	Volt/In (V/in)
No filter	>40	-2.37	7.69	10.0600	5	2.0120
0%	>40	-3.83	0.26	4.0900	5	0.8180
6%	>40	-4.16	-3.33	0.8300	5	0.1660
13%	>40	-4.18	-3.33	0.8500	5	0.1700
19%	>40	-4.06	-2.69	1.3700	5	0.2740
25%	40.00	-3.66	-2.21	1.4500	5	0.2900
31%	30.37	-3.21	-2.38	0.8300	5	0.1660
38%	21.28	-2.96	-0.74	2.2200	5	0.4440
44%	16.36	-3.05	-0.76	2.2900	5	0.4580
50%	15.21	-2.85	0.03	2.8800	5	0.5760
56%	14.96	-2.85	-0.35	2.5000	5	0.5000
63%	12.39	-2.39	0.17	2.5600	5	0.5120
69%	11.47	-3.24	0.12	3.3600	5	0.6720

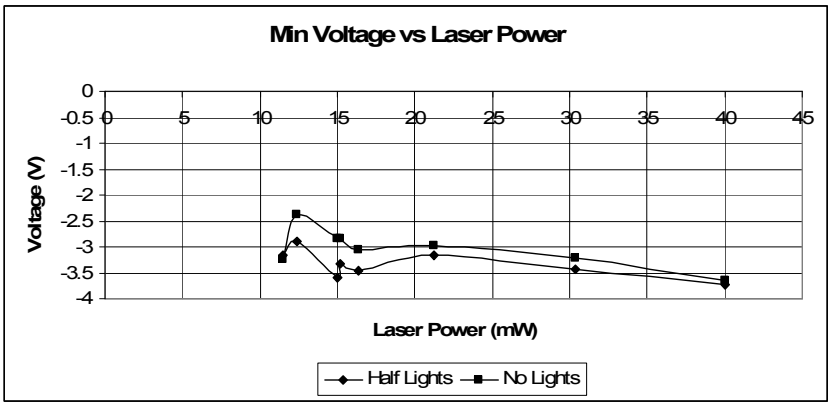

Figure 5.23: The minimum voltage tends to be higher with no background lights.

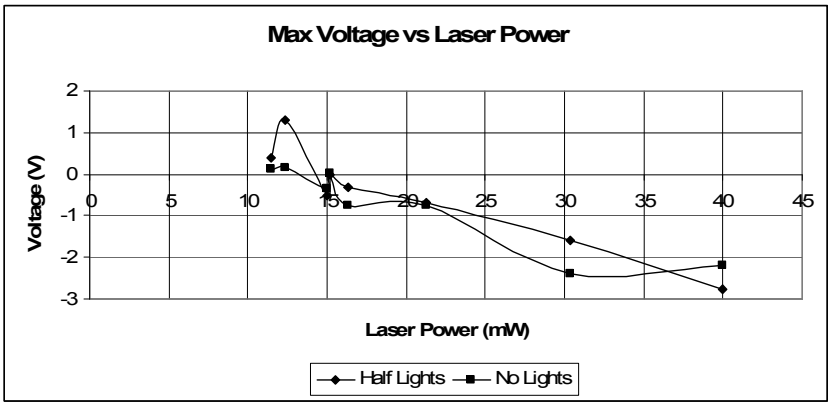

(a)

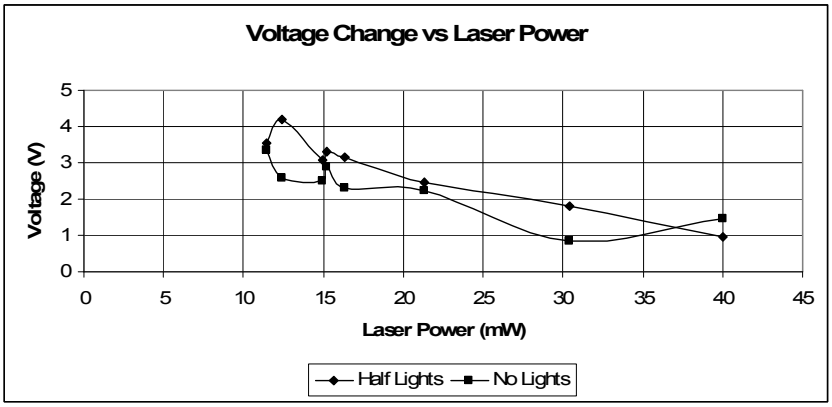

(b)

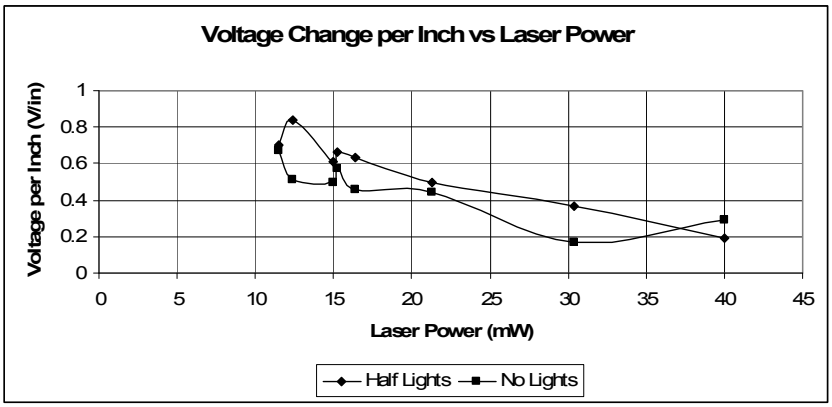

(c)

Figure 5.24: (a) The maximum voltage decreases as laser power increases. (b) The voltage change tends to decrease as laser power increases. (c) The resolution becomes worse with no light and as laser power increases.

The voltage change can be divided by the distance between the two points, or 5 inches in this case, to determine the volts per inch. A higher volts per inch corresponds to better resolution. The volts per inch tends to decrease as laser power increases and is usually lower with no light. This trend is opposite of the trend for the poster experiment.

5.3.6 Voltage at Same Point at Different Distances

A point was marked on the mirror by drawing an arrow on the white paper, as seen in Figure 5.25.

The procedure was:

1. Line up the lens/LPSM with the table.
2. Line up with the tape on the floor and with the table at 1.5 feet.
3. Turn on the laser and point it directly under the arrow.
4. Record the voltage reading.
5. Move the mirror back by six inches, re-align, and repeat.

The data in Table 5.20 was collected.

Figure 5.26 was generated with the data. The voltage tends to increase as the distance increases, again opposite of the trend with the poster. As the mirror is moved backwards, the reflection angle changes. When the reflection angle hits the lens, as indicated by the green low level indicator light, then the reading is usually higher. If the reflection misses the lens, then the low level indicator light is red, and the lens picks up a small portion of the laser light, if any, causing a lower voltage level. Due to the size of the mirror, it is very difficult to keep it perfectly aligned. Small changes in the angle of the mirror cause different reflection angles and could be the cause of some inconsistencies in the data. Like the poster, the voltage at a set point does not remain the same at different depths.

Figure 5.25: The set point was marked by an arrow on the white paper.

Table 5.20. Voltage of set point at different distances

Distance (ft)	Voltage (V)	Red/Green Light?
1.5	-7.33	red
2	-8.59	green
2.5	-5.47	green
3	-6.06	red
3.5	-6.07	red
4	-7.93	green
4.5	-1.73	red
5	-3.13	red
5.5	1.15	red
6	-2.7	red
6.5	-2.51	red

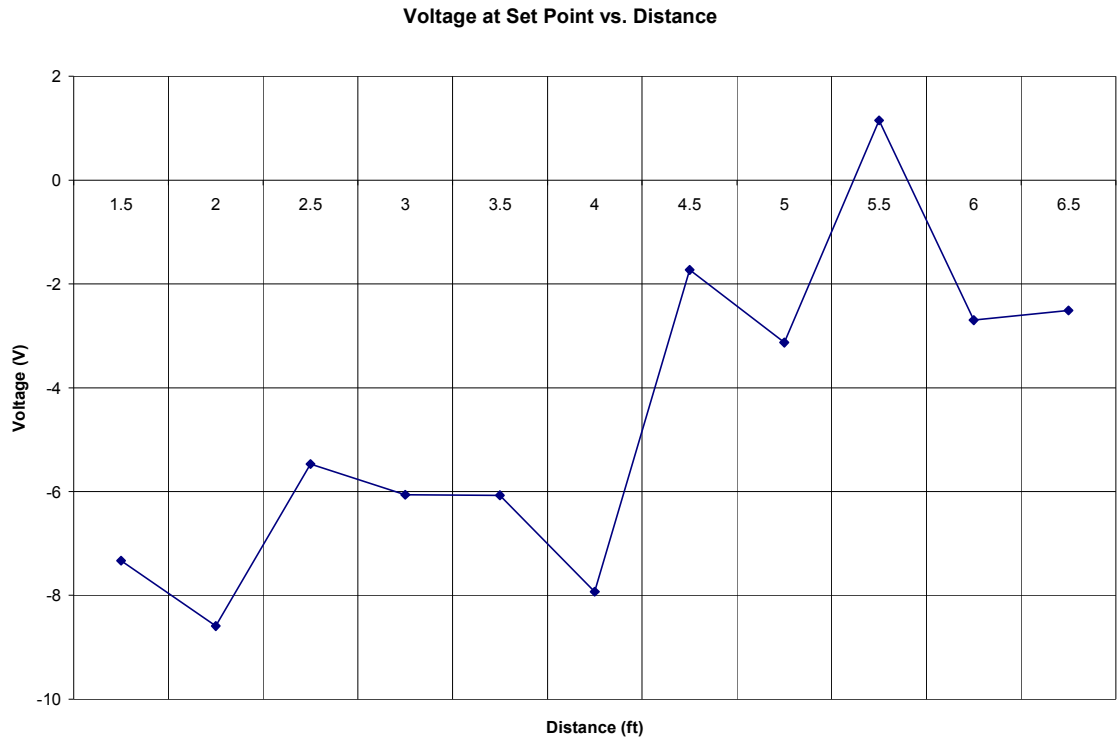

Figure 5.26: The voltage tends to increase as distance increases.

5.3.7 Within Threshold Experiments

A mirror is a specular surface. When light hits the mirror at an incident angle, it is reflected at the same angle, unlike on a diffuse surface where the reflected light is spread out uniformly in all directions. If the reflected light from the mirror strikes the lens, then the low level indicator light turns green, meaning that sufficient power is hitting the lens to provide valid readings on the outputs. The distance between the laser and the lens affects the angle where the laser reflection will hit the lens.

The laser was placed approximately 9.5 inches from the lens. The laser was then turned on and the leftmost point where the low light indicator light turned green was found. The voltage and point on the mirror was noted. The light was then moved to the right until the light turned red. The voltage and point on the mirror right before the light turned red was found. This experiment was tested with different distances between the laser and lens and at different light levels.

It was found that the area on the mirror that reflected onto the lens, giving a green indicator light, was only about 0.25 inches wide. There was very little variation in this distance, regardless of the baseline. In this 0.25 inch window, the voltage would change dramatically, usually between 2 to 3 volts.

The change at the red light to green light edge was studied. Big voltage jumps occurred between the transition from red to green. When the reflection stayed in the red light level area or the green light level area, the voltage seemed to change fairly linearly. However, the transition between the two areas was characterized by a large jump in voltage, as seen in Figure 5.27.

(a) (b)

Figure 5.27: The voltage level jumps from (a) just inside the green light area to (b) just outside the green light area.

5.3.8 Conclusions

In these tests, the laser power, the background light level, and the distance were varied. Voltage readings were taken at the boundaries of the field of view, as well as in the middle of the field of view.

The laser power was within the threshold for the LPSM when the reflection was directed at the lens. If the reflection did not hit the lens, then the light level was below the LPSM threshold. The laser light would hit the mirror and reflect at an angle governed by Snell's Law. Therefore, as the laser moved through the field of view, there was only about an inch long area where the reflection would hit the lens. Since the area was so small, the behavior of the LPSM for several of the tests could not be studied in depth.

Therefore, another method must be used to try to get within the threshold of the LPSM. It may be possible to move the poster board closer to the LPSM and repeat the same experiments. By moving the poster closer, the laser may appear more focused, causing the power to be more concentrated.

5.4 Tests at Close Range

The mirror was replaced with the white poster board. Although the poster board was a diffuse surface, absorbing more power than the mirror, it uniformly reflected the laser. To try to increase the apparent laser power, the white poster board was moved much closer to the LPSM than in the original experiments. If a distance could be found that increased the laser power to the given good operation region, then tests could be conducted to try to find consistent behavior of the LPSM.

5.4.1 Laser Power Behind Lens

At all distances up to fifteen inches, the low light indicator light was green when the laser was in the field of view of the lens. The indicator light turned green when the light was within the threshold range of 0.001 mW to 1 mW. The laser power behind the lens was measured for all distances up to fifteen inches to ensure that the power was beyond the minimum threshold.

The procedure followed was:

1. Align the lens with the table.
2. Align the poster with the 3 inch tape marks and the table.
3. Turn on the laser.
4. Point the laser at the marked point.
5. Hold the laser power meter behind the lens and focus the point.
6. Record the power reading.
7. Move the poster back 3 inches and repeat.

Table 5.21. Power at different distances and light levels

Distance (in)	Power Lights On (uW)	Power Lights Off (uW)
3	100.7	76.3
6	64.8	27
9	62.6	13.5
12	58.3	8.2
15	49.3	5.6

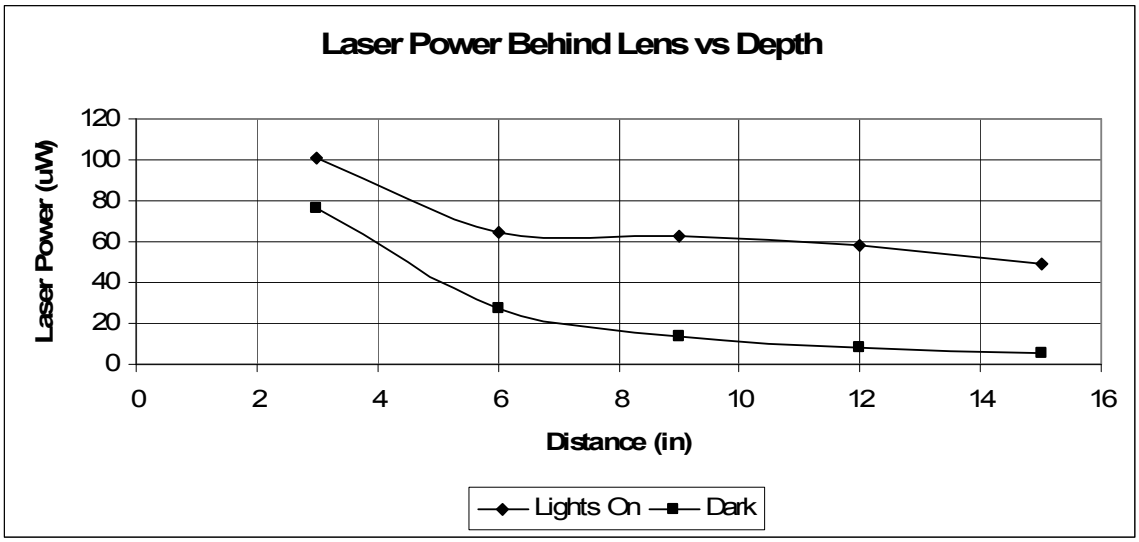

Figure 5.28: All power levels within fifteen inches is above 1 uW.

8. Change the light level and repeat.

The data in Table 5.21 was collected.

The data is graphed in Figure 5.28. All power levels within fifteen inches are above the 1 μW minimum power level, proving that the indicator light should be green for distances within fifteen inches.

5.4.2 Within Threshold Experiments

All of the experiments up to this point did not have a good operation range within the valid threshold of the LPSM. When the low light indicator light on the LPSM is red, then there is not enough light hitting the LPSM to give valid outputs. When the light turns green, then there is enough light to give valid outputs.

When the poster, a white diffuse surface, was moved close to the laser/lens setup and the <500mW laser was used with no filters, then there was enough light incident on the LPSM to give valid readings. Distances were marked in front of the laser and lens setup every three inches from three inches to fifteen inches. After fifteen inches, the low light indicator light became red. Within fifteen inches, there was enough light to give valid readings for the entire expected field of view.

First, the field of view and voltage range were found for all valid depths to ensure good operation of the LPSM. The procedure used was:

1. Align the lens/LPSM with the table.
2. Place the poster at the 3 inch marks, aligned with the edge of the table.
3. Turn on the laser.
4. Move the laser as far to the left as possible while still seeing a green indicator light, as seen in Figure 5.29.
5. Record the voltage.
6. Mark the point on the poster.
7. Move the laser as far to the right as possible while still seeing a green indicator light.
8. Record the voltage.
9. Mark the point on the poster.
10. Measure the distance between the two points and record.
11. Move the poster three inches further away and repeat.
12. Change the light level and repeat.

Tables 5.22-5.25 give the data collected for all experiments.

(a) (b)

Figure 5.29: (a) Move the laser all the way to the left while still staying in the valid threshold. (b) Move the laser all the way to the right while still staying in the valid threshold range.

Table 5.22. Data with lights on

Distance (in)	Min Voltage (V)	Max Voltage (V)	Distance (in)	Change in Voltage (V)	Volts per Inch (V/in)
3	-7.54	6.29	2.75	13.83	5.029
6	-7.5	8.74	3.75	16.24	4.331
9	-7.54	8.03	4.75	15.57	3.278
12	-7.48	8.15	5.25	15.63	2.977
15	-6.96	7.74	5.75	14.7	2.557

Table 5.23 Data with lights on and lens filter

Distance (in)	Min Voltage (V)	Max Voltage (V)	Distance (in)	Change in Voltage (V)	Volts per Inch (V/in)
3	-8.65	8.76	1.5	17.41	11.607
6	-8.8	9.33	3	18.13	6.043
9	-8.54	7.91	0.5	16.45	32.900
12	*no green	--	--	--	--
15	*no green	--	--	--	--

Table 5.24. Data with half lights on

Distance (in)	Min Voltage (V)	Max Voltage (V)	Distance (in)	Change in Voltage (V)	Volts per Inch (V/in)
3	-7.98	9.1	2.25	17.08	7.591
6	-8.29	9.36	3.5	17.65	5.043
9	-8.84	9.43	4.75	18.27	3.846
12	-8.77	9.49	5.5	18.26	3.320
15	-8.48	9.5	6.25	17.98	2.877

Table 5.25. Data from no background lights

Distance (in)	Min Voltage (V)	Max Voltage (V)	Distance (in)	Change in Voltage (V)	Volts per Inch (V/in)
3	-9.05	8.76	2.25	17.81	7.916
6	-8.5	9.44	3.5	17.94	5.126
9	-8.86	9.46	4.5	18.32	4.071
12	-8.71	9.2	5	17.91	3.582
15	-8.52	9.4	6.24	17.92	2.872

First, it can be seen in Figure 5.30 that the minimum voltage at all distances remains fairly constant at -9 V. The voltage changes slightly with background light, but all light levels maintain the same trend at all distances.

Next, the maximum voltage is graphed in Figure 5.31. Like the minimum voltage, the maximum voltage remains fairly constant at approximately 9 V at all depths, regardless of light level. Since the minimum voltage and maximum voltage remain constant, the voltage change also remains fairly constant for all depths.

It is expected that as the depth increases, the field of view should get bigger. The field of view is directly proportional to the depth by a factor of approximately 1/3, so it is expected that the field of view should increase linearly. The field of view does increase at a linear rate.

By dividing the voltage change by the field of view distance, the volts per inch can be found. Since the lens filter did not seem to help the results, that data is not included in the graph. It can be seen that the volts per inch decreases as depth increases. This result is expected because the voltage change remains constant even though the field of view distance increases with depth. Therefore, at larger depths, the same amount of voltage levels is describing a larger distance, giving poorer resolution and a smaller volt per inch reading.

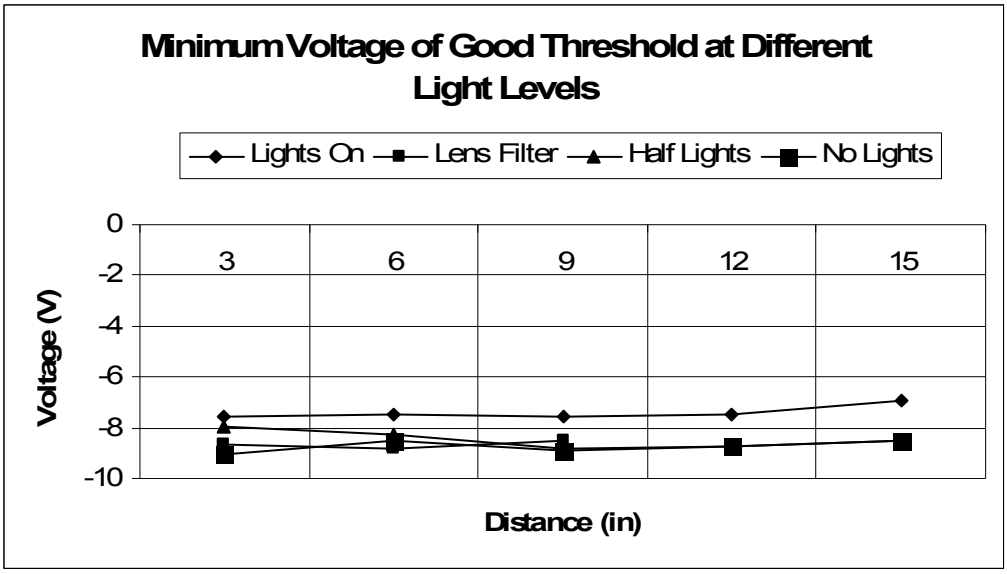

Figure 5.30: The minimum voltage remains constant at all depths.

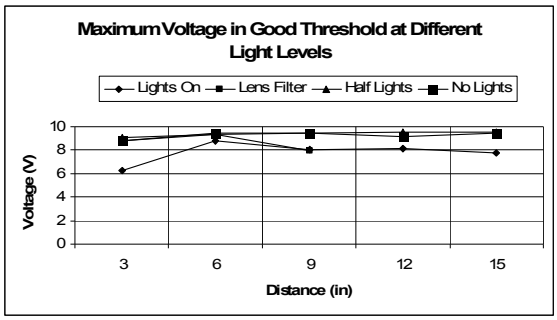

(a)

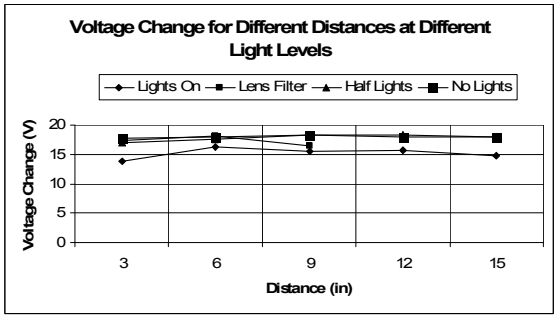

(b)

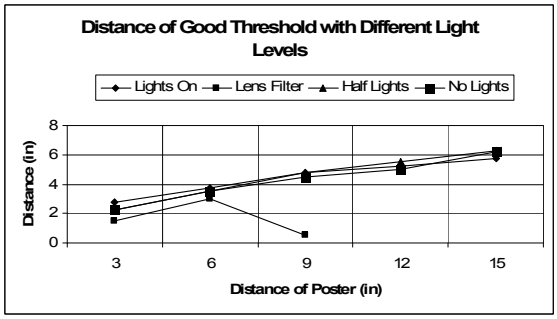

(c)

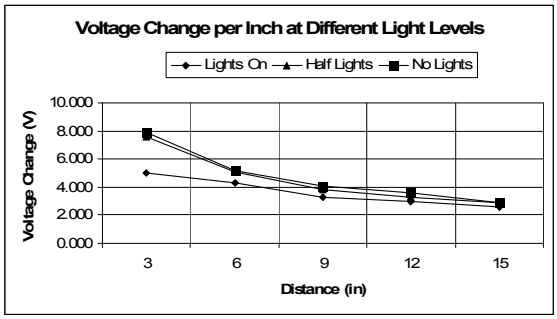

(d)

Figure 5.31: (a) The maximum voltage remains constant at all depths. (b) The voltage change remains constant at all depths. (c) The field of view increases linearly with depth. (d) The volts per inch decreases as depth increases.

5.4.3 Voltage at Set Distance

For this experiment, two points that lie within the good threshold at all depths were found. Since the 3 inch depth has the smallest field of view, a one-inch wide distance within the 3 inch field of view was marked, as seen in Figure 5.32.

The procedure followed was:

1. Align the lens/LPSM with the edge of the table.
2. Place poster along 3 inch tape marks and align with table.
3. Turn on the laser and point to the left mark.
4. Record the voltage.
5. Move the laser to the right point.
6. Record the voltage.
7. Move the poster back 3 inches and repeat.
8. Change the light level and repeat.

Tables 5.26-5.29 give the data collected in the experiment.

Figure 5.32: Two points, one inch apart, were marked.

Table 5.26. Data with lights on

Distance (in)	Min Voltage (V)	Max Voltage (V)	Distance (in)	Change in Voltage (V)	Volts per Inch (V/in)
3	-4.98	8.37	1	13.35	13.350
6	-3.52	5.05	1	8.57	8.570
9	-2.24	3.47	1	5.71	5.710
12	-0.43	2.99	1	3.42	3.420
15	-0.76	2.24	1	3	3.000

Table 5.27. Data with lights on and lens filter

Distance (in)	Min Voltage (V)	Max Voltage (V)	Distance (in)	Change in Voltage (V)	Volts per Inch (V/in)
3	-3.43	8.88	1	12.31	12.310
6	-3.35	7.1	1	10.45	10.450
9	0.25	5.88	1	5.63	5.630
12	--	--	--	--	--
15	--	--	--	--	--

Table 5.28. Data with half lights on

Distance (in)	Min Voltage (V)	Max Voltage (V)	Distance (in)	Change in Voltage (V)	Volts per Inch (V/in)
3	-6.36	7.03	1	13.39	13.39
6	-3.23	4.3	1	7.53	7.53
9	-2.37	5.13	1	7.5	7.5
12	-0.56	3.8	1	4.36	4.36
15	-1.24	2.44	1	3.68	3.68

Table 5.29. Data with no background lights

Distance (in)	Min Voltage (V)	Max Voltage (V)	Distance (in)	Change in Voltage (V)	Volts per Inch (V/in)
3	-6.85	7.2	1	14.05	14.05
6	-3.25	4.11	1	7.36	7.36
9	-2.36	2.35	1	4.71	4.71
12	-0.56	3.36	1	3.92	3.92
15	-1.14	2.09	1	3.23	3.23

Figure 5.33 shows the minimum voltage graphed against the depth. The minimum voltage tends to increase as depth increases.

Next, the maximum voltage is graphed against the depth. The max voltage tends to decrease as depth increases. Light level does not have a large affect on either minimum of maximum voltage levels.

The voltage change is found by subtracting the minimum and maximum voltages. The voltage change is the same as the volts per inch since the distance between points was one inch. The volts per inch decreases as distance increases. These results agree with the results from the green threshold experiment.

From the green threshold experiment, it is shown that different depths correspond to different volts per inch. Therefore, when two points are marked in this experiment and held constant, it is expected that the voltage change should decrease as depth increases. This trend is observed in the experiment.

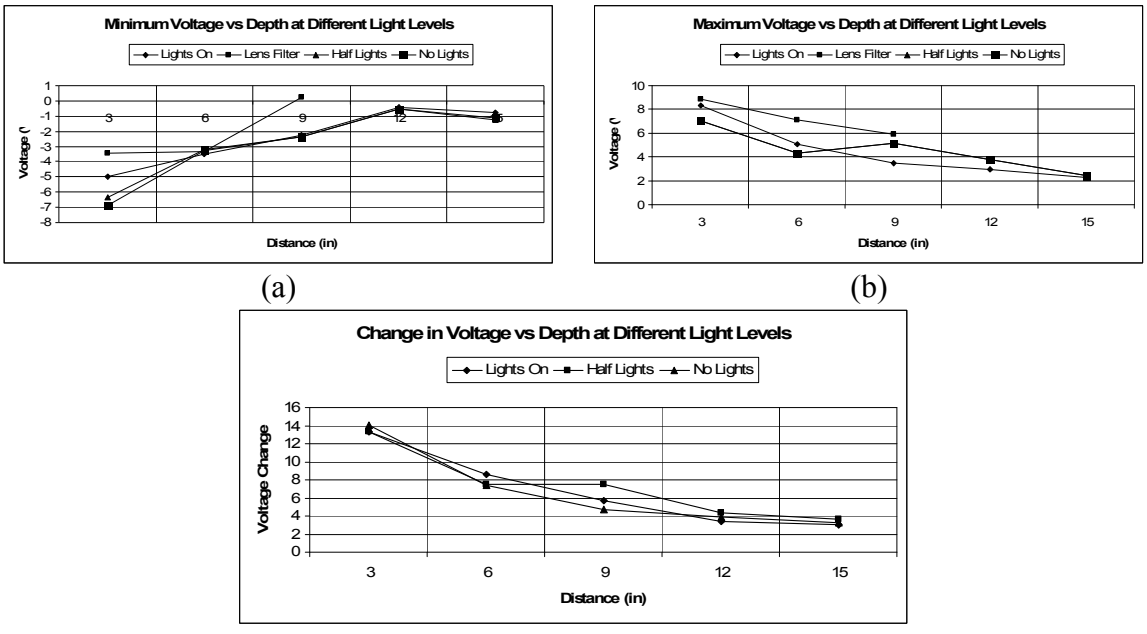

Figure 5.33: (a) The minimum voltage tends to increase as depth increases. (b) The maximum voltage tends to increase as depth increases. (c) The minimum voltage tends to increase as depth increases.

5.4.4 Voltage at Set Point

A point was marked on the poster, as seen in Figure 5.34. For this experiment, the alignment of the lens and poster had to be kept very constant. Due to projective geometry, the voltage should change slightly as the poster is moved further away. However, a 4.5 V change should not occur, as it did in previous setups.

The procedure followed was:

1. Align the lens/LPSM with the table edge.
2. Put the poster on the 3 inch tape marks and align with table edge.
3. Turn on the laser and shine on the point.
4. Record the voltage.
5. Move the poster back three inches, re-align, and repeat steps.
6. Change the light level and repeat.

The data in Table 5.30 was collected.

The data is graphed in Figure 5.35. The voltage increased by about 4 V. A smaller voltage change was expected.

Figure 5.34: A point was marked on the poster so that the x distance would remain constant.

Table 5.30. Data from experiment

Distance (in)	Voltage Lights On (V)	Voltage Half Lights (V)	Voltage No Lights (V)
3	-3.27	-3.34	-3.34
6	-3.49	-3.53	-3.52
9	-1.46	-1.61	-1.58
12	0.35	0.39	0.3
15	0.42	0.51	0.51

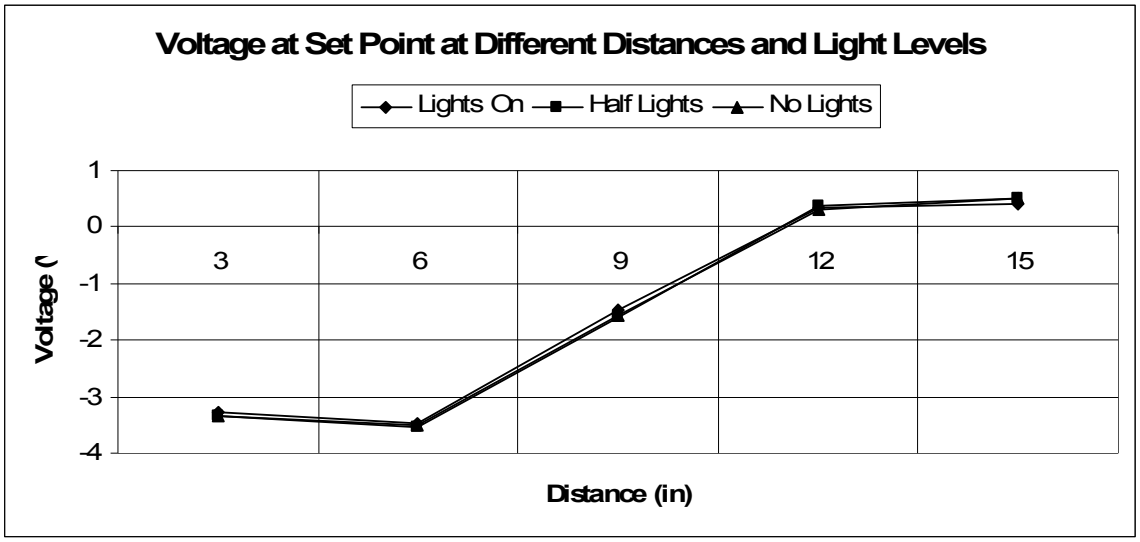

Figure 5.35: The voltage level changes with depth.

5.4.5 Distance Threshold Range

It was noticed that if the laser was on and the poster was moved, that the threshold light on the LPSM would remain green. However, if the laser was off, the poster was moved to the same distance, and then the laser was turned on, then the LPSM indicator light would not always turn green. Therefore, an experiment was conducted to determine a good operating threshold.

The poster was moved to a given distance away from the LPSM and the laser was kept on. The laser was focused to a point where the LPSM indicator light was green and the X position read 0 V. The center of the field of view was used because it should have the least distortion. The laser was turned off for a few seconds, and then turned back on. If the indicator turned green, then the distance was within the operational threshold, and the poster was moved further away by a very small distance. If the indicator light stayed red, then the distance was outside of the operational threshold, and the poster was moved closer to the LPSM by a very small distance, as shown in Figure 5.36.

It was found that the indicator light turned green when the laser was turned on up to and including 11 inches. The indicator light did not turn green at distances 11.25 inches away and further.

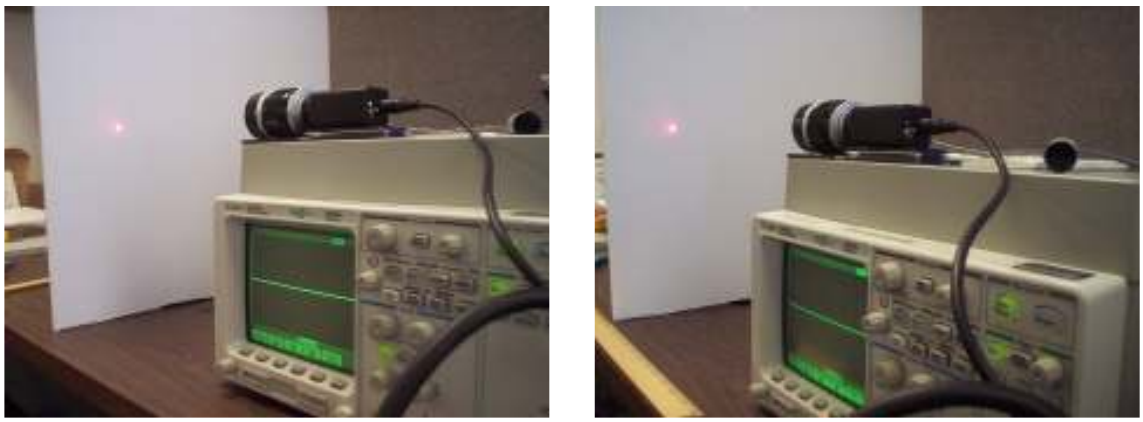

(a) (b)

Figure 5.36: The distance in (a) is within the operational threshold, while the distance in (b) is outside of the operational threshold.

5.4.6 Conclusions

In these tests, the laser power, the background light level, and the distance were varied. Voltage readings were taken at the boundaries of the field of view, as well as in the middle of the field of view.

At distances within fifteen inches, the light level was within the threshold of the LPSM. Once the experiments were performed within the proper threshold, the expected outputs were seen. Consistent results were seen regardless of background light levels. It was seen that the laser power needs to be about 500 mW to reach the 15 inch distance, so the laser filters were no longer used.

Now that the working threshold is found, boundaries can be defined for the system.

6 SLIDER EXPERIMENTS

In the final system, two LPSMs will be placed next to each other, facing a scene. When the laser is present in the scene, an x and y voltage will be output from each LPSM. Using these voltages, the depth of the scene can be calculated.

The process of acquiring corresponding x and y voltages for a laser point can be accomplished with one LPSM. The LPSM can face the scene and one x and y voltage recorded. Keeping the laser at the same spot, the LPSM can be moved to a second position and the new x and y voltages recorded. Using this system, objects can be modeled so that the resolution and accuracy of the system can be tested.

6.1 Slider Setup

In stereo vision, two cameras are placed parallel to each other, facing a scene. They are separated by a distance known as the baseline. Each camera sees a slightly different picture, and by finding the position of the same point in each picture, the depth of the point can be determined. For these experiments, only one LPSM is used. If the LPSM can be moved to a slightly different distance while staying the same distance away from the scene, then stereo vision can be simulated manually. Therefore, something must be built so that the LPSM can be moved.

The LPSM and lens were mounted on a piece of metal that slid along a metal bar. Lines were drawn on the bar 0.5 inches apart to help to move the LPSM known distances during experiment, as seen in Figure 6.1. Next, something had to be built to ensure that the scene was parallel to the bar where the LPSM slid.

At either end of the LPSM sliding bar, two mounts were placed ninety degrees to the LPSM bar. Two more bars were slid into the mounts and were again checked to ensure perpendicularity. Marks were also placed on these bars in half inch increments. If both bars are placed to protrude the same distance from the LPSM bar, then the poster could be placed next to the two bars and be parallel to the LPSM bar.

6.2 Manual Data Point Collection

The lab currently has only one LPSM. Therefore, a test needed to be done to simulate stereo vision with two LPSMs. The following procedure was used:

1. The slider setup was placed on the table. The laser was deflected off of a mirror onto the poster board. The two distance bars on the slider were set to 3 inches away from the front of the LPSM lens. The poster was pushed against the two bars and held in place by

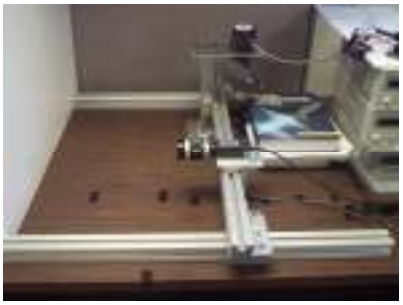

(a)

(b)

(c)

Figure 6.1: (a) The LPSM is mounted on a metal piece that slides along a metal bar with half inch increments marked to make data collection easier. Two bars are placed perpendicular to the LPSM bar and have half inch increments marked. The bars can be slid (b) closer or (c) farther from the LPSM bar, depending on where the poster is placed.

two heavy batteries. The LPSM was hooked up to power and the outputs hooked up to an oscilloscope, as seen in Figure 6.2.
2. Place the laser in the right side of the field of view and make sure that the indicator light on the LPSM is green. The laser is placed in the right side of the field of view because the LPSM will be moved to the right, causing the laser to move closer to the left side of the field of view.
3. Record the x and y voltage levels.
4. Move the LPSM to the right by a quarter of an inch.
5. Record the x and y voltage levels. Repeat at quarter inch increments until the LPSM has been moved a total of 1.25 inches to the right or until the light spot is out of the field of view (the indicator light becomes red).
6. Move the two distance bars 1 inch further away. Reset the poster and laser and repeat up to thirteen inches.

Figure 6.3 shows how the waveforms change as the LPSM is slid over, at the 6 inch distance.

As the LPSM is moved to the right, the laser appears to move further to the left of the field of view. Therefore, it is expected to see that the x voltage level should decrease. The y voltage level is expected to remain fairly.

Figure 6.2: The setup for the experiment had a poster held next to the two distance bars, the slider setup, the laser deflected off of a mirror, the power supply, and oscilloscope.

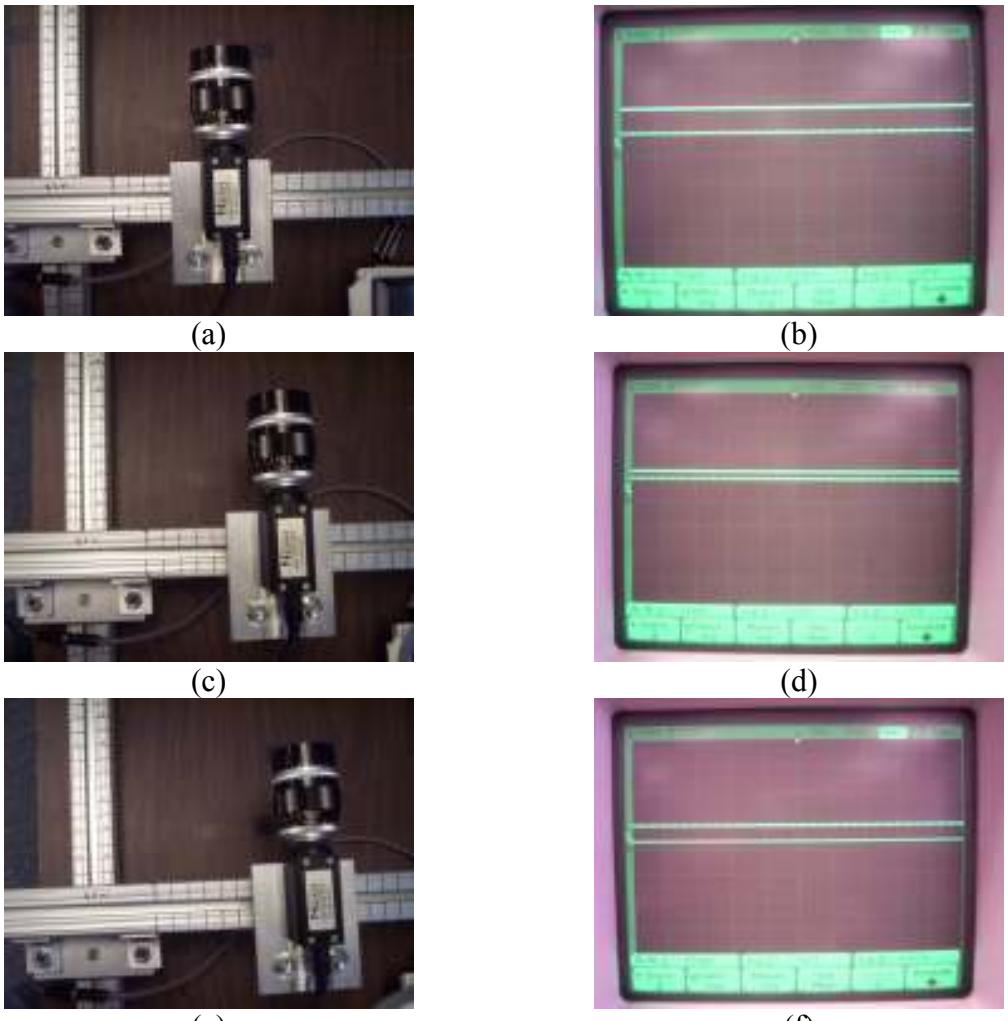

(a) (b) (c) (d) (e) (f)

Figure 6.3: The LPSM starts in (a) the original position, producing (b) a waveform. The LPSM is (c) moved over a small distance, such as 0.5 inches, producing (d) another waveform. The process is repeated, (e) moving the LPSM and (f) recording the waveforms.

6.3 Edge Distortion

In the performed experiments, a laser moves through the field of view of the LPSM in the horizontal direction, from the +10V point to -10V. A triangular wave is expected. However, the waveform actually appeared to be a curve, where the rise time and fall time on the edges were much longer than expected.

During the slider experiments, it was noticed that the absolute maximum voltage and absolute minimum voltage did not always occur at the edge of the LPSM threshold where the indicator lights turns from green to red. When the voltage readings from the LPSM are mapped to the corresponding distance on the active area of the LPSM, the voltage must be multiplied by a constant. The constant was found assuming that the absolute maximum and absolute minimum voltages occurred at the edges of the LPSM active area at 2 mm and -2 mm. If the max and min voltages did not really occur at the edges of the LPSM, then the constant was incorrect, meaning that the mapping of the voltage to a distance was also incorrect.

6.3.1 Light as Enter Field of View

The laser is not a point when it strikes the poster surface. There may be enough incident light on the LPSM to get a valid reading before the entire light spot is within the field of view. Once enough light is within the field of view, the LPSM will give the voltage reading of the center of light of all light seen, as shown in Figure 6.4.

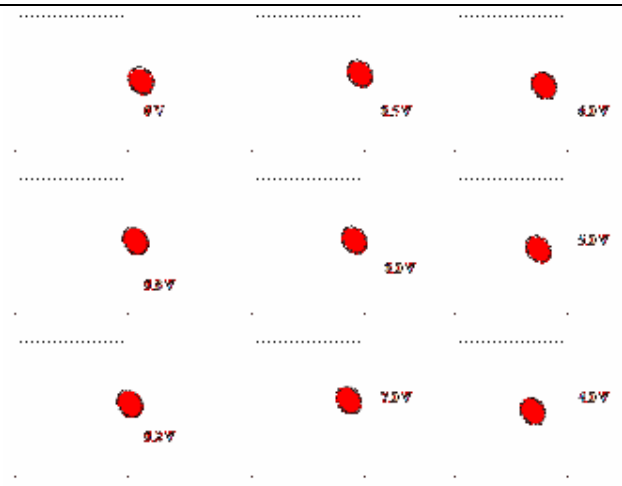

Figure 6.4: A possible light spot and voltage values are noted as the light spot enters the field of view. The pictures are ordered from top to bottom and then from left to right.

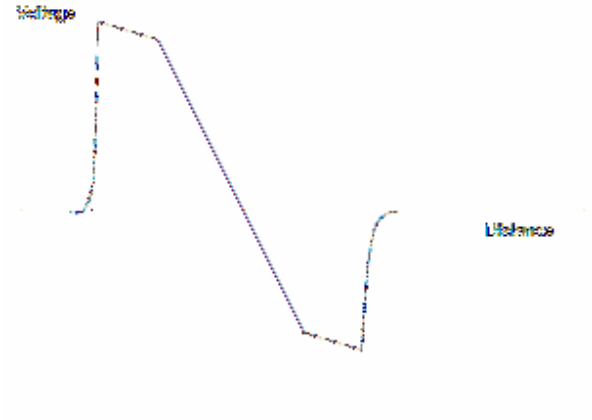

Figure 6.5: As the light spot moves through the field of view, the voltage should decrease. The voltage will probably decrease at different slopes depending on whether or not the entire light spot is in the field of view.

It can be seen that once enough light is present, the LPSM should give the maximum voltage. As the laser spot continues to move into the field of view, the voltage should decrease, although it may not decrease rapidly. Once the entire light spot is in the field of view, the voltage should decrease linearly at a faster rate. When the laser spot begins to exit the field of view, the voltage should continue to decrease until it reaches the minimum voltage, but at a smaller slope. The expected behavior is graphed in Figure 6.5.

From previous experiments, as the laser moves across the field of view, the voltage increases to the maximum voltage before decreasing linearly to the minimum voltage. The problem does not appear to be because the laser spot is not always entirely in the field of view.

6.3.2 Laser Focus Problem

The 500 mW laser creates an elliptical beam when it strikes a surface. However, the 1 mW point laser creates a small point, about 1 mm wide. To test to see whether or not the voltage problem is due to the focus of the laser, tests are done using the 1 mW laser shining directly into the LPSM.

When the laser strikes an object, it diffuses according to a Gaussian curve. The mean of a Gaussian curve is at its center. Since the LPSM outputs the voltage corresponding to the center of light, it is expected that the focus of the laser should not affect the output. Tests are performed to test this theory.

The 1 mW laser is shined directly into the LPSM with lens. The response time is taken by placing a piece of cardboard between the laser and LPSM and then quickly removing the cardboard. The experiment is done with the laser sitting 3 inches, 7 inches, and 14 inches away from the LPSM. The lens is then removed from the LPSM and the

experiment is repeated. The experiment is repeated several times for the same distance so that an average response time can be taken. Table 6.1 shows the data collected.

At different distances, the response time changes, as was seen with the 500 mW laser. However, the response time is closer to the expected response time of 100 µs. The decrease in response time could be due to the intensity of the laser.

Next, the maximum voltage is tested pointing the 1 mW laser directly into the LPSM. Table 6.2 shows the data collected.

The maximum voltage never reaches the cited 10V in the LPSM specification. When the lens is placed on the LPSM, the maximum voltage decreases even more. Since the same behavior is noted with the 1 mW laser as with the 500 mW laser, then the laser focus is probably not the cause of the edge error.

6.3.3 Lens Focus Problem

The lens focuses the light onto the LPSM. The lens has been set to focus light coming form infinity to the LPSM. Although experiments were done to determine how far back the LPSM should sit from the lens, it cannot be determined if the light is focused or not since it cannot be seen. Therefore, tests are done to see whether the lens is introducing blur to the laser light to cause the edge error.

Table 6.1. Response time with 1 mW laser

Distance	Response Time, no lens (µs)			Avg	Response Time, with lens (µs)			Avg
(in)	1	2	3	(µs)	1	2	3	(µs)
3	240	300	220	253	--	--	--	--
7	60	100	120	93	260	200	300	253
14	120	200	140	153	280	220	320	273

Table 6.2. Maximum voltage with 1 mW laser directly into LPSM

Distance (in)	Max Voltage with Lens (V)	Max Voltage without Lens (V)
5	--	9.7
6	4.7	9.7
7	6.1	9.7
8	7.2	9.4
9	6.9	9.2
10	6.9	9.4
11	6.9	9.2

Table 6.3. The max and min voltages are recorded at different lens apertures.

Distance (in)	Aperture (m)	Max Voltage (V)	Min Voltage (V)
7	Infinity	3.9	-2.5
7	3	3.9	-2.5
7	1.5	3.9	-2.3
7	1	3.8	-2.3
7	0.7	3.6	-2.3
7	0.5	3.6	-2.3
7	0.4	3.3	-2.3
7	0.3	2.5	-2.8

The lens introduces blur in the form of a Gaussian curve. Again, a Gaussian curve averages to the center, so even if the light is not in focus when it hits the LPSM, it should not affect the output voltage reading.

The 1 mW laser was pointed directly into the LPSM with lens. The maximum voltage reading and minimum voltage reading were recorded. The aperture of the lens was then changed and the voltages were again found and recorded. The 1 mW laser sat 7 inches away from the LPSM/lens. Table 6.3 shows the data collected.

The maximum and minimum voltages changed very little as the aperture changed from infinity to 0.3 meters. If the lens aperture caused the edge error, then different maximum and minimum voltages should have been seen as the light was focused differently. Therefore, it can be concluded that the lens focus does not greatly affect the response of the LPSM at its boundaries.

6.3.4 Light Scattering and Conclusions

The white poster was placed 9 inches away from the lens/LPSM. The laser was placed on a pan-tilt for easier control. The laser was turned on and shined at the rightmost point before the indicator light turns from green to red, on the X-axis so that theyY voltage was 0 V. The point was marked on the poster and the voltage recorded. The laser was then moved slightly to the left, further inside the field of view. The y voltage was checked to ensure that the laser was still on the X-axis. The voltage was recorded and the point marked. This process was repeated until the indicator light turned red, meaning that the laser light was out of the field of view. The data collected can be found in Table 6.4.

Table 6.4. Data collected from calibration experiment

Marks Count from Right	Distance (in)	X (V)	Y (V)	Red/Green
1		0.588	0.741	R
2	0.0000	3.314	0.017	G
3	0.1250	4.661	0.030	G
4	0.3125	6.137	0.038	G
5	0.5000	6.975	0.040	G
6	0.6875	7.192	0.030	G
7	0.8125	7.313	0.038	G
8	1.0000	7.046	0.039	G
9	1.1250	6.706	0.034	G
10	1.3125	6.022	0.011	G
11	1.4375	5.356	0.041	G
12	1.6250	4.645	0.035	G
13	1.8125	3.582	0.015	G
14	2.0000	2.650	0.039	G
15	2.1875	1.609	0.040	G
16	2.3750	0.499	0.039	G
17	2.5625	-0.223	0.030	G
18	2.7500	-1.220	0.034	G
19	2.8750	-2.037	-0.009	G
20	3.0625	-2.980	0.039	G
21	3.2500	-3.752	0.009	G
22	3.3750	-4.638	0.040	G
23	3.5625	-5.353	0.041	G
24	3.6875	-5.970	0.030	G
25	3.8750	-6.811	0.018	G
26	4.0625	-7.317	0.016	G
27	4.2500	-7.552	0.035	G
28	4.5000	-7.382	0.030	G
29	4.6250	-6.751	0.038	G
30	4.8750	-5.350	0.039	G
31	4.9375	-4.651	0.039	G

Once all of the points had been marked, the distance of the marks was measured. The point on the rightmost part of the field of view was called 0 in. All of the other marks were measured in comparison to this point. The voltages can be graphed versus the distance, giving the curve shown in Figure 6.6.

Ideally, it is expected for the voltage to spike to its maximum value as soon as it enters the field of view and decrease linearly to the minimum voltage. Instead, it is seen that the voltage slowly increases to the maximum voltage. The voltage then begins to decrease, fairly linearly, to the minimum voltage before slowly increasing again. The points between the maximum and minimum voltages can be plotted showing a linearly decreasing trend, as expected.

It is necessary to find out the distance on the LPSM that the voltage refers to in order to compute the stereo vision equations. One explaination for the plot having curves is that there is edge distortion intrinsic to the PSD.

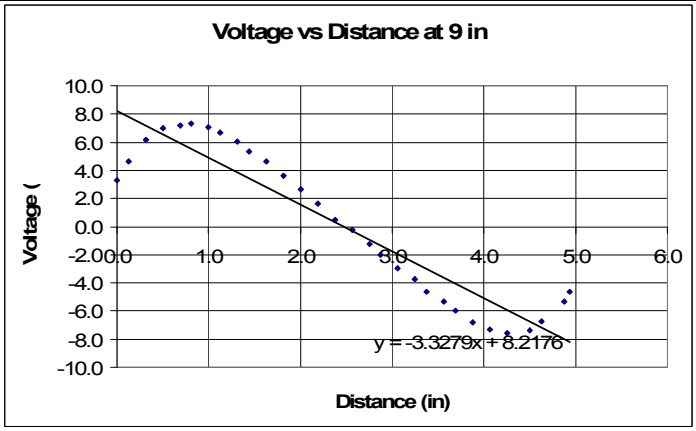

(a)

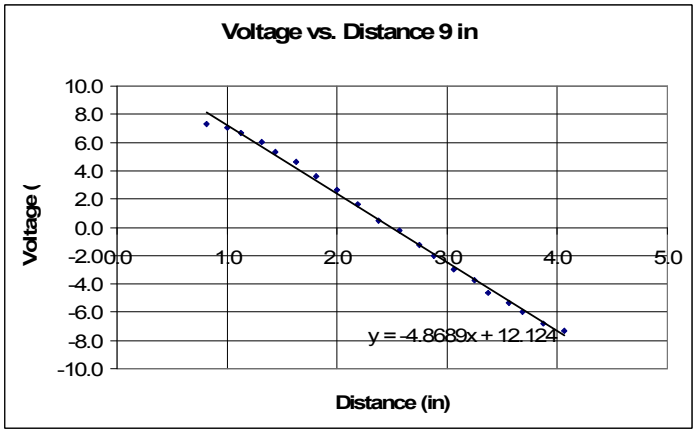

(b)

Figure 6.6: (a) The voltage can be plotted against the distance on the poster. (b) The voltage can be plotted against the distance on the poster between the minimum and maximum voltages, giving a linearly decreasing line.

In this case, it is assumed that the 4.9375 in field of view must be mapped to the 4 mm PSD area. The device acts linearly from approximately 6 V to -6 V, or from 1.3125 in to 3.6875 in. This linear distance, or 2.375 in, is about 48.1% of the entire field of view. Therefore, 2.375 inches must be mapped to 48.1% of the PSD area, or 1.92 mm. Since the voltage is linearly decreasing with distance and it is assumed that the center of the PSD is equivalent to 0 V, the equation for the line mapping voltage to PSD distance becomes:

$$V = 6.23269 D_{PSD}. \tag{30}$$

Therefore, to map a voltage to a distance on the PSD, the voltage must be between 6 V and -6 V, and it needs to be divided by the constant 6.23269. To test this, the laser was pointed within the linear region of the field of view in front of the LPSM. The voltage was recorded. The LPSM was slid 0.5 in and the voltage recorded. This process was repeated at 1 in and 1.5 in. The poster sat 9 inches from the LPSM, so the answer given from stereo vision can be checked.

The voltages can be divided by the previously found constant to give the PSD distance, and then can be applied to stereo vision equations to give a calculated distance, as shown in Table 6.5.

As can be seen from the table, the calculated depths are incorrect. Next, the assumption that the minimum and maximum voltages occur at the edges of the 4 mm PSD area was tried. The field of view at 9 inches was expected to be approximately 3 inches. The distance between the maximum and minimum voltages is 3.25 inches, much closer to the expected value than the distance of the entire field of view.

The lens is removed from the LPSM and a slightly opaque piece of paper was held behind the lens at about the same distance away as the LPSM. The laser was moved at a constant rate through the field of view. The light spot on the paper also moved at a constant rate, with no extraneous reflections seen. Since there were no extraneous reflections, the behavior cannot account for the slow curve up to the maximum voltage.

A front view of the LPSM can be seen in Figure 6.7. The PSD is centered in the middle of the device, behind a piece of glass. Around the glass is a small gold-colored circle. Black plastic fills the area between the gold circle and the C-mount for the lens. As the laser moves over this area, most of the reflections are absorbed in the black area. However, when the laser strikes the gold circle, the light is spread out, reflecting into the PSD area. Once the laser passes the gold area, it begins to hit the active area of the PSD.

Table 6.5. Stereo vision calculations 1

Distance (in)	Baseline (in)	Vx1 (V)	Vx2 (V)	V1 Dist (mm)	V2 Dist (mm)	Depth (mm)	Depth (in)
9	0.5	3.456	0.985	0.55449	0.158038	416.437523	16.39518
9	1	3.456	-1.373	0.55449	-0.22029	426.182282	16.77883
9	1.5	3.456	-4.192	0.55449	-0.67258	403.641652	15.8914

(a) (b) (c)

Figure 6.7: As the laser moves across the LPSM face, it first hits (a) black plastic, then (b) a gold ring where the light is scattered, and then (c) the active area.

The green indicator light may be turning green while the laser is on the gold circle, measuring the reflection of light. When the voltage reaches the maximum value, the laser may have moved off of the gold circle onto the PSD. The same reflective behavior is seen as the laser exits the PSD and again hits the gold circle.

Using the minimum and maximum voltages at the edges of the 4 mm area, the same method from above yields a constant of 3.6565. Points were again collected at several distances and several baselines, resulting in Table 6.6.

The new constant seems to give good results for the stereo vision calculation. The plot of the voltage against distance between the minimum and maximum voltages appears fairly linear, with some discrepancies near the minimum and maximum voltages. The offset of these points can be attributed to some edge distortion. Points outside of the linear region need to be ignored since they are actually reflections instead of points taken when the laser is focused on the PSD.

6.4 Intensity vs Voltage Problem

Different amounts of light have been incident on the LPSM according to the laser used and the deflection of the laser. In the final system, the object to be modeled will be unknown, meaning that the color and surface material will also be unknown. The laser will reflect differently according to the surface, so tests need to be run to ensure that the intensity of the incident light does not affect the voltage, as long as the amount of light is within the threshold range of the LPSM.

Table 6.6. Stereo vision calculations 2

Distance (in)	Baseline (in)	Vx1 (V)	Vx2 (V)	V1 Dist (mm)	V2 Dist (mm)	Depth (mm)	Depth (in)
9	0.5	3.3	0.802	0.902502	0.219335	241.668595	9.514512
9	1	3.3	-1.949	0.902502	-0.53302	230.020251	9.055915
9	1.5	3.3	-4.649	0.902502	-1.27143	227.835508	8.969902
6	0.5	5.666	2.024	1.549569	0.553535	165.757317	6.525879
6	1	5.666	-2.425	1.549569	-0.6632	149.224608	5.874985
6	1.5	5.666	-6.256	1.549569	-1.71093	151.909449	5.980687
3	0.5	6.868	0.153	1.878299	0.041843	89.9014371	3.539427
3	1	6.868	-7.26	1.878299	-1.98551	85.4598174	3.36456

Figure 6.8: The 1 mW laser is pointed directly into the LPSM to ensure a focused point.

6.4.1 1mW Laser at Different Distances

The first experiment removes the issues of the laser being well-focused and the lens not focusing the laser on the LPSM correctly. The 1 mW point laser is pointed directly into the LPSM without the lens, as shown in Figure 6.8.

The laser was pointed into the LPSM at a distance of 5 inches. The LPSM was manually moved, while watching the oscilloscope. The LPSM was moved until the absolute maximum voltage value was read on the oscilloscope, while the indicator light was green. This voltage value was recorded. The laser was then moved one inch further away, and the process repeated. Table 6.7 summarizes the results.

As the laser distance increases, the maximum voltage decreases. At larger distances, the laser must travel further to reach the surface of the LPSM, meaning that it will diverge more. Higher divergence results in lower intensity. Therefore, as laser intensity decreases, the maximum voltage decreases.

Table 6.7. The maximum voltage is recorded at different distances.

Distance (in)	Max Voltage (V)
5	9.7
6	9.7
7	9.7
8	9.4
9	9.2
10	9.4
11	9.2

6.4.2 High Power Laser with Different Colors

In this experiment, the true system setup of a laser reflecting off of an object was used. The 500 mW laser was deflected off of a mirror onto the surface of an object that sat 3 inches from the LPSM with lens. The voltage was recorded. The object was then replaced by an object of a different color. The distance from the object to the LPSM remained constant and the laser remained stationary. Therefore, for correct operation, the LPSM needed to give the same voltage reading regardless of the object in the field of view. The objects used can be seen in Figure 6.9.

Table 6.8 summarizes the results.

From this experiment, it can be seen that different color surfaces give different voltage readings for the same point. Therefore, depending on the object placed in the scene, the voltage could change. If the voltage reading for a specified point is inconsistent, then the depth cannot be calculated.

6.4.3 High Power Laser with Different Surfaces

It may be possible to change the object so that it remains the same color. Therefore, an experiment was performed to test the voltage of the same point when the laser was reflected off of different surface types that were all the same color.

In this experiment, the laser was reflected off of a mirror onto the given object. The object sat 3 inches away from the LPSM with lens. The voltage was read from the oscilloscope and recorded. Four surfaces were tested including white poster board, a slightly glossy book cover, cast metal painted white, and a magazine cover that was not glossy, as seen in Figure 6.10.

(a) (b) (c)

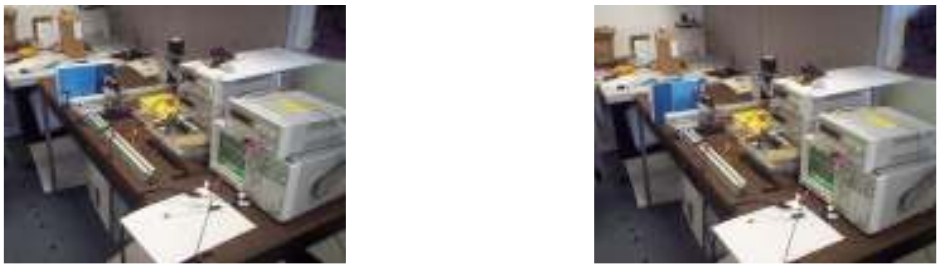

(d) (e)

Figure 6.9: The laser was reflected off of different color surfaces to see if the LPSM would give the same voltage reading. The surfaces used were (a) white poster board, (b) brown cardboard, (c) yellow plastic, (d) dark blue slightly glossy book cover, and (e) light blue slightly glossy book cover.

Table 6.8. The voltage was recorded for different colored surfaces

Distance (in)	Surface	Voltage (V)
3	White poster board	3.9
3	Brown cardboard	1.1
3	Yellow plastic	2.2
3	Dark blue book cover	6.3
3	Light blue book cover	7.0

(a) (b) (c)

Figure 6.10: The surfaces tested included (a) white poster board, (b) a glossy book cover, and (c) metal painted white.

Table 6.9. Voltage readings at different white surfaces

Distance (in)	Surface	Voltage (V)
3	White poster board	3.9
3	White slightly glossy book cover	8.0
3	White-painted cast metal	6.9
3	White cover of magazine, not glossy	4.1

As can be seen in Table 6.9, different surfaces gave different voltage readings even though the laser position and distance did not change.

6.4.4 Conclusions

The different surfaces and colors result in different voltages. The amount of laser power that a surface reflects and absorbs is dependent on both color and on the surface material. Therefore, both the color and surface material affects the intensity of the light incident on the LPSM. From the above experiments, it is seen that intensity affects the output of the LPSM. Since the object to be modeled is of unknown color and not necessarily of uniform material, then the voltage readings when the laser strikes the object will be inconsistent, giving incorrect values to be applied to the stereo equations.

Even when the laser is shined directly into the LPSM from different distances, the voltage changes. The LPSM seems to be extremely sensitive to laser intensity, and the performance changes accordingly. Therefore, even if an object of the same material and color were being modeled, readings may be inconsistent because the entire object will not lie the same distance away.

6.5 Fifteen Point Stereo with Absolute Error

Using the slider, it is possible to point the laser a scene, read the x and y voltages, and then move the LPSM by a pre-determined baseline distance to get another x and y voltage pair. The four voltages and baseline distance give enough information to use stereo equations to calculate the depth of the given point in the scene.

The poster can be placed a given distance away from the lens/LPSM. The field of view for the camera in its first position can be marked. The camera can then be moved by 1 inch, and the new field of view marked. The overlap area is the active field of view for the entire system.

At 9 inches, the active field of view is about 2 inches wide by 3 inches tall. The laser was pointed at a spot in the field of view and the voltages were taken. The LPSM was then slid 1 inch to the right, and the values were taken again. The point was then marked with a black pen. The laser was moved to a new spot and the process repeated.

A total of 15 points were taken, spread throughout the active field of view. The points were divided into five points in three columns. Table 6.10 shows the collected data and the calculated X, Y, and Z positions.

Since the true values for X, Y, and Z are known for each point, the error can be found. The percentage error and actual error in inches can be seen in Table 6.11.

To see where the majority of the error occurs, the calculated errors were placed in a graph relative to the position of their corresponding points. Figure 6.11 shows the graphs for the error calculations in relation to where the error occurs in the field of view.

It can be seen that the error seems to be smaller in the middle of the field of view and gets larger towards the edges. This behavior is expected because the PSD inside the LPSM is known to have some edge distortion. Overall, the depth seems to have about a 10% error, or about one inch.

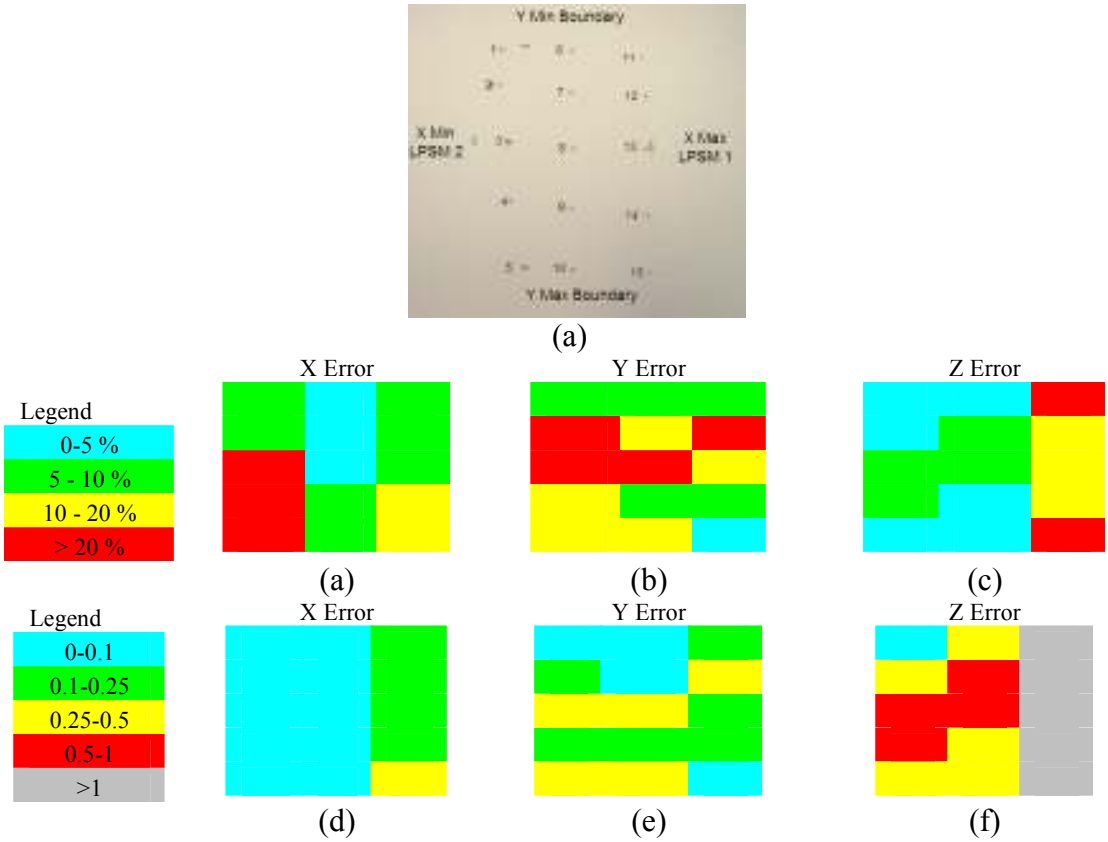

Figure 6.11: (a) Fifteen points were taken on the poster board sitting 9 inches from the LPSM. The error is placed into the area of the field of view where it occurs and color-coded for better readability. The percentage area is shown for (b) X, (c) Y, and (d)Z, and the inches error is shown for (e) X, (f) Y, and (g) Z.

Table 6.10. Data with calculates X, Y, and Z positions

Point	Xdist (in)	Ydist (in)	X1 (V)	Y1 (V)	X2 (V)	Y2 (V)	Z (in)	X (in)	Y (in)
1	0	0	-1.7	-5	-6.5	-5	8.938	0	0.000
2	0	0.5	-1.7	-3.8	-6.7	-3.6	8.580	-0.014	0.269
3	0.125	1.25	-0.9	-0.2	-6.1	0	8.250	-0.181	0.960
4	0.125	1.875	-0.7	3.6	-5.9	3.8	8.250	-0.220	1.659
5	0.125	2.625	-0.7	6	-5.3	6	9.326	-0.202	2.244
6	0.875	0	2.5	-5	-2.5	-5	8.580	-0.854	0.040
7	0.875	0.5	2.7	-3.2	-2.5	-3.1	8.250	-0.873	0.408
8	0.875	1.25	2.7	0	-2.5	0.1	8.250	-0.873	0.996
9	0.875	1.875	2.9	3.8	-2.1	4	8.580	-0.934	1.723
10	0.875	2.625	2.7	5.8	-1.9	5.8	9.326	-0.941	2.202
11	1.75	0	5.7	-4.8	1.9	-4.8	11.289	-1.854	-0.212
12	1.75	0.5	6.1	-3.2	2.1	-3	10.725	-1.879	0.231
13	1.75	1.25	6.3	0.2	2.1	0.4	10.214	-1.854	1.042
14	1.75	1.875	6.3	4.2	2.3	4.4	10.725	-1.929	2.001
15	1.75	2.625	5.3	5.6	2.1	5.8	13.406	-2.010	2.670

Table 6.11. Data with calculated error by percent and distance

Point	X (%)	Y (%)	Z (%)		X (in)	Y (in)	Z (in)
1	--	--	0.694444		0.000	0.000	0.063
2	--	46.11594	4.666667		0.014	0.231	0.420
3	44.87179	23.233	8.333333		0.056	0.290	0.750
4	75.64103	11.54218	8.333333		0.095	0.216	0.750
5	61.5942	14.51376	3.623188		0.077	0.381	0.326
6	2.380952	--	4.666667		0.021	0.040	0.420
7	0.18315	18.45039	8.333333		0.002	0.092	0.750
8	0.18315	20.28986	8.333333		0.002	0.254	0.750
9	6.761905	8.088889	4.666667		0.059	0.152	0.420
10	7.556936	16.09806	3.623188		0.066	0.423	0.326
11	5.952381	--	25.4386		0.104	0.212	2.289
12	7.380952	53.76812	19.16667		0.129	0.269	1.725
13	5.952381	16.64596	13.49206		0.104	0.208	1.214
14	10.2381	6.705314	19.16667		0.179	0.126	1.725
15	14.88095	1.725328	48.95833		0.260	0.045	4.406
Average:	**18.73676**	**19.76473**	**12.09977**		**0.078**	**0.196**	**1.089**

6.6 Scope Stereo with Absolute Error

Taking points by hand results in a low density of points in the active field of view. Therefore, a way to collect more points in the field of view must be found.

An oscilloscope, the Tektronix TDS 340A, can output a waveform as a set of points in a table. The new oscilloscope was hooked up to the LPSM and the poster was placed 9 inches away. The laser was placed on the pan tilt so that it could be moved very precisely and at the same speed. Starting at the top left of the field of view, the laser was moved at a constant rate down through the field of view until it reached the bottom edge. The waveform was captured on the oscilloscope and saved as a table of data points. The LPSM was moved 1 inch to the right, and the process repeated. The laser was moved to a point on the vertical line and the voltage was read for both positions. When the data was moved to the computer, the data in the tables could be correctly aligned using this known point from both positions.

The maximum and minimum voltages were also taken during the experiment so that the depth could be calculated. The oscilloscope took data at a faster rate than the LPSM could provide data. All duplicate entries were discarded. The rest of the entries were used to find the depth. The depth was then compared to the true 9 inch depth and the error found. Since each vertical line had at least 100 points, the average error was calculated and is displayed in Table 6.12 for each vertical scan.

Even with a much faster rate of data collection and with a much higher point density, the error remains about the same as the 15 point collection error. The percentage error ranges from about 7% to 16%, or about 1 inch.

Table 6.12. Average error for each vertical scan

	Average Z Error (in)	Average Z Error %
Scan 1	0.714	7.937
Scan 2	0.813	9.039
Scan 3	0.908	10.097
Scan 4	1.154	12.824
Scan 5	1.499	16.661
Scan 6	0.899	9.997
Scan 7	0.610	6.788

6.7 Nine Point Stereo with Differential Error

The absolute error has been found to be approximately 10%. If an object is placed in the scene that has known depth differences, then points can be collected and a differential error can be calculated.

The foam poster board is used to create the object. The object is made a total of 2 inches wide by 2.75 inches tall because the active field of view at a 9 inch depth is 2 in by 2.75 in. The object is made up of 3 steps, each 1 inch apart, as seen in Figure 6.12. The closest part of the object is placed 8 inches from the LPSM. The field of view at 8 inches will be smaller than the field of view at further away depths, so it is a concern that the points chosen on the 8 inch area are still within the field of view.

The object was placed in front of the LPSM and the laser shined at a point. The voltage was taken and the LPSM moved to the right by 1 inch. The new voltage was recorded. The point where the laser hit the calibrated object was marked. The laser was then moved to another point and the procedure was repeated. The points were counted going from top to bottom and then left to right.

Table 6.13 summarizes the data collected. Point 1 is used as a reference point. The data, along with the recorded max x and max y values, can be used to calculate the coordinates of each point. The calculated coordinates are then adjusted so that they represent the distance from the reference point. Table 6.14 shows the calculation results.

Using the calculated data, the error in the expected results versus the actual results is found. The error is reported in both inches and percentage difference, as seen in Table 6.15.

(a) (b)

Figure 6.12: (a) A calibrated object was placed in the field of view. (b) The object was placed in front of the LPSM and points were recorded.

Table 6.13. Data collected from experiment

Point	X (in)	Y (in)	Z (in)	X1 (V)	Y1 (V)	X2 (V)	Y2 (V)
1	0	0	0	0.9	-2.5	-2.3	-2.7
2	0.125	0.9375	1	1.9	-5.3	-6.1	-5
3	0.3125	1.75	2	1.1	2.7	-7.8	3.1
4	0.6875	0	0	2.8	-2.5	-0.8	-2.7
5	0.6875	0.9375	1	6.1	-5.5	-2	-5.2
6	0.875	1.8125	2	6.1	3.3	-3.1	3.4
7	1.25	0.0625	0	4.2	-3.3	0.8	-3
8	1.125	1	1	8.3	-5.6	1.3	-5.5
9	1.3125	1.8125	2	8.6	3.8	0.6	3.9

Table 6.14. Position calculated with point 1 as reference

Point	Z (in)	X (in)	Y (in)	Adjusted X (in)	Adjusted Y (in)	Adjusted Z (in)
1	15.234	-0.219	0.901	0.000	0.000	0.000
2	6.094	-0.263	0.764	-0.044	-0.137	-9.140
3	5.478	-0.376	-0.350	-0.157	-1.251	-9.756
4	13.542	0.278	0.801	0.497	-0.100	-1.692
5	6.019	0.253	0.783	0.472	-0.118	-9.215
6	5.299	0.163	-0.414	0.382	-1.315	-9.935
7	14.338	0.735	1.120	0.954	0.219	-0.896
8	6.964	0.686	0.923	0.905	0.022	-8.270
9	6.094	0.575	-0.548	0.794	-1.449	-9.140

Table 6.15. Error in calculated positions

Point	X Error in	X Error %	Y Error in	Y Error %	Z Error in	Z Error %
1	--	--	--	--	--	--
2	0.387	310.000	0.800	85.431	8.140	814.025
3	0.688	220.44	0.498	28.511	7.756	387.823
4	0.409	59.595	0.099	#DIV/0!	1.692	#DIV/0!
5	0.434	63.187	0.819	87.464	8.215	821.548
6	0.711	81.366	0.497	27.454	7.935	396.754
7	0.514	41.176	0.281	450.255	0.895	#DIV/0!
8	0.439	39.047	1.022	102.207	7.269	726.971
9	0.737	56.190	0.363	20.050	7.140	357.012

Table 6.16. Error recalculated with point 5 as reference

Point	X Error in	X Error %	Y Error in	Y Error %	Z Error in	Z Error %
1	0.468	68.181	0.819	87.366	10.215	1021.54
2	0.300	53.333	0.018	#DIV/0!	0.074	#DIV/0!
3	0.001	0.374	0.320	39.451	1.541	154.147
4	0.277	#DIV/0!	0.919	98.049	8.522	852.267
5	0.253	#DIV/0!	0.0004	#DIV/0!	0.0004	#DIV/0!
6	0.024	13.043	0.321	36.786	1.720	172.008
7	0.172	30.718	0.538	61.496	9.319	931.92
8	0.248	56.734	0.202	324.12	0.945	#DIV/0!
9	0.050	800	0.456	52.123	0.925	92.525

Point 1 was chosen as the reference point in the previous calculations. Point 1 lies in a corner, where more distortion is probably occurring. Therefore, a new reference point is chosen, this time in the middle of the field of view. Point 5 is chosen as the reference point and the error is recalculated, as shown in Table 6.16.

Using a reference point in the middle of the field of view does improve the differential error. However, the error in both cases is significantly greater than the absolute error from previous experiments.

6.8 Pipe Weld

One possible application of this system would be to reverse engineer objects. Since the object must be of the same size and material, a pipe weld is modeled. The laser scanning system is not yet built, so the point collection has to be done manually. Attempting to model the pipe weld will help to see flaws in the current data acquisition system and study test accuracy.

6.8.1 Manual Point Collection

A pipe weld, shown in Figure 6.13, of constant color and material was to be modeled.

The laser was pointed at the pipe weld within the active field of view. The voltages for both positions of the LPSM were recorded. The laser was moved slightly and the process repeated. About 200 points were collected for the 3 in by 4 in area.

Figure 6.13: A pipe weld was to be modeled.

6.8.2 Manual Point Calculation and Modeling

The points were entered into an excel spreadsheet and the corresponding X, Y, Z coordinate was found. These points were then entered into a VRML file and imported into RapidForm 2004, giving Figure 6.14.

Since the points were not very dense, the volume function was used to add points. The triangulate function could then be used to create a 3D model.

A bump can be seen in the 3D model corresponding to where the weld should be. The area flattens out away from the bump. The shape is not very good because the points are not very dense. The program had to add some points and make assumptions to connect the points. From the model, it can be seen that a way to collect more points needs to be found.

When looking at the points, it seems that the majority of the points are concentrated in a small area, along with some extraneous points. These points were deleted and the remaining points were re-triangulated to try to get a better shape.

The deletion of extraneous points did not seem to help the shape a lot. Sampling points at a higher density may help to give a better shape.

6.8.3 Scope Point Collection

The Tektronics TDS 340A oscilloscope can save a waveform and output it as a table of points. The pipe weld was placed in front of the LPSM and the laser scanned a vertical

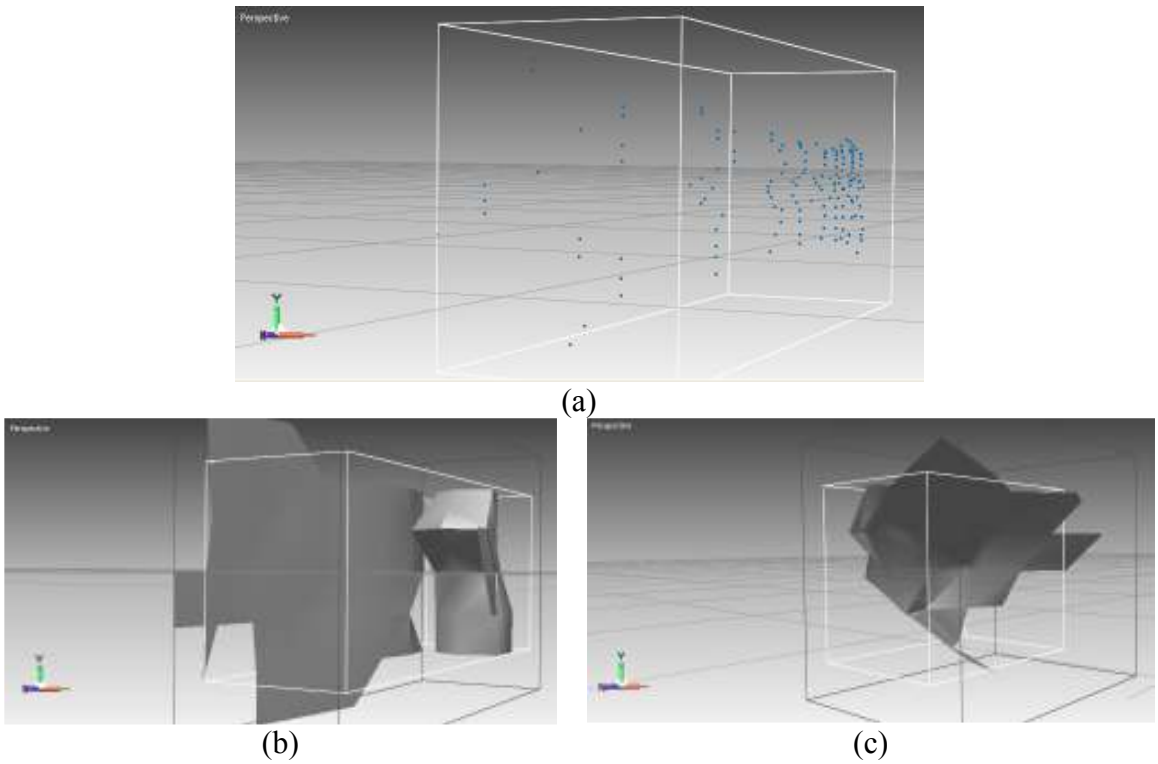

(a) (b) (c)

Figure 6.14: (a) The manually collected data points were entered into RapidForm 2004. (b) Functions in RapidForm allowed the points to be connected to form a 3D shape. (c) Extraneous points were deleted to try to create a better 3D shape.

line in the field of view, as seen in Figure 6.15. The waveform was captured on the oscilloscope and saved to a disk as a table of points. The LPSM was moved by 1 inch and the laser traced the same scan. By taking the voltage of one point along this line at both positions, the data in the two tables could be aligned.6.8.4 Scope Point Calculation and Modeling

About 10 scans of data were taken, consisting of about 600+ points per vertical scan. The oscilloscope outputs points at a faster rate than the response time of the LPSM. Therefore, not all the data was good data. Duplicate points were removed from the data. The X, Y, and Z coordinates were calculated for the remaining data. The coordinates were then sampled every 0.033 inches in the Y direction. The coordinates were filtered for 4 vertical scans, giving the dataset to be modeled.

The points were imported into RapidForm 2004 and then triangulated. Figure 6.15 shows the resulting 3D form. The section modeled is about 0.25 in wide by 1 in tall and consists of 400+ points.

(a)

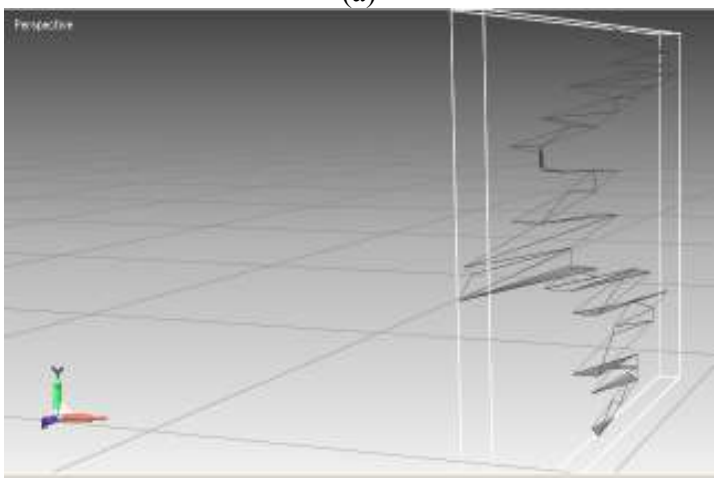

(b)

Figure 6.15: (a) The oscilloscope was used to take data at a high density. (b) Functions in RapidForm connected the dense points to form a 3D shape.

It can be seen that the shape is not very smooth, even with a denser sampling of points. As was seen from the poster experiments, the error tends to be about 10%, or 1 inch. The pipe weld was sitting about 9 inches away from the LPSM, meaning that 10% error corresponds to 0.9 in. The pipe weld is less than 1 inch in height. Therefore, the average error seen is actually larger than the change in height.

The expected error is larger than the height change to be detected. Therefore, it is not surprising that the 3D model is very jagged. It can be seen that there is a bump in the middle, about where the weld should be. The areas on top of the bump and below the bump are supposed to be slightly further away and flatter. This general shape can be seen, but it is not smooth and probably contains considerable error.

6.9 Object Modeling

From modeling the pipe weld, a good system using an oscilloscope was found for point collection. It was also seen that the system seems to have a lot of error. To test the error, calibrated objects need to be modeled so that the calculated points can be compared to where the true points lie in space. By analyzing the error of the calibrated objects, correction methods can be developed and tested.

6.9.1 Final System Setup

The system needs to be tested on calibrated objects to test for performance boundaries and error. Objects that can easily be modeled are used, such as a rectangular prism and a triangular prism. The objects also need to be of the same material and the same color as the background or the constant will be incorrect, as shown from previous experiments.

Since the field of view at a 9 inch distance is only 2 inches by 3 inches, small wooden toy objects, as seen in Figure 6.16, are used in the final system test. The objects include a rectangular prism, a triangular prism, a cylinder, a cone, a pyramid, and a cone with the top cut off.

A wooden board was found that was about the same color as the wooden objects. The board was placed 10 inches away from the LPSM and aligned to be parallel with the slider. Books were placed in front of the board so that when an object was placed in front of the board, it was high enough to be in the field of view of the LPSM. A piece of white poster board was placed on the top of the books so that any reflections that hit the surface would be uniformly reflected. The laser was placed on a pan tilt behind the LPSM, a little to the right of center, so that it did not interfere with the output cable from the LPSM. When modeling an object, the object was placed on the books and pushed back until it touched the wooden board.

The laser was then turned on and pointed to hit the board within the field of view of the LPSM. The laser was moved along the X-axis until the maximum x value was found. The value was recorded, and the process repeated to find the minimum x value. The laser was then moved to the middle of the field of view and moved along the Y-axis to find the maximum and minimum y values. These values would later be used to find the constant for converting the output voltages from the LPSM to distances.

The x and y outputs of the LPSM were attached to a Tektronics TDS400A oscilloscope. The oscilloscope was set to take 200 samples per second. Using the pan tilt, the laser made one vertical scan in the field of view, and the waveform was captured on the oscilloscope. The output was saved as a table of points to a floppy disk. The laser was then moved to a set point along the vertical line, and the x and y values were recorded. The LPSM was slid one inch to the right, and the new x and y values were recorded for the same point. The laser scanned the original vertical line, and the data was again

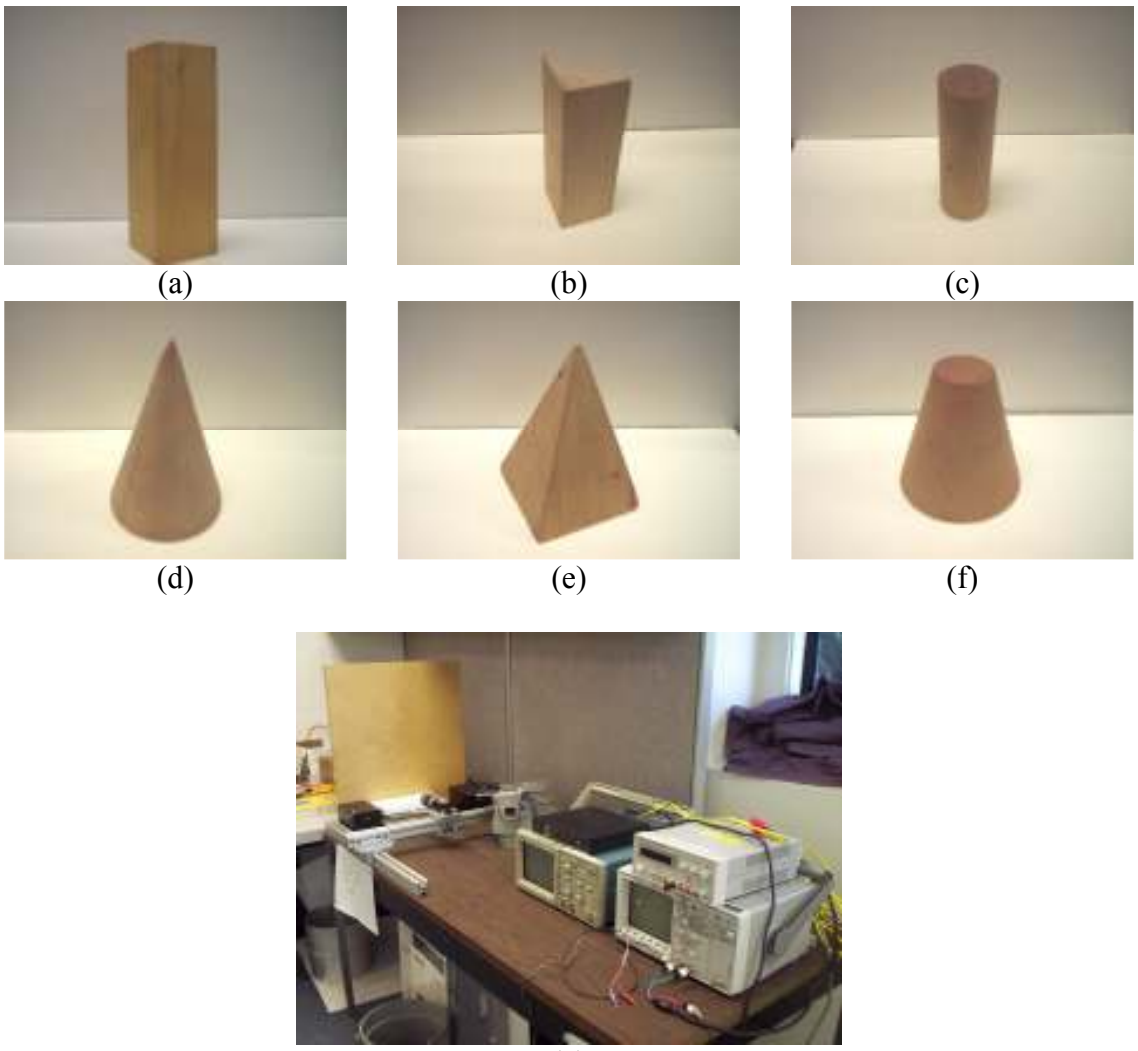

(a) (b) (c)

(d) (e) (f)

(g)

Figure 6.16: Six wooden objects were modeled including (a) a rectangular prism, (b) a triangular prism, (c) a cylinder, (d) a cone, (e) a pyramid, and (f) a cone with the top cut off. (g)In the final system setup, a board was placed ten inches from the slider. The object was placed directly in front of the board for modeling.

captured and saved. The x and y values recorded were used to find which data points in each of the vertical line scans corresponded to the same point. The laser was then moved slightly to the right, and the process was repeated until the entire field of view was scanned.

6.9.2 Modeling Objects and Data Acquisition

All of the data taken for an object was saved as a spreadsheet. Each vertical scan contained four columns of data: x from LPSM at position 1, y from LPSM at position 1, x from LPSM at position 2, and y from LPSM at position 2. Two more points were also saved for each scan telling an x and y point from position 1 that corresponded to an x and y point from position 2. Since the laser was moving at a constant speed for both scans and since data was being sampled at a constant rate, then if these two points could be lined up, then the rest of the data in the table would also be correctly aligned. Therefore, this reference point was used to align data from the LPSM at position 1 to data from the LPSM at position 2.

Assuming linearity, the maximum x value and the maximum y value were divided by 2 mm, the position where the maximum value should occur on the active area of the LPSM, giving two constants. The voltages in the table were converted to distances by dividing by the respective constant. The distances, along with the known focal length and baseline, were applied to stereo vision equations to give an X, Y, Z coordinate for each set of points in the table.

Since each scan represented one vertical sweep in the field of view, the X distance should be approximately the same. Therefore, the average X value was found and used for all points within one vertical sweep. The Y and Z coordinates were filtered so that only unique points were left. This process was repeated for each vertical scan, leaving approximately 100 to 150 points per vertical scan.

All of the points from each of the vertical scans were combined and imported into RapidForm to create a final model of the entire field of view. To easily see the depth of each point, a color map was to be added to the point cloud. To add a color depth map in RapidForm, a surface must be present. Therefore, the triangulate→3D command in RapidForm was used to fit a surface to the points. The inconsistent density of points in the color depth maps appears after RapidForm processing, possibly due to an automatic redundant data removal algorithm.

Once the surface was created, the contour line command was used to add a color depth map to the remaining points. Blue colors meant that the point was closer to the LPSM, while red and yellow colors meant that the point was further away. The map allowed the viewer to easily see the depth of all points to see whether the object was correctly modeled.

6.9.3 Background

The background wooden board was modeled with no object to create a base of comparison. Ten vertical scans comprised the entire field of view, an area two inches wide and three inches tall. Figure 6.17 shows the results.

The position of the board was measured to within 0.0625 inches using a ruler. To attempt to reduce this error, a plane can be fitted to the data. If the wooden board is not truly parallel to the slider, this error will also be filtered out by using a best fit plane. The program lsplane.m from Eurometros was used to find the best fit plane for the data using Matlab. The plane was then created in RapidForm. It was expected that the plane be perpendicular to the *Z*-axis. However, it can be seen in Figure 6.17 that the plane is very skew. Although the data fits the plane, the data has so much error that the best fit plane probably contains more error than the plane measured with a ruler. Therefore, the plane measured by hand that sits perpendicular to the Z-axis at 10 inches was created in RapidForm for comparison.

To study the error, the calculated depth was compared to the actual depth. The actual depth was set at the measured distance of the plane, or 10 inches, for all points. The percent error was calculated as:

$$\%Error = \left(\frac{|\ ActualDepth - CalculatedDepth\ |}{ActualDepth} \right) 100\ . \qquad (31)$$

The error was first plotted as a depth map, where the error at each point was plotted at its X,Y coordinate. Since the laser made vertical sweeps through the scene, many points were grouped at certain X values. Therefore, all points that occurred at a given X value were grouped together and the average error was found and graphed. The points were scattered along the Y axis. Points within 0.2 inches were grouped together and the average error found and graphed. A similar procedure as to the X values was used to create the plot for error versus the depth. The error versus the x distance and y distance can be seen in Figure 6.18. Since all points should have been on a plane at 10 inches, the error versus the depth was averaged and found to be 6.5%.

The error versus the x distance does not seem to have a pattern. The error versus the y distance shows that the error remains fairly constant in the middle of the field of view and increases at the edges of the field of view.

6.9.4 Rectangular Prism

The first object modeled was the rectangular prism. The prism was placed directly in front of the wooden board background. Ten vertical scans were taken to create the color depth model. The color depth model is measured in inches.

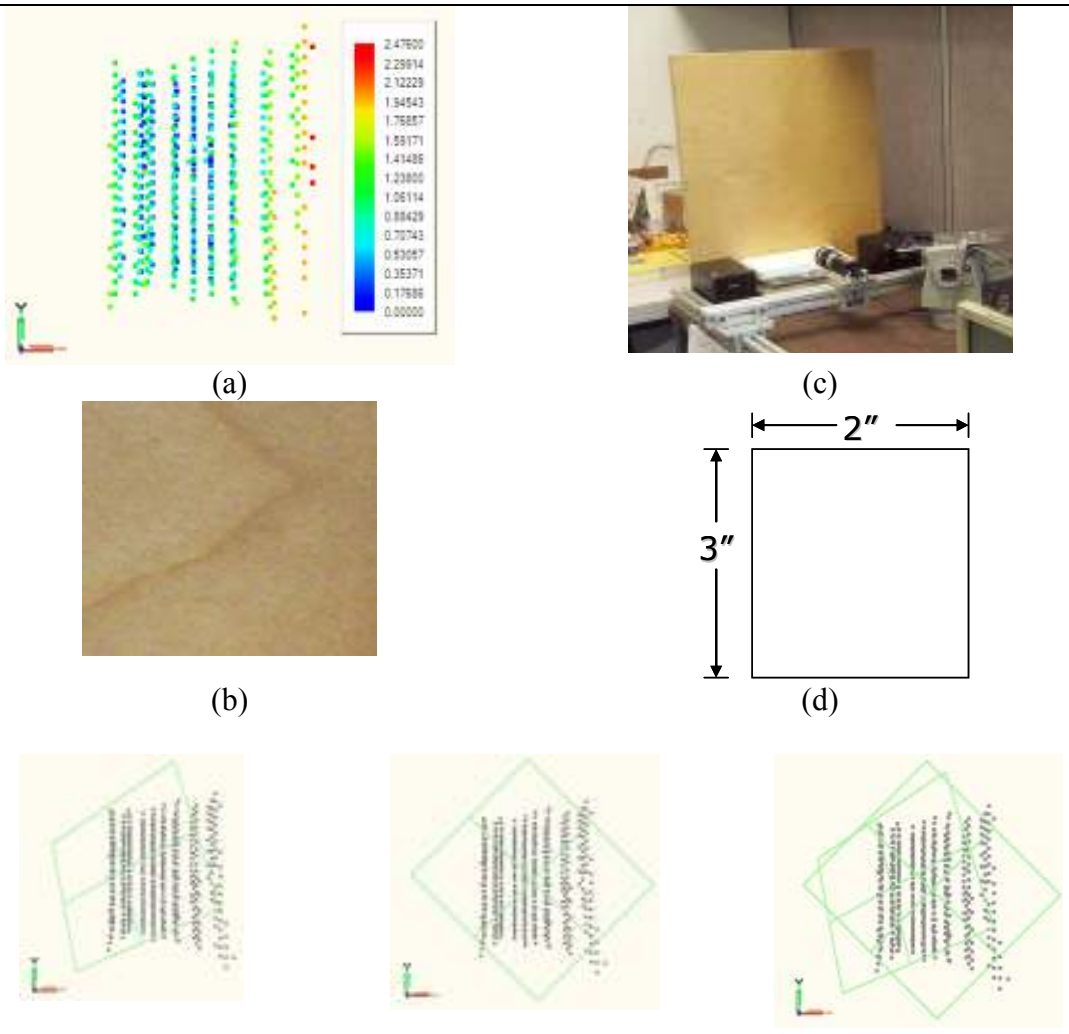

(a) (c)

(b) (d)

(e) (f) (g)

Figure 6.17: (a) The color depth map in inches and (b) visual photo of the triangular prism can be seen as well as (c) the triangular prism in the entire system and the (d) actual dimensions of the object. (e) The best fit plane is calculated and placed in RapidForm. Since the best fit plane is skew, the (f) measured plane is also created in RapidForm and (g) can be compared to the best fit plane.

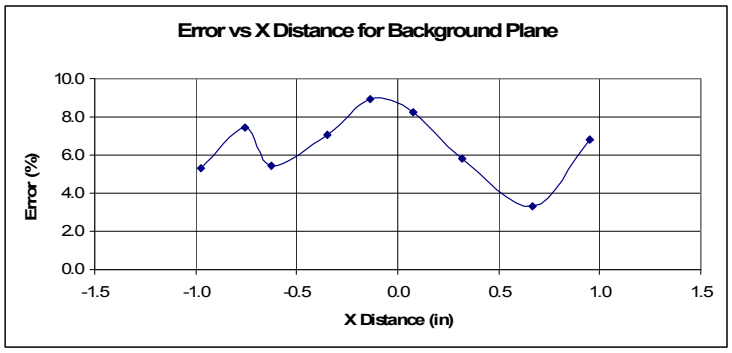

(a)

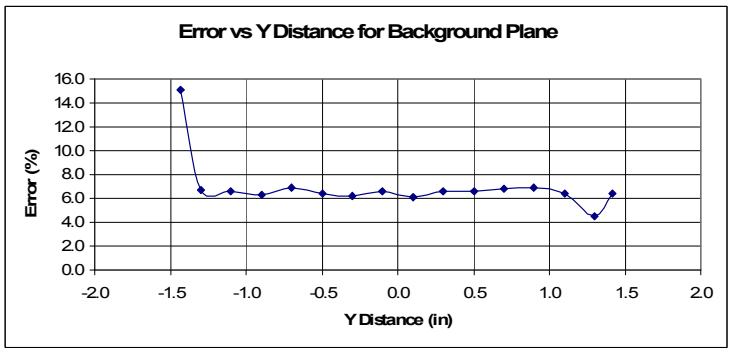

(b)

Figure 6.18: The average error or the background plane is graphed against (a) the x distance and (b) the y distance.

The depth model can be compared to the visual picture in the field of view and also to the actual dimensions of the object.

The cluster of blue dots in the center of the color depth map indicates an object close to the LPSM. The green, yellow, and red dots on either side of the blue cluster represent the backdrop, which is further away. The inconsistency of the dots is due to processing by RapidForm.

Since the data points on the object should be on a plane perpendicular to the *Z*-axis at 9 inches, the best fit plane method was again tried. The best fit plane was created in RapidForm, along with the expected plane, as seen in 6.19. The best fit plane was even more skew than the best fit plane for the background, so it was again decided that absolute error calculations would probably give a better indication of the true error.

The same methods as were used for the background plane were used to compare the error to the x distance, y distance, and depth. The four graphs can be seen in Figure 6.20.

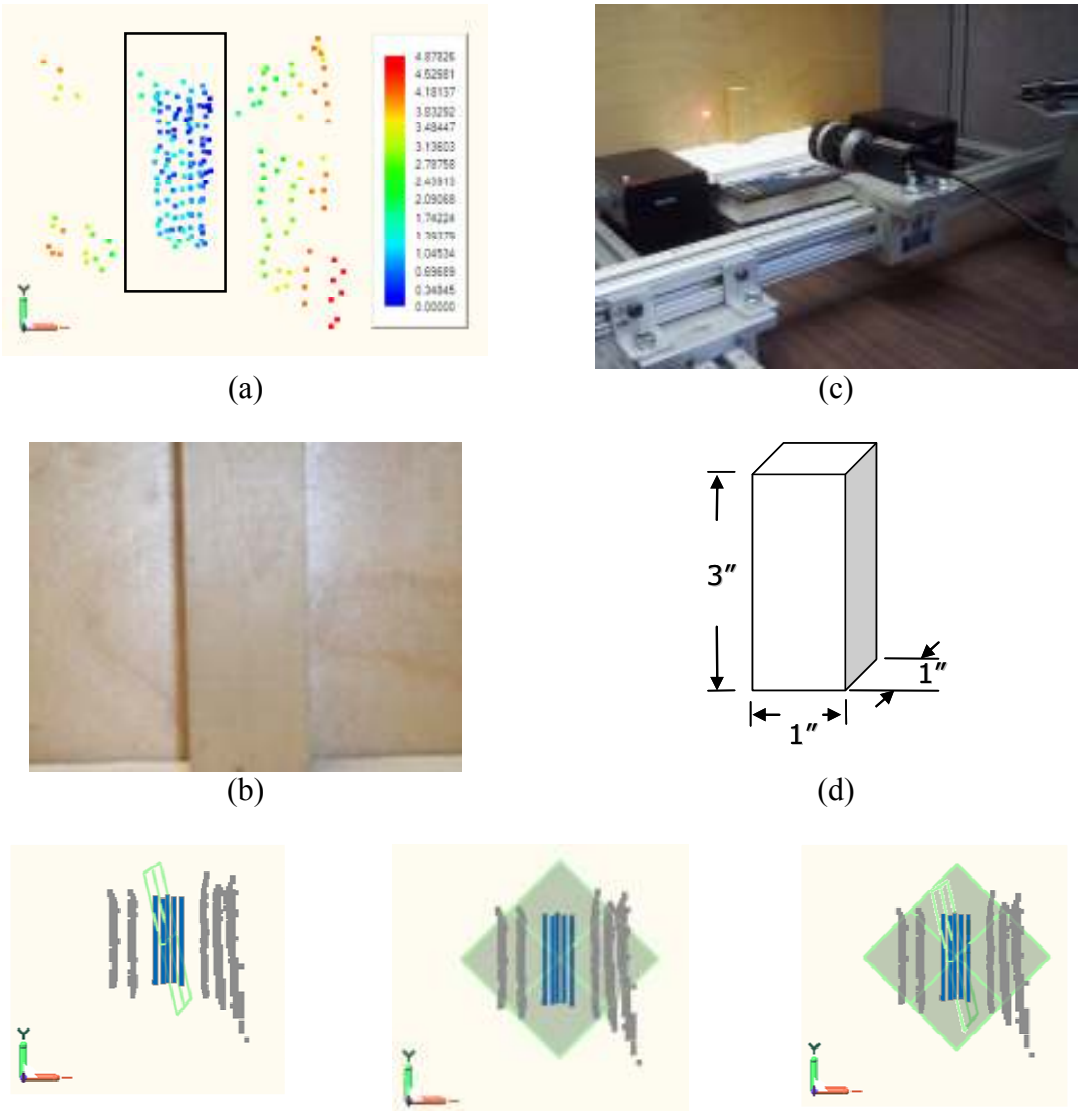

(a) (c)

(b) (d)

(e) (f) (g)

Figure 6.19: (a) The color depth map in inches and (b) visual photo of the rectangular prism can be seen as well as (c) the rectangular prism in the entire system and the (d) actual dimensions of the object. (e) The best fit plane is calculated and placed in RapidForm. Since the best fit plane is skew, the (f) measured plane is also created in RapidForm and (g) can be compared to the best fit plane.

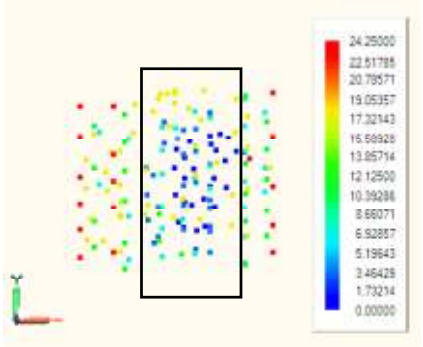

(a)

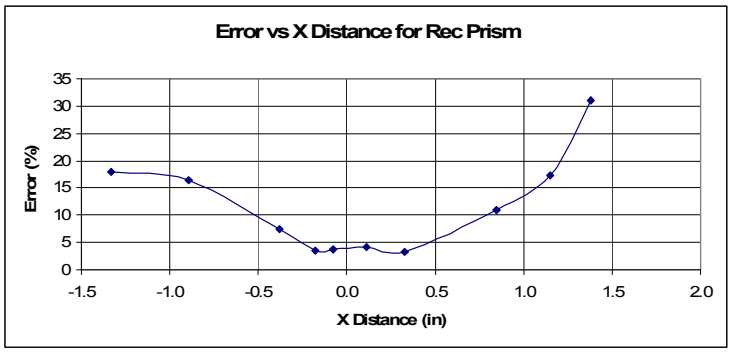

(b)

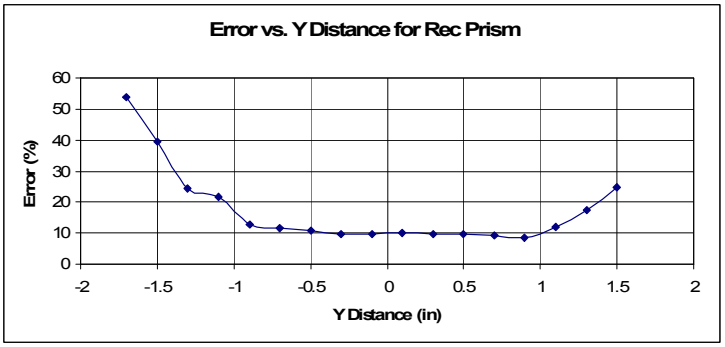

(c)

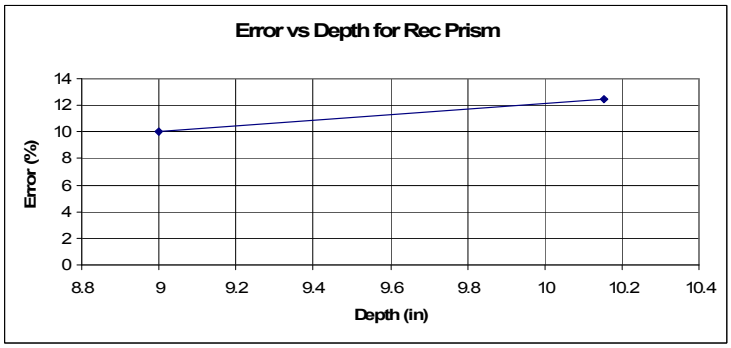

(d)

Figure 6.20: The percent error is graphed against (a) the (x,y) position, (b) the x distance, (c) the y distance, and (c) the depth for the rectangular prism.

The error against the x distance has less error in the middle of the field of view and has larger error at the edges. The y distance follows the same trend as the background, with constant error in the middle of the field of view and larger error at the edges. The error against depth has smaller error at closer areas and larger error at further away areas of the scene. From the depth plot, the least amount of error seems to occur on the object, which is the closest part of the scene.

6.9.5 Triangular Prism

Figure 6.21 shows the modeling of the triangular prism. The color depth map can be seen compared to the visual photo of the field of view of the LPSM and the actual object dimensions.

It is known that the back of the triangular prism is 10 inches away from the LPSM. Since the geometry of the triangular prism is known, the depth of the rest of the shape can be calculated with three equations, an equation for the background, for the left face, and for the right face of the prism. Error is then calculated in the same way as the rectangular prism and is graphed, as seen in Figure 6.22.

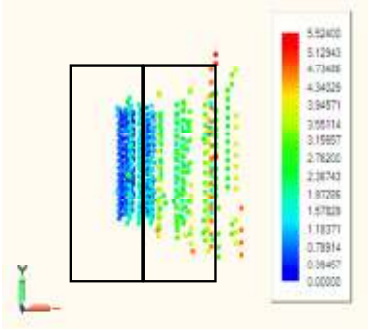

(a)

(c)

(b)

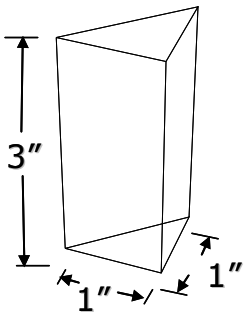

(d)

Figure 6.21: (a) The color depth map in inches and (b) visual photo of the triangular prism can be seen as well as (c) the triangular prism in the entire system and the (d) actual dimensions of the object.

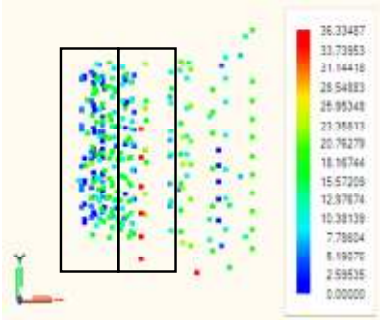

(a)

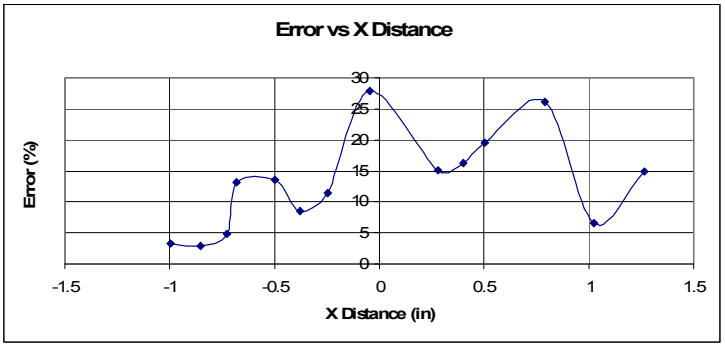

(b)

(c)

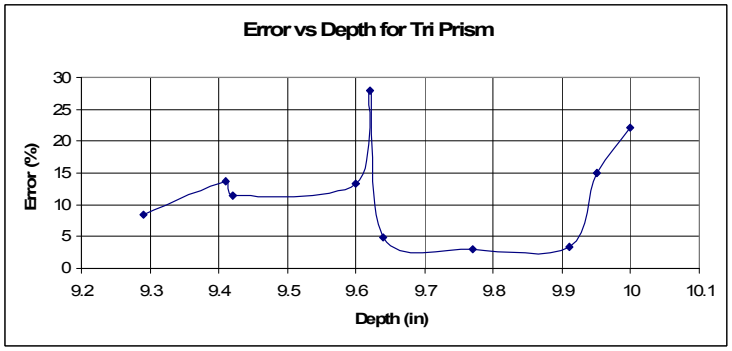

(d)

Figure 6.22: The percent error is graphed against (a) the (x,y) position, (b) the x distance, (c) the y distance, and (d) the depth for the triangular prism.

It can be seen from the graph that the error does not follow a clear pattern when compared to the x distance. When compared to the y distance, the error is again constant in the middle of the field of view, but is less towards the bottom and is larger towards the top of the field of view. The error versus depth is also not constant or linear, but it can be seen that there is more error at 10 inches than at 9 inches away. According to the depth plot, the most error occurs in the middle of the right face of the prism. The least amount of error occurs on the left face.

6.9.6 Cylinder

The next object modeled was the cylinder, shown in Figure 6.23. Ten vertical scans were taken to model the entire cylinder. The color depth map can be seen compared to the visual photo of the field of view of the LPSM and the actual object dimensions.

The error was calculated using the same method as the other shapes. Figure 6.24 shows the percent error plotted at its x,y point, against the x distance, against the y distance, and against the depth.

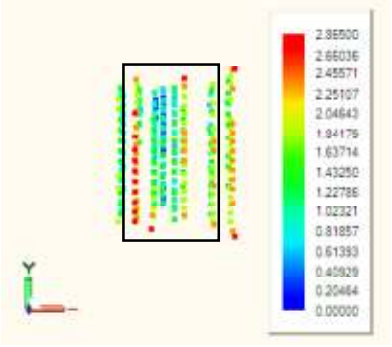

(a)

(c)

(b)

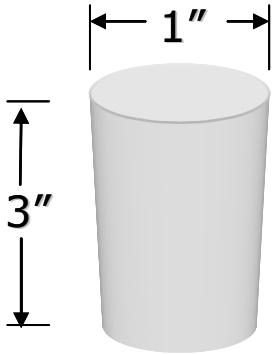

(d)

Figure 6.23: (a) The color depth map in inches and (b) visual photo of the cylinder can be seen as well as (c) the cylinder in the entire system and the (d) actual dimensions of the object.

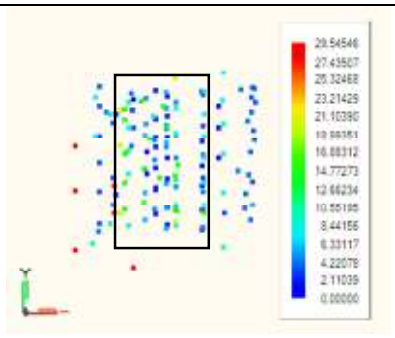

(a)

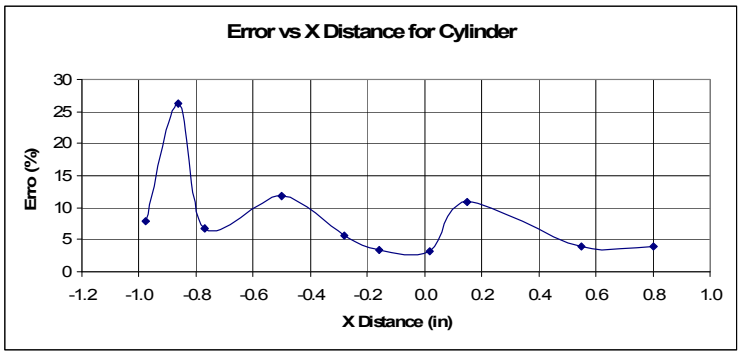

(b)

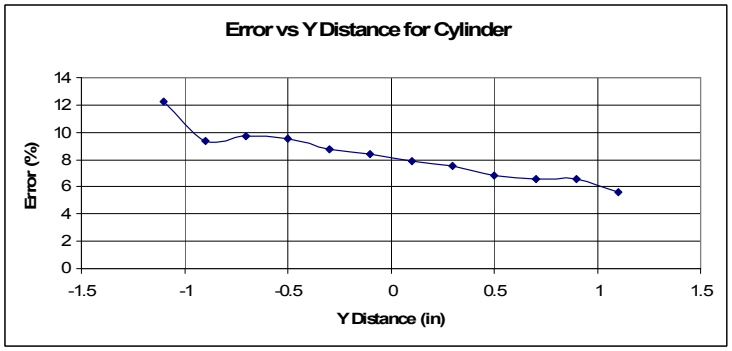

(c)

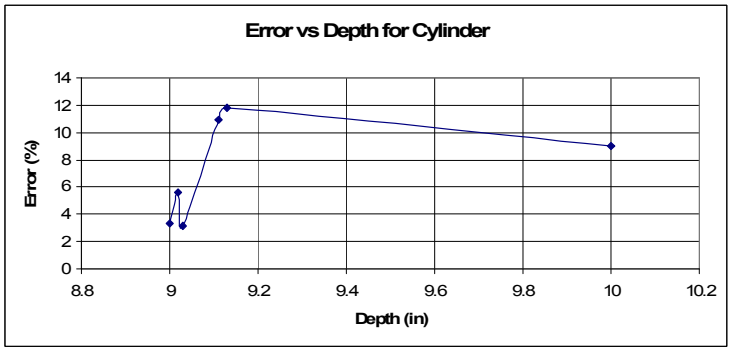

(d)

Figure 6.24: The percent error is graphed against (a) the (x,y) position, (b) the x distance, (c) the y distance, and (c) the depth for the cylinder.

The error against the x distance still shows no clear pattern. The error against the y distance is still constant in the middle of the field of view and changes at the edges. Although the maximum error does not occur at the 10 inch point when compared to the depth, the error is greater at 10 inches than at 9 inches away. From the depth plot, it appears that the error is more evenly spread throughout the scene than it was for the rectangular prism or triangular prism.

6.9.7 Cone

Three shapes, a cone, a pyramid, and a cone with the top cut off, were also modeled. The error was not calculated for these objects since their shape was increasingly difficult to correctly and accurately model. However, the user should be able to see the shape using a depth map and subjectively determine how good the model is. The cone was first modeled and can be seen in Figure 6.25.

Red, yellow and green dots in the upper right corner indicate the background. It was expected that dark blue dots be at the bottom of the cone, and lighter blue or green dots be at the top of the cone, since the top is further away than the bottom of the cone.

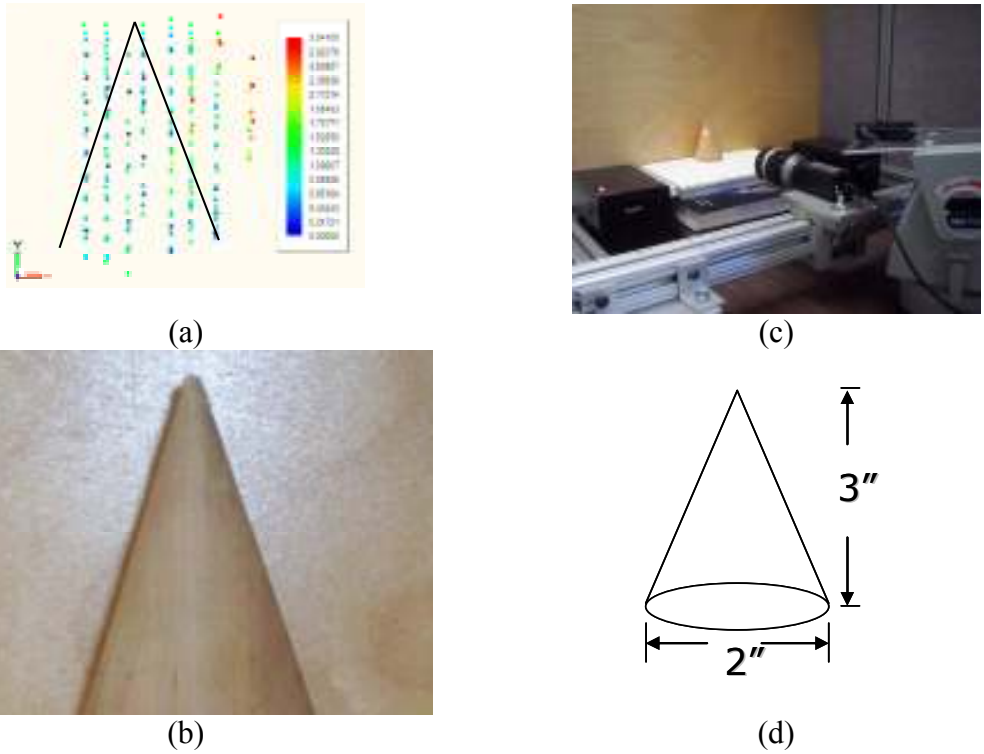

(a) (c)

(b) (d)

Figure 6.25: (a) The color depth map in inches and (b) visual photo of the cone can be seen as well as (c) the cone in the entire system and the (d) actual dimensions of the object.

However, the depth plot shows a fairly constant mix of blue and green dots along the entire cone area. Since the cone face is at a different angle than the triangular prism and cylinder, the laser intensity being reflected back to the LPSM may be different, causing different error. The top left part of the background may not be seen because the laser was placed slightly to the right of the center of the scene. Then, when the laser was pointed to the left part of the scene, some of the beam may have been hitting the cone instead of the entire beam hitting the background.

6.9.8 Pyramid

A four-sided pyramid was the next shape to be modeled and can be seen in Figure 6.26.

The laser was placed slightly right of the center, so when the beam hit the background to the right of the pyramid, it was hidden from the LPSM. Therefore, only the left side of the pyramid was modeled. The upper left area of the plot has green, yellow, and red dots indicating the background. The pyramid had more blue and green dots. There should have been more dark blue dots towards the bottom of the pyramid and light blue or green dots at the top of the pyramid.

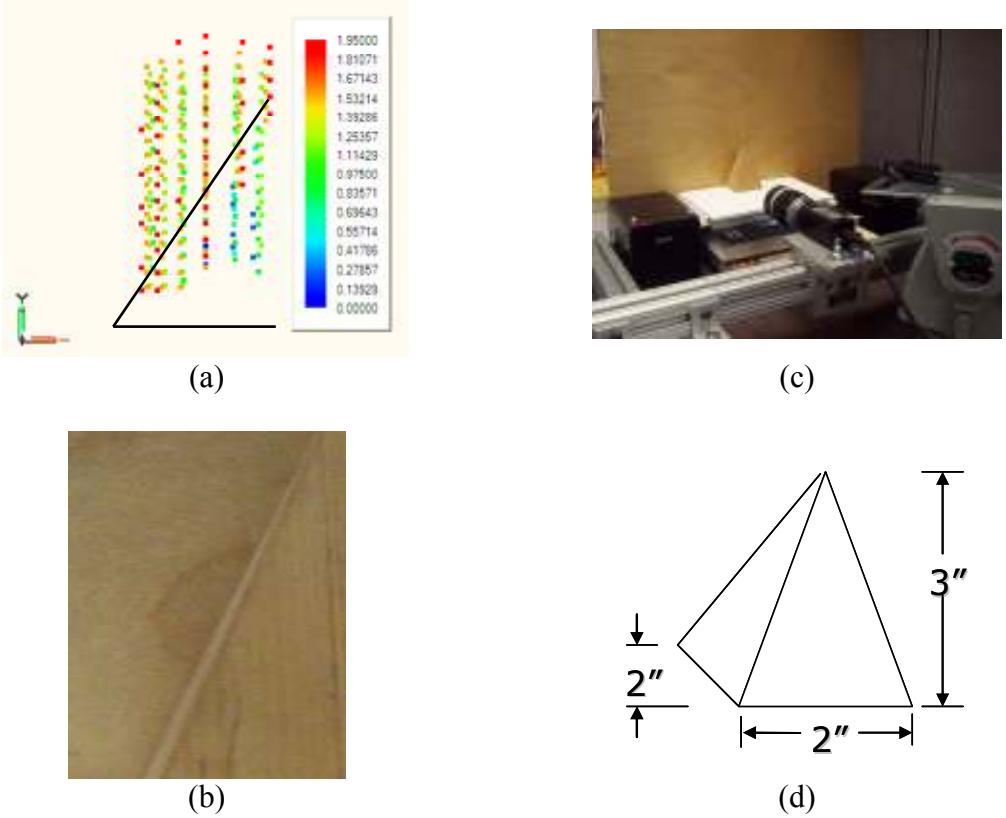

Figure 6.26: (a) The color depth map in inches and (b) visual photo of the pyramid can be seen as well as (c) the pyramid in the entire system and the (d) actual dimensions of the object.

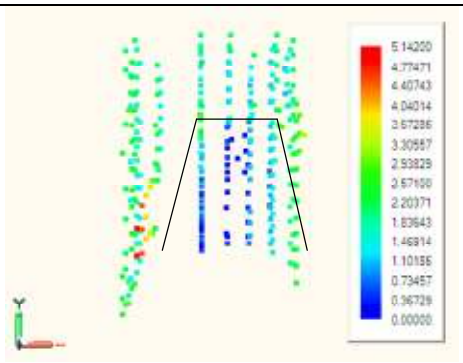

(a)

(c)

(b)

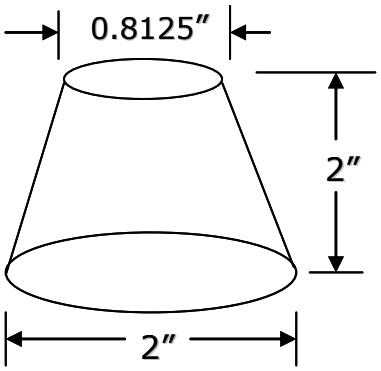

(d)

Figure 6.27: (a) The color depth map in inches and (b) visual photo of the cone with the top cut off can be seen as well as (c) the cone with the top cut off in the entire system and the (d) actual dimensions of the object.

6.9.9 Cone with Top Cut Off

The last object modeled was a cone with the top cut off and can be seen in Figure 6.27.

The cluster of dark blue dots indicates the object. The green, yellow, and red dots represent the background. There should be more dark blue dots concentrated at the bottom of the object and lighter blue or green dots at the top. However, all of the dots on the object seem to be spread out fairly consistently.

6.9.10 Conclusions

The error versus x distance is first studied. When comparing the graphs from the rectangular prism, triangular prism, cylinder, and background, no pattern seems to

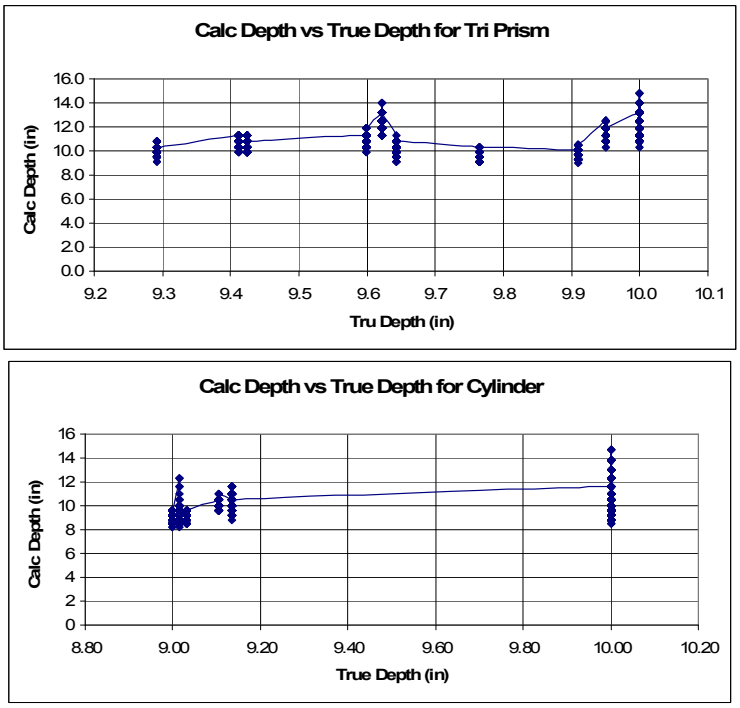

Figure 6.28: Calculated depth is plotted against measured depth for (a) the triangular prism and (b) the cylinder.

emerge. Each object has different depths at different points along the x axis, which could cause the irregular patterns in each graph.

When the error versus y distance graphs are compared for the same objects, the only obvious pattern is that the error becomes constant in the middle of the field of view. At the edges of the field of view, the error changes, but the change at the edge is not predictable.

The error versus depth plots are not very consistent for intermediate depths. However, it can be seen that the error at 9 inches is always smaller than the error at 10 inches. This suggests that error may be a function of depth. To see if there is a fixed constant that can be applied to correct the calculated depth, the calculated depth is graphed against the measured depth. These plots for the triangular prism and cylinder can be seen in Figure 6.28.

From the graphs, it can be seen that multiple points occur at the same absolute depth. Therefore, there is no one-to-one correspondence between the calculated depth and absolute depth, meaning that a single constant does not exist to correct the calculated depth.

There have been many problems with laser intensity. From previous experiments, it was proven that laser intensity changes with depth. Therefore, the LPSM is probably seeing different levels of intensity of the laser according to the depth of the object. The objects

being modeled are also different shapes. The laser hits the face of the object, but according to the angle of the object surface, the laser is being reflected in different directions. Unless the object surface is facing the LPSM, not all of the reflections will be directed back to the LPSM, again affecting laser intensity. Intensity may also be reduced according to how sharp of an angle the laser beam is directed at the object. If the laser is perpendicular to the object face, then the amount of the laser beam striking the surface will be greater than if the beam strikes the surface at a 45º angle.

6.10 Object Modeling Correction

Three methods were tried to correct the models. First, non-linearity of the LPSM was assumed. Next, multiple new constants were used to try to calculate the depth. Finally, multiple constants were again used to calculate the depth, but the constants were based on the original constant found for each model. Only the third attempt created consistently better models.

6.10.1 Non-Linearity

To create the models, it was assumed that the LPSM was linear throughout the voltage range. Therefore, the constant used to convert voltages from the LPSM to distances was based on the maximum voltages found. The maximum voltage for x or y was divided by 2 mm, the farthest away distance of the active area. The constant was used to convert positive and negative voltages.

When recording the maximum and minimum voltages, it was seen that the two values were usually different, suggesting that the LPSM may not be linear. Therefore, four constants were created to convert voltages to distances: a negative x constant using the x minimum voltage, a positive x constant using the x maximum voltage, a negative y constant using the y minimum voltage, and a positive y constant using the y maximum voltage. The depth was then recalculated using the new distances.

The 4-constant attempt was tried on the rectangular prism. The error was calculated in the same way as for the original model. Figure 6.29 shows the percent error per point of the corrected model versus the percent error per point of the original model.

The corrected model had more error along the left side of the field of view. The error in the rest of the corrected model was about the same as the error in the original model. Therefore, the assumption that the LPSM is linear stands and only two constants are needed to convert voltages to distances.

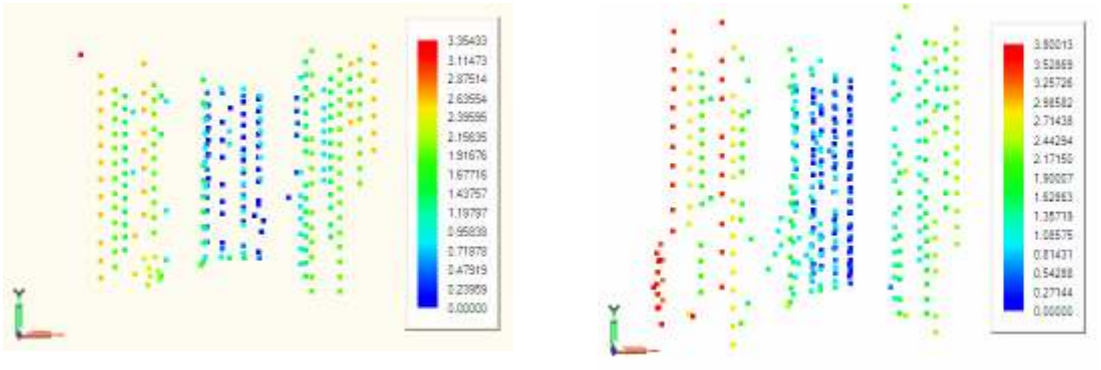

(a) (b)

Figure 6.29: The color depth plots show the percent error according to the point for (a) the original model and (b) the corrected model for the rectangular prism.

Table 6.17. New constants used to change voltages from LPSM to distances

Distance (in)	Max X (V)	Min X (V)	Max Y (V)	Min Y (V)	Xconst (V/mm)	Yconst (V/mm)
10	7	-8.4	6.8	-5.8	3.50	3.40
9.75	7.2	-8.4	7.2	-6.2	3.60	3.60
9.5	7.6	-8.8	7.2	-6.2	3.80	3.60
9.25	7	-8.4	7.4	-6	3.50	3.70
9	7	-8.2	6.6	-5.8	3.50	3.30

6.10.2 Several Constants

From previous experiments, it was seen that the maximum and minimum voltages change with distance. To create the models, the constant found using data from a 10 inch distance was used to convert all voltages, regardless of the depth at which the voltage was taken.

Using the background wooden board, maximum and minimum voltages were recorded when the board was 10 inches, 9.75 inches, 9.5 inches, 9.25 inches, and 9 inches away. Using prior knowledge of the depth from where the voltage was taken, the most appropriate constant was selected and the voltage converted to a distance. The depth was then calculated with the new distances. The new constants can be found in Table 6.17.

The new constants were applied to the triangular prism. The percent error per point for the original model along with the percent error per point for the corrected model can be seen in Figure 6.30.

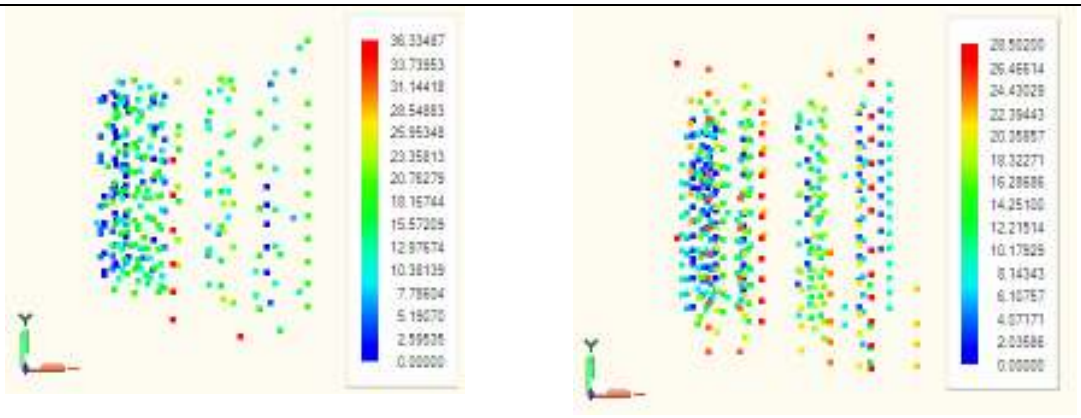

(a) (b)

Figure 6.30: The color depth plots show the percent error according to the point for (a) the original model and (b) the corrected model for the triangular prism.

From the plots, it can be seen that much more error is introduced, especially along the bottom of the field of view. More error was also introduced along specific vertical scans, as shown by the three columns of yellow and red dots in the corrected model.

It was noticed that the new constant for 10 inch distances was not the same as the original constant. The constant at 10 inches changed for each model because the maximum voltage was recorded before the data for the object was taken. Different background light levels and other environment variables may contribute to a change in the constant. Therefore, the data for modeling the object would have to be taken at the same time as when the constants were recorded.

6.10.3 Decreasing Constants

When the minimum and maximum voltages were taken at different distances, it was expected that the maximum voltages would linearly increase as the board moved closer and that the minimum voltages would linearly decrease as the board moved closer. However, the maximum and minimum voltages changed, but without a pattern. Instead of constantly increasing or decreasing, they increased as the board moved from 10 inches to 9.5 inches and then began to decrease. The cause of the inconsistency in the constants was probably due to environment variables, such as background light, reflections, and shadows.

It was decided to attempt to correct the model by changing the constant, based on the original 10 inch constant. For every 0.25 inches closer in depth, the constant was decreased by 0.05 V/mm. All of the calculated depths for a given vertical scan were averaged. The constant used to change LPSM voltages to distances was changed, and the calculated depths averaged again. The constant was changed until the calculated depth was closer to the known depth. Using this method, a 0.05 V/mm decrease in the constant was decided upon for every 0.25 inch decrease in depth.

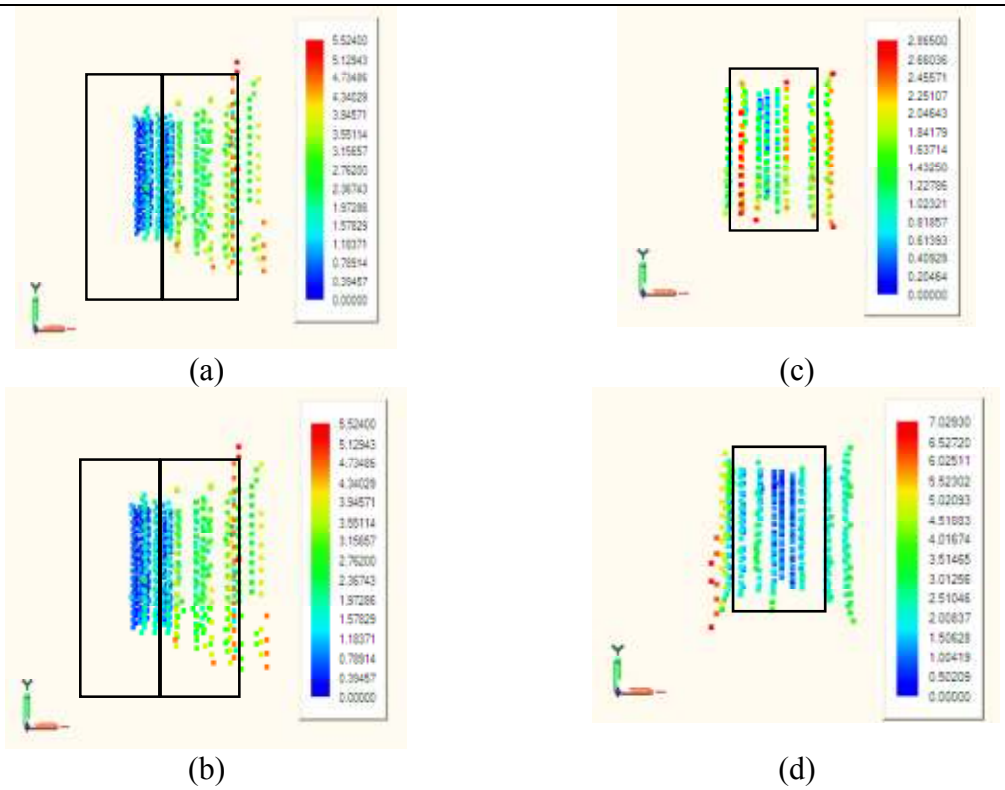

(a) (c)

(b) (d)

Figure 6.31: (a) The original model for the triangular prism can be compared to (b) the corrected model. (c) The original model for the cylinder can be compared to (d) the corrected model.

The rectangular prism, triangular prism, and cylinder were all recalculated using the new formula for the constant. Each object gave less error than the original model. Figure 6.31 shows the original and corrected models for the triangular prism and cylinder.

There is little different between the original and corrected model for the triangular prism. The left face still has blue dots, indicating the closest part of the object, towards the left edge. The dots gradually change from blue to green and yellow towards the right edge of the left face. The background has more red dots, indicating that the background is further away.

The cylinder has more noticeable differences in the original and corrected model. The new model has more dark blue dots at the center of the cylinder. The dots go from dark blue at the center to light blue to green at the edges. The background has green, yellow, and red dots indicating that it is further away. Unlike the original image, all red and yellow dots occur on the background instead of on both the cylinder and the background.

The average error per depth was recalculated for the three objects. The corrected object percent error was graphed along with the original percent error for each object and can be seen in Figure 6.32. In each graph, the error for the corrected model is better than the error for the original model.

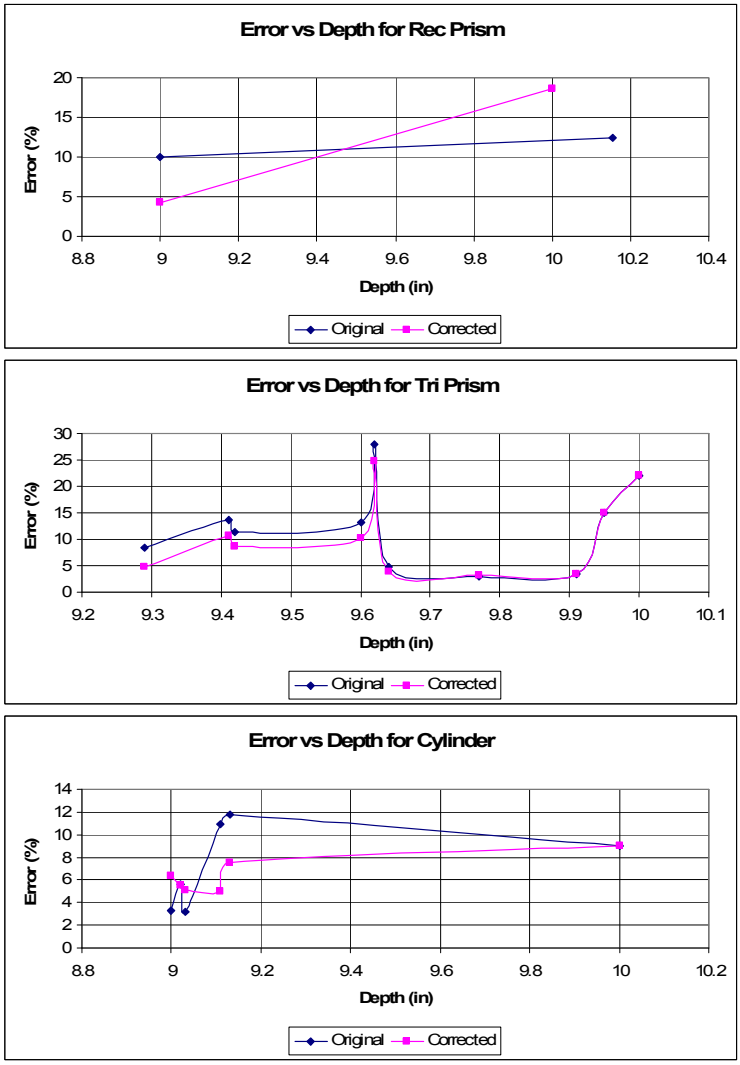

(a)

(b)

(c)

Figure 6.32: The error for the corrected model is compared to the error in the original model for (a) the rectangular prism, (b) triangular prism, and (c) cylinder.

6.10.4 Conclusions

The error in the models seems to be caused by a combination of factors. The main problem appears to be due to laser intensity. The LPSM is very sensitive to laser intensity and its behavior changes according to how much power is incident on its active area.

When pointing a laser directly into the LPSM, different voltages can be seen by changing the depth at which the laser sits. If the laser is reflected off of a piece of white poster board, the maximum and minimum voltages change as depth changes. Therefore, even

small changes in depth seem to change the laser intensity, causing inconsistencies in the output of the LPSM.

There are two factors that may be causing the laser intensity to dramatically change. First, the laser is not well focused. When the laser has a larger fanout angle, the beam spreads out more quickly and thus the same amount of power is being put into a larger area, decreasing the intensity. If the laser were more focused, then the beam would appear more intense because the same amount of power would be concentrated in a smaller area.

Another cause of the difference in laser intensity is the shape of the object being modeled. Each object has a surface at a different angle. The laser strikes the object, but the reflections coming off of the object change due to the angle of the surface. If the surface is facing the LPSM, then the majority of the reflections will come back to the LPSM. However, if the surface is at a 45º angle, such as the surface of the triangular prism, then many of the reflections are being deflected away from the LPSM, reducing the laser intensity seen by the LPSM.

7 SYSTEM EXPERIMENTS

Performance boundaries for the LPSM are now known. The next step is to create a laser scanning system using this data to control the area that the laser should scan and the speed at which the laser moves. Once the laser scanning system is tested, data can be sent from the data acquisition system to the A/D converter to test the performance of the A/D board. Finally, the algorithm for the FPGA can be developed and tested using data sets gathered from the data acquisition tests.

7.1 Laser Scanning System

Now that the LPSM has been characterized and the system boundaries set, the laser scanning system can be developed. The scanning system must take into account the speed that the laser will move, the size of the field of view to scan, and other factors. The LPSM must be tested with the scanning system to make sure it can respond to a moving light spot, since the laser has been stationary or very slow moving in all previous experiments.

7.1.1 Stepper Motor Basics

A motor is comprised of two parts: the stator and the rotor. The stator is stationary, with a hole in the middle. The rotor is a small stick inside of the stator that rotates, as seen in Figure 7.1. Pairs of poles lie along the stator. Complement pairs lay 180º from each other. Different motors contain a different number of poles.

The stepper motor is based on the principle of magnetism. When a current is applied correctly to a pole, then the pole becomes either “North” or “South.” The rotor is attracted and repelled from these poles to create mechanical movement.

For the motor with two pole pairs to turn, electric current must first be sent to P1a, so that P1a is “on” or “North”. The complement current signal, or ground, must be sent to P1b so that it is “off” or “South.” Poles P2a and P2b are also off. Using current to create poles causes the rotor to begin rotating either clockwise or counterclockwise, until it becomes aligned with poles P2a and P2b. Then, a signal will be sent to P2a, creating “North,” and the other three poles will be off. This action continues to push the rotor in the same direction until it is 180º from its original position. This sequence continues

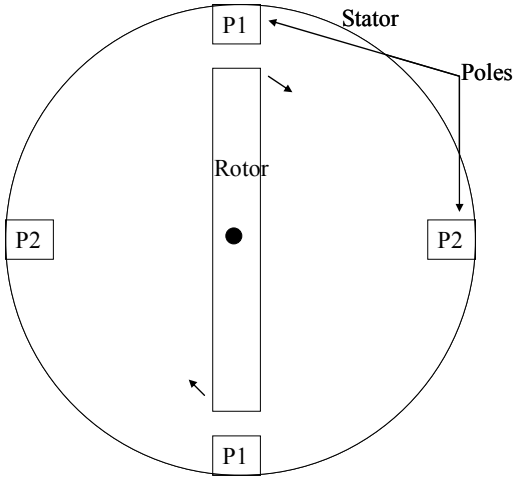

Figure 7.1: A stepper motor has a stator with poles and a rotor.

until the user no longer wants the motor to spin. To move in the opposite direction, the order in which the poles are turned on and off is reversed.

Each rotation of the rotor from one pole to the next pole is known as a step. Therefore, in the above motor, one step is equal to ninety degrees. As more poles are placed on the stator, the step size decreases. Smaller step sizes increase resolution and accuracy, but require more changes in current to turn the rotor.

Stepper motors provide very precise control. Since each step corresponds to a given degree rotation and a new position, the position of the rotor can be easily controlled. The speed at which the rotor turns can also be tightly controlled.

Stepper motors can be either unipolar or bipolar, depending on the way the coil is wound around a pole. Unipolar motors, or four-phase steppers, have two windings on each pole. The north pole is created when one winding is energized and the south pole is created if the other winding is energized. Therefore, the current flow is never reversed.

In bipolar motors, one winding exists at each pole. When current flows through the wire in one direction, the north pole is created. Reversing the current direction creates the south pole.

7.1.2 Motor/Mirror System 1

The laser can be deflected by a mirror that turns via a stepper motor. The mirror will reduce some of the laser power. The laser will also be moving through the scene at a much faster rate than the LPSM has seen before. When moving the laser horizontally through the field of view, the output of the LPSM is expected to resemble a triangular wave.

7.1.2.1 Stepper Motor/Mirror System 1

The first motor/mirror system can be seen in Figure 7.2. The stepper motor can be attached to one of four places. The shaft that the motor attaches to determines the ratio of motor turns to mirror turns. The motor was connected to the 1:1 shaft, since all of the other ratios did not turn the mirror through a full turn for every motor turn. The mirror was attached to the motor shaft using a set screw.

The stepper motor had four wires, red, white, blue, and yellow, coming out of it. The wires were attached to a 2x4 black connector. Since four wires were protruding from the motor, it was concluded that the stepper motor was bipolar. To determine which wires were complements of one another, a multimeter was used. The multimeter was set to measure Ohms, and the positive and negative terminals were placed to two different wires. If the multimeter read 0 Ohms, then the two wires were not connected, and were not complements of one another. If the multimeter read hundreds of Ohms, then the wires were complements of one another. Using this method, the pinout diagram was found.

(a)

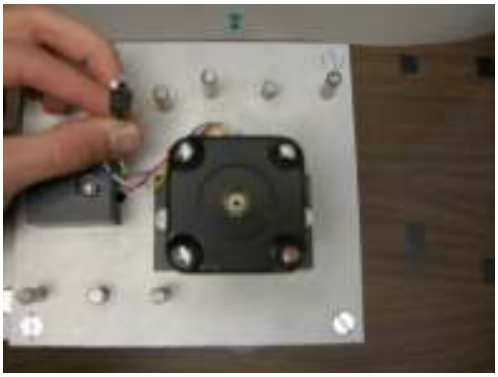

(b)

Signals

B	A’
B’	A
Empty	Empty
Empty	Empty

Wires

Red	Yellow
Blue	White
Empty	Empty
Empty	Empty

(c)

Figure 7.2: (a) The first motor/mirror setup had four places to attach the motor to the mirror. (b) The stepper motor had four wires, corresponding to (c) the outputs of a stepper motor driver card.

A stepper motor driver is needed to create the necessary signals to attach to A, A', B, and B'. The driver in Figure 7.3 was found in the IRIS lab. The driver is an IB Series driver from Intelligent Motor Systems.

The Enable', Logic ground, and Ground pins are connected to ground. H'/F is tied to ground for half step operation and power for full step operation. CW'/CCW is tied to ground for clockwise rotation and tied to power for counterclockwise rotation. Power, or 15 V, is attached to V+. The resistor is placed between the current adjust pin and ground. The value of the resistor can be found in the IB Series specifications. The step clock is attached to a function generator which outputs a 0 V to 5 V square wave. The period of the square wave determines the speed that the driver runs the motor. Pins A, A', B, and B' are outputs and connect to the stepper motor.

The clock step causes the mirror to turn slowly at a period of 20 ms with 50% duty cycle. As the period is decreased, the angular velocity of the mirror increases. However, the torque produced by the motor decreases. Therefore, at a certain point, the motor does not have enough power to turn the mirror. This point is reached at approximately 1.0 ms, depending on the resistor attached to the Current Adjust pin. Larger resistors allow the motor to turn at slower periods, but only by a few hundred microseconds.

7.1.2.2 System 1 Test Results

Several variables can change the output of the LPSM. The distance of the poster from the LPSM, half step versus full step operation of the stepper motor, manual control of the mirror versus stepper motor control, and the speed of the laser can all be controlled. The distance of the poster affects the size of the field of view. Half step operation versus full step operation and the speed of the laser affects how smooth the laser moves through the scene. Manual control of the mirror allows a signal to be found where the laser moves smoothly across the scene instead of moving across the scene in steps. However, the speed cannot be measured for manual control.

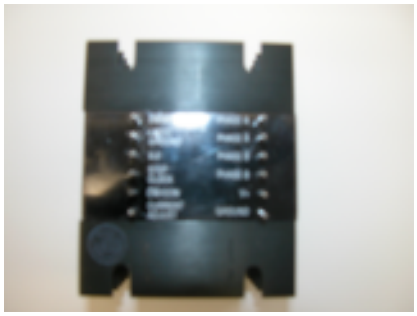

Signals

Enable'		A
Logic gnd		A'
H'/F		B'
Step Clk		B
CW'/CCW		V+
Current Adjust		GND

(a) (b)

Figure 7.3: (a) The driver has 12 pins, corresponding to (b) the inputs and outputs listed.

The procedure to test all of these variables was:

1. Set up the system so that the LPSM points at a white poster board and the laser shines at a height within the field of view of the LPSM.
2. Set the function generator to a period of 20 ms.
3. Set the poster 3 inches away from the LPSM.
4. Set up the oscilloscope so that it triggers on the rising edge of the input signal and set the acquire time so that the signal can be seen for the entire field of view. The time varies according to how far away the poster sits from the LPSM.
5. Set the driver to half speed operation by connecting the H'/F signal to ground, as seen in Figure 7.4.
6. Turn on the motor by connecting power. The mirror should begin to rotate, directing the laser through the scene.
7. Wait for the oscilloscope to trigger and acquire the signal.
8. Save the waveform and record the max and min voltage levels
9. Change the function generator period to 10 ms and repeat.
10. Change the function generator period to 6 ms and repeat.
11. Change the driver setting to full step by connecting the H'/F signal to power
12. Repeat the measurements with the function generator at 20 ms, 10 ms, and 6 ms.
13. Turn the motor off. Turning the mirror with your hand, direct the laser through the field of view at a constant, slow pace. Record the waveform and min/max voltage levels.
14. Turning the mirror with your hand, direct the laser through the field of view at a constant, fast pace. Record the waveform and min/max voltage levels.
15. Move the poster 3 inches further away from the LPSM and repeat all of the above measurements.

First, the difference between running the motor at half step and full step is examined. Figure 7.5 shows the half step and full step waveforms of the motor at a distance of 3 inches and a speed of 6 ms. The waveforms can be compared to the half step and full step waveforms of the motor at a distance of 12 inches and a speed of 6 ms.

(a) (b)

Figure 7.4: (a) The driver is set to half step when the H'/F signal is tied to ground. (b) The driver is set to full step when the H'/F signal is tied to power.

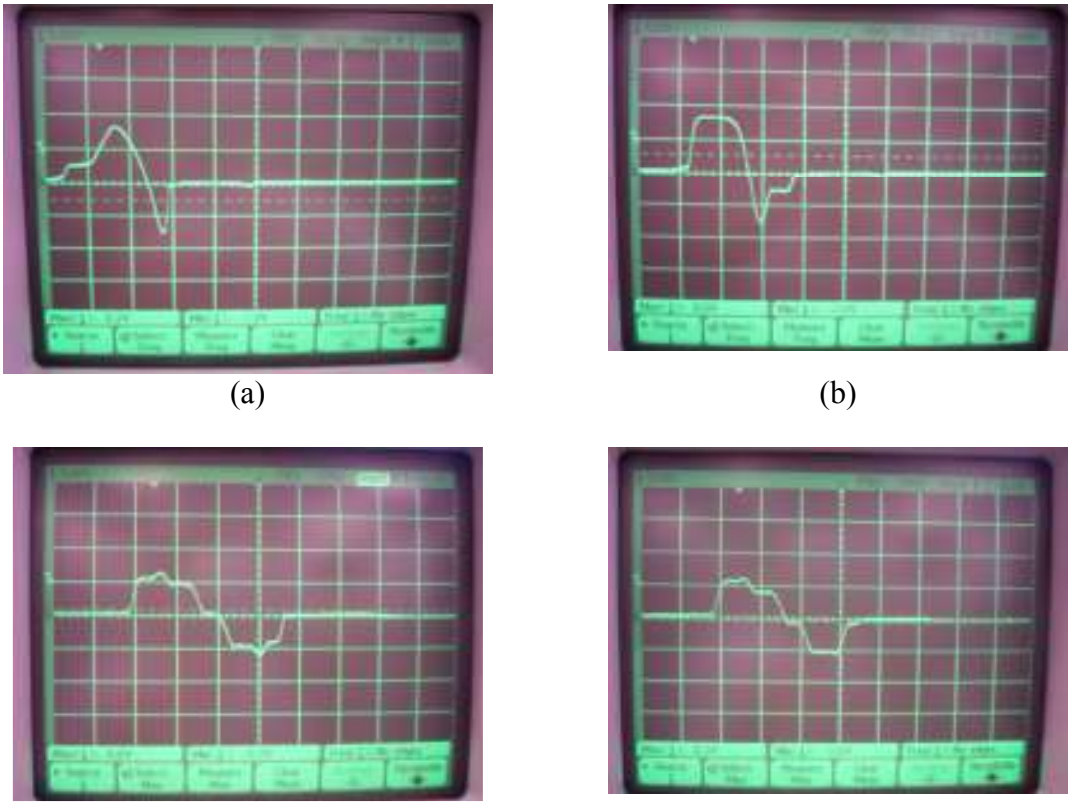

(a) (b)

(c) (d)

Figure 7.5: The waveform is generated at a distance of 3 inches and a speed of ms with the motor at (a) full speed and (b) half speed. The waveform is generated at a distance of 12 inches and a speed of 6 ms with the motor at (c) full speed and (d) half speed.

At the 3 inch distance, the half step waveform remains at the maximum voltage for approximately 50 ms before decreasing linearly. The full step waveform also waits for about 50 ms before decreasing linearly, but the signal is increasing to the maximum voltage during that time. At the 12 inch distance, the signals look almost identical.

The 3 inch field of view is only about 1 inch wide, while the 12 inch field of view is about 4 inches wide. For both half step and full step, the laser could visually be seen to jump from step to step. In other words, the laser did not scan through the scene at a constant rate, but instead move an increment, paused, and then moved another increment. Depending on where the laser paused as it moved into the field of view could cause the difference in the 3 inch waveforms. In other waveforms for the other distances, the full step and half step waveforms look almost identical, so it is concluded that the half and full step functionality of the stepper motor does not affect the operation of the system.

Next, operation at different speeds is compared. As the speed increases, the laser should move more smoothly through the scene. However, even at the top speed of 6 ms, the laser can still be visually seen to jerk through the scene instead of moving at a constant

rate. Figure 7.6 shows the waveforms at 20ms, 10ms, and 6ms speeds at a distance of 6 inches. Waveforms at various speeds at a distance of 15 inches can also be seen.

The waveforms are expected to decrease linearly. However, the waveforms seem to decrease in steps. The flat portions of the waveforms tend to decrease slightly as the speed increases. The flat portions are probably due to the pauses and jumps in the laser movement. As the pause decreases, the flat portion decreases. Therefore, to get the expected waveform, the laser needs to move at a constant, smooth rate through the scene.

To compare the irregular laser pattern to a smooth laser pattern, the mirror was rotated by hand. Since the 6 ms period caused the shortest pauses in laser movement, those waveforms were compared to the manual control of the laser. Figure 7.7 gives the waveforms at a distance of 6 inches and shows waveforms generated in the same manner at a distance of 15 inches.

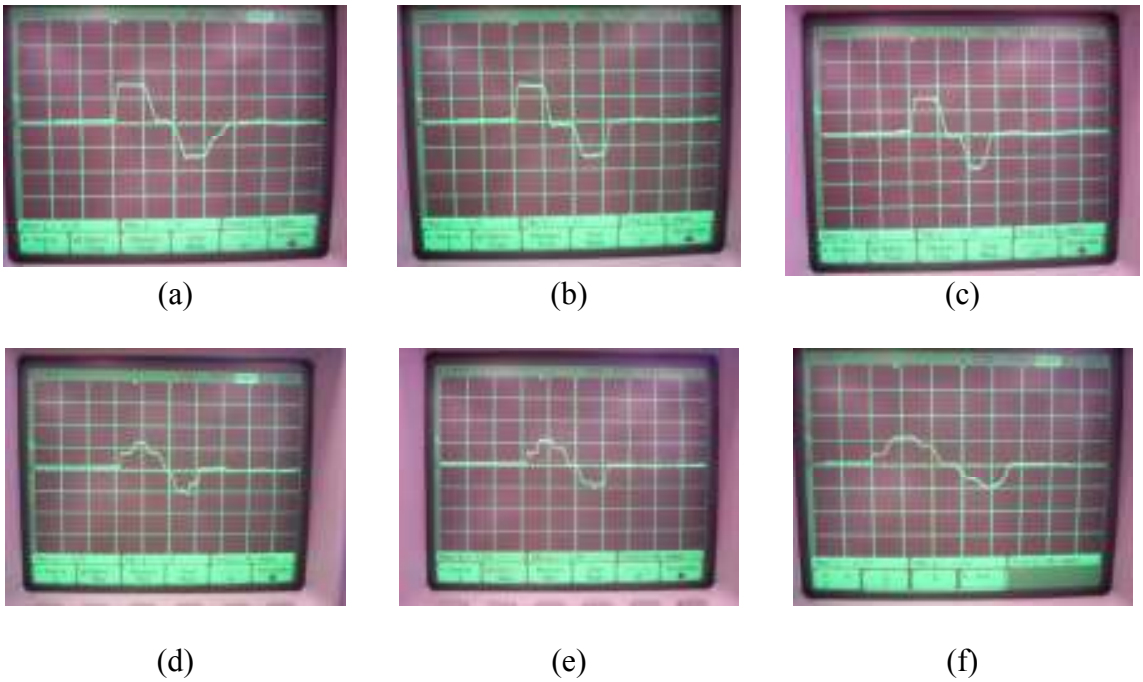

(a) (b) (c)

(d) (e) (f)

Figure 7.6: Waveforms are gathered at a distance of 6 inches at half step with a speed of (a) 20ms, (b) 10ms, and (c) 6ms. Waveforms are gathered at a distance of 15 inches at half step with a speed of (d) 20ms, (e) 10ms, and (f) 6ms.

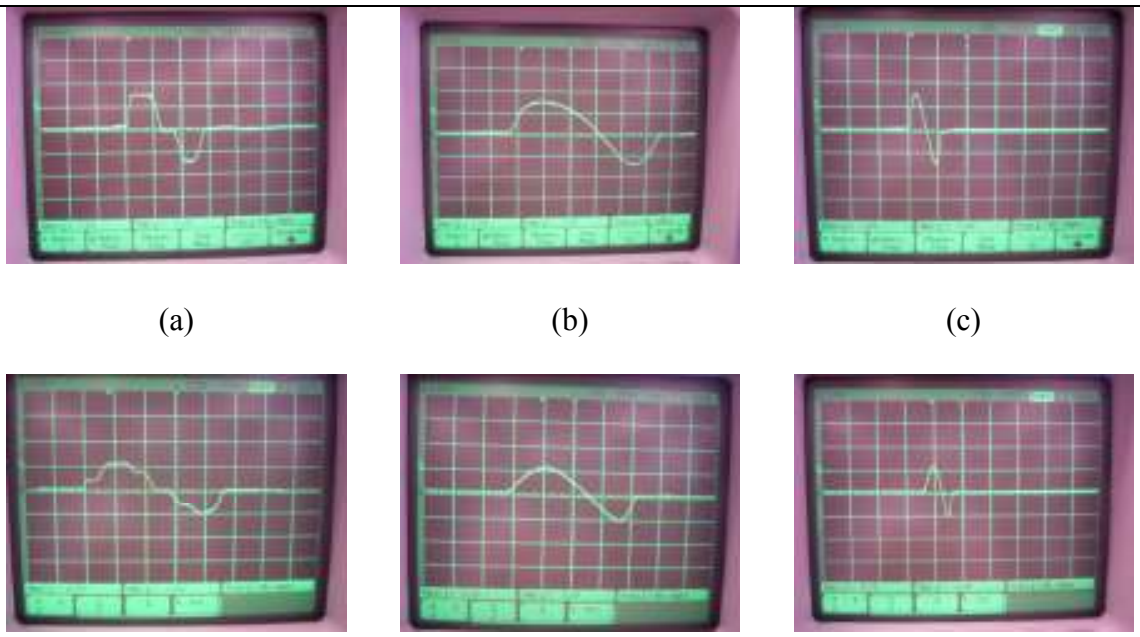

(a) (b) (c)

(d) (e) (f)

Figure 7.7: Waveforms were generated at 6 inches using (a) the stepper motor at a speed of 6ms, (b) by hand moving slowly, and (c) by hand moving fast. Waveforms were generated at 15 inches using (d) the stepper motor at a speed of 6ms, (e) by hand moving slowly, and (f) by hand moving fast.

As can be seen, when the laser moves smoothly and constantly through the scene, the waveform decreases linearly, as expected. Therefore, it can be concluded that the reason that the waveforms generated using the stepper motor are not linearly decreasing is due to the inconsistencies introduced by the motor. To improve the waveform, the motor either needs a smaller step size, needs to run faster, or another motor needs to be used.

7.1.2.3 Conclusions

The main problems seen in system 1 are the speed of the motor and the step size. The motor can be physically seen to move in increments instead of moving smoothly. Either the increment size needs to decrease or the speed of the motor needs to increase. The current motor does not have enough torque at higher speeds to move the mirror, so another motor must be found.

The waveforms reflect the jerkiness in the laser movement because the waveform has flat areas in the area where it should be linearly decreasing. A new motor should fix this problem.

7.1.3 Motor/Mirror System 2

The waveforms of the first motor and mirror system did decrease, as expected. However, the movement of the laser due to the jerkiness of the motor caused the waveforms to not

be smooth. The motor could not reach very high speeds, causing only one waveform to be seen instead of a periodic wave. Therefore, a faster, smoother motor and mirror system must be developed to test the LPSM.

7.1.3.1 Stepper Motor/Mirror System 2

A motor that had more torque and that rotated at a faster speed was needed. Another stepper motor was found, already connected to a different driver, along with another metal bracket. The metal structure only had one place to mount the motor at a ratio of 1:1. The mirror was attached to the shaft, as seen in Figure 7.8.

The motor had four wires, so it was classified as bipolar. The wires were already attached to a driver controller. The driver accepted inputs from a computer via a serial port. Therefore, a USB to serial port converter was also necessary.

Power had to be supplied to the motor and to the driver controller. Since both the motor and driver needed at least 0.5A, separate power supplies were used to power each component. The power supplies were set to +7.5V.

(a)

(b)

(c)

(d)

Figure 7.8: (a) A second motor was mounted to a mirror with a ratio of 1:1. The (b) stepper motor was controlled with a (c) driver that accepted inputs from the computer via (d) a USB to serial port converter.

Next, the driver controller had to be connected to a computer. The Windows XP operating system comes with a communication device called HyperTerminal, found under Start→All Programs→Accessories→Communications. HyperTerminal first asks the user to name the terminal. In the next window, the user needed to choose the correct COM port in the "Connect using" drop-down menu. A properties window appeared, and the drop down windows were set to:

Bits per Second: 9600
Data bits: 8
Parity: None
Stop bits: 1
Flow control: None.

Next, the File→Properties window was opened. Under the Settings tab, the Emulation was changed to TTY. The user then clicked the "ASCII Setup…" button, which brought up another window. The "Echo typed characters locally" checkbox needed to be selected, and then both properties windows could be closed by clicking the "OK" buttons. If the driver controller was powered on, a message appeared in the HyperTerminal window, along with a "*" on the last line, indicating that the driver was ready to accept commands.

Since two motors could be connected to the driver, the correct motor must be selected. Either "x" or "y" selected the correct motor, depending on which outputs from the card were connected to the motor. The driver accepted commands to control the speed of the motor, position, acceleration, and other parameters.

7.1.3.2 System 2 Test Results

The slow motor/mirror system was taken out of the full system and replaced by the faster motor/mirror system. The new system ran much faster and much smoother than the old system, allowing multiple pulses to be seen in a given frame of the oscilloscope. More consistent waveforms could also be seen since the motion of the laser was much smoother through the field of view of the LPSM.

The speed of the mirror rotation was controlled by the computer. The driver allowed the rate to be changed through the "R" command by setting the number of microsteps per second. A slow speed of 9000r, medium speed of 13000r, and fast speed of 17000r were tested. The motor could not run above 17000r without getting out of sync and thus getting stuck. The slow speed corresponded to about three rotations per second, the medium speed was about five rotations per second, and the high speed was about six rotations per second.

Figure 7.9: The setup for System 2 was the same as the setup for System 1 except that the motor/mirror system was replaced.

The distance of the poster could also be changed. The poster was placed from 3 inches to 15 inches away from the LPSM and laser setup and was changed in increments of 3 inches. As the distance increased, the field of view became larger.

The procedure used was:

1. Set up the system the same way as for system test 1 except with the faster mirror/motor system, as shown in Figure 7.9.
2. Start with the poster at a distance of 3 inches from the LPSM/laser. Start the mirror rotating at a speed of 9000r.
3. Once the signal appears on the oscilloscope, push the run button on the oscilloscope to stop to capture the signal.
4. Turn the motor off. Measure the max/min voltages of the signal and the necessary time intervals of the signal.
5. Change the speed of the motor to 13000r and then to 17000r and repeat.
6. Move the poster back 3 inches and repeat.

As can be seen from the collected data, the time between signals changed with speed but not with distance, as expected. For a rotation of 9000r, the time between signals was about 356 ms. For 13000r, the time was 246 ms, and for 17000r, the time was 188 ms, as seen in Figure 7.10.

The minimum and maximum voltages changed with distance. As the distance increases, the field of view increases, and the power of the laser incident on the LPSM will decrease. It was expected that the boundary voltages of the field of view would remain constant, but the distance at which the boundary was physically located changed. However, the minimum voltage became smaller as the distance increased, and the maximum voltage decreased as distance increased, which does not remain consistent with projective geometry.

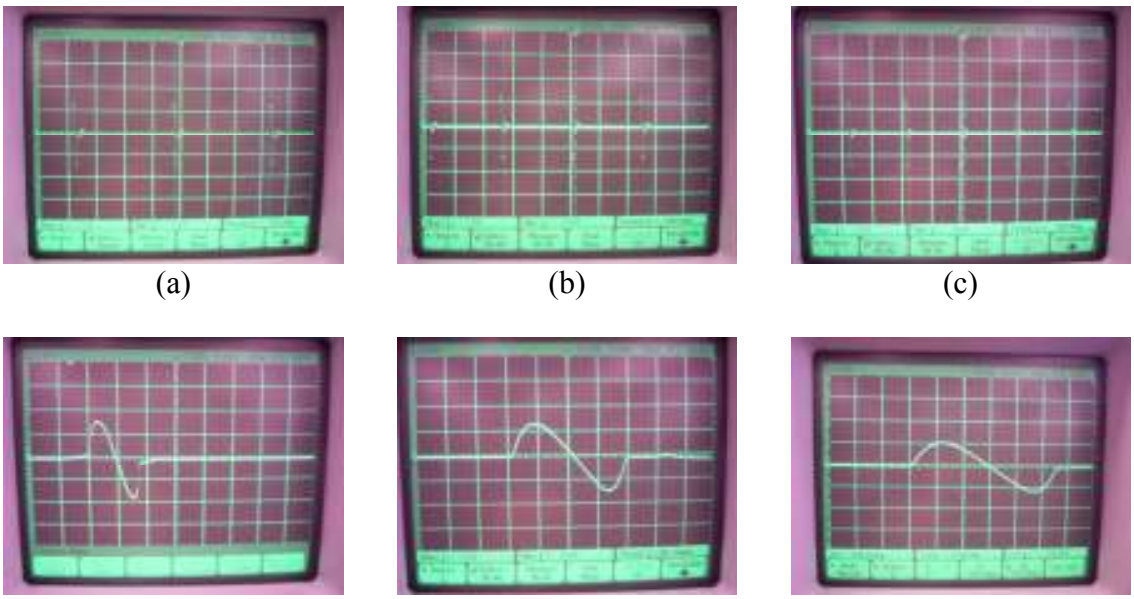

(a) (b) (c)

(d) (e) (f)

Figure 7.10: As the speed of the motor increases, the time between pulses decreases, as can be seen in the (a) 9000r waveform, (b) 13000r waveform, and (c) 17000r waveform at a distance of 9 inches. At a constant speed, the time between minimum and maximum voltages increased with distance, as can be seen in (d) the waveform at 3 inches, (e) the waveform at 9 inches, and (f) the waveform at 15 inches at a rate of 17000r, where each interval in the x direction corresponds to 2.0ms.

The distance between the minimum and maximum voltage was expected to increase as the distance increased. Therefore, as expected, the time between the minimum and maximum voltages increased as distance increased, with a constant speed, as seen in Figure 7.11.

If the distance was held constant and the speed increased, it was expected that the time between minimum and maximum voltages would decrease.

7.1.3.3 Black Object Test

In this test, the affect of a non-reflective area within the field of view was tested. Any black object does not reflect any light, so the LPSM should not be able to give a valid reading when the laser strikes the black area. It is expected to see a linearly decreasing signal from the maximum voltage to the minimum voltage with a small area where the signal goes to 0 V before returning to the original decreasing signal.

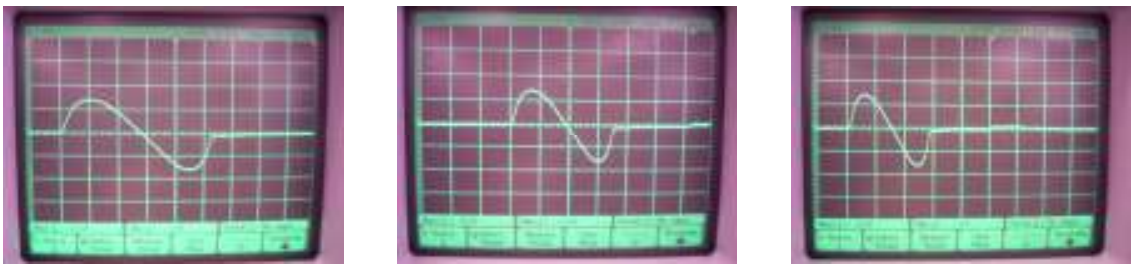

(a) (b) (c)

Figure 7.11: At a constant distance, the time between minimum and maximum voltages decreased with increased speed, as can be seen in (a) the waveform at 9000r, (b) the waveform at 13000r, and (c) the waveform at 17000r at a distance of 6 inches, where each interval in the x direction corresponds to 2.0ms.

The same setup was used for this setup as was used in the System 2 test procedure. The poster was held at a constant distance of 9 inches from the LPSM/laser. The speed of the motor was varied between the same three speeds. The procedure followed was:

1. Setup the system the same as the previous experiment, with the poster at a distance of 9 inches.
2. Place the 0.5 inch black object in the field of view of the LPSM, to the right of the center, as seen in Figure 7.12.
3. Turn the motor on at 9000r and record the waveform.
4. Record the minimum and maximum voltages and the necessary time intervals.
5. Repeat at speeds of 13000r and 17000r.
6. Replace the black object with the 1 inch black object and repeat.

The waveforms for the half inch object can be seen in Figure 7.12. The duration of the 0 V region decreases as the speed increases, as expected. The region occurs in the positive voltage region of the curve since the black object was placed to the right of the center of the field of view. The 0 V region was 1.92 ms long at a speed of 9000r, 1.4 ms long at 13000r, and 1.12 ms at 17000r.

Since the 1 in object is double the length of the 0.5 in object, it is expected that the 0 V region be about twice as long.

At 9 inches, the field of view should be approximately 3 inches long. Therefore, for the 0.5 inch black object, the 0 V region time interval should be about $1/6^{th}$ of the entire time interval from minimum voltage to maximum voltage. At 9000r, the time from minimum to maximum voltage was 10.44 ms, and the 0 V region was 1.92 ms, which is slightly more than $1/6^{th}$ of the time interval.

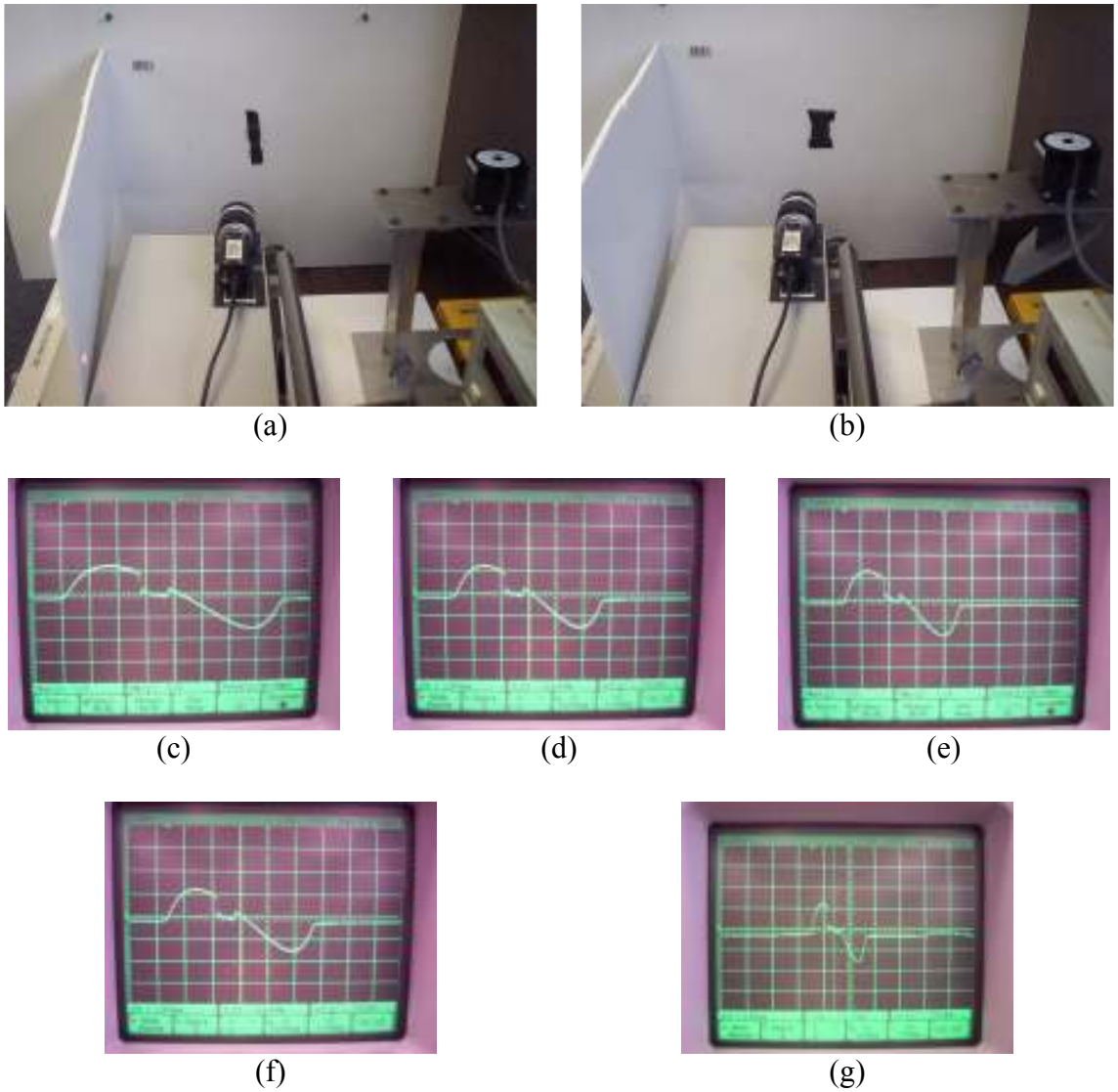

Figure 7.12: (a) A 0.5 inch black object was taped to the poster in the field of view of the LPSM. (b) A 1 inch black object was taped to the poster in the field of view of the LPSM. Using a 0.5 in black object, the waveforms were gathered when the motor rotated at (c) 9000r, (d) 13000r, and (e) 17000r, at a distance of 9 inches, with the x interval set at 2.0ms. At a rate of 13000r and a distance of 9 in, (f) the waveform with a 0.5 in object with an x interval of 2.0ms should have a 0 V region of about half the time length as (g) the waveform with a 1 inch object at an x interval of 5.0ms.

For the 1 in object, the 0 V time interval should be about 1/3rd of the time from minimum to maximum voltage. At 9000r, the time from minimum to maximum voltage was 10.3 ms, and the 0 V region was 3.6 ms, which is slightly more than 1/3rd of the time interval.

7.1.3.4 Conclusions

The motor in this system has a different step size and can move at much faster rates than the motor in system 1. The human eye cannot observe any jumps in the laser movement. The waveforms now display the expected shape of a linear decreasing curve. The curve to the left and right of the linearly decreasing region are due to response time and the scattering of light due to the gold circle surrounding the PSD in the LPSM.

7.1.4 Final 2D Scanning System

Many 2D laser scanning systems use a polygonal mirror that rotates vertically, moving the laser in vertical lines. The laser and mirror is then mounted on a base that rotates so that the laser also scans in the horizontal direction, such as for the Riegl Scanner. [Riegl, 2000]

At high speeds, it is very important that the mirror is well-mounted and balanced. Therefore, systems can be purchased that already have a polygonal mirror mounted, along with a controller to turn the mirror. It is recommended to purchase a pre-built kit, such as the Polygon Mirror Scanner Motor by Samsung Electro-mechanics [Samsung, 2003] for safety reasons.

The bottleneck of the system is the response time of the LPSM. As shown from experiment, the worst case response time is approximately 1 ms when the scene is 15 inches away from the laser and LPSM setup. The largest scene also occurs at 15 inches, corresponding to a 3 inches wide by 4 inches tall field of view.

Table 7.1 compares the frame rate and resolution possibilities of the system.

As the frame rate increases, the resolution decreases. Therefore, to get better resolution, the frame rate must decrease. For good resolution, the laser should also be well-focused.

The first system proposal aims to achieve the 30 fps rate. The polygonal mirror scanner motor can be mounted vertically on a circular base. The 500 mW laser can be placed directly under the mirror. The entire base will rotate, controlled by a stepper motor. Of the entire 360º circle that the base can turn, the laser is only directed into the field of view for a portion of the circle. Using a 30 inch diameter field of view, it can be calculated that the laser is in the field of view for about 4% of the sphere. However, at the speed necessary to achieve 30 fps using a stepper motor, there may be too much inertia in the system to stop the rotation and change direction.

Table 7.1. Resolution and frame rate trade off at 1000 positions per second

Distance (in)	Baseline (in)	Window Size (in)			Frame Rate (fps)	Pos/Frame	Pos/Row or Col	Resolution (in)		
12	1.2	2.800	x	4.000	1	1000.00	31	0.09	x	0.13
12	1.2	2.800	x	4.000	10	100.00	10	0.28	x	0.40
12	1.2	2.800	x	4.000	20	50.00	7	0.40	x	0.57
12	1.2	2.800	x	4.000	25	40.00	6	0.47	x	0.67
12	1.2	2.800	x	4.000	30	33.33	5	0.56	x	0.80
12	1.2	2.800	x	4.000	35	28.57	5	0.56	x	0.80
12	1.2	2.800	x	4.000	40	25.00	5	0.56	x	0.80
12	1.2	2.800	x	4.000	45	22.22	4	0.70	x	1.00
12	1.2	2.800	x	4.000	50	20.00	4	0.70	x	1.00
12	1.2	2.800	x	4.000	60	16.67	4	0.70	x	1.00
12	1.2	2.800	x	4.000	75	13.33	3	0.93	x	1.33

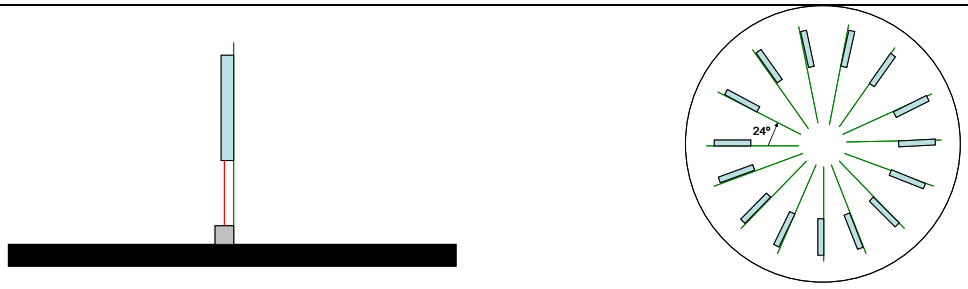

(a) (b)

Figure 7.13: The scanning system is comprised of (a) 15 vertically placed polygonal mirrors and lasers placed (b) in a wheel-spoke configuration.

Therefore, multiple motor and laser systems can be placed on the base in a wheel-spoke configuration, as seen in Figure 7.13. As the laser exits the field of view from one system, the next system's laser should enter the field of view. This system would allow the base to continually rotate in one direction at a constant rate. The vertically rotating mirrors would also be able to rotate in one direction at a constant rate. Therefore, there would be less inertial stresses on the system due to changes in speed and direction. The wires could be run through the center of the base and strung to the necessary components.

The two main concerns with this system are the cost and the physical constraints. Although the polygonal mirror and motor are fairly cheap, each system must have its own laser. A single 500 mW laser costs at least a few hundred dollars, and 15 are needed. Next, this system has a mirror spinning vertically at a fairly high rate. The mirror is then turned horizontally. A gyroscope effect may be seen at these speeds. Stress is also placed on the vertically standing card, so extra precautions must be used to ensure that it does not move during operation. Calibration of the system could also cause problems. The cards must be placed at the correct positions so that 2 light spots are not present in the same field of view. The cards must also be perfectly vertical and the laser must be

pointing directly into the mirror. All of these components must not move during system operation, or the laser will be deflected in the wrong direction.

Stepper motors also tend to be limited to about 2000 rpm. To achieve various speeds, gear ratio systems would have to be developed. To change the speed, the entire gear ratio system would then have to be re-worked. Stepper motors also move in discrete steps, limiting the resolution.

Another option is to use servo motors. One of the laser and polygonal mirror systems can be mounted on a horizontally rotating platform, controlled by a servo motor, as seen in Figure 7.14. Servo motors can commonly reach speeds of up to 10000 rpm. They also rotate smoothly, so better position resolution can be reached than with stepper motors. Servo motors change speed and direction according to the applied voltage. [Danaher, 2006]

A switch can be placed on the top, rotating base that hangs down past the bottom, stationary base. On the bottom, stationary base, two pegs can be placed. As the top rotates, the switch will hit one of the pegs. When the top has rotated far enough, the switch causes the voltage to be flipped, causing the motor to spin in the other direction. When the switch hits the other peg, the voltage and thus the direction will change again. The two pegs can be manually placed by the user of the system, based on the field of view desired.

(a) (b)

Figure 7.14: (a) The polygonal mirror and laser can be mounted to the top circular base. The top base is attached to a servo motor so that the top base can rotate horizontally, while the bottom base remains stationary. (b) The second system proposal uses a servo motor to rotate the base horizontally and changes direction based on a switch.

This system is a lot cheaper than the first system. It also has better position resolution, if the speed is desired to be slower. The speed can be easily controlled by changing the applied voltage. It is also possible to make the system less mechanically dependent by applying voltage to the servo using a waveform generator instead of using the switch and screws, allowing for less moving parts and thus a more reliable system.

The calibration of the system can be done fairly easily. By turning the top, rotating base, the two boundary conditions can be established and the pegs can be inserted. The speed of rotation can be determined simply by changing the applied voltage. The final necessary voltage can be found either by experiment or by calculation from the motor spec.

The major concern for this system is the physical stress placed on the vertical mirror and card. They will be stopping abruptly and changing direction. Therefore, the card will have to be mounted more carefully and with more support.

Another system possibility is to use two mirrors. The laser is deflected from one mirror into another mirror and then onto the scene. One mirror controls the vertical motion of the laser, while the other controls the horizontal motion of the mirror. Usually one of the mirrors is flat and rectangular shaped. The other mirror can also be flat and rectangular, or it can be shaped like a cone.

The 2 mirror system would be very difficult to calibrate. The mirrors would have to not only be calibrated to hit the field of view, but also calibrated so that their movements correspond to one another to correctly move the laser. The laser would also lose twice as much power as in the other systems because it is being deflected off of two surfaces instead of just one surface. Depending on whether the mirrors were rotated constantly in one direction or made to change direction, inertia problems may not be as big of a concern.

Table 7.2 summarizes the pros and cons of the three considered systems.

Table 7.2. Comparison of the three proposed laser scanning systems.

	System 1: Wheel Spokes	**System 2: Servo Motor**	**System 3: Two Mirrors**
Cost	Very Expensive	Reasonable	Medium expense
Physical Stress	Gyroscope Concerns	Stress on Motor Card	Variable
Calibration	Medium Difficulty	Not too difficult	Very difficult
Speed	Able to get to 30fps	Variable, constrained by stress on card	Variable
Resolution	Constrained by stepper motor	Able to get very good resolution	Dependent on mirror controller
Laser Power	1 Deflection	1 Deflection	2 Deflections

System 2, the servo motor solution, is recommended. System 2 gives the widest range of frame rate and resolution options. Servos can be easily controlled and are programmable, allowing for less mechanical parts. The main concern is the stress placed on the mirror card. Extra support can be built in to the system by mounting the card on PCB or other material. The main calibration of the system would be in programming the servo, which could be done by looking at the specification of the motor, or by experiment.

7.2 A/D Converter

The outputs of the LPSM must be converted to binary before they can be sent to an FPGA. The speed and resolution of the necessary A/D converter cannot be found on a development board, so a separate chip and board must be used. The TI ADS7805 is a 16-bit SAR A/D converter. A sample was requested and received for testing and to validate the specifications.

7.2.1 A/D Control Line Validation

The ADS7805 User's Manual from Texas Instruments shows how the chip should be connected for basic operation. The chip was mounted on a breadboard to make the necessary connections. The chip is high speed, operating at 100 kHz, so the extra capacitance added by the breadboard may cause operational problems. Figure 7.15 shows the chip completely connected.

The A/D chip has two control lines, CS' and R/C'. CS' can be tied to ground and ignored for basic operation so that only R/C' controls the read and conversion cycles. The BUSY' signal tells when valid data is present on the outputs and when the chip is doing a conversion. When the user makes R/C' go low, then BUSY' automatically goes low, meaning that the chip is going into conversion mode. At this time, data on the output pins is at High-Z. R/C' can go high again once the chip is in conversion mode. The conversion cycle take a few microseconds. When finished, the BUSY' signal goes high, meaning that the data on the output pins is valid. The cycle can repeat every 10 µs.

A function generator was used to create the R/C' signal, as shown in Figure 7.16. The generator was set to a period of 10 µs, frequency of 100kHz, amplitude of 5 V, high voltage of 5 V, low voltage of 0 V, offset of 2.5 V, type of square, and duty cycle of 80%. The input analog signal was created using a second function generator set to a period of 10 µs, frequency of 100 kHz, amplitude of 50 mV, high voltage of 0 V, low voltage of -50 mV, offset of -25 mV, type of square, and duty cycle of 80%. The voltage could be moved up and down to see the changes on the data pins.

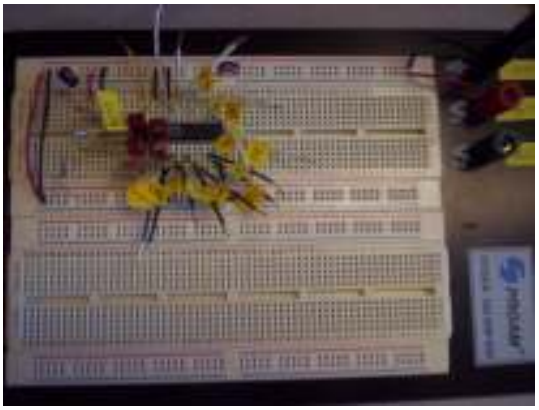

Figure 7.15: The A/D chip was mounted on a bread board.

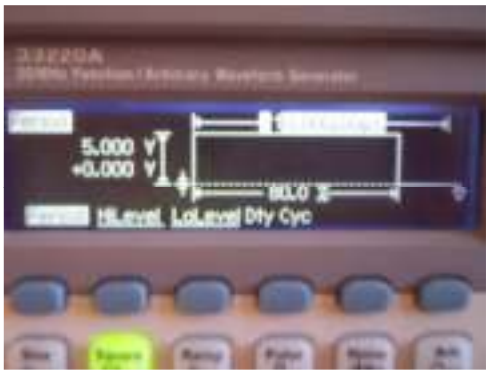

Figure 7.16: A function generator was used to create the control signals.

Figure 7.17 shows the oscilloscope screen with R/C' connected to signal 1, the bottom signal, and BUSY' connected to signal 2, the top signal. It is expected that after the R/C' signal goes low, the BUSY' signal should go low. The BUSY' signal should go high after a conversion cycle is finished and should remain high until the R/C' signal goes low, signaling the beginning of anther conversion cycle.

7.2.2 Conclusions

The A/D converter can be controlled as expected. As shown earlier, the data input to the FPGA only needs to be 8 bits long. One option is to reduce the input voltage to the A/D chip using a resistor network and to use a converter that outputs 8 bits. The resistor network would add more noise into the system. Therefore, it is decided that it is best to use the 16-bit converter and to only connect the top 8 bits.

A digital logic analyzer is required to study the outputs of the converter. To check that the outputs are changing as expected and at the speed required, the inputs would need to become automated. If the LPSM is chosen as the final sensor to be used in the system,

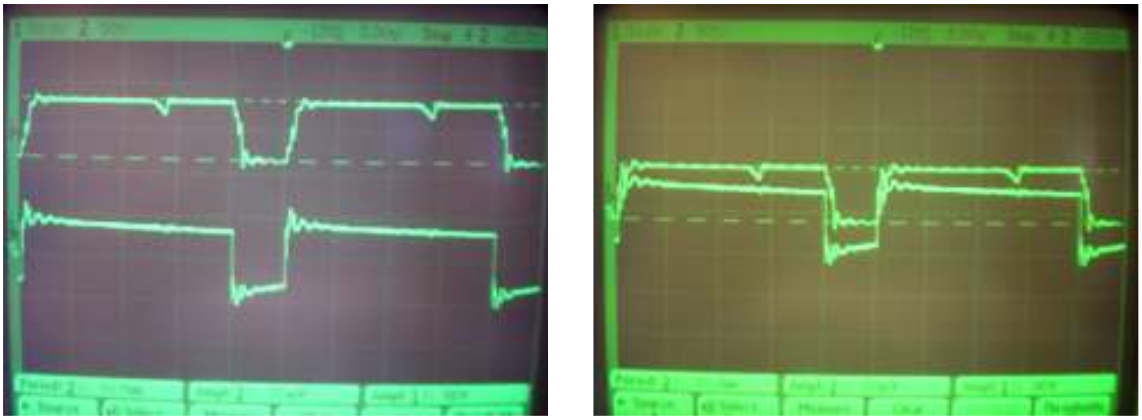

(a) (b)

Figure 7.17: (a) An oscilloscope was used to see the R/C' signal on the bottom of the screen, and the BUSY' signal on the top of the screen. (b) When moved to overlap, it can be seen how the BUSY' signal follows the R/C' signal, as expected.

then the outputs could be connected to the converter and the rest of the chip functions tested.

7.3 FPGA Algorithm

Once all of the information from the data acquisition system is collected and digitized, it will be sent to the FPGA for computation. The FPGA will first need to receive the focal length and baseline. Next, the minimum or maximum voltages in the x and y direction for each LPSM must be sent to the FPGA so that the constant to convert voltages to distances can be calculated. Once this calibration information is setup, the FPGA must start reading in voltages at a given rate and continuously output 3D points.

It is possible to break up these steps into separate state machines. All of the small state machines can be combined using a main, overhead state machine. Using this method, if new procedures are developed, then they can be programmed and easily inserted by creating a new state in the main state machine.

The entire process can be separated into 4 smaller state machines. An *INPUT* state machine can read in the baseline, focal length, maximum voltages, and minimum voltages. A *CALIBRAITON* state machine can take the information and create and store the voltage-to-distance constants. Four *SAMPLING* state machines can start polling the data signal from the A/D converter to select when valid voltages are on the FPGA input

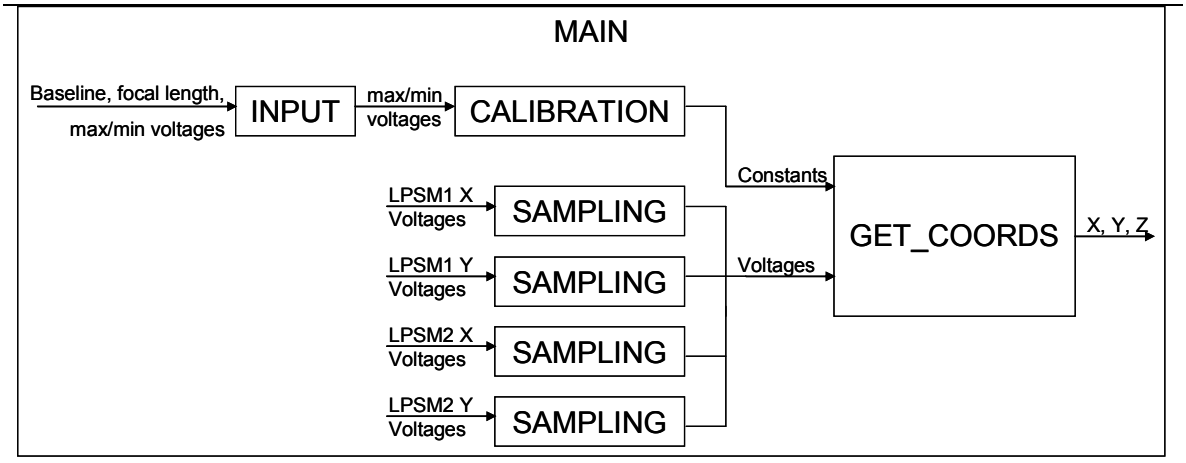

Figure 7.18: The FPGA algorithm could be split up into smaller state machines controlled by a main state machine using enable and done bits.

pins. Finally, a *GET_COORDS* state machine can take the voltages and calibration information and output the stereo points.

All of these machines can be controlled by a *MAIN* state machine, as seen in Figure 7.18. Each smaller state machine can have an enable bit. When the enable bit is turned on by the main state machine, then the smaller state machine operates. When the smaller state machine finishes, it sends a signal back to the main state machine. The main state machine then turns the enable bit off and turns on the enable bit for the next state machine.

7.4 Computer Software

The computer will be receiving the points via USB 2.0. USB API's are available online for C++. Using the preprogrammed API, data from the FPGA can be read and stored in a text document. The text document can then be displayed with a program of the user's preference. For example, headers can be added to the text to create a VRML file to be viewed using VRMLPad. Another option would be to keep the data in a text file and use RapidForm 2004 to view the points. Other options for viewing points that need to be refreshed for every new scene would have to be looked into.

7.5 Conclusions

The entire 3D scene reconstruction system can be broken into three main parts: the data acquisition system, the data conversion, and the data computation. The data acquisition, as studied in previous chapters, determines most of the performance boundaries of the system. Using data from the testing of the data acquisition system, a laser scanning system could be designed.

Once the laser scanning system is designed and developed, the entire data acquisition system can be put together and tested. Data sets from the data acquisition system can be fed into the data conversion element of the system.

A sample A/D converter was ordered from TI. Although it is not yet possible to connect the LPSM outputs to the A/D converter, it was possible to check the control signals and ensure that the A/D converter operated as stated in the specification. Using the converter on an EVM board instead of on a breadboard should reduce noise and increase performance.

The FPGA algorithm can also be designed without the data acquisition system. Although certain variables, such as sampling rates, are not yet determined, they can be changed once they are known. The algorithm can also be designed to be flexible and allow for future changes by using a series of state machines. With these state machines, it is easy to remove, add, or change the existing model to allow for more error correction or other changes.

8 CONCLUSIONS

The goal of this thesis was to develop a new 3D scene reconstruction system that could model scenes at mid-range distances in real-time. A physical and logical block diagram of the proposed system was developed. A literature review was conducted and showed that no current system exists that uses PSDs in a stereo vision configuration. The system theory was studied and a hardware overview conducted to choose the best parts for the system.

The LPSM was purchased as part of the data acquisition system. The focus of the thesis shifted to characterizing this sensor due to its performance in experiments. The LPSM was characterized to help determine system performance boundaries and the necessary hardware for the rest of the system.

The rest of the system was designed and hardware recommendations were offered, as well as algorithms for developing the necessary code.

8.1 Summary

A survey of current 3D systems was first studied. Background of laser triangulation, stereo vision, PSDs, and FPGAs was also examined. Then, a survey of available products was conducted to try to find the appropriate hardware for the system. Criteria to determine the best hardware choices was developed and hardware recommendations were made, creating a paper design of the system, and fulfilling the contribution of designing a 3D scene reconstruction system based on PSDs in a stereo vision configuration.

Before the entire system could be built or designed, the data acquisition system needed to be built to determine performance boundaries and inputs for the rest of the system. It was decided to base the data acquisition system on the LPSM from Noah Corp. In conversations with Noah Corp, the LPSM was found to be used in applications where a <10mW laser is shined directly into the LPSM or reflected off of a shiny surface that is very close to the LPSM. However, in this application, a laser was going to be reflected off of a diffuse surface from 3 feet to 15 feet away.

The LPSM was extensively tested to find out how it performed for this type of application. At first, a laser was reflected off of a white poster board placed from 3 feet to 15 feet away. However, even using a <500mW laser did not supply the necessary laser power for the LPSM to operate within its specified light threshold range. Therefore, a mirror was used to reflect more laser power. Although the mirror did reflect enough laser power for the LPSM to register a good threshold from 3 feet to 15 feet away, the threshold was only reached when the laser's angle of reflection directly hit the LPSM. This meant that the distance on the mirror that gave readings within the threshold was only a few inches wide.

It was decided to try using the white poster board again at a closer distance to try to reach the good light threshold region. From experiment, it was found that if the poster was within 15 inches of the LPSM and a red <500mW point laser was used, then the LPSM gave good readings. The maximum and minimum voltages seemed to be more consistent throughout this range and linear behavior could be seen when moving the laser in the field of view. These experiments demonstrated the contribution of characterizing the LPSM as a vision sensor.

A slider was built so that stereo points could be taken even though only one LPSM was present. A system of moving the laser with a pan tilt while collecting data points on an oscilloscope gave high enough point density to model small objects. The modeling of a rectangular prism, triangular prism, and cylinder were studied in depth.

Data was taken for the rectangular prism and a plane was fitted to the data. It was expected that the plane be fairly perpendicular to the *Z*-axis. However, the plane was almost perpendicular to the *Z*-axis. Therefore, fitting a plane to the data added more error than measuring where the object sat with a ruler. Consequently, the error was found using the absolute distance of the object as measured by a ruler.

The percent error was found for the three objects and compared to the x distance, y distance, and depth. No correlation could be found between error and x or y distance. However, there was always more error at the 10 inch depth than at the nine inch depth. From this observation, three correction models were applied to the data.

The first correction model assumed that the LPSM may not be perfectly linear. In previous calculations, one constant had been used to convert voltages on one axis to distances. In this model, two constants were used: one for positive voltages and one for negative voltages. When applied to the data, this model caused more error.

The next correction models took into account the intensity problems that had been seen. The LPSM seemed extremely sensitive to even slight changes in laser power level. Even moving the scene further away or closer by one inch would cause a change in the minimum and maximum voltages, changing the conversion constant. Therefore, a model was attempted where the constant changed with depth. For every 0.25 inches closer to the scene from the original 10 inch distance, the constant was decreased by 0.05 mm/V. Using this model, the error was improved for each object. These experiments demonstrated the contribution of testing the LPSM as a vision sensor.

8.2 Lessons Learned

It was determined that the error in the model is probably due to the LPSM sensitivity to changes in light intensity. Although the LPSM is able to operate within a light power range of 0.001 mW to 1 mW, the boundaries of the voltage remain inconsistent within

that range. Since the scene is far away and the surface reflecting the laser is diffuse, the laser intensity changes too much for the LPSM to give consistent readings.

Other factors besides distance could be contributing to the change in intensity. For example, the rectangular prism face is parallel to the LPSM. When the laser strikes the rectangular prism, the majority of the reflections bounce directly back to the LPSM. However, the triangular prism face is at a 45º angle to the LPSM. When the laser hits the triangular prism face, the majority of the reflections will be directed at an angle away from the LPSM, so less intensity is seen.

Another factor could be the entry angle of the laser. The largest laser intensity should be seen when the laser is pointing directly at a surface. However, to scan the entire scene, the laser must be pointed at different angles. If the reflecting surface is not perpendicular to the entry angle of the laser beam, then the intensity will be reduced.

Laser intensity is also affected by surface material and color. From experiment, it was shown that different colored surfaces give inconsistent voltage readings. Even if the surface is the same color, different materials also cause inconsistent voltage readings. Therefore, surfaces in the field of view must be the same color and material to get somewhat consistent readings.

These restrictions along with the amount of error seen in the models severely limits the possible applications of the system. The system could still be used for reverse engineering of objects that are the same color and material, such as pipe welds. However, other systems currently have better error and could probably make better models.

8.3 Future Work

Several options exist to try to improve the system. First, steps could be taken to try to make the laser intensity more consistent at different depths. This could be accomplished by purchasing a more focused laser. Most of the laser power may be getting lost in the diffusion of the laser beam. Therefore, a more focused laser would cause the power to stay in a more concentrated area, giving higher apparent laser intensity. Red well-focused lasers that have an output power of <500 mW are approximately $5000-$10000. Another option to better focus the laser is to develop a two lens system. The curvature and placement of the lenses would be found through optics equations. The makers of the <500mW laser recommended purchasing a new laser rather than building a two lens system.

Another option would be to change the sensor. The LPSM is based on a PSD made by UDT Sensors. The main manufacturer of PSDs is Hamamatsu. It may be possible to purchase a PSD from Hamamatsu and perform similar tests to see if it performs better than the LPSM for this application. Different PSDs may prove to be less sensitive to slight changes in light intensity, but that can only be determined through testing. It is

possible to buy a PSD from Hamamatsu for about $30 per piece, usually with a minimum of a five piece purchase. Using a PSD instead of the LPSM would also mean that the outputs would be sets of currents. The distance would then have to be computed using equations found in Chapter 3. These calculations could be done on the FPGA. The computations could easily be added by coding a new state machine.

Although using a PSD sounds like it may add extra computations, it actually reduces the amount of computations. The LPSM sees a light spot, takes the outputs of the PSD, and creates a voltage, with a response time of at least 100 µs. The voltage must then be changed back to a distance on the FPGA. A PSD outputs the currents so that only one calculation must be made to determine the distance. Since only one calculation needs to be made, and the response time of many PSDs is recorded as less than 10 µs, the response time may improve, allowing for better frame rates and resolutions.

If it is shown that PSDs work well, it may also be possible to change the system to a line laser system, again improving frame rates. A line laser system may work better than a point laser system because more of the beam is present in the field of view of the PSD, possibly helping to keep the laser intensity more constant. Using a line laser would mean that more PSDs are required. However, if the PSDs are $30 per piece, and the LPSM is $1700, then using about 56 PSDs would be equivalent to one LPSM. This method would cause the resolution to be more fixed than using a point laser, but would improve the frame rate. Using a line laser would also cause the laser scanning system cost to decrease dramatically because the laser would only have to move in one direction and at a much slower speed. A less complicated laser scanning system would allow more money to be put into the sensors.

8.4 Conclusions

For the current system, the LPSM is probably not a good choice for the sensor. It may be possible to get improved error by purchasing a more focused laser, but other options are also available. Using PSDs may help reduce the system cost and allow for faster response times.

The elimination of the correspondence problem is possible by using a laser. However, the LPSM is too sensitive to light intensity to accurately be used in this application.

REFERENCES

3D Digital Corporation, "Optix 400 Series," 2005, http://www.3ddigitalcorp.com/products.htm

Altera, "Cyclone II Device Family Data Sheet," 2005.

Altera, "Stratix II Device Family Data Sheet," 2005.

K. Araki, M. Shimizu, T. Noda, Y. Chiba, Y. Tsuda, K. Ikegaya, K. Sannomiya, and M. Gomi, "High Speed and Continuous 3-D Measurement System," in *Conference D: Architectures for Vision and Pattern Recognition*, 1992, pp. 62-65.

Atmel, "5k-50k Gates Coprocessor FPGA with FreeRam," 2004.

K. Benkrid, D. Crookes, J. Smith and A. Benkrid, "High Level Programming for Real Time FPGA based Video Processing," in *Acoustics, Speech, and Signal Processing*, 2000, pp. 3227-3230.

J. –A. Beraldin, F. Blais, L. Cournoyer, G. Godin and M. Rioux, "Active 3D Sensing," April 2000, http://www.iit-iti.nrc-cnrc.gc.ca/iit-publications-iti/docs/NRC-44159.pdf

J.-A. Beraldin, F. Blais, L. Cournoyer, M. Rioux, S. H. El-Hakim, R. Rodela, F. Bernier and N. Harrison, "Digital 3D Imaging System for Rapid Response on Remote Sites," in *3-D Digital Imaging and Modeling*, 1999, pp. 34-43.

J. –A. Beraldin, F. Glais, M. Rioux, J. Domey, L. Gonzo, F. DeNisi, F. Comper, D. Stoppa, M. Gottardi and A. Simoni, "Optimized Position Sensors for Flying-Spot Active Triangulation Systems," 2003, http://ieeexplore.ieee.org/iel5/8779/27810/01240229.pdf

S. Brown and J. Rose, "Architecture of FPGAs and CPLDs: A Tutorial," *IEEE Transaction on Design and Test of Computers*, vol. 13, pp. 42-57, 1996.

Callidus Precision Systems, "Callidus CP 3200 Technical Specifications," 2005, http://www.callidus.de/en/cp3200/techn_daten.html

Carnegie Mellon University, "The CMUcam1 Vision Sensor," November 2005, http://www.cs.cmu.edu/~cmucam/qanda.html

"Chapter 9, 3D Vision (Part I): Geometry for 3D Vision," October 2005, http://www.icaen.uiowa.edu/~dip/LECTURE/3DVisionP1_2.html

B. Chen, W. Lou, C. Chen and H. Lin, "A 3D Scanning System based on Low-occlusion Approach," in *3-D Digital Imaging and Modeling*, 1999, pp. 506-515.

J. Chen, D. Yang, H. Zhou and S. Buckley, "Avoiding Spurious Reflections from Shiny Surfaces on a 3D Real-Time Machine Vision Inspection System," in *Instrumentation and Measurement Technology Conference*, 1998, pp. 364-368.

Danaher Motion, "Servo Handbook: Stepper versus Brushless," 2006, http://www.danahermotion.com/education/learn_about_mc/servohandbook/motor/comparison/stepper_vs_brushless.php

"DARPA Grand Challenge Overview," 2005, http://www.darpa.mil/grandchallenge/overview.html

M. de Bakker, P. W. Verbeek, F. vandenOuden and G. K. Steenvoorden, "High-speed Acquisition of Range Images," in *Pattern Recognition*, 1996, pp. 293-297.

F. De Nisi, F. Comper, L. Gonzo, M. Gottardi, D. Stoppa, A. Simoni and J.-A Beraldin, "A Novel CMOS Sensor for Position Detection," *IEEE Transactions on Sensors*, vol. 2, pp. 1277-1282, 22-24 Oct. 2003.

C. Donninger, A. Kure and U. Lorenze, "Parallel Brutus: the First Distributed, FPGA Accelerated Chess Program," in *Parallel and Distributed Processing Symposium*, 2004, p. 44.

M. Dumberger, "Taking the Pain Out of Laser Triangulation," July 2002, http://www.sensorsmag.com/articles/0702/laser/main.shtml

Edmund Optics, "Edmund Optics: Optics and Optical Instruments Catalog," 2005, www.edmundoptics.com

A. Ejnioui and N. Ranganathan, "Routing on Switch Matrix Multi-FPGA Systems," in *Thirteenth International Conference on VLSI Design*, 2000, pp. 248-253.

O. Faugeras, *Three-Dimensional Computer Vision: A Geometric Viewpoint*. Cambridge, Massachusetts and London, England: The MIT Press, 1993.

F. Ferrari, E. Grosso, G. Sandini and M. Magrassi, "A Stereo Vision System for Real Time Obstacle Avoidance in Unknown Environment," *IEEE Transactions on Intelligent Robots and Systems*, vol. 2, pp. 703-708, 3-6 July 1990.

L.Md A. Filho, A. F. Barbosa, H. P. Lima, Jr. and P. R. B. Marinho, "A TDC-Based System for X-Ray Imaging Detectors," *IEEE Transactions for Nuclear Science*, vol. 52, pp. 932-937, Aug. 2005.

R. Fujita and M. Idesawa, "New Types of Position Sensitive Device for Accurate Sensing," in *Information, Intelligence and Systems*, 1999, pp. 141-148.

S. Funabiki and T. Tanaka, "Binocular-vision-based Position Sensor with PSDs and its Application to Mobile Robot Following," *IEEE Transactions on Science, Measurement and Technology*, vol. 149, pp. 79-84, March 2002.

D. Geiger, "Binocular Vision," October 2005, http://www.cs.nyu.edu/courses/fall02/622.2271-001/stereo.doc

L. Gonzo, A. Simoni, M. Gottardi, D. Stoppa and J.-A Beraldin, "Sensors Optimized for 3-D Digitization," *IEEE Transactions for Instrumentation and Measurement*, vol. 52, pp. 903-908, June 2003.

L. Gonzo, A. Simoni, M. Gottardi, D. Stoppa and J.-A Beraldin, "Smart Sensors for 3D Digitization," in *Instrumentation and Measurement Technology*, 2001, pp. 117-122.

P. T. Grey, "Digital Stereo Vision Camera: Bumblebee," Feb 2005, http://www.ptgrey.com/products/bumblebee/bumblebee.PDF

Hamamatsu Solid State Division, "PSD (Position Sensitive Detector)," 2003, http://usa.hamamatsu.com/assets/pdf/catsandguides/Psd.pdf

Hamamatsu, "Two-dimensional PSD, S1200, S1300, S1880, S1881, S2044," 2004, http://sales.hamamatsu.com/assets/pdf/parts_S/S1200_etc.pdf

Hamamatsu, "Two-dimensional PSD S5990-01, S5991-01," 2001, http://sales.hamamatsu.com/assets/pdf/parts_S/S5990-01_S5991-01.pdf

Hamamatsu, "Two-dimensional PSD S7848 series," 2005, http://sales.hamamatsu.com/assets/pdf/parts_S/S7848_series.pdf

R. Hartley and A. Zisserman, *Multiple View Geometry in Computer Vision*. United Kingdom: Cambridge University Press, 2000.

W. P. Kennedy, "The Basics of Triangulation Sensors," May 1998, http://www.sensorsmag.com/articles/0598/tri0598/main.shtml

M. Kim, H. Cho and H. Lee, "An Active Trinocular Vision System for Sensing Mobile Robot Navigation Environments," in *Intelligetn Robots and Systems*, 2004, pp. 1698-1703.

R. Klette, K. Schluns and A. Koschan, *Computer Vision: Three-Dimensional Data from Images*. Singapore: Springer-Verlag, 1998.

H. Konodo (a), T. Maki, T. Ura, Y. Nose, T. Sakamaki and M. Inaishi, "Relative Navigation of an AUV Using a Light-section Ranging System," in *Control, Automation, Robotics, and Vision Converence*, 2004, pp. 425-430.

H. Konodo (b), T. Maki, T. Ura, Y. Nose, T. Sakamaki and M. Inaishi, "Structure Tracing with a Ranging System using a Sheet Laser Beam," in *Underwater Technology*, 2004, pp. 83-88.

Leica Geosystems, "HDS3000 Specifications," 2005, http://www.leica-geosystems.com/hds/en/lgs_6506.htm

A. Makynen, T. Rahkonen and J. Kostamovaara, "Digital Optical Position-Sensitive Detector (PSD)," in *Instrumentaiton and Measurement Technology*, 2004, pp. 2358-2360.

L. Marques, F. Moita, U. Nunes, and A. T. de Almeida, "3D Laser-based Sensor for Robotics," in *Electrotechnical Conference*, 1994, pp. 1328-1348.

L. Marques, U. Nunes, and A. T. de Almeida, "A New 3D Optical Triangulation Sensor for Robotics," in *Advanced Motion Control*, 1998, pp. 512-517.

Minolta, "VIVID 9i Specifications," 2005, http://kmpi.konicaminolta.us/eprise/main/kmpi/content/ISD/ISD_product_pages/Vivid_9i?mDetail=Specifications

S. Mizuno, H. Funakoshi and K. Yamamoto, "3D Realtime Imaging System with PSD Array Combined with Charge Amplifier Array," in *Instrumentation and Measurement Technology*, 1994, pp. 457-460.

H. G. Nguyen and M. R. Blackburn, "A Simple Method for Range Finding via Laser Triangulation," San Diego, CA: United States Navy Technical Documentation, Janurary 1995.

Y. Oike, M. Ikeda and K. Asada, "A 375 x 375 3D 1k Frame/s Range-finding Image Sensor with 394.5 kHz Access Rate and 0.2 Subpixel Accuracy," in *Solid-State Circuits Conference*, 2004, pp. 118-517.

Y. Oike, M. Ikeda and K. Asada, "Design of Real-time VGA 3-D Image Sensor Using Mixed-signal Techniques," in *Design Automation Conference*, 2004, pp. 523-524.

Y. Oike, M. Ikeda and K. Asada, "High-sensitivity and Wide-dynamic-range Range Finder and its Application," in *World Automation Congress*, 2002, pp. 417-422.

Y. Oike, H. Shintaku, S. Takayama, M. Ikeda and K. Asada, "Real-time and High-resolution 3D Imaging System using Light-section Method and Smart CMOS Sensor," *IEEE Transactions on Sensors*, vol. 1, pp. 502-507, 22-24 Oct. 2003.

J. V. Oldfield and R. C. Dorf, *Field Programmable Gate Arrays*. New York: Wiley-Interscience Publication, 1995.

Parks, J. and Evans, P. Personal Visit. February, 2006.

P. J. Rajda, "Optimizatino of Logic Use on Stereo Vision Algorithm Example," in *Field-Programmable Custom Computing Machines*, 2001, pp. 307-308.

X. Reves, A. Gelonch and F. Casadevall, "Software Radio Implementation of a DS-CDMA Indoor Subsystem based on FPGA Devices," in *Personal, Indoor and Mobile Radio Communications*, 2001, pp. D-86—D-90.

Riegl Laser Mirror Scanner LMS-Z10 Technical Documentation and User's Instructions, May 2000

C. R. Rose, J. P. Hammonds, R. A. Nelson, J. T. Weizeorick, "The LANL Neutron Science Center TOF/PSD Module: Status and Progress," in *Real Time Conference*, 1999, pp. 137-139.

H. Russell, "Vision Systems Face a Grand Challenge," October 2005, http://www.advancedimagingpro.com/publication/article.jsp?pubId=1&id=1939

Samsung Electro-mechanics, "Polygon Mirror Scanner Motors," 2003, http://www.sem.samsung.com/

L. C. Silva, A. Petraglia and M. R. Petraglia, "Stereo Vision System for Real Time Inspection and 3D Reconstruction," *IEEE Transactions on Industrial Electronics*, vol. 1, pp. 607-611, 9-11 June 2003.

A. Simoni, L. Gonzo and M. Gottardi, "2.1: Integrated Optical Sensors for 3-D Vision," 2002, http://ieeexplore.ieee.org/iel5/8046/22242/01036976.pdf

Sitek, "What's a PSD", 2005, http://www.sitek.se/whats_a_psd.htm

"Stereopsis," October 2005, http://www.cim.mcgill.ca/~siddiqi/308-558-2001/danicl_stereo.pdf

"Stereo Vision," October 2005, http://www.cs.bris.ac_uk/Teaching/Resources/COMS30121/slides3D/lec2v.pdf

Trenz Electronics, "Spartan-3 FPGA Micromodule," 2005, http://www.trenz-electronic.de/prod/proden18.htm

S. M. Trimberger, *Field Programmable Gate Array Technology*. Boston/Dordrecht/London: Kluwer Academic Publishers, 1994.

User Documentation MAPP Ranger System. Sweden: IVP, Integrated Vision Products AB, 1998-2000.

L. Viarani, D. Stoppa, L. Gonzo, M. Gottardi and A. Simoni, "A CMOS Smart Pixel for Active 3-D Vision Applications," *IEEE Transactions on Sensors*, vol. 4, pp. 145-152, Feb. 2004.

Videre Design, "STH-MDCS/-C Stereo Head User's Manual," 2003, http://users.rcn.com/mclaughl.dnai/sthmdcs.pdf

W. Wang and I. J. Busch-Vishniac, "The Linearity and Sensitivity of Lateral Effect Position Sensitive Devices—An Improved Geometry," *IEEE Transactions on Electron Devices*, vol. 36, pp. 2475-2480, Nov. 1989.

M. Williams (mwilliams@nuhorizons.com), "FW: University of Tennessee in Knoxville," October 21, 2005.

Xilinx, "Spartan-3E FPGA Family: Complete Data Sheet," 2005.

Xilinx, "Virtex-4 User Guide," 2005.

VITA

Julie Anne Morris was born in Springfield, VA on June 9, 1983. Her family moved to Raleigh, North Carolina where Julie attended Jeffrey's Grove Elementary School and Pleasant Union Elementary School. They moved to Libertyville, IL, where she attended Oak Grove Middle School. Julie's family settled in Brentwood, Tennessee, where she attended Brentwood High School, graduating salutatorian in 2001.

Julie began attending Virginia Polytechnic Institute and State University in Blacksburg, VA in August 2001. Julie participated in the Residential Leadership Community, Baptist Student Union, and intramural basketball program. She also played for the open Ultimate Frisbee Club. She received her B.S in Electrical Engineering from Virginia Tech in May 2005, graduating suma cum laude. While working on her undergraduate degree, Julie interned at Sparta in Huntsville, AL, Northrop Grumman Missile Systems in Huntsville, AL, Micron in Dallas, TX, and IBM in Raleigh, NC.

Julie began working as a graduate research assistant for the Imaging, Robotics, and Intelligent Systems Laboratory at the University of Tennessee in Knoxville, TN, in August 2005. She will be graduating with an M.S in Electrical Engineering in August 2006.

After graduation, Julie will move to Raleigh, North Carolina, where she has taken a position as a hardware engineer with IBM in the Retail Store Solutions group.